CENTRE FOR INTERDISCIPLINARY PLASMA SCIENCE

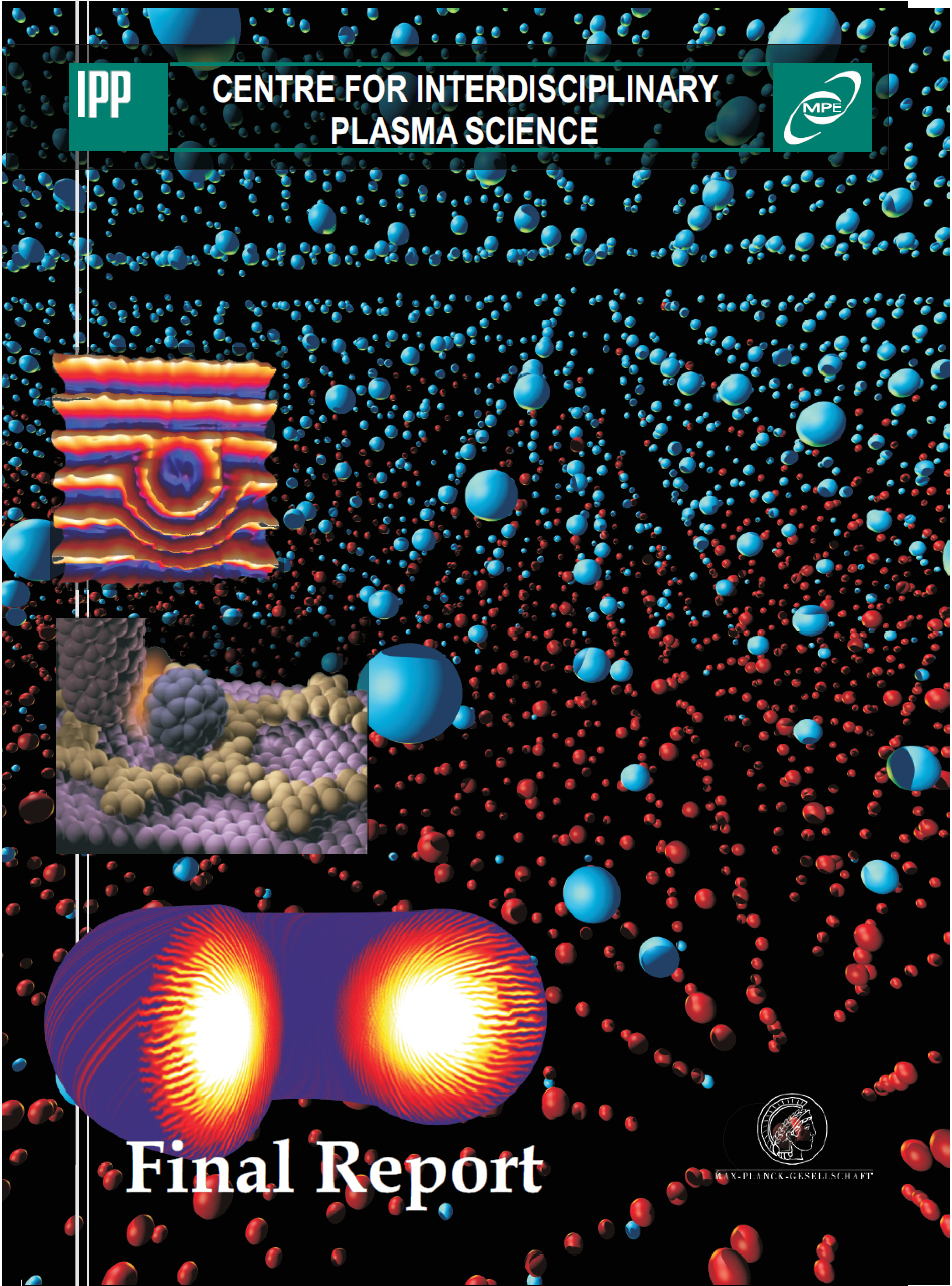

Final Report

Cover image:

The background shows the 3-dimensional particle positions of a plasma crystal observed under gravity conditions.

The inlay is divided in 3 sections, representing the different groups of CIPS:

1. The figure visualizes for each pixel of a noisy binary speckle image obtained from a test surface the probability to be zero. The probability map has been computed with Bayesian Neural Networks using hyperplane priors. Subsequently this probability map is used to extract information about surface changes (eg. erosion).

2. The image shows a dynamic force-field simulation of the manipulation of Buckminsterfulleren-molecules, which are imbedded in a template grid of trimesinacid molecules. The bucky-balls are moved with a Carbon nano-tube.

3. Spin up of global zone flows in a Tokamak turbulence computation. The torus cut shows the turbulent temperature fluctuations, which are just about to be sheared by the poloidal zone flow velocity.

Table of content:

I. EXECUTIVE SUMMARY

1. Introduction

In our previous report (2000/2001) we described the role and purpose of the "Centre for Interdisciplinary Plasma Science" CIPS, the hoped-for synergies in the cooperation between IPP and MPE, the possibility to focus energy and manpower on new aspects of plasma science, fostering in particular the interdisciplinary research with fields such as colloid physics, condensed matter physics, kinetic physics, plasma technology, medicine etc. We described the three research topics that form the backbone of CIPS:

- Theoretical Plasma Science
- Experimental Plasma Science
- Analysis Techniques and Applications

We described the new laboratories that were in the process of being built, the complementary space laboratory programme, the cooperations, outreach and science output of the first two years.

We will not repeat this here, since this introduction to CIPS is well-known and can be found in our Fachbeirat-Report 2000/2001. Instead, we will use this Executive Summary to describe the changes and developments since the last Fachbeirat-meeting in 2002.

2. Institutionalisation of CIPS

At the end of 2004, CIPS will officially come to an end, as envisaged by the special Max-Planck research programme under which it was funded. Obviously, the aim of this MPG programme is to create new and innovative science. Equally obvious should be the answer to the question: What happens if such a programme is successful? The simple answer is that the research should be continued – the not so simple answer is how this should be done. The level of success is evaluated by the independent Fachbeirat, who reports to the President of the Max-Planck Society.

In 2002 the Fachbeirat concluded that CIPS had become very successful and recommended "that steps are taken to initiate the process within MPG that can lead to the transformation of CIPS into a separate institute". This recommendation precipitated a whole range of reactions and activities, which we summarise in some detail, because of their unquestioned importance.

Boundary conditions

The situation of MPG in 2002/3 was not good. Due to budget cuts some 20 departments had to be closed down. Starting a new Institute under those circumstances was not easy.
MPE and IPP strongly supported the Fachbeirat's recommendation to institutionalise CIPS as an independent Max-Planck Institute.
MPE pledged support at the current level of Prof. Morfill's resources until 2010 as "start-up funds". After 2010 MPE plans to become a "pure" astronomy/astrophysics institute – further support from MPE will then not be possible any more.
IPP pledged to provide laboratory and office space on the Garching campus for this new Institute. IPP decided not to contribute manpower or financial resources. Consequently, the current IPP resources dedicated to CIPS will be re-integrated in January 2005, when CIPS ceases to exist.

The proposed CIPS successor institute

Subject to these "boundary conditions" a plan was developed to start CIPS as an independent institute in 2005 with the minimum of financial resources. The plan was to begin as a "**virtual institute**", accepting the start-up offers from MPE and IPP, using the workshops of the two institutes and their administration to save cost. After some years the "virtual institute" would then develop into a "real" institute. Also, the science was "descoped". The plan was to start with two departments – "experimental complex plasmas", and "kinetic theory" – with the latter also including nonlinear dynamics, simulations and data analysis. Later, so the plan, a third department should be added (e.g. low temperature plasma science). This proposal was presented to the President.

The formal procedures

At the request of the President, the "standard MPG-procedure" for institutionalisation was started:

- Presentation of the research portfolio for pre-screening to the "Perspektiven-kommission" of the CPT-Sektion

(2/11/2002). Recommendation to take this on to the Sektion.

- Presentation to the Sektion (4/6/2003). Unanimous recommendation to prepare a proposal for institutionalisation and proceed with the usual evaluation process. Election of an "Expert Commission".
- Presentation of the proposal to the Expert Commission (29/8/2003). Unanimous recommendation to proceed with the institutionalisation – but not as an independent institute, instead as a department in an existing institute. This department should receive additional central funding from MPG.
- Discussion of this recommendation in the next Sektionssitzung (16/10/2003). Institutionalisation, as recommended by the Expert Commission, was unanimously approved.

Attempts to implement this recommendation

An attempt to merge the CIPS "complex plasma" activities with the reconstituted Max-Planck-Institut für Strömungsforschung in Göttingen (for which some scientific overlap – kinetic theory of liquids, classical plasma-nano-fluidics – exists) was not possible. MPG was not willing to commit the extra funds for an additional department.
IPP also voted not to act as "host" institute for the new field of "complex plasmas", since this would diversify the institute away from its primary research goal of "plasma fusion".
MPE had already decided to become a 'pure' astronomy/astrophysics institute.
No other attempts were made to "find an institute" – in particular, since the outcome of the negotiations with the Max-Planck-Institut für Strömungsforschung showed that the MPG administration was not yet willing to commit resources.

Interim solution and current status

Meanwhile, time was not standing still. The concern grew that the whole investment in CIPS could be wasted, the scientific leadership (as attested by the Fachbeirat, 2002) would disappear with the scientists and the huge innovation potential would just not be taken up within MPG in spite of all the recommendations.

At a meeting in January 2004, the President promised to provide some interim support and gain time for a solution to the CIPS succession, by providing some limited resources for a "Research-Group" headed by Dr. Thomas starting in January 2005.

The current status is, therefore, that subject to an appropriate recommendation from this (second) Fachbeirat-Evaluation the issue of founding a new Max-Planck-Institute as successor to CIPS is not closed. The situation of MPG has improved substantially since 2002/3, a fact that has to be borne in mind, too.

Effects of these events on CIPS

On the positive side are the excellent scientific evaluations, the sustained exponential growth of the field of "complex plasmas" (see Fig. I.1), the many publications in top-class journals and all the other measurable international successes. These have ensured a good team spirit in CIPS in spite of the negative side of things – where the apparent failure of MPG to acknowledge the success of CIPS and to appreciate its innovation potential, and the decision by IPP to not expand into interdisciplinary plasma science are the most important.

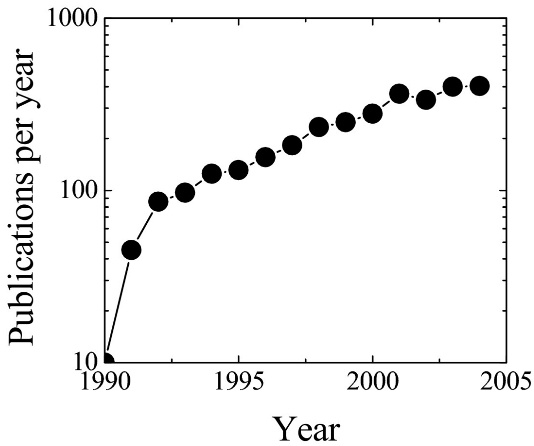

Fig. I.1: The figure shows the publication rate in complex (dusty) plasmas over the last 15 years.

A significant negative effect has been the slow-down in the growth of joint IPP/MPE projects, which would have been significantly more if the scientists had been able to continue a joint scientific vision.

The most notable joint MPE/IPP projects are:

- Diamond production in low temperature rf plasmas
- Development of a rf strip electrode for particle manipulation and dust-free plasma deposition

- Astrophysical data analysis using advanced Bayesian techniques
- Simulation studies of collisionless shocks

The strength of these cooperations is underscored by the fact that MPE and IPP now hold three joint patents.

The second negative effect has been the (quite understandable) decision by some CIPS scientists to seek opportunities elsewhere, and the fact that retirements could not be replaced with fresh personnel due to central cuts in resources.

Ten established scientists have left CIPS since 2002, including three retirements. Only two could be replaced with a new person from outside.

On the other hand, the growth and attractiveness of the "interdisciplinary plasma sciences" does not go unnoticed with the students and young post-docs. Therefore, we were able to add six post-docs (three of them funded from outside sources), six PhD students (two of which were funded from outside sources) and many short-term visitors (mostly self-funded). Thus CIPS has continued to be scientifically alive and vibrant in spite of all the difficulties associated with the forthcoming changes.

3. Research Highlights

Some research highlights in the present reporting period (2002-2004) were:

Experimental plasma science

- Analysis of the melting phase transition using localised Γ, kT, Δ
- Phase boundaries with attractive potentials (shadow effect) and investigation of the "critical point"
- Non-Hamiltonian Physics – kinetic effects in complex plasmas
- Universality concepts in crystal growth and nucleation
- Nanofluidics – first experiments with liquid complex plasmas
- Magnetised complex plasmas – first experimental results
- Two-stream-flows – nonlinear non equilibrium coordinate space phase transition, wave excitation
- Charge-induced runaway coagulation (gelation), statistical analysis of charges, Q/m etc.
- Diamond growth experiments at higher temperatures
- Generalised theory of ion drag, comparison with new experiments
- Propagation of phonons in plasma crystals, thermal conductivity measurements
- Chemical sputtering of carbon materials by combined bombardment with ions and thermal hydrogen atoms
- Growth in pulsed plasmas – the role of the mean energy per particle
- Contributions of different species (neutrals, radicals, ions) to hydrocarbon film growth – the dominant growth precursors

Theoretical plasma science

- Understanding the physics of collisionless magnetic reconnection
- The structure of collisionless shocks
- MHD turbulence – origins and development
- Instabilities in collisionless plasmas

Analysis Techniques and applications

- Robust signal-background separation employing mixture modeling
- Quantitative analysis of multicomponent mass spectra with unknown cracking structure
- Development and application of Bayesian neural networks
- Integrated data analysis of heterogeneous plasma diagnostics
- Bayesian experimental design of future fusion diagnostics
- Bayesian nonparametric function estimation of climate and phenology data time series
- Real time tomographic inversion of soft X-ray measurements on fusion devices
- Parameter estimation of the dynamics of cell migration on different time scales
- Segmentation of images using a neural formulation of scaling indices
- Non-Gaussian signatures in the cosmic microwave background
- Quantitative determination of the information content of images
- Dermatoscopic workplace for skin cancer diagnosis
- Detection of carcinogenic lung (micro-) nodules in high resolution CT images

- AFM-analysis of nano-structures
- Early detection of osteoporosis
- “In vivo” sterilisation using low temperature plasmas

4. New laboratory activities

The low-temperature (complex) plasma laboratories for the investigation of strongly magnetised systems, paramagnetic complex plasmas, thermophoretic suspension of particles, adaptive electrode development and diamond formation have been continuously improved and are working satisfactorily.

Thanks to some special MPG-funding and industry support, we have been able to initiate new projects:

- Development of a large area strip-electrode, which has the capability of manipulating large (~ 10^9 particles) plasma crystals, thus allowing "boundary free" experiments.
- Development of "plasma medicine" – using a rf "plasma torch" to sterilise wounds and treat bacteriological and fungoid skin diseases. The plasma torch is cold (just above room temperature) and a substantial "in vivo" study will be undertaken to investigate clinical implementation.
- Development of a "stochastic laser manipulator" to "heat" predetermined regions of complex plasmas (plasma crystals) to a given kinetic temperature.
- Time-resolved mass spectrometry in pulsed plasma was started.
- Installation of a new inductively-coupled plasma device dedicated to the study of particle fluxes. This experiment is equipped with a new plasma process monitor allowing to measure mass-resolved neutral and ion fluxes and ion energy distributions.

Future experiments

The German/Russian cooperation in space is proceeding as planned, although there are some delays, which are beyond our control (to some extent precipitated by the space shuttle uncertainties). PK-3 Plus will now be launched in 2005. PK-4 was cancelled by DLR due to budget cuts, but it is now planned that ESA and DLR will finance it jointly – as it is an essential technology for IMPF. The currently projected start of PK-4 is 2007. The new cornerstone project IMPACT (International Microgravity Plasma, Aerosol and Cosmic particle Twin) Laboratory, which merges the two projects IMPF and ICAPS – with substantial cost savings and without any science descoping – is now planned on the ISS for 2009. Thus the research strategy – to have laboratory experiments on Earth and a continuous succession of microgravity laboratories on the ISS – appears to remain feasible.

ESA's new Announcement of Opportunity (AO 2004) has paved the way for new proposals and ideas. Together with many partner institutes we have responded to this AO, suggesting five new projects for international evaluation:

- Investigation of the physics at the "critical point" at the kinetic level using complex plasmas (liquid state).
- Particle beam manipulator for IMPF to investigate charged particle beam – dust interactions.
- Diamond production in space – a prototype to investigate long-term particle growth in the low temperature main plasma (theoretically it should be possible to grow cm-sized pure diamonds this way).
- Study of "quantum gases" and "quantum plasmas" by developing a "Bose-Einstein condensate (BEC) experiment drawer" for IMPF. Under microgravity, the condensates can be trapped much longer, allowing studies of interacting BEC’s and external manipulation.
- A "GRID Science Net" to link all researchers with common interests in "space complex plasmas" (and beyond) providing optimised communication and data exchange capabilities. This project is an infrastructure project of great importance for the wider scientific community (it complements the current EU-GRID initiative) and we propose IMPACT as a pilot project for ESA.

6. Organisation of this report

This report covers the scientific work of the years 2002 – 2004, but it includes all the publications from 2000 – 2004.

II. Theoretical Plasma Science

The plasma theory group of the Centre for Interdisciplinary Plasma Science has concentrated on the following main activities: Understanding the physics of collisionless magnetic reconnection, particle acceleration during reconnection in relativistic pair plasmas, the structure of quasi-perpendicular collisionless shocks, MHD turbulence, and instabilities in collisionless plasmas.

When some dynamical energy release occurs in dilute astrophysical plasmas collisionless shocks arise where the macroscopic flow is regulated by microscopic dissipation and where part of the thermal population is accelerated to high energies. Collisionless shocks are found in the Corona of the Sun, in the solar wind, in front of planetary magnetospheres, and in many other astrophysical settings. The two main questions in collisionless shock physics are: (1) how is dissipation achieved in a plasma where two-body Coulomb collisions are unimportant, and (2) how is a certain part of the thermal plasma accelerated to high energies. We have actively investigated these questions over the last decades by numerical simulations. Most of these simulations have been performed with hybrid codes, where the ions are treated as macro-particles and the electrons as a massless fluid. Naturally, such a code does not describe physics on the electron scale. However, certain shock acceleration processes require shock potential scales of the order of the electron inertial scale. In order to resolve electron physics we have therefore performed full particle simulations of collisionless shocks. While such simulations have been done in the past by a number of groups, we have demonstrated that in many cases use of the physical ion to electron mass ratio is unavoidable in order to describe correctly the dissipation processes in collisionless shocks. In particular, the modified two-stream instability has a growth rate which strongly depends on mass ratio and thus has not been found before in low ion to electron mass ratio simulations.

Reconnection is a fundamental process in astrophysical and laboratory plasmas, whereby magnetic field energy is converted into plasma bulk and thermal energy, and large topological changes occur. In a collisionless plasma reconnection requires either an anomalous resistivity, inertia-based processes, or nonzero off-diagonal terms of the electron pressure tensor, which all support an electric field along a neutral line. Numerical simulations have recently clarified the details of the reconnection process within a two-dimensional configuration. However, these 2D simulations of reconnection (1) eliminate instabilities along the reconnection line, (2) do not provide any information whether reconnection is patchy or remains two-dimensional with an extended neutral line, and (3) do not provide information why reconnection sets in in the first place, i.e., they have to start already with a perturbation akin a reconnection configuration. We have investigated with a three-dimensional full particle (Particle-in-cell) code the onset of reconnection in thin current sheets. It has been found that the lower hybrid drift waves excited in thin current sheets lead to quick triggering of reconnection within several inverse ion gyrofrequencies. In order to investigate reconnection in the regime of non-Hall reconnection in thin current sheets PIC simulations of pair plasmas have been performed. These are by their nature fully relativistic requiring the definition of a fully relativistic Harris equilibrium and using the Jüttner equilibrium particle distribution function. It is found that non-Hall reconnection is possible in 2D and 3D, proceeds very fast on the electron time scale, and causes intense particle acceleration.

The work on plasma instabilities has been continued mostly in the direction of very low frequency instabilities of about zero frequency in the mirror mode range. These calculations have been linear analytical in nature either for wave-particle interaction or wave-wave interaction. Emphasis was put on the modification of the linear growth rates of mirror waves in the presence of modified ion distributions, finite electron temperatures, and electron temperature anisotropies. General dispersion relations have been derived which include the effects of these modifications and of plasma gradients. The inclusion of electron temperatures led to the discovery of new branches of mirror modes. The inclusion of wave-wave interaction for kinetic Alfven waves led to the excitation of electrostatic convection cells by such waves which might be applicable to the auroral region and contribute to the understanding of the appearance of auroral shear flows in relation to the detection of kinetic Alfven waves. Finally, in the high frequency electrostatic range calculations of the evolution of phase space holes gives some indication of deformation of these holes in phase space which should contribute to the excitation of auroral kilometric radiation. This mechanism seems very promising and will be investigated in greater depth in the next months. We have also continued research the direction of the nonlinear evolution of the mirror mode, which will be discussed more deeply in the simulation section, and of the physics of the generalized-Lorentzian distribution functions which has been one of the issues of central interest in view of the continuous observation of kappa distributions in collisionless space plasmas.

Turbulence is a nearly omnipresent state of many astrophysical systems and laboratory plasmas. Advancing the theory of these flows is important for a better understanding of as diverse observations as, e.g., the generation of large-scale magnetic fields accompanying many celestial objects by the turbulent dynamo effect, the dynamics of stellar winds and their interaction with planetary magnetospheres, the discrepancy between observed and predicted life-times of star-forming molecular clouds in the insterstellar medium, and the angular momentum transport within accretion disks prone to magnetorotational instability. Moreover, the anomalous particle and energy transport in magnetically confined plasmas in tokamak and stellarator experiments for nuclear fusion is assumed to be caused by small-scale turbulence. Fundamental numerical studies on the macroscopic and statistical scaling properties of magnetohydrodynamic and magnetoconvective turbulence are carried out to extend the theoretical framework of astrophysical plasma turbulence. Two-fluid simulations focus on the nonlinear turbulent interplay of micro-instabilities present in the cool edge region of fusion plasmas, investigating the impact of turbulence on the mass and heat losses.

The turbulence in magnetically confined nuclear fusion plasmas transcends simple descriptions by overall scaling laws in the dimensionless parameters. The reason is its ability to spontaneously create large structures in the electromagnetic field or the plasma itself, which strongly act back on the turbulence, thereby potentially improving the confinement by orders of magnitude. The explorations in this area target the principles for the creation of such structures and their interaction with the background turbulence. A comprehensive understanding of these global structures would lead to more trustworthy predictions of future machine performance and could lead to schemes to more directly access the favorable confinement regimes. Apart from nuclear fusion, analogous interactions between microscopic and macroscopic scales generally occur in quasi-two dimensional turbulence systems, e.g., between the convective turbulence and the zonal bands in the atmosphere of gas planets.

1. Collisionless Shocks

Reformation of quasi-perpendicular shocks has been extensively investigated by full particle (Particle-in-cell) simulations in the past. In high Mach number shocks part of the incoming ions are reflected at the ramp and form during their gyration a foot in front of the ramp. At the upstream edge of the foot these ions are accumulated in time and are eventually responsible for reformation, i.e., a new ramp emerges at the upstream edge of the foot. The reformation process inseparably related to ion dynamics. In addition, electron dynamics may become important in the foot region and can lead to the excitation of the Buneman instability with subsequent electron hole formation. However, most of the past full particle simulations assume, because of computer limitations, unrealistically small ion to electron mass ratios. Using a one-dimensional full particle code we have investigated the role of the ion to electron mass ratio in quasi-perpendicular shock simulations. At medium Mach number shocks ($M_A \sim 5$) and mass ratios below about 100 the Buneman instability arises, resulting in a wave electric field with a component parallel to the shock normal and to electron holes in the electron normal velocity component. Reformation is due to ion accumulation in the foot. When increasing the mass ratio to several hundred the Buneman instability disappears, since it is Landau-damped due to the larger thermal velocity of the electrons. Increasing the ion to electron mass ratio to the physical value results in the Modified-Two-Stream instability (MTS) in the foot: because of the presence of the reflected ions the total bulk velocity of the ions in the foot decreases. The electron bulk velocity has then also to decrease when requiring zero current in the shock normal direction. As a result a finite difference of the bulk velocity between the

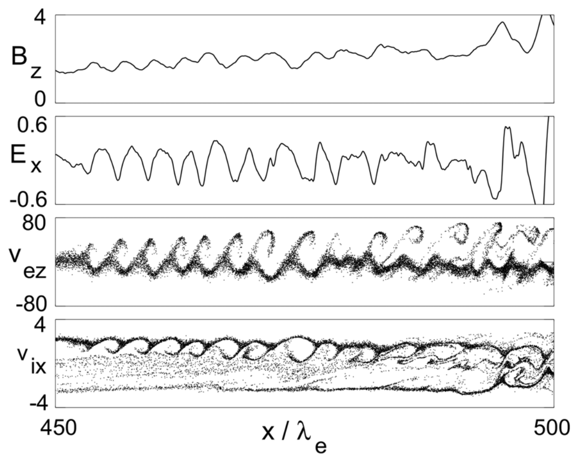

Fig. II.1: From top to bottom: magnetic field, electric field component in the shock normal direction, v_{ex} phase space distribution of electrons, and v_{ix} phase space distribution of ions in the foot region (within 50 electron inertial lengths upstream of the ramp) of a quasi-perpendicular collisionless shock.

electrons and the incoming as well as between the reflected ions arises. This velocity difference leads to the MTS instability. Since the growth rate of this instability depends strongly on the mass ratio, it has not been seen in the low mass ratio simulations.

Fig. II.1 shows from top to bottom the main magnetic field component, the electric field component in the shock normal direction x, the v_{ez} phase space distribution of the incoming electrons, and the v_{ix} phase space distribution of the incoming and reflected ions in the foot region. The scale is in units of the electron inertial lengths. One can clearly see electron acceleration parallel to the main magnetic field and the instability of the incoming ions. At a later state the MTS instability grows nonlinearly and phase mixing between incoming and reflected

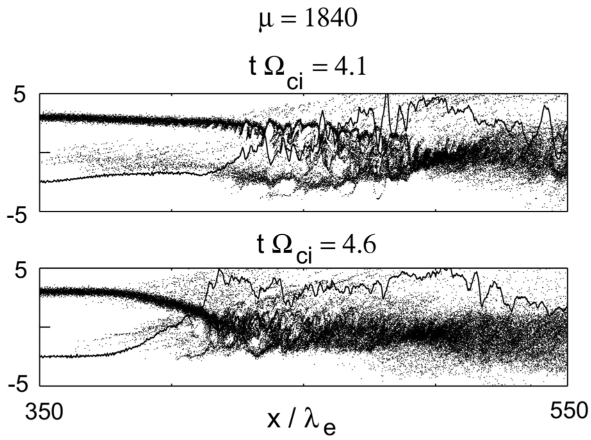

Fig. II.2: Ion v_{ix}-x phase space plots at two different times during a reformation cycle of a quasi-perpendicular collisionless shock. The solid lines denote the magnetic field profile.

ions results in a hot ion distribution in the foot. Fig. II.2 shows snapshots of the ion v_{ix} phase space distribution at two different times with the magnetic field profile superposed. It can be seen how the phase mixing and heating eventually leads to a newly emerging ramp at the upstream edge of the former foot. Thus, realistic mass ratio simulations confirm the process of shock reformation of almost perpendicular shocks; however, the physical mechanism is totally different from the one envisaged before. This clearly demonstrates the necessity of using the physical ion to electron mass ratio in collisionless shock simulations.

2. Reconnection

Numerical simulations have recently clarified the details of the reconnection process within a two-dimensional configuration. However, these 2D simulations of reconnection (1) eliminate instabilities along the reconnection line, (2) do not provide any information whether reconnection is patchy or remains two-dimensional with an extended neutral line, and (3) do not provide information why reconnection sets in in the first place, i.e., they have to start already with a perturbation akin a reconnection configuration. We have investigated with a three-dimensional full particle (Particle-in-cell) code the onset of reconnection in thin current sheets. Instead imposing reconnection ab initio, reconnection is allowed to develop out of the numerical noise. In the case of exactly antiparallel magnetic fields the lower hybrid drift instability is excited at the boundaries of the current sheet in the region of steepest pressure gradients. The electric field of the lower hybrid waves accelerates the electrons in the current sheet center in the current direction. Fig. II.3 is a color-coded representation of the electron density and the electric field in a plane perpendicular to the antiparallel magnetic field configuration, i.e., a plane containing the current direction and the direction normal to the current sheet. Fig. II.3 shows the excitation of the lower

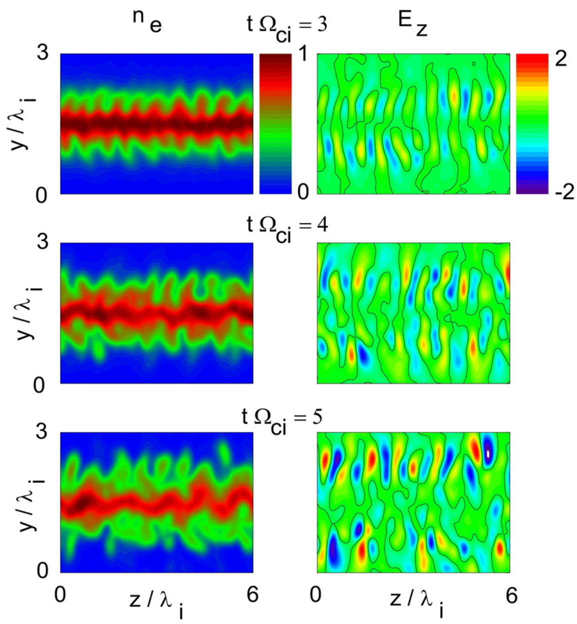

Fig. II.3: Color-coded representation of electron density (left) and of electric field component in the current direction z (at three different times in the plane perpendicular to the antiparallel magnetic field (plane containing the current). Time is in units of the inverse ion gyrofrequency.

hybrid drift waves at three different times. The acceleration of the electrons in the current sheet center results in an increase of the electrical current density by a factor of about 3. Due to the current sheet collapse quick reconnection is triggered. Initially reconnection has a patchy appearance in the current plane. Fig. II.4 shows

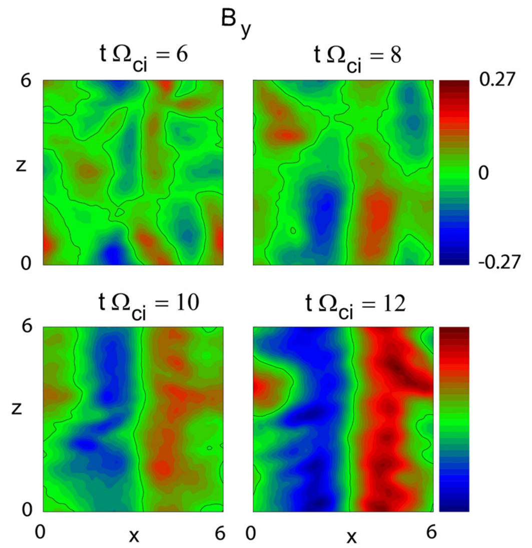

Fig. II.4: Color-coded representation of the magnetic field component normal to the current sheet in the centre of the current sheet at four different times. Blue represents a negative magnetic field component, red a positive magnetic field component. A neutral line separates red from blue areas.

how the reconnection patches merge and a single X line results within a few inverse ion gyrofrequencies.

When imposing a guide field of the same order as the antiparallel field in the current direction (sheared field configuration) the onset is considerably delayed, but after reconnection sets in the reconnection rate is the same as in the exactly antiparallel case. This indicates that so-called component merging may be delayed with respect to antiparallel merging.

3. Reconnection and Acceleration in Pair Plasmas

Reconnection in collisionless electron-proton plasmas unavoidably develops Hall currents and is thus subject to Hall modulation of reconnection. In order to investigate reconnection clean of Hall effects PIC simulations of pair plasmas have been performed in two and three dimensions (see Fig. II.5). This requires a fully relativistic treatment. Very thin current relativistic Harris current sheets have been taken as initial condition with thickness comparable to the inertial length scale. Under such conditions reconnection develops very fast with the current sheet containing several X-points similar to tearing instability. This demonstrates that in thin current sheets reconnection evolves very fast in absence of Hall currents and is driven solely by electron dynamics. In the X-point geometry the latter induces deviations of the electron pressure from diagonality which implies electron viscosities. Larger X-point show a stronger dynamics and in the course of the evolution of the current sheet interact with smaller X-points and merge. The

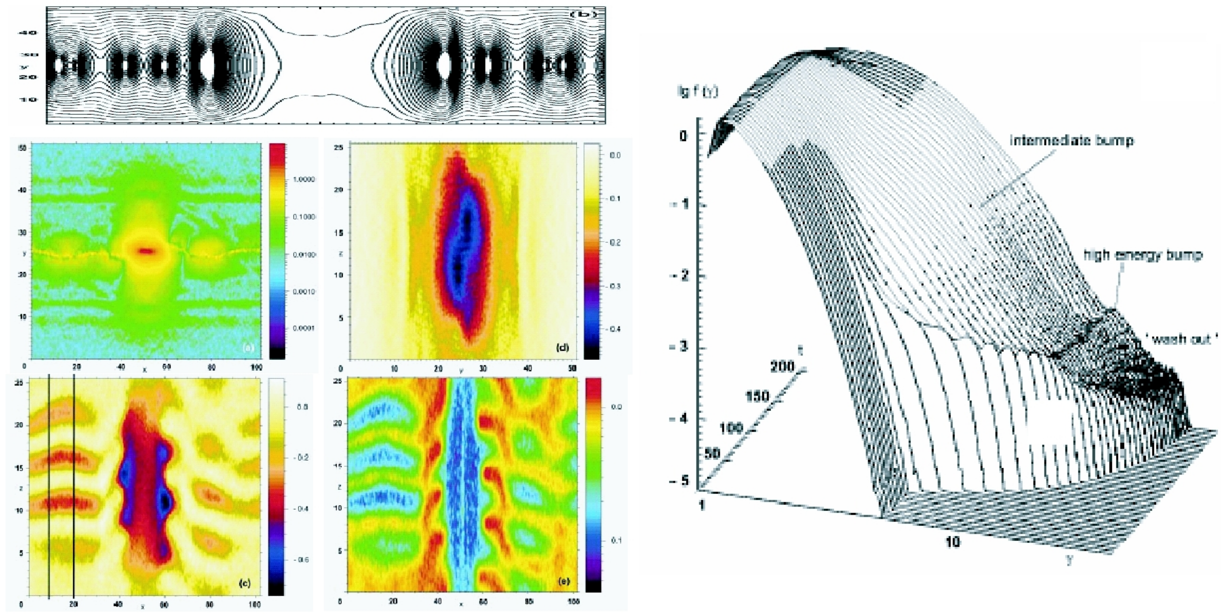

Fig. II.5: PIC simulation of relativistic pair reconnection in a thin current sheet in three dimensions. The top left shows the evolution of several X point reconnection regions. Below the electric field near the dominant X point is shown in the centre of the current sheet and above the centre indicating the three dimensional structure of the field and the development of electric field ripples. On the right the evolution of the particle distribution integrated over the full box is shown. The initial relativistic Boltzmann-Juettner distribution function readily evolves into a power law distribution.

most interesting effects are observed in three-dimensional reconnection. The reconnection electric field in the direction of current flow breaks off into three-dimensional structures indicating that the neutral line has finite extension and that the magnetic field in reconnection is truly three-dimensional. The electric field is essentially the electric induction field related to the annihilation and topological reorganization of the magnetic field. In addition the electrostatic wave modes related to density fluctuations evolve at the boundaries of the current sheet and may contribute to anomalous resistivity effects. Pronounced acceleration of particles has been found. The particles are accelerated along the finite X-line by the induction electric field but are turned around by the magnetic field near the X point and escape along the magnetic field. Particles can be accelerated by collisions with successive X-points reaching very high energies when escaping along the field from the current sheet. The resulting particle distribution is power law. During acceleration such a distribution emits intense synchrotron radiation. This has been calculated using radiation theory. Since synchrotron absorption can be shown to be negligible even on much larger scales, such calculations have been used to model synchrotron emission from intense astrophysical sources near AGNs yielding excellent agreement with observation. On larger spatial scales the power law distributions will generate bremsstrahlung and can thus explain the X ray emissivity from such sources as well.

4. Magnetic Mirror Modes

Research on magnetic mirror modes has been continued in the direction of numerical simulation of the mirror instability using a PIC particle code and in the direction of the analytical investigation of the evolution of the mirror instability (see Fig. II.6). The physical mechanism of evolution of the mirror mode in an homogeneous anisotropic plasma is based on the assumption that an infinitesimal localized fluctuation in the magnetic pressure causes trapping of the zero parallel/large perpendicular velocity particle component in the small magnetic depression and thus induces growth of the depression. Linear theory of this process has been extended to arbitrary ion distribution functions including plasma gradients and finite electron temperatures. The most interesting effects observed are that finite electron temperatures introduce some damping of the original ion mirror mode. At the same time two new branches of mirror modes appear in which the electrons play a fundamental role. These branches are of kinetic nature and vanish when the electrons have zero temperature. Under certain conditions they can have larger growth rate than the ordinary ion-mirror mode. Since the maximum growth rate of all mirror modes is attained at short wavelengths comparable to the ion gyroradius, inclusion of finite gyroradius effects was necessary. Finite ion gyroradii increase the threshold for the mirror instability while maximum growth remains at wavelengths comparable to the ion gyroradius. One therefore expects to find mirror modes of transverse wavelength comparable to ion gyroradii which is in gross agreement with observation. However, mirror modes are never observed in their linear states. Investigation of the final nonlinear state of the mirror mode has been done by numerical (PIC) simulation and analytically. Simulations under conditions when the mirror instability should set on showed that mirror modes readily

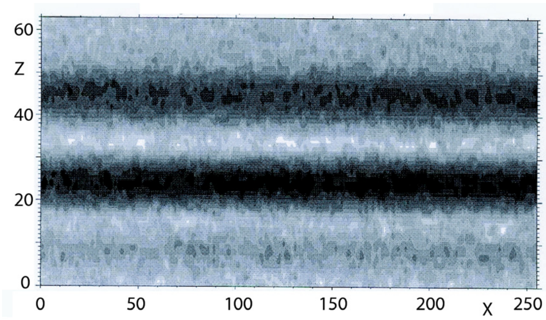

Fig. II.6: The final state of the 3D simulation of mirror modes in an electron-proton plasma under conditions when the mirror instability is unstable. Long magnetic field depleted mirror tubes (dark) evolve which are separated by magnetic walls (bright).

evolve nonlinearly forming a macroscopic quasi-crystalline network of magnetic field depressions wih parallel wavelengths longer than the simulation box. These structures are about regularly arranged in the simulation box, are of hexagonal nearly circular geometry and about one ion gyroradius in diameter. They are separated by magnetic walls. The magnetic field depression inside the magnetically depressed tubes is compensated by plasma pressure enhancements essentially due to an increase in plasma density. However, the depression itself is caused by diamagnetic electron currents of cold electrons flowing along the boundaries of the tubes. Analytical investigation shows that the final state is a state of marginal stability with the parallel wavelength growing beyond limits thereby confirming the simulations. The marginal stability threshold is understood as a condition for phase transition from homogeneous to structured plasma containing mirror tubes separated by magnetic walls. Attempts of applying Ginzburg-Landau theory to this transition encounter severe difficulty, as the free plasma energy is not precisely known. Nevertheless, formally a Maxwell-London set of equations can be derived. It defines the magnetic screening length in terms of the diamagnetic electron density. Taking this length from simulations and observations and comparing it with the correlation length of the diamagnetic electrons from simulation one finds that the ratio of the two lengths, the Abrikosov-Ginzburg-Gorkov parameter, is larger than one. This is in agreement with the observation of structuring the plasma into magnetic depressions and magnetic walls. In a certain sense the ideally collisionless plasma behaves in this case as a superconducting medium of the second kind. The quasi-crystalline arrangement of the magnetic depressions is then caused by the repulsive Lorentz forces of the antiparallel diamagnetic electron currents flowing on the surfaces of neighbouring tubes.

5. Acceleration and Radiation from Electron Holes

Formation and effects of electron holes in the auroral plasma have been a vital issue of interest in this group. It had been identified that auroral kilometric radio emission is basically due to elementary emitters which had been proposed to be electron holes. This research has been continued and extended to the investigation of the energy flux fluctuations of the auroral electron beam in the upward current region, the source region of auroral kilometric radiation (see Fig. II.7). It was found that the electron and ion energies fluctuate in strict anti-correlation and by the same amount, which is an unambiguous sign of the presence of electric fields. These fields are concentrated in layers along the magnetic field of 10 km parallel extension, comparable to the theoretically estimated width of auroral electron holes in the low-density auroral plasma. Investigation of the observed wave spectra show indication of localized electric fields and power law spectra. Numerical 1D PIC simulations have been performed for the transition region between the upward and downward current regions where the wave intensities are strongest. These simulations nicely reproduce both the observed wave spectra as the time modulation of the wave form. Three kinds of waves are excited in this region: the auroral beam excites intense electron plasma waves at the plasma frequency and at its harmonic and a broad spectrum of ion acoustic waves which modulate the former. Initially, the presence of cold and hot electrons also excites electron acoustic waves which however are quickly damped heating the plasma. In the late stage weak electron acoustic waves reappear as a result of wave coupling and deformation of the electron distribution function. In order to arrive at even more realistic wave spectra 2D simulations are needed to be performed in which case ion cyclotron waves would also be excited and contribute to wave modulation.

Concerning the generation of radiation we have made an essential step ahead in realizing that the electron holes excited in the upward auroral current region are at very low frequencies below 10 kHz. This range is in the Buneman range such that the holes are excited by the parallel difference velocity between the downward auroral beam and the upward ion beam of the ring-shell distribution. In fact the distribution is extended but the electron thermal velocity is lower than the difference speed between electrons and ions for a substantial range of perpendicular velocities such that the Buneman mode is excited strongly. Since there

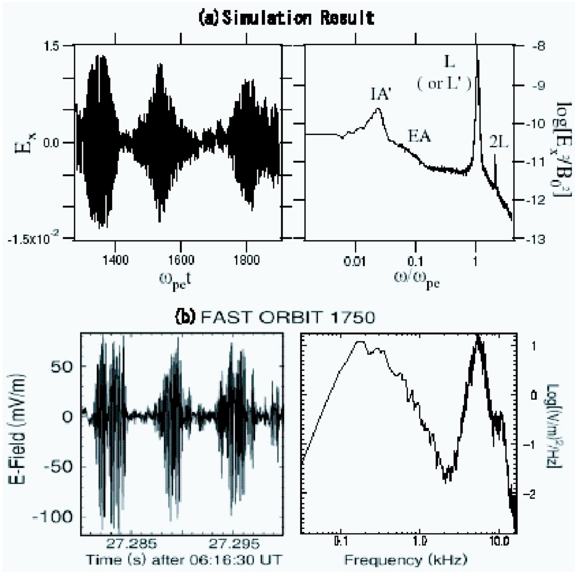

Fig. II.7: Simulation (top) and observation (bottom) of electrostatic waves in the auroral upward current region. Wave forms are shown on the left, spectra on the right. The similarity of the wave forms is striking. The high frequency auroral beam excited waves are modulated by low frequency ion acoustic oscillations. Less agreement is seen in the spectra where the ion acoustic and electron plasma wave bumps are more intense and broader than in the simulations. But the general agreement is excellent.

is no background electrons the plasma frequency is low and the mode appears at so low frequencies that it had not been recognized before. The holes which evolve experience a deformation in the phase plane thereby generating a local perpendicular gradient in the perpendicular velocity distribution which excites radiation. It is this gradient which is responsible for the elementary radiators, and the radiation need not to be strictly perpendicular anymore.

6. Residual Energy Spectrum in Incompressible Magnetohydrodynamic Turbulence

In MHD turbulence the spectral distribution of total energy does not give sufficient insight in the only partially understood nonlinear energy dynamics of the system. This becomes obvious in simulations of isotropic MHD turbulence which display a growing excess of magnetic energy with increasing spatial scales (see Fig. II.8). In contrast, turbulent magnetofluids threaded by a mean magnetic field display approximate equipartition of kinetic and magnetic energy at all scales of motion.
By making use of the eddy-damped quasi-normal Markovian approximation, a statistical turbulence theory giving differential evolution equations for the second-order moments of incompressible MHD, we are able to describe the behaviour of the difference between kinetic and magnetic energy spectra by a simple phenomenology. The theory assumes a quasi-equilibrium of the turbulent small-scale dynamo amplifying the magnetic field and the effect of Alfvén waves leading to equipartition of kinetic and magnetic energy. The main result of this work is a spectral relation between total energy and residual energy, the latter being the difference of magnetic and kinetic contributions.
The relation yields scaling predictions for the residual energy spectrum in isotropic systems, $\sim k^{-7/3}$, and for flows permeated by a mean magnetic field, $\sim k^{-2}$. High-resolution numerical simulations of the respective setups are in very good agreement with theoretical expectation.

7. Tokamak Turbulence Code Developments

The principal nonlocal effects of the pedestal structure of density and temperature as pertaining to the edge of a tokamak had been explored with the massively parallel, three-dimensional, electrostatic, nonlocal two-fluid turbulence code NLET. The code had also been used to study the zonal flows for various edge regimes in a tokamak. The edge zonal flows were found to be oscillating geodesic acoustic modes, different from the core, where the flows are known to be nearly static. Depending on the regime encountered in the tokamak edge, ITG or ballooning, either a condensate of global flow modes or a spectrum of local microscopic flows had been observed.

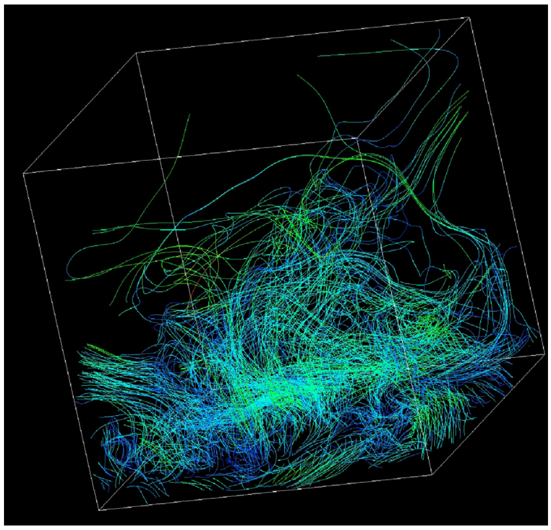

Fig. II.8:. Snapshot of magnetic field lines in a simulation of isotropic MHD turbulence.

The turbulence code NLET originally running on the Cray T3E has been expanded to take into account magnetic field fluctuations and general tokamak magnetic field geometry information, such as generated by the EFIT equilibrium code. Moreover it has been ported to the Regatta IBM-SP supercomputers of the Rechenzentrum Garching, as well as to parallel Linux Clusters supporting the MPI message passing standard.
We have started to compare comprehensive electromagnetic edge turbulence simulations by the new NLET code with the turbulence in Alcator C-mod discharges, which has been measured to unprecedented detail by ultra-fast GPI imaging. For the comparison, an L-mode reference discharge was used. Open and closed field lines as well as the effect of limiter-like boundary conditions have been tested. The atomic emission efficiency curves for the D-alpha line have been applied to the code results. Linear growth rates from the fluid code have been found to agree with gyrokinetic results for the same plasma parameters in the relevant regime for the C-Mod L-Mode edge. These comparisons are still in progress owing to the uncertainty in the edge parameters and the sensitivity of the turbulence with regard to the background gradients.

8. Zonal Flow Studies

The excitation and saturation of the stationary core zonal flows has been studied with NLET for various parameter sets located in the vicinity of the cyclone-base case, a well know reference point. As expected, stationary zonal flows were found (Fig. II.9). Differing from the present notion of the flow mechanics, at their final saturation amplitude, the zonal flows continue to

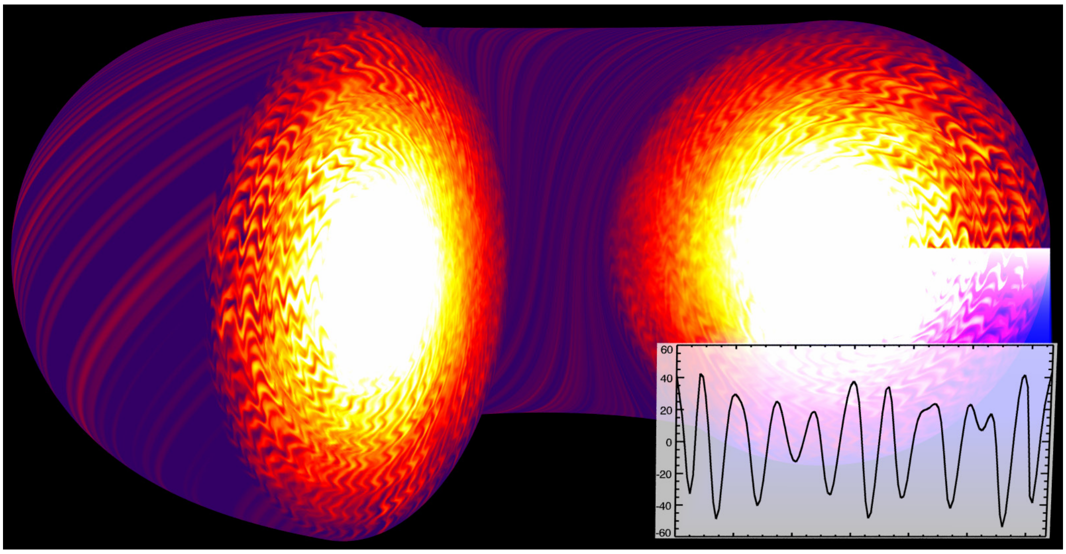

Fig. II.9: Spin up of global zonal flows in a turbulence computation. The torus cut shows the turbulent temperature fluctuations, which are just about to be sheared by the poloidal zonal flow velocity, displayed in the inset.

be driven strongly by perpendicular turbulent forces. The saturation is caused by parallel forces, which brake the parallel flow component of the zonal flows, which is required to cancel the divergence of the perpendicular flow component. The importance of the parallel turbulence force requires an augmentation of current comprehensive transport models. In all studied cases around the reference case, the braking parallel stress was due to quasilinear transport of the parallel momentum by the ambient ITG turbulence and not due to instabilities of the zonal flows themselves.

A new way to compute the effective inertia of collisionless zonal flows has been studied. A very small fraction of the passing ions is found to nearly cancel the large inertia of the trapped ions. The effect of collisions on this small fraction of ions could dramatically increase the effective mass density of the plasma with respect to the zonal flows. This would result in an enhancement of turbulence in comparison to current expectation.

9. Particle Transport in Tokamaks

High resolution gyrokinetic turbulence computations with the GS2 code augmented by NLET fluid simulations have been used to study the particle transport in the tokamak core and edge plasma. Although the particle diffusivities are small compared to the heat diffusivities, they determine the final density profile, with obvious consequences for the energy confinement time. Especially important is the occurrence of an inward particle transport (pinch) for realistic parameters, as it can lead to a profile instability incurring a steepening of the density, and result in a barrier for ITG turbulence.

Contrary to common wisdom, the residual particle transport in ITG and TEM turbulence is not only due to the trapped electron fraction. Instead it is controlled to a great extent by the passing electrons. In all ITG or TEM scenarios where a pinch effect has been found, the inward electron current is carried only by the circulating electrons, while the trapped electrons are advected outward. Analysis shows, that the ITG/TEM pinch effect is caused by the non-adiabatic part of the collisionless parallel circulating electron response. Analogously for ETG turbulence, the residual particle transport is determined by the nonadiabatic part of the ion response at the electron gyroradius scale, and can also cause inward particle transport.

10. Statistical Mechanics and the kappa Distribution

The investigation of the properties of generalized Lorentzian distributions in plasmas far from thermodynamic equilibrium has been extended into three directions. The first direction refers to the behaviour of such distributions at high energies. The formal derivation of the generalized Lorentzian from a generalization of the Boltzmann collision integral as it has been done in our earlier attempts of constructing statistical mechanics far from equilibrium was based on the assumption that the medium is subject to internal correlations which dominate its behaviour under conditions when it is strictly collisionless. These attempts led to the generalized Lorentzian distribution as a fundamental stationary state far from equilibrium. Clearly, since the medium evolves as time progresses, the medium will ultimately, after enough time enter a collisional state and the generalized Lorentzian distribution will tend to deform until it merges into the ordinary collisional Boltzmann (or Maxwell) distribution. Hence a more extended theory should take into account a competition between collisions and correlations. This idea has been included into theory assuming that the collisions are basically Coulombian. The result is that the generalized Lorentzian is cut-off at high energy with the cut-off energy determined by both the initial kappa and the residual Spitzer collision frequency. This cut-off energy is far greater than the thermal energy, but nevertheless assures convergence of calculating moments of the distribution up to arbitrary order. This fact is satisfactory, since in the previous theory no convergence was attained. This distribution was applied to various measured Lorentzian distribution functions in solar wind, magnetosphere and the aurora leading to the determination of temperatures and chemical potentials for these cases. A further extension of theory focused on the relation between the generalized Lorentzian distribution and the celebrated kappa distributions inferred from measurements in high temperature collisionless space plasmas. These distributions are trivially normalized to the density and thus contain a kappa-dependent equivalent temperature. The generalized Lorentzians, on the other hand, contain a chemical potential which is related to the density. There is a relation between the chemical potential and the kappa-equivalent temperature which has been determined. Usually the chemical potential will not vanish, but will be very large and negative (for classical conditions). However, in one special case when the free correlational energy is at its minimum, the derivative of the free energy with respect to the particle number (or density) vanishes, and thus the chemical potential vanishes as well. This is the case when the experimental kappa distribution is correct and agrees with theory. Hence, one concludes that the correlations leading to the experimental kappa distribution should be such that the correlational free energy is minimum.

11. Astrophysical relativistic jets

1. X-ray observations

BL Lac objects are thought to be dominated by relativistic jets seen at small angles to the line of sight. As BL Lac objects show remarkably featureless spectra at all energies, from the radio to the X-ray band, the structure of the jets remains largely unknown and the measured spectra can be reproduced by models with widely different assumptions.

A substantial part of the information we possess about these objects is obtained from the analysis of the temporal variations of the emission and the combined spectral and temporal information can greatly constrain the jet physics. Time scales are related to the crossing time of the emission regions which depend on wavelength and/or the time scales of the dominant physical processes. The measured lags between the light curves at different energies as well as spectral changes during intensity variations allow to probe the physics of particle acceleration and radiation in the jet.

We performed a detailed spectral and temporal analysis of all currently available XMM-Newton observations of the bright BL Lac object Mrk 421 using the EPIC-PN data. The source was found in various intensity states differing by up to a factor of five in count rates. In general, the source is more variable and shows a harder spectrum during higher intensities than when it is in lower states. We find that the flux variations on time scales of a few thousand seconds are associated with significant and sometimes very complex spectral changes. The Cross-Correlation analysis shows that the soft and hard band light curves are often well correlated near zero lag, in other cases the hard band variations lead the soft band variations by typically 5 min, in two cases we find the soft band leading the hard band variations.

This complex behavior is demonstrated in Fig II.10. for a particular observation of XMM which shows in the upper panel the normalized hard (black) and soft (reddish) band light curves and the hardness-ratio (HR) plot (lower panel). The red points in the upper right part of the HR plot correspond to the first ~ 15 ksec part of the observation (``Part A'' in the upper panel) when the total band count rate was decreasing (as indicated by the overlying red arrow). During ``Part B'', the total count rate increased, and the corresponding HR variations are shown by the green points. The red and blue points in the lower left part of the HR plot correspond to the the first and second part part of the last ~ 17

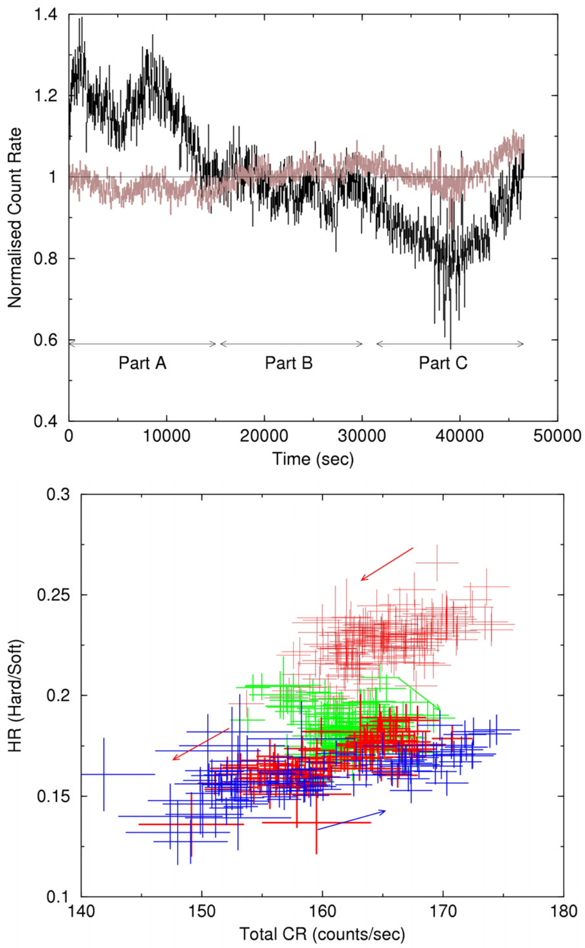

Fig. II.10: Normalized hard (black) and soft (red) band light curves of MrK 421 during the XMM orbit 171. Bottom: hardness ratio versus count rate plot.

ksec of the observation, when the source flux decreased and then increased again.
Correspondingly, it appears hard to deduce uniquely the underlying physical parameters for the emission process from the observations. For the currently favored 'shock-in-jet' model for the BL Lac emission this implies that we are seeing the emission from multiple shocks which have either largely different physical parameters or that we detect the emission from similar shocks at very different states of their evolution, heavily confused by relativistic beaming and time dilatation effects. More observations with longer exposures, more sophisticated (perhaps non-linear) data analysis methods and explicit jet simulations are required for a better understanding of these objects.

2. Numerical Hydrodynamics

In oder to get more insight into the physical processes governing the emission from these blazar jets we performed two- and one-dimensional relativistic numerical simulations of collisions of density inhomogeneities (shells) within the jet, in order to study the influence of the initial properties (mass, temperature, size, velocity) on the characteristics of X-ray flares. It was found that the jet medium external to the shells has a significant influence on the shells prior to their interaction. The total radiated energy in the observer frame depends on the total initial rest mass of the shells and the relative velocity, but does not depend on the way in which the mass is distributed in the shells. One-dimensional simulations of collisions of a large number (>500) of shells indicate that, in order to reproduce global characteristics of observed X-ray blazar light curves, the central engine must work intermittently, ejecting discrete shells instead of continuous fluid.

III. EXPERIMENTAL PLASMA SCIENCE

A. Complex Plasmas

1. Introduction

Complex plasma research is a new and rapidly developing field, with complementary investigations under gravity and microgravity conditions. The complex plasma consists of a common plasma – with electrons, ions and neutrals - and an additional component of small solid particles typically in the range of micrometers. This heavy component in the plasma makes it necessary to perform experiments under microgravity conditions although levitation of the particles in the laboratory allows many interesting experiments here, too. The microparticles in the plasma are charged through the absorption of free electrons and ions to thousands of elementary charges. This is responsible for the strong coupling of the particles and for the transition to liquid and crystalline states.
The first two years of CIPS from 2000-2001 were devoted to the design, development, and assembly of new laboratories for the investigation of complex plasmas. Since the completion of the labs the scientific work in our group could be increased dramatically.

2. Laboratory Research

The most dominant property of complex plasma research is the investigation on the most fundamental – the kinetic – level. This provides new insights into the physics and allows easy comparison with theory and numerical simulations. Therefore the Institute built many experimental laboratories, each with special features and diagnostics for the investigation of complex plasmas. The equipment for these laboratories was financed by a special grant from MPG in the framework of CIPS. The laboratory infrastructure is provided by IPP and MPE, the manpower is largely supplied by MPE.
The laboratories are:

1. The GEC-Laboratory: Radio-frequency (rf) discharge plasmas using GEC reference cells for investigations of strong coupling phenomena in "complex plasmas".
2. PK-3 Plus laboratory. Development laboratory for the next space experiment.
3. PK-4 laboratory. Development laboratory for a future space experiment.
4. Magnetic Laboratory, involving a superconducting magnet up to ~5 Tesla of high homogeneity. In this laboratory strongly coupled and strongly magnetised systems will be studied at the most fundamental (the kinetic) level for the first time.
5. Paramagnetic Laboratory, for studying strongly coupled systems with magnetic dipole interactions – in contrast to the electrostatic interactions discussed in (1). These systems are thermodynamically "closed", whereas electrostatic systems are thermodynamically "open". Weakly damped closed systems have not been studied before at the kinetic level.
6. Adaptive Electrode Laboratory, a large plasma chamber which can be manipulated electronically (through addressing a pixelled electrode) to generate and investigate controlled dynamical processes in complex plasmas.
7. Plasma crystal educational laboratory for student research (cooperation with Universities).

Beside the experimental investigation on Earth our group performs experiments under microgravity conditions using different apparatus. The most prominent experiment is PKE-Nefedov, our laboratory on the International Space Station ISS, a close cooperation between the Russian Academy of Science Institute for High Energy Densities and MPE/CIPS.

2.1 The GEC-Laboratory

The GEC-laboratory consists of two modified GEC-rf-Reference Cells with different configuration and diagnostics. One of these plasma chambers is equipped with a large electrode system specially suited for the investigation of large 2-dimensional plasma crystals and long-term particle motion in high resolution. But also single particle experiments, as shown below, can be performed.

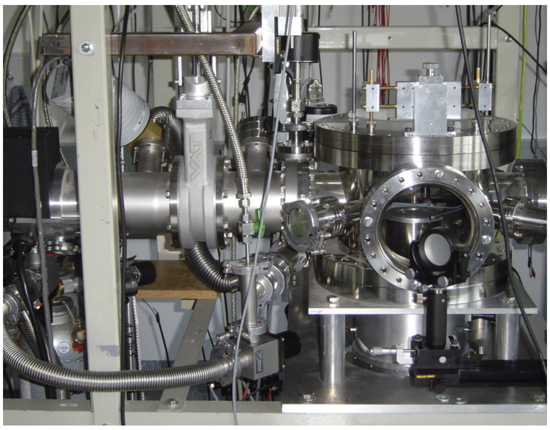

Fig. III.A.1: The first GEC-RF-Reference Cell with diagnostics and vacuum parts.

Vertical pairing of identical particles suspended in a rf plasma sheath

In the laboratory the complex plasma forms in the sheath or pre-sheath of an rf discharge. In this environment ion streaming has a very strong effect on the complex plasma behaviour. When the ions stream with Mach speed through the complex plasma they generate a highly non-uniform non-symmetric environment. Due to deflection on the dust grains of the complex plasma the ions form a complicated density pattern in the wake of each particle. This leads to a region of high positive space charge behind the particle that has a fixed relative position. These positive space charges result in an attractive force between layers of crystallised complex plasma stacked upon each other. Due to the fast directed streaming of the ions this attraction force is asymmetric and only affects the lower (down stream) plane.

In our experiment we show that identical particles that are initially suspended at the same height in an rf plasma sheath can separate vertically and form vertically stacked pairs (see Fig. III.A.2). The transition to pairs is related to the symmetry breaking by the ion streaming and develops in two distinct phases. First, there is a continuous transition from a purely horizontal configuration to a vertical displacement of the particles. The particles can swap vertical positions in this phase, so they can be considered identical for the instability. Second, there is a sudden discontinuous transition to the vertical pairing. The transition is reversible. The control parameter is the plasma power.

To explain this transition a simple model of Coulomb interaction between two negatively charged particles with each other and their respective shadow charges that are induced by the streaming ions was developed. No other external symmetry breaking (like particles of different size) is necessary. Without the shadow charges, the system of two negatively charged particles could only have two stable states – either vertically or horizontally aligned – with a sudden transition when the confinement in horizontal direction becomes weaker than in the vertical direction. The measurement of the vertical and horizontal free oscillation frequency of the particles as function of the plasma power shows that the vertical separation happens when the vertical confinement is still much stronger than the horizontal, and that pairing occurs long before the two confinements become equal.

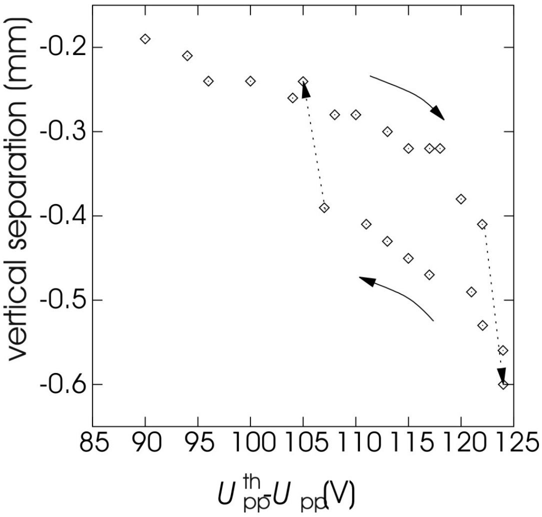

Fig. III.A.2: The figure shows the characteristics of the vertical separation of the two particles, whereas the arrows show the transition to a vertical pair (in the lower right corner). With the decrease of the voltage a hysteresis of the transition process sets in.

Nonlinear vertical oscillations of a particle in the sheath

The experiment uses single particle oscillations to "non-invasively" measure the local potential in the plasma. To do this, the driven oscillation of a single particle in response to an external electrical excitation is measured. As the excitation amplitude increases, the oscillations become strongly non-linear and secondary harmonics are generated. The data are described using the theory of anharmonic oscillations, and the first two anharmonic terms in an expansion of the sheath around the particle equilibrium position are estimated. This technique is currently the best way to measure the sheath potentials in plasma devices, since it disturbs the plasma only minimally.

The electrical excitation voltage U_{ex} is applied through a 0.5mm diameter wire, 8mm above the electrode, located vertically below the particle. The excitation frequency is varied from 0.1Hz to 40Hz, and back, in steps of 0.1Hz. After each step the system is allowed to oscillate for 10 full periods before the oscillation curve and amplitude are evaluated.

For very low U_{ex} <30mV, usual linear (harmonic) oscillations are observed, with a single symmetric narrow maximum of the amplitude to frequency response at the resonance frequency ϖ_0 of 17Hz (primary resonance). For higher U_{ex} values the oscillations become non-linear. Several effects can be observed: 1) The maximum of the resonance shifts to lower frequencies as U_{ex} increases. 2) If U_{ex} is larger than a critical value, hysteresis appears, i.e. the resonance curves for increasing and decreasing frequency follow different paths. In addition to this characteristic behaviour of the primary resonance, the superharmonic resonance at $1/2\varpi_0$, and the sub harmonic at $2\varpi_0$ are measured and exhibit all characteristics of anharmonic oscillations.

Vertical wave packet experiment

Propagation of vertical wave packets (Fig. III.A.3) was observed experimentally in a crystallised hexagonal monolayer complex plasma. They were excited by an electrostatic pulse applied to a wire placed below the crystal lattice. The vertical motion was visualized by measuring the change of particle brightness as they moved out of the illuminating beam. It was found that the phase velocity exceeded the group velocity by a factor 65 and was directed into the opposite direction, as expected for an inverse optical-like dispersion relation. The wave packets propagated keeping their width constant. The theoretical investigation of this behaviour is based on three-dimensional equations of motion and uses a long-wavelength weak dispersion weak inhomogeneity approximation. While the wave dispersion causes the wave packet to spread, lattice inhomogeneity and neutral gas drag counteract spreading. A new plasma diagnostic method was developed that is based on the ratio between vertical and dust-lattice wave speeds. This ratio is very sensitive to the lattice parameter κ (ratio of the particle separation to the screening length) in a very useful range of $\kappa<2$.

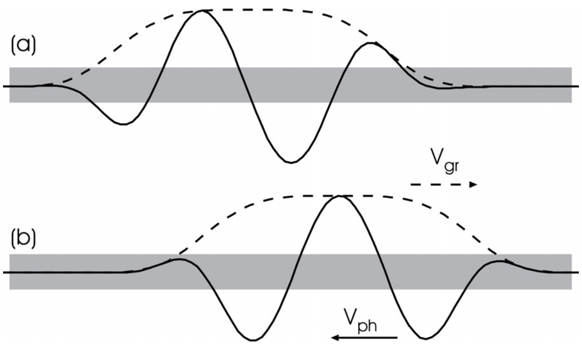

Fig. III.A.3: Side view of the vertical wave packet propagating in a monolayer lattice. (a) Initial position of the packet. (b) Displaced packet. The group velocity V_{gr} (the velocity of the packet envelope marked by the dashed line) is directed to the right, while the phase velocity V_{ph} (the velocity of the modulating wave marked by the solid line) points left. The illuminating laser beam is indicated by the grey bar. We observe only the areas where it intersects the lattice (solid line), which appear as moving stripes in the experiment.

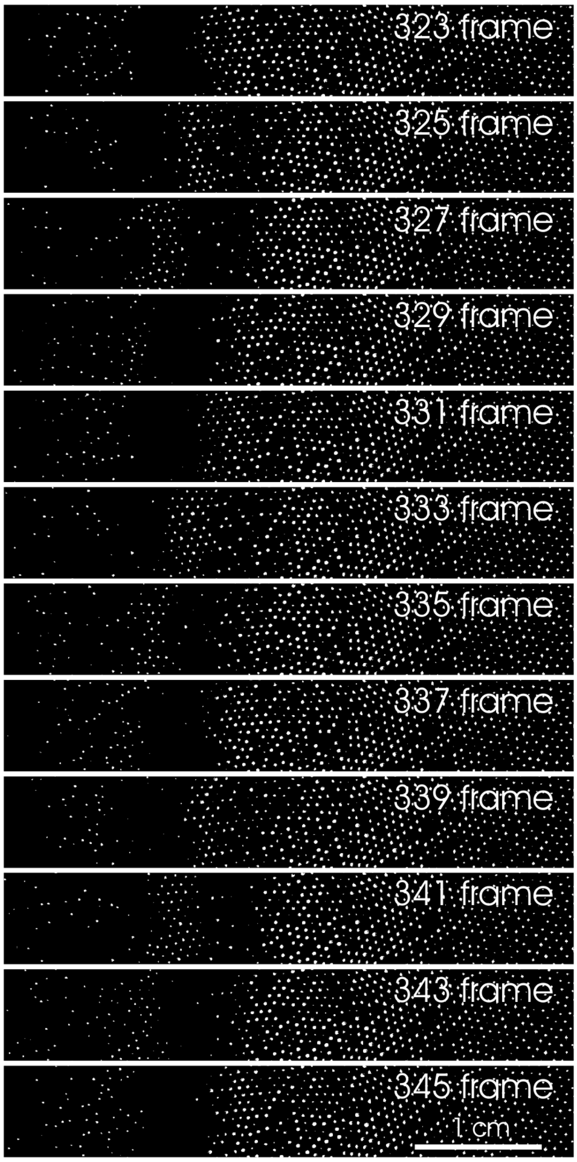

Fig. II.A.4: Top view of the lattice at time 1.4-1.5 s after the excitation, when the wave packet was well formed. A wire, positioned at the left edge of the field of view below the lattice excited the wave packet. The particles are visible only if they are in the plane of the illuminating laser sheet. The stripes of particles apparently move from right to left due to the vertical wave motion. They correspond to the lines of constant phase (phase motion). Individual particles do not move horizontally. The numbers on the images indicate the frame number (at 230.75 fps).

Solitons and nonlinear waves

An analytical model for weakly dispersive and weakly non-linear longitudinal and transverse (shear) waves and solitons propagating in a two-dimensional screened Coulomb (Yukawa) crystal was developed. The possibility of formation of soliton-like compressional and shear waves is demonstrated. It is shown that the compressional solitons have a small but non-vanishing anisotropy, whereasa the shear solitons are strongly anisotropic. This is due to the strong anisotropy of the transverse shear waves in both dispersion and non-linearity. It was shown that there are directions in a crystal where shear solitons don't form. The obtained analytical results are in a good agreement with the experiments on finite amplitude compressional and shear waves propagating in a monolayer hexagonal dust lattice.

Mach cones

Mach cone propagation in an inhomogeneous medium was studied analytically. The shape of Mach cones formed by nondispersive linear sound waves in a non-uniform complex plasma was calculated using the method of wave rays.

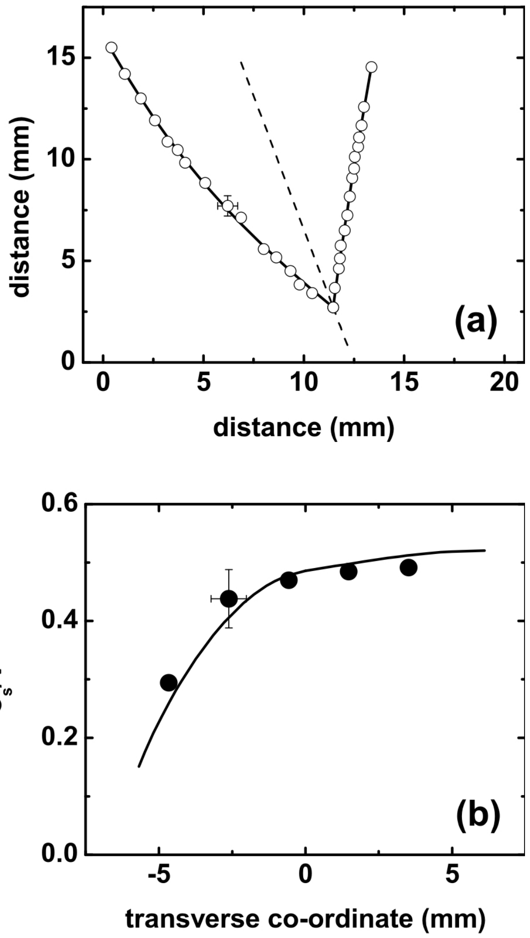

Fig. III.A.5: (a) Shape of a Mach cone in a transversely inhomogeneous medium. The experimental data points are shown with open circles. Both cone wings are fitted to a third order polynomial (solid lines). The trajectory of the cone vertex is marked by a dashed line. (b) Inverse Mach number (ratio of the acoustic speed C_s to the speed of a perturbing body V) across the Mach cone trajectory. The negative direction corresponds to the left cone wing, the positive to the right. Filled circles indicate the values calculated directly from the particle number density map. The solid line is calculated from the shape of the Mach cone. Typical error bars are marked on one of the data points in both plots.

The cases of transversely and longitudinally inhomogeneous media, as well as a medium with a sound speed maximum were considered. The theory was compared with experimental observations of Mach cones with curved wings (dynamic Mach cones) in a two-dimensional complex plasma. A diagnostic method was developed to measure the change of complex plasma parameters from the observed shape of the Mach cones (Fig. III.A.5).

Shock waves

Shock waves with a linear front (Fig. III.A.6) were experimentally studied in a monolayer hexagonal Yukawa lattice which was formed from charged monodisperse plastic microspheres levitated in the sheath of a radio-frequency discharge. It was found that the shock can cause phase transitions from a crystalline to gas- and liquid-like states. Melting occurred in two stages. First, the lattice was compressed in the direction of the shock propagation and second, the particle velocities were randomized a few lattice lines downstream. The Mach number of the shock reached 2.7. The shock structure is characterised by a peak in the compression factor and the particle speed at the shock front, and a discontinuity in the kinetic temperature and the defect density (Fig. III.A.7). A molecular dynamics simulation was performed (Fig. III.A.8) and good qualitative agreement was achieved using a model based on particles interacting via a Yukawa potential and confined in a parabolic potential well (strong vertically and weak horizontally).

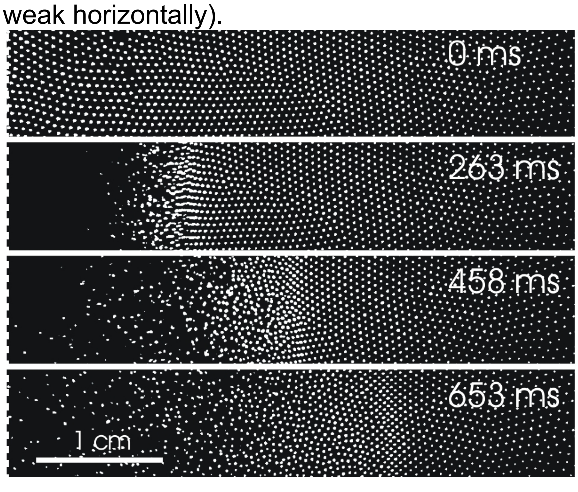

Fig. III.A.6: Shock wave propagating in a monolayer hexagonal lattice. The excitation pulse was applied to the wire placed at the left edge of the field of view (dashed line) 2 mm below the lattice plane. Initially undisturbed particles (at 0 ms) were swept from left to right (at 263 ms and 458 ms) forming a shock with a sharp linear front. The lattice melted behind the front. At later times (653 ms) the amplitude of the disturbance was reduced due to neutral drag and a soliton was formed.

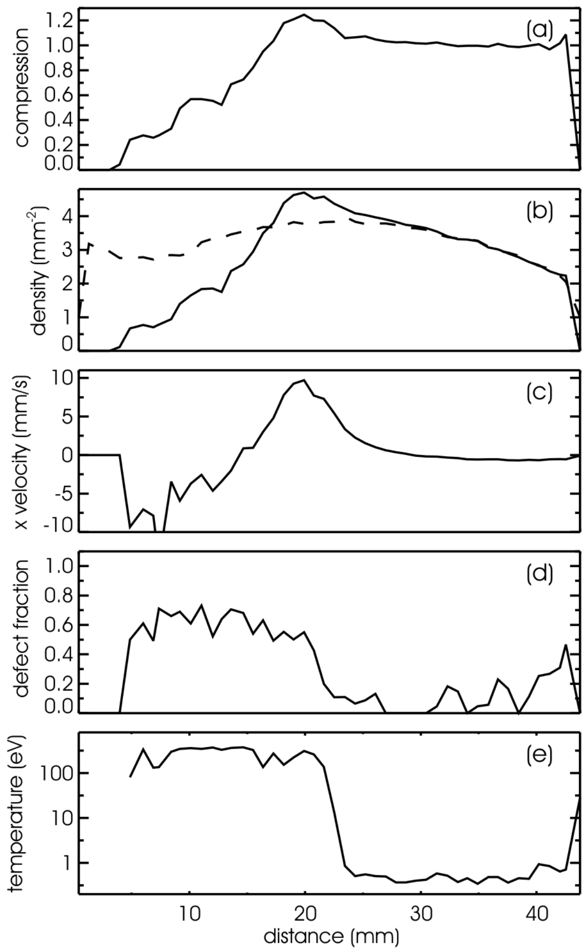

Fig. III.A.7: Structure of the experimentally observed shock front at time 0.38 s. (a) compression factor, (b) particle number density (dashed line indicates unperturbed number density), (c) particle velocity in the direction of the shock propagation, (d) defect fraction, and (e) particle kinetic temperature, plotted versus distance to the excitation source. The compression factor, number density, and particle speed have a peak at the shock front, whereas the defect fraction and the kinetic temperature have a jump.

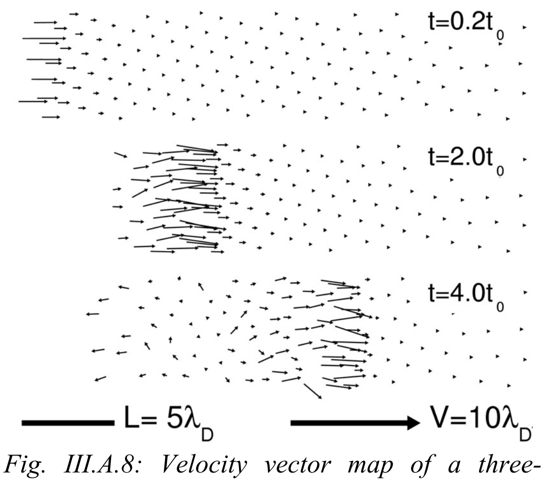

Fig. III.A.8: Velocity vector map of a three-dimensional molecular dynamics simulation (MDS) of a shock in a monolayer hexagonal lattice. The shock propagates melting the lattice.

Statistics of particle transport in a two-dimensional dusty plasma cluster

In spite of the appealing aspects of tracking and visualization of dust grain trajectories, such observations do not provide direct information about the interaction between the grains and between grains and the surrounding plasma. However, results based on detailed statistical analysis of the experimentally observed dust particle transport could serve as a foundation for the development and verification of dynamical models which, in turn, could be used to estimate generic quantities like the particle charge or the coupling parameter. A statistical analysis of increments of dust particle positions in a 2D plasma cluster has been performed and revealed non-Gaussian self-similarity of the time series and a weak superdiffusion with Hurst exponent H=0.6 on time-scales for which the displacement range is greater than the mean interparticle distance. The analysis demonstrates that superdiffusion (H>1/2) is associated with long range dependence in the data and is not due to power-law tails in the probability distribution function PDF of the position increments (Levy flights). It was found that particle transport (diffusion coefficient) is determined by persistent slip events, but the elevated diffusion exponent H is caused by the fact that these slips exist on all timescales and therefore implies a long range dependence in the increment signal. The self-similar nature of slip durations extends to time-scales on which rearrangements of particle positions in the lattice take place indicating that there is no characteristic timescale for the growth, propagation, and decay of lattice defects. This interpretation is supported by the observation that PDF analysis of the duration of slipping events for individual particles yields power law distributions for all different levels of coarse graining, confirming the self-similar nature of the dynamics. PDFs of the number of particles simultaneously participating in slip events, and "snapshots" of the spatial distribution of slipping particles during big slips, indicate that there is some spatial correlation with formation of clusters of slipping particles, and intermittent slip activity. Hence it appears likely that the long-range dependence is spatial as well as temporal.

Dynamical Properties and Ergodicity in Plasma Crystals

Ergodic behaviour in a plasma crystal is understood as the equivalence of the dynamic behaviour of a single particle in time and the ensemble of particles as components of the crystal at one particular time, as it is expressed in general in terms of ergodic theory. Ergodicity

is often presupposed in the interpretation of particle dynamics of a plasma crystal, as for temperature or charge calculation.
In the experiments long time series of over 5 minutes length of single layer plasma crystals with approximately 200 particles have been recorded. The investigation was focused on the time series of particle displacements *r* and velocities *v*.
The distribution functions of both *r* and *v* were obtained for each particle and compared among each other to get an idea of the dynamical uniformity of the crystal.

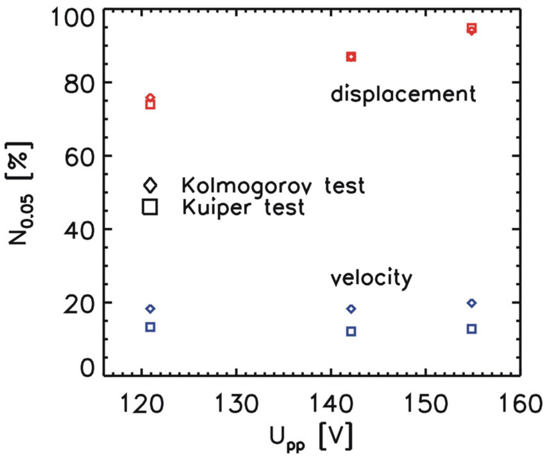

Fig. III.A.9: Result of the comparison of distributions of single particles with ensembles. The fraction of comparisons which are significantly different are shown for displacements (red) and velocities (blue).

Finally, a direct comparison of the distributions of *r* and *v* inside a particle ensemble given by one image were compared to that of single particle time series in *r* and *v* by means of statistical tests (Kolmogorov-Smirnov- and Kuiper-Test). If the system behaves ergodically, time- and ensemble distributions would be expected to be equal.
The velocity distributions of the particle time series were fitted by Maxwellian distributions and yielded equal temperatures for all particles. The result of the statistical test, the comparison of time- and ensemble distributions, could not prove ergodic behaviour of the velocity uniquely, but the agreement was still good enough in order to not reject the idea of ergodicity for the velocities.
The displacements were fitted by a distribution dependent on the interparticle potential, but the shape of the distribution showed a dependence on the position of a particle inside the crystal. This evidence on nonergodic behaviour with respect to *r* was confirmed by the results of the Kolmogorov-Smirnov test.
Figure III.A.9 shows the fraction $N_{0.05}$ of results of comparisons between time- and ensemble distribution of *r* and *v* which exhibited significant differences. The total number of comparisons was of the order of 1 million, and was repeated for three different electrode voltages U_{PP}.

Complex plasma fluids in the GEC-chamber
Investigations of fluid phenomena at the kinetic level promises to be a major new development, made possible using complex (fluid) plasmas. To establish a continuous flow we built up an electric pumping device for complex plasmas. (We applied for a patent for this pumping mechanism.) Due to the circular geometry the flow is practically infinite and it behaves like an

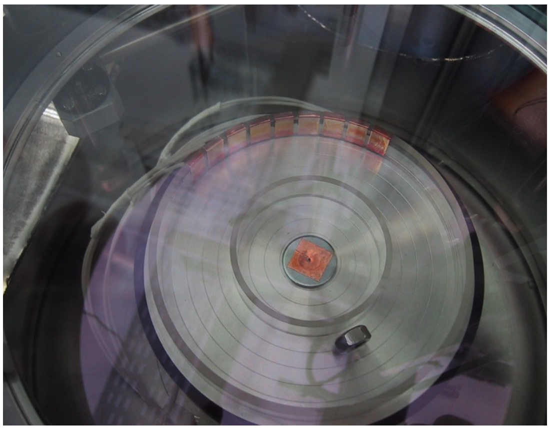

Fig. III.A.10: Picture of the setup in the GEC chamber, with the screw nut working as obstacle. Pumping is done by a propagating wave along the copper electrodes on the side.

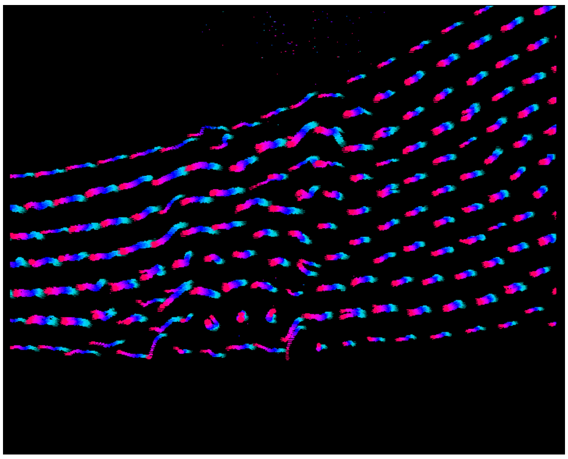

Fig. III.A.11: Consecutive frames colour-coded and overlayed (particles from the first picture in blue and from the last picture in red to show the particle movement, which is from upper right to lower left).

ideal fluid. This gives us the ability to perform long time flow experiments. So far we can establish flow velocities up to 6 mm/s, which is already comparable to supersonic velocities within a plasma crystal.
In a first step we studied the movement of the fluid around an obstacle. The fluid moves in stream lines and reacts to the reduced cross section, which is induced by the obstacle,

according to classical hydrodynamics (the law of Hagen-Poiseuille).

In our experiments we can investigate the process at the kinetic level. If the cross section is reduced, two stream lines merge and this continues until the fluid can pass through the reduced cross section. This is shown in Fig. III.A.11. On the other side of the constriction this process reverses and stream lines split up.

In future we plan to investigate this picture of fluid flow in more detail. We will also try to increase the velocity of the particles to reach values that produce turbulent flows behind the obstacle.

2.2 Magnetic field laboratory

Since the delivery of the high magnetic field system in February 2002, the support environment for the magnetic field laboratory has been built up to perform first experiments, taking into account safety issues.

In first experiments a plasma chamber compatible to the PK3-Plus experiment was introduced into the experimental setup, supplemented by a laser illumination and new camera system that keep functional at high magnetic fields as well as the necessary gas support and electronic system. Starting in 2004 the experimental setup was extended by a plasma chamber previously used as a test device for the IMPF- (International Microgravity Plasma Facility) experiment. The new plasma chamber allows more flexibility in the design of the electrode system for the plasma generation including the possibility to include transparent electrodes to establish a top view on the complex plasma. Several kinds of electrode setups and plasma generations have been tested.

Because of safety concerns extensions to the experimental support structure - like an automatised, remote controlled positioning and adjustment system for the plasma chamber - as well as the laboratory environment are in progress. As a “side effect”, experiments are expected to be performed more easily keeping the experimentalists in a safe, low magnetic fields environment.

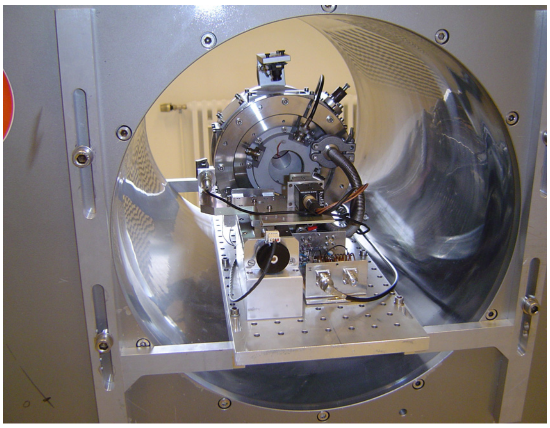

Fig. III.A.12: Strong magnetic field assembly with the IMPF-RF Predevelopment Plasma chamber.

Crystallization of plasma filaments

The magnetic field has a strong influence on the behavior of complex plasmas and even on the standard particle free plasma. In first experiments within the high magnetic field setup (up to 4 Tesla) we observed that at low pressures and low discharge powers of a radio frequency parallel plate discharge the produced plasma can break up into filaments. These filaments are plasma columns between the electrodes that are aligned with the magnetic field direction and (as expected) do not show up for low magnetic fields.

In a more detailed investigation a layer of microparticles was introduced into the plasma environment, levitated a few millimetres above the lower electrode, confined by the plasma distortion produced by an Aluminium ring on the lower electrode. Since the particle react strongly on local electric field variations and the ion-drag, the micro particles can be used as probes to visualize the structure of the plasma by imaging their position.

We observed that by increasing the vertically aligned magnetic field a transition from a 'monolayer' crystalline complex plasma to a rotating complex plasma disc takes place (see Fig. III.A.13a). This phenomenon has been observed in different experiments at low magnetic field already a few years ago. But, after a further increase first 2d-voids that are correlated with the positions of the filaments show up (see Fig. III.A.13b). Keeping the field strength fixed and reducing the pressure of the gas the number of filaments increase and they start to slowly move around (see Fig. III.A.13c). Finally at even lower pressures the plasma filaments settle in a “crystalline”, stable structure as can be seen in Fig. III.A.13d.

We plan to take a much closer look into the “crystallization” of the plasma columns by using the complex plasma as a probe system to derive the plasma parameters within the filaments and thus to investigate the reason why this kind of crystallizations takes place.

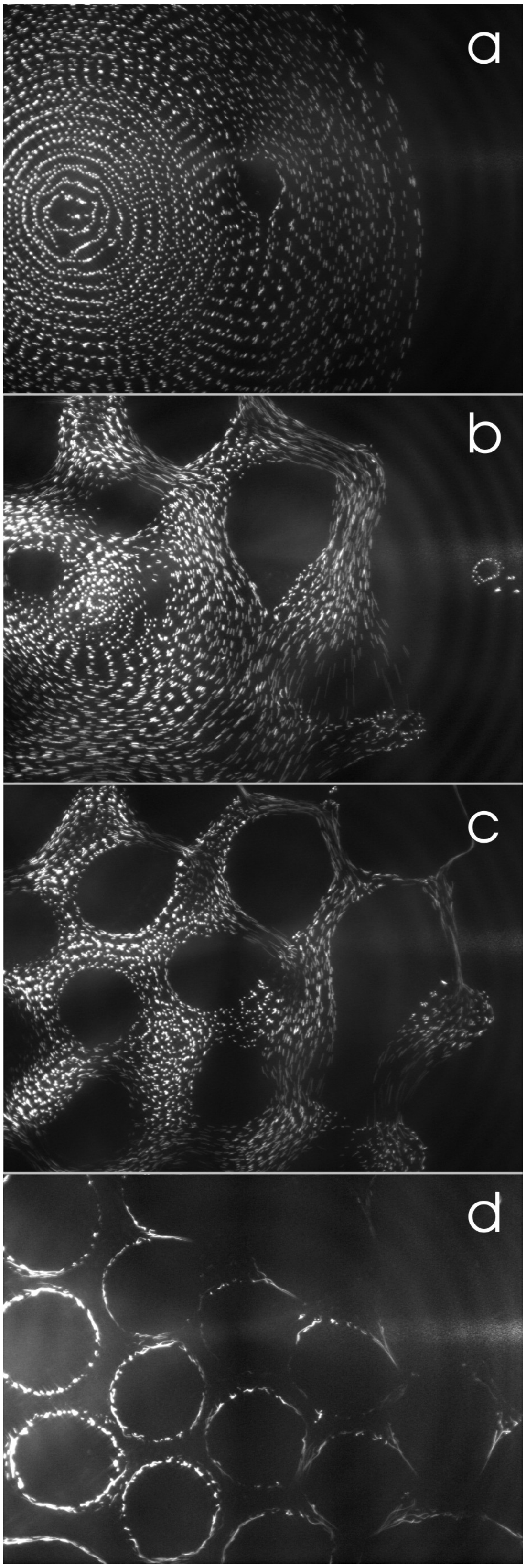

Fig. III.A.13: Overlay of 8 consecutive image of particle positions within a layer perpendicular to the magnetic field axes for different pressures and magnetic field strength. a) p=20 Pa, B=0.3T, b) p=18 Pa, B=1.0T, c) p=17 Pa, B=1.0T, d) p=16 Pa, B=1.0T (reduced particle number)

Wave dispersion relation of two-dimensional plasma crystals in a strong magnetic field

Micro particles that are introduced into a plasma environment charge up to a high negative value due to ion and electron bombardment. As a result of the strong Coulomb interaction between the particles often so-called ``plasma crystals'' are built up. The inter-particle potential is considered to be of the Yukawa type. There have been many theoretical and experimental studies on wave phenomena in ``plasma crystals''. In these studies two wave modes, named ``longitudinal dust lattice waves'' and ``transverse dust lattice waves'', have been identified and extensively analyzed. However, the influence of an external magnetic field on the wave dispersion has been considered barely, although magnetic fields play an important role for many common complex plasma environments.

In this study, we analytically derive the wave dispersion relation in a two-dimensional plasma crystal under magnetic field influence, where the wave propagation and particle displacement are perpendicular to the magnetic field B.

Fig. III.A.14 show the wave spectra due to thermal motion of the dust particles in a simulated plasma crystal in a magnetic field, where the dashed lines are from theory. When we apply a magnetic field though, the longitudinal and transverse modes in the plasma crystal are coupled due to the Lorentz force, and a high-frequency ϖ_H and low-frequency branch ϖ_L can be observed. Then, the dispersion relation has a cut-off at ϖ_c in the limit of long wave lengths where $k_x \rightarrow 0$. The profile of the dispersion relations that we obtained from the thermal particle motion are in good agreement with our theoretical predictions.

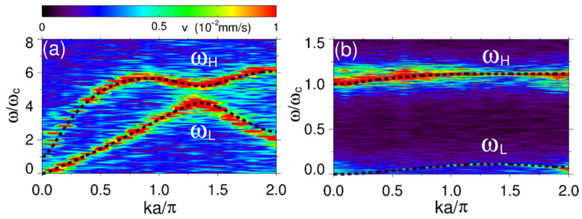

Fig. III.A.14: Dependence of the dispersion relation on the magnetic field strength which is represented by the parameter ϖ_c/ϖ_0, where ϖ_c is the dust cyclotron frequency and ϖ_0 the dust plasma frequency. Figure (a) and (b) are for ϖ_c/ϖ_0=0.52 (ϖ_c/ϖ_0<1; a weakly magnetized plasma crystal), and for ϖ_c/ϖ_0=6.85 (ϖ_c^2/ϖ_0^2>>1; a strongly magnetized plasma crystal), where a screening parameter $\kappa = a/\lambda_D$ is 1.0.

2.3 Paramagnetic-Laboratory

A new chamber with interchangeable electrodes made of non-magnetic materials was developed, manufactured and installed on the frame under the DC magnetic coils. The chamber was equipped with a large diameter electrode which allows us to obtain large monolayer crystals at low gas pressure to study lattice dynamics. A set of AC magnetic coils was manufactured and installed. A power supply for the AC coils was upgraded. The magnetic coils can be used to apply a constant or periodic lifting force on magnetic particles in order to compensate gravity or excite vertical motion. The top window was coated with a conductive (indium-tin oxide) layer to prevent formation of a ring discharge in the presence of the magnetic field.
A laser particle manipulation system was developed and installed on the optical table placed near the chamber. The system contains a 4.8W Ar-ion laser, galvanometer beam scanner and intensity modulator, as well as a focusing device. It allows us to excite different wave modes, to heat the lattice as well as obtain shear flows and vorticies. The laser system is being upgraded now by installing two 30 W diode lasers and two scanning systems in order to provide symmetric wave excitation without net particle flow.

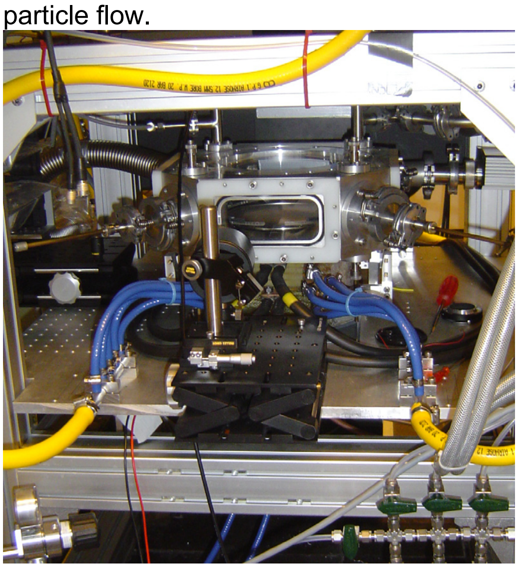

Fig. III.A.15: New plasma chamber with large electrode system installed in the paramagnetic laboratory.

The high speed camera was mounted on a computer-controlled 3-dimensional translation stage, it is intended to do the same for the laser illumination system. A Langmuir probe was installed to provide measurements of plasma parameters.

Linear waves (phonons)
Linear (small amplitude) waves (or phonons) can be studied kinetically, by observing the thermal motion of individual particles in a complex plasma. A Fourier analysis of such motion yields phonon spectra of lattice waves (Fig. III.A.16). It was found that there are two wave modes with polarization alternating between longitudinal and transverse. In the long-wavelength regime, the modes separate and become purely longitudinal (compressional) and transverse (shear), as was known before. In the short-wavelength regime the spectra strongly depended on the wavelength and the direction of propagation. We developed a molecular dynamics simulation based on the equations of motion written for particles interacting via a Yukawa potential and confined in a parabolic potential well (strong vertically and weak horizontally). The results obtained from the experiment, theory, and simulation agreed well with each other.

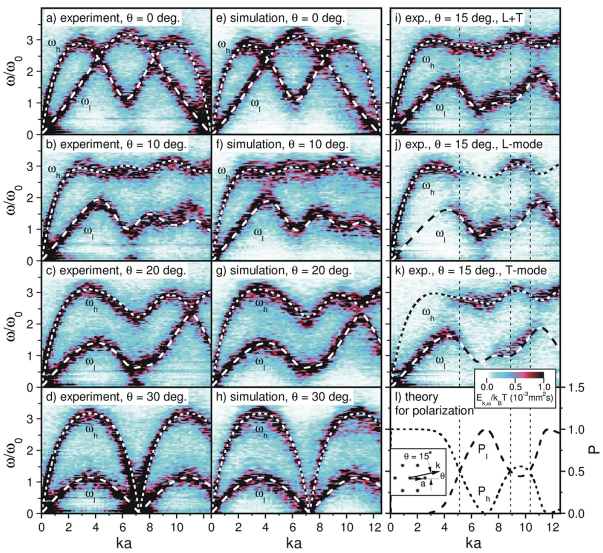

Fig. III.A.16: Phonon spectra of thermally excited waves in the first and second Brillouin zone at different angles of propagation, (a)-(d) experiment, (e)-(h) simulation. The theoretical dispersion relations are superposed: dotted line (high frequency mode) and dashed line (low frequency mode). The dispersion relation is periodic for 0° and 30° but it is aperiodic in general. (i) Phonon spectra of the waves propagating at 15° measured experimentally. The high and low frequency branches have mixed longitudinal (j) and transverse (k) polarization. (l) Polarization of the high frequency (P_h) and low frequency (P_l) modes predicted by the theory. At low wavenumbers (long wavelengths) the high frequency mode is purely longitudinal (P_n=1), and the low frequency mode is purely transverse (P_l=0).

At an arbitrary wavenumber the modes have mixed polarization. Spectra of longitudinal and transverse waves were obtained experimentally in liquid and solid two-dimensional complex (dusty) plasmas at different kinetic temperatures (Fig. III.A.17). As the temperature increased and the phase state of the plasma changed from solid to liquid, the phonon spectra of both longitudinal and transverse modes broadened (especially at high wavenumbers) indicating increased damping. The transverse mode disappeared and a new thermal (compressional) mode appeared.

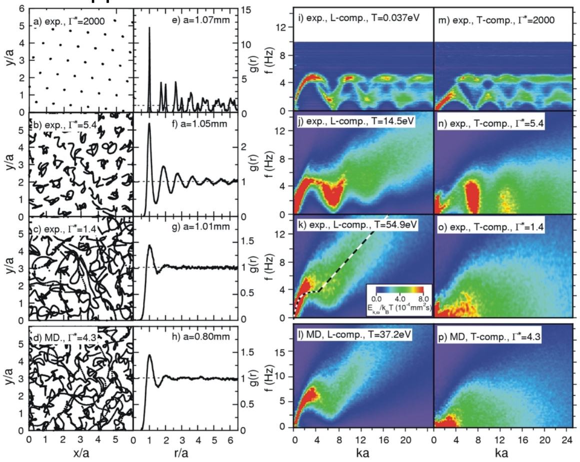

Fig. III.A.17: Results of experiments and a molecular dynamics (MD) simulation for different kinetic temperatures T and coupling parameter Γ. (a-d) Particle orbits. (e-h) Pair correlation function. (i-l) Spectra of the longitudinal (compressional) waves averaged over all directions. (m-p) Spectra of the transverse (shear) waves. The figures are arranged in rows corresponding to different conditions: (a,e,i,m) Experiment at T=0.037eV, Γ*=2000, a=1.07 mm (particle separation). The lattice is in a highly ordered crystalline state, the phonon spectra are periodic and have a cutoff frequency. (b,f,j,n) Experiment at T=14.5eV, Γ*=5.4, a=1.05 mm. The particle cloud is in a partly melted state, the longitudinal mode has no cutoff, the width of both modes increases. (c,g,k,o) Experiment at T=54.9 eV, Γ*=1.4, a=1.01 mm, the lattice is melted. The overlayed dotted line (k) indicates a fit to the well known dust-acoustic mode (C_{DA}=26.9 mm/s), the dashed line is a fit to the thermal mode (v_{DT}=5.98 mm/s), the frequency of longitudinal waves grows linearly with ka at high wave numbers. The transverse wave mode (o) almost disappears in the fluid state. Finally, (d,h,l,p), we show a MD simulation at T=37.2 eV, Γ*=4.3, a=0.8 mm. The cloud is melted, the result closely reproduces that of the experiment.*

Heat transfer experiment

Heating and heat transfer were studied in a two-dimensional crystalline complex plasma at the kinetic level. The lattice was formed of microspheres levitated in a plasma sheath. One half of the crystal was heated anisotropically (by a randomly scanning laser beam) to obtain higher kinetic temperatures in one direction. Heat conduction was observed in real time (Fig. III.A.18). It was found that the longitudinal phonons conduct heat better than the transverse. The temperature conductivity coefficient was measured to be 53 mm^2/s for longitudinal heating and 30 mm^2/s for transverse heating. In terms of "natural (kinetic) properties" (a, c_L, and c_T) the conductivity coefficients turn out to be ~2-3ac_i respectively, suggesting that most of the thermal transport is due to the shortest wavelengths (λ~2a).

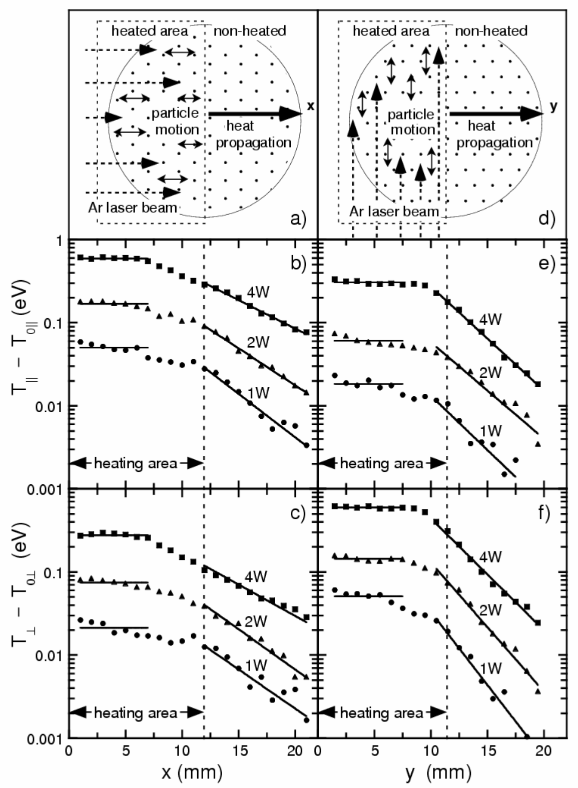

Fig. III.A.18: Kinetic temperature distribution in a monolayer plasma crystal. The left side of the lattice was heated by light pressure of a randomly scanned laser beam. (a) Sketch of the longitudinally heated area. The heating beam is directed perpendicular to the hot/cold interface (dotted line) and parallel to the direction of the heat propagation. (b) Kinetic energy component parallel to the direction of heat propagation. (c) Kinetic energy component perpendicular to the direction of heat propagation. (d) Sketch of the transverse heated area. The heating beam is directed parallel to the hot/cold interface (dotted line) and perpendicular to the direction of the heat propagation. (e) Kinetic energy component parallel to the direction of heat propagation. (f) Kinetic energy component perpendicular to the direction of heat propagation. $T_{0//}$ and $T_{0\perp}$ are the equilibrium kinetic energies without the lattice heating. This shows that the kinetic energy decays exponentially outside of the heated area (solid lines).

Magnetic experiments

Interaction of magnetic particles with each other and with a magnetic field was studied experimentally in a complex plasma. Monodisperse plastic microspheres with magnetic filler were suspended in an rf symmetrically driven discharge to form a multilayer dust cloud. The magnetic field induced a magnetic moment in the grains. The particles were pulled upward in the direction of the magnetic field gradient and their levitation height increased (Fig. III.A.19). This was used as a new diagnostic method to calculate the particle charge and the thickness of the plasma sheath. It was demonstrated that the magnetic gradient can compensate gravity. Some particles formed agglomerates due to magnetic attraction between the grains. Analysis of the particle interaction forces showed that at intermediate magnetic fields (used in the experiment) the particles can agglomerate only if their kinetic energy is high enough to overcome the barrier in the electrostatic interaction potential.

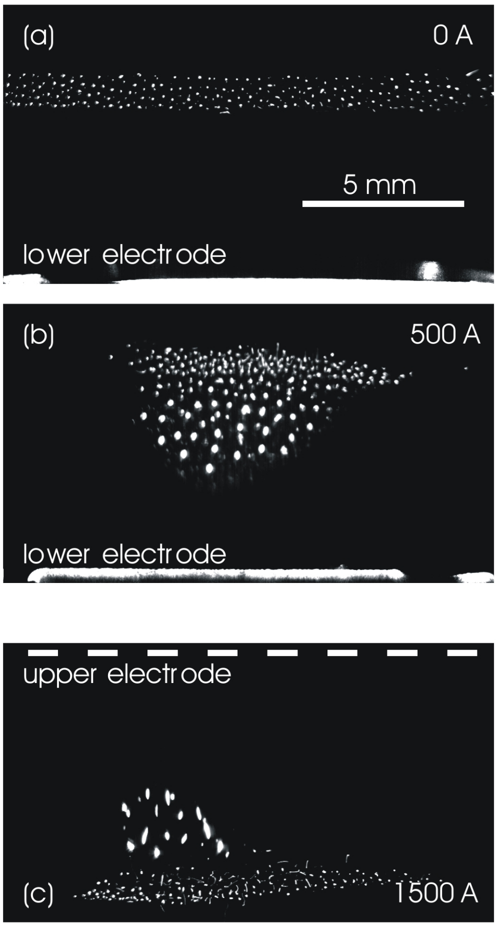

Fig. III.A.19: Particles levitated in the plasma. The current in the magnetic coils is indicated in the upper right corner. (a) Without the magnetic field. Particles form a multilayer cloud in the lower plasma sheath (lower viewing area). (b) Magnetic field of 0.04 T. Some particles agglomerate and levitate in the lower sheath below the main cloud (lower viewing area). The main cloud is compressed and slightly shifted upwards. (c) Magnetic field of 0.12 T. The cloud is levitated towards the upper sheath (upper viewing area). The larger agglomerated particles levitate above the main cloud. Gravity can be compensated by the magnetic force

The possibility of magnetically induced formation of a plasma crystal was discussed (Fig. III.A.20). Various mutual dust–dust interactions, including the forces due to induced magnetic and electric moments of the grains were theoretically considered. It turns out that the electromagnetic forces from particle magnetization and polarization may result in mutual repulsion as well as attraction. It is found that magnetized grains can coalesce, forming field-aligned chains. Since the "disruptive" electrostatic forces increase with the distance from the centre of a chain, whereas the "cohesion" magnetic forces decrease, there is an intrinsic length scale for these particle chains. A model was developed to determine the length of these structures. These finding were then applied to recent complex plasma experiments with paramagnetic particles. The theoretical estimations have revealed good agreement with experimentally observed data.

Our results are of direct interest to laboratory studies of magnetized complex plasmas, indicating several new effects. In particular, the model predicts that the chain length will increase when the magnetic field is increased, when the permeability of the particle material is higher and the grain size is larger.

.

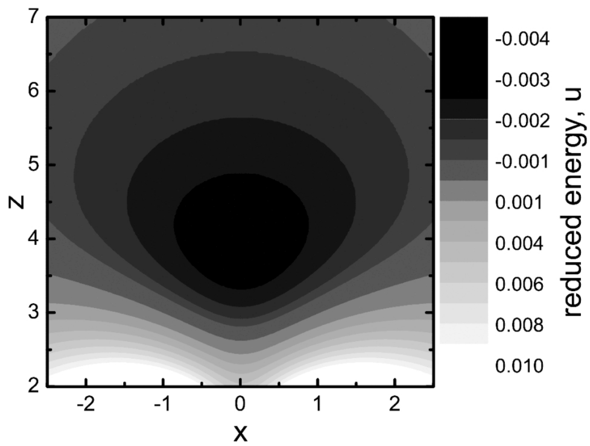

Fig. III.A.20: Interaction energy of two charged and magnetized particles as a function of their relative position, normalized by the Debye length. The particles are aligned vertically along the magnetic field, their induced magnetic moments are also vertical. There is a weak potential well which can in principle lead to the formation of linear chains of particles along the magnetic field, with particle separation of about $4\lambda_D$.

2.4 Adaptive Electrode Laboratory

The adaptive electrode (an assembly of small contiguous electrodes) research had developed substantially since its first assembly.
To study the transport of particles and the time varying regime we have improved the control of the pixels. We have now the possibility of an independent control of 93 channels in DC and of 3 channels in DC and RF (amplitude and phase). With pre-calculated data generation we can choose waveforms up to 100Hz.
The first two prototypes of the adaptive electrodes are currently used in two different experiments and laboratories. A third adaptive electrode with improved design is being realised with one 50Ohm pixel for the measurement of the complex plasma impedance and a thermocouple pixel for the measurement of the power deposited from the plasma.
The study of the local modification of the plasma boundary has been extended to magnetic perturbation where a magnetic spot is inserted in one of the electrodes. An electron gun is available.

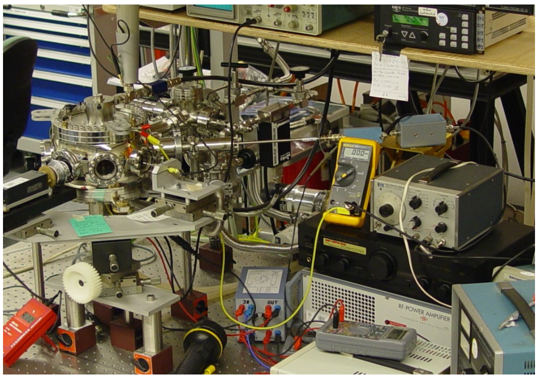

Fig. III.A.21: Image of the AE-Laboratory with diagnostics and electronics.

The plasma diagnostics, Langmuir probe and emission spectroscopy, are now an essential routine accompanying most of the experiments. We are developing a new method to monitor the negative ion density by absorption spectroscopy in the continuum.

Complex plasma manipulation and 3-D clusters
This work presents a new plasma configuration with localised RF on the boundary, useful for particle manipulation. The theoretical analysis of the RF sheath, and of the charging of particles in it, has disclosed a levitation force on particles, which is substantially different from the DC one often used in complex plasmas modelling. Experimentally the electrostatic structures have been visualised by nano-particles grown in the plasma and by injected micro-particles. The 3-D visualisation diagnostic simultaneously

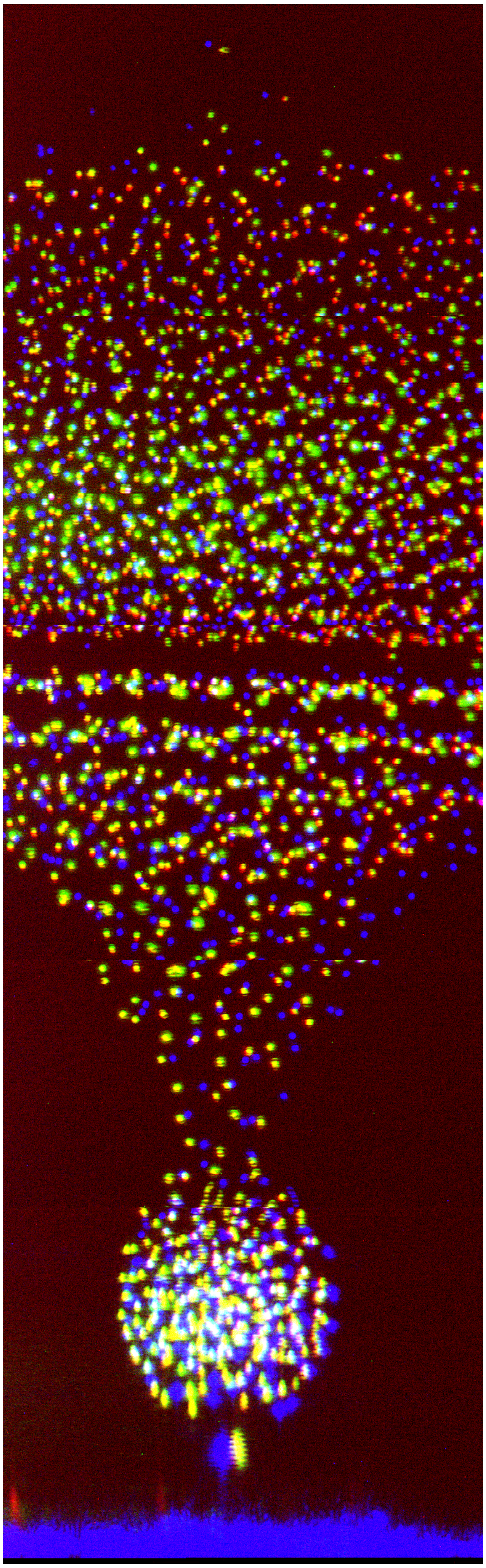

Fig. III.A.22: A plasma sheath with localised RF effects heavily loaded with particles. The green-red picture shows 2.3 x 1.7mm^2. Colours indicate the particle positions in the perpendicular direction.

monitored the position of the particles in a volume 2.3 x 1.7 x 2.3mm^3 based on two super-imposed laser light sheets, modulated in intensity in a complementary way. We found regions of extra ionisation and complex electrostatic structures in which it is possible to obtain uniform gravity compensation in 3-D.
In equilibrium the vertical confinement is provided by the electric field of double layers/striations combined with suitable conditions for particle charging. The analysis of the structures will clarify whether the horizontal confinement is due to plasma pressure or by internal forces among the cluster component (Lennard-Jones like potential) or by ion drag.

Particles in an electronegative plasma sheath
Electronegative discharges are often used in plasma processing of materials because they are highly chemically reactive and show peculiar plasma characteristics, such as transport and plasma boundaries, useful for etching and deposition. Although widely used, the physics of the discharge is not well understood, due to difficulties with the plasma diagnostics. The electronegative sheath presents several physical effects, which have been un-ravelled by a new (non invasive) diagnostic; we have injected micro-particles of different sizes in the sheath and recorded their equilibrium positions. These depend on the presence of negative ions in two ways: the electric field of the sheath can be a non-monotonic function of the electronegativity and the particle charge is strongly affected by the modified Bohm flux of positive ions.
The experiments agree well with a model of a structured electronegative plasma sheath, a possibility so far only mathematically and numerically investigated. Using the most probable reactions we have demonstrated the existence of cold and energetic negative ions in RF Oxygen plasma.

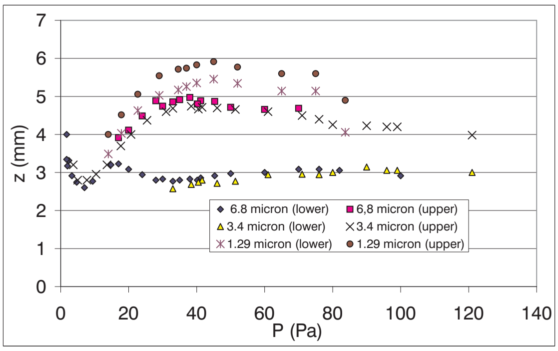

Fig. III.A.23: The position of the particles above the electrode versus pressure. The medium and large particles settle on the two sides of a secondary plasma as predicted by theory.

Levitation of microparticles in a weak magnetic field
The estimation of the charge acquired by microparticles in a magnetic field is a difficult issue. For weak magnetic fields only the electrons are magnetised. This causes a decrease of the charge when the Larmor radius of the electrons, which are energetic enough to reach the particle, is comparable to the particle radius *a*. The cross section for magnetised electrons is then πa^2.
We study this regime in a magnetised plasma sheath by the introduction of a magnetic spot on the lower electrode of an RF plasma reactor. The charge of the injected particles is deduced by the levitation height when the magnetic field is vertical. It was found that oscillations of the particles around this position have a relatively high frequency, related to gradients of the electric and magnetic field.

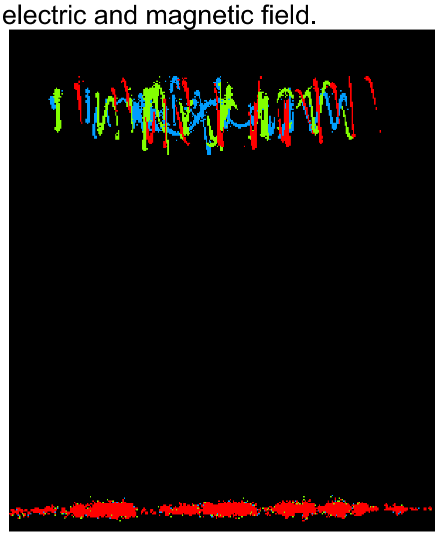

Fig. II.A.24: Oscillation of particles in the plasma sheath with a non- uniform magnetic field applied. The colour corresponds to three consecutive frames, 15 frames per second, and the trace is recorded in 62ms.

3. Theory and simulation

Kinetics of non-Hamiltonian ensembles
One of the remarkable features distinguishing complex (dusty) plasmas from usual plasmas is that charges on the grains are not constant, but fluctuate in time around some equilibrium value which, in turn, is some function of spatial coordinates. Ensembles of particles with variable charges are *non-Hamiltonian systems*, because the mutual collisions do not conserve energy.
Therefore, the use of thermodynamic potentials to describe such systems is not really valid. An appropriate way to investigate their evolution is to use the kinetic approach. We studied two cases: (i) *inhomogeneous charge* – it depends

on the particle coordinate but does not change in time, and (ii) *fluctuating charge* – it changes in time around the equilibrium value, which is constant in space. For both cases we used the Fokker-Planck approach to derive the collision integral which describes the momentum and energy transfer in collisions. From the solution of the corresponding kinetic equation we obtain the result that the mean particle energy grows in time. In case (i) the energy changes as $\propto(t_{cr}-t)^{-2}$, exhibiting the explosion-like growth with t_{cr} a critical time scale. In case (ii) it grows exponentially. The obtained solutions can be of significant importance for laboratory dusty plasmas as well as for space plasma environments, where inhomogeneous charge distributions are often present. For instance, the instability can cause "dust heating" in low-

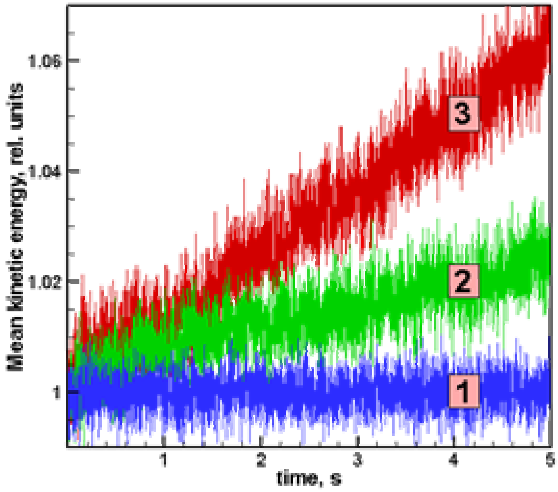

Fig. III.A.25: Initial stage of the mean energy growth, as obtained from the molecular dynamics simulations of case (i). The particle energy (normalized to the initial temperature) is plotted as function of time for different values of dimensionless charge gradient.

pressure complex plasma experiments, it can be responsible for the melting of plasma crystals and it might operate in protoplanetary disks where it could affect the kinetics of the planet formation, etc.

Oscillations and coupled dust-lattice solitons in monolayer plasma crystal

We have studied the nonlinearly coupled dust-lattice (DL) waves in monolayer plasma crystals. It was shown that the nonlinear longitudinal and transverse oscillations in a monolayer plasma crystal can form a coupled DL soliton – characterized by a spatially localized transverse wave envelope with increased particle density (Fig.III.A.26).

Transverse waves in complex plasmas are analogous to the well known *plasmons* in usual (electron-ion) plasmas. Treating the transverse oscillations as quasi-particles-*oscillatons*, we have shown that the region of higher density is an effective 'potential well' for such quasi-particles. Accumulation of oscillatons in the region with higher density causes further density increase, and therefore a modulational instability of coupled dust-lattice waves might be possible. The modulational instability can be suppressed due to a nonlinearity resulting from the spatial localization of vertical oscillations, i.e. formation of a solitary wave. There is a clear analogy with Langmuir waves (plasmons), except that in this case the oscillations cause an increase of the density, whereas the high-frequency pressure of plasmons creates cavities. Using molecular dynamics simulations, has been shown that DL solitons are stable.

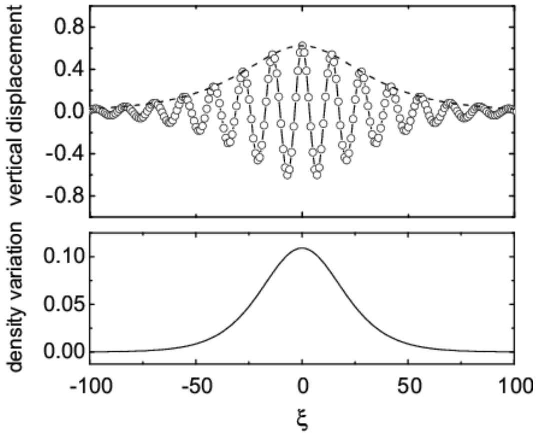

Fig. III.A.26. Normalized transverse (top) and longitudinal (bottom) structure of the dust-lattice soliton.

Comprehensive approach for the ion drag force

The ion drag force – the momentum transfer from the flowing ions to charged microparticles (grains) embedded in a plasma – is an inevitable and exceptionally important factor in (dusty) complex plasmas. The ion drag force determines the location and configuration of complex plasmas in experiments, in particular – it causes the formation of the "void" in the centre of rf discharges, a phenomenon discovered in microgravity ("PKE-Nefedov") experiments. Also, ion drag affects properties of dust-acoustic and dust-lattice waves and can cause, e.g., melting of plasma crystals. Therefore, knowledge of the ion drag force as a function of the plasma parameters (which may vary over a broad range) is necessary in many of the complex plasma experiments. Microgravity experiments clearly showed that the so-called "Barnes formula", which had been traditionally used to calculate the ion drag force, cannot explain the formation of the void. This stimulated further investigations of this topic. It turned out that the Barnes formula in fact is only applicable when the ion-grain interaction is linear, and when the ion neutral collisions can be neglected.

a. Binary collision approach

The traditional way to derive the ion drag force on a charged test particle – the *binary collision approach* – is based on the solution of the mechanical problem of the ion motion in the field of the particle. Once the ion trajectories have been calculated, the momentum transfer cross section is obtained. The force is then derived by averaging the momentum transfer cross section over the velocity distribution function of ions. We calculated the cross section numerically assuming an isotropic Debye-Huckel (Yukawa) potential of interaction between the ions and the point-like grain. The obtained cross section is shown in Fig.1 along with different analytical approximations. The normalized cross section is a function of the so-called "scattering parameter" β, which is the ratio of the Coulomb radius to the screening length (λ) and characterizes the "linearity" of the scattering: In the linear limit $\beta<<1$ the range of nonlinear interaction – the Coulomb radius – is much shorter than the screening length and the standard Coulomb scattering theory is applicable (on which the Barnes theory is based). It yields the following scaling for the cross section: $\sigma/\lambda^2 \sim \beta^2 \ln(\beta^{-2})$. In the opposite limit of nonlinear scattering $\beta>>1$ the nonlinear range is much larger than the screening length and the Coulomb scattering theory is not applicable. We developed a different approach, which provides an accurate analytical expression for the cross section which scales as $\sigma/\lambda^2 \sim \beta^2 \ln^2\beta$ in this limit.

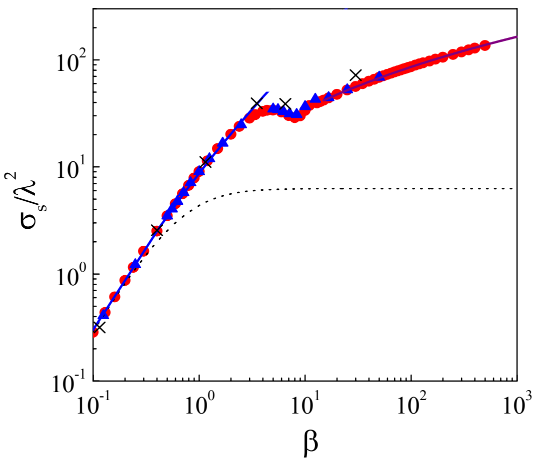

Fig. III.A.27: Momentum-transfer cross section, σ_S, normalized to the squared screening length λ, versus the scattering parameter β. Symbols represent numerical calculations, solid lines correspond to the analytical formulas. The dotted line is for the Coulomb scattering theory. One can see that the Coulomb theory underestimates the cross section for $\beta>1$ considerably.

Also, the role of the ion absorption on the grain was investigated. It could be shown that absorption provides the dominant contribution to the momentum transfer when $\beta>>1$. We integrated the obtained cross sections over a Maxwellian distribution function to obtain an expression for the ion drag force. The most important result is that in the linear regime the obtained expression is close to the Barnes formula, whereas for the nonlinear regime (which often occurs in dusty plasmas) the ion drag force can be considerably larger (more than by one order of magnitude) than that predicted by the Barnes theory.

b. Linear kinetic approach

The binary collision approach requires the following assumptions: (i) The ion-neutral collisions are neglected. (ii) The potential distribution around the test charge is presumed to be isotropic (although the ion flow velocity introduces anisotropy). (iii) The distribution function for ions has to be presumed. All these issues can be successfully resolved by employing the self consistent *kinetic approach*. Instead of calculating single ion trajectories and then integrating the resulting momentum transfer, one can solve the Poisson equation coupled to the kinetic equation for ions and obtain the self consistent electrostatic potential around the particle. The polarization electric field at the origin of the test charge gives us the force on the particle. As long as the linear approximation is applicable – the so-called "linear dielectric response formalism" – the whole problem is basically reduced to the calculation of the appropriate plasma response function (permittivity). The generalized kinetic

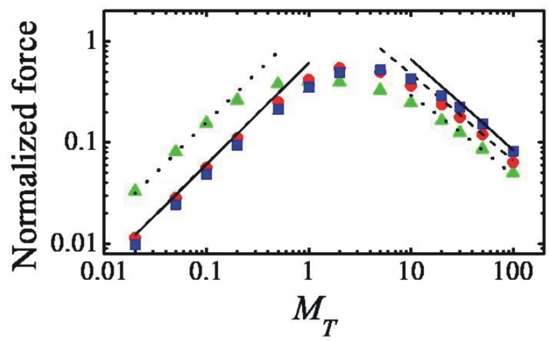

Fig. III.A.28: Normalized ion drag force versus the thermal Mach number M_T (ratio of the ion flow velocity to the ion thermal velocity). Symbols represent numerical results for weakly collisional (square), transitional (circle), and strongly collisional (triangle) cases – when the ion mean free path is much longer, comparable, and much shorter than the screening Debye length, respectively. Lines show analytic asymptotes at small and large Mach numbers for the same cases.

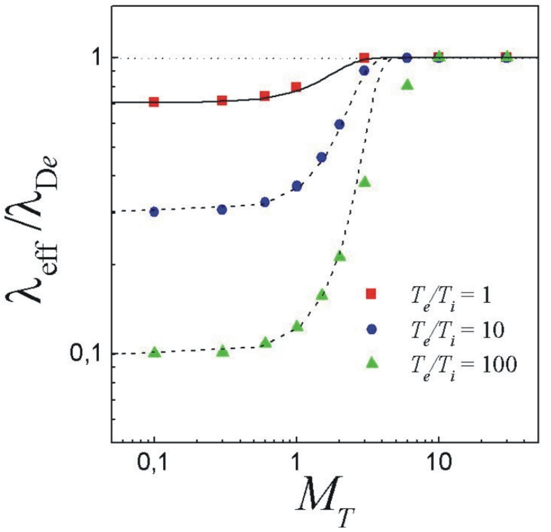

Fig. III.A.29: The effective screening length λ_{eff} of the charged grain in the flowing plasma versus the thermal Mach number M_T (ion flow velocity normalized to the ion thermal velocity) for different electron-to-ion temperature ratios. Symbols are numerical calculations, lines are simple fits.

approach allows us to obtain the ion drag force for arbitrary frequency of the ion neutral collisions and arbitrary velocity of the ion flow, as shown in Fig. III.A.28. For a subthermal flow the force grows $\propto M_T$ and collisions enhance it, for a suprathermal flow the force falls off as $\propto M_T^{-1}$ and collisions reduce it. The kinetic approach also allows us to determine how the effective screening length changes with the ion velocity. Fig. III.A.29 show that the transition from the linearized Debye length in bulk plasmas (small M_T) to the electron Debye length in the sheath (large M_T) occurs in a fairly narrow range of velocities around M_T~1.

c. Complementarity and hybrid approach

Comparing the results of the linear kinetic approach and the binary collision approach, the most important conclusion to be dawn is that these approaches are not really competitive but rather complementary: The binary collision approach is more suitable to describe the nonlinear collisionless cases. This situation is typical for subthermal ion flows (bulk plasmas). Since small Mach numbers imply only weak distortions of the potential around the grain and the ion distribution, there is no need to employ the kinetic approach in this case. Also, with the binary collision approach the effects of finite grain size and charging collisions can be consistently taken into account. On the other hand, for suprathermal ions (pre-sheath regions) – when the linear theory can be better applied – both the particle potential and ion distribution function are highly anisotropic, and then the self consistent kinetic approach is necessary. Also, in contrast to the binary collision approach, the kinetic approach allows us to consider collisional linear cases. Figure III.A.30 illustrates this complementarity. In the linear collisionless case both approaches, of course, converge to the traditional Barnes formula. Current activity is focused on the investigation of the strongly nonlinear collisional case – as yet the only region inaccessible for theory, as one can see from Fig. III.A.30.

Momentum transfer in complex plasmas

In order to characterise complex plasmas and determine the "states" (e.g. crystalline, liquid, gaseous, granular) it is necessary to determine the interactions between all components. Hence momentum transfer between the different charged components in complex plasmas was investigated, and a detailed analysis of grain-electron, grain-ion, and grain-grain binary collisions was performed (electron-ion collisions are well described within standard plasma theory). Assuming a screened Coulomb (Debye-Hückel or Yukawa) interaction potential (attractive or repulsive) the momentum-transfer cross sections are calculated numerically. In Fig. III.A.31 these cross sections are shown as functions of the so called *scattering parameter* β, which is the unique parameter describing scattering of point-like particles for any short-range potential. For typical complex plasma parameters the characteristic values of β for different types of collisions are: electron-grain β<<1, ion-grain 1<β<30, and grain-grain β>>1. The standard Coulomb scattering theory is applicable only for electron-grain collisions, whereas for ion-grain and grain-grain collisions different approaches should be used. Based on

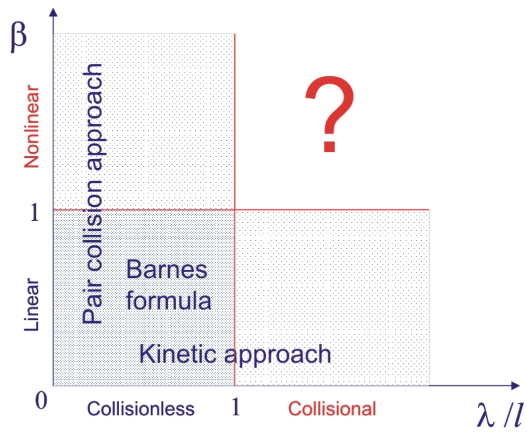

Fig. III.A.30: "Phase diagram" of the ion drag force showing schematically the applicability of different approaches in the "nonlinearity-collisionality space". The measure of nonlinearity is the ion-grain coupling parameter β, for collisionality the ratio of the screening Debye length λ to the ion mean free path l is employed.

our numerical calculations the required approaches are developed, the role of the finite grain size is investigated, and analytical approximations for the momentum transfer cross sections are proposed. The latter are used to estimate the characteristic momentum-transfer rates in complex plasmas. The obtained results have various applications, including calculation of the ion drag (see earlier) and electron drag forces.

The analysis of grain-grain binary collisions also allows us to obtain further insight into the properties of complex plasmas: We developed criteria to classify the possible states of complex plasmas in terms of the momentum transfer. Fig. III.A.31 represents different "phase states" of complex plasmas as functions of the electrostatic coupling parameter $\Gamma_{ES}=U(\Delta)/T$ (where $U(r)$ is the potential energy of pair interaction) and the mean grain separation Δ, normalized either to the grain size *a* or the screening length λ. The vertical dashed line at $\kappa=1$ conditionally divides the system into Coulomb and Yukawa parts. The following states can be identified: Above the red solid line we have Coulomb or Yukawa crystals, the crystallization condition is $\Gamma_{ES}>106(1+\kappa+\kappa^2/2)^{-1}$. (ii) Above the blue solid line we have Coulomb or Yukawa non-ideal plasmas - the characteristic range of grain-grain interaction (in terms of the momentum transfer) is larger than the intergrain distance (in terms of the Wigner-Seitz radius), $(\sigma/\pi)^{-1/2}>(4\pi/3)^{-1/3}\Delta$, which implies that the interaction is essentially multiparticle. (iii) Regions below blue solid line correspond to Coulomb or Yukawa ideal plasmas -- the range of grain-grain interaction is smaller than the intergrain distance and only pair collisions are important. (iv) Below the lower dotted line the electrostatic interaction is not important and the system is like a usual granular medium. (v) In the region between the upper dotted line and the solid blue line the pair Yukawa interaction asymptotically reduces to the hard sphere limit and the complex plasma forms a "Yukawa granular medium".

Another important application of the obtained results is to investigate the complex plasma properties in terms of the competition between the momentum transfer rate in mutual grain-grain collisions ν_{dd} and the interaction with the surrounding medium (neutral gas), characterized by the rate ν_{nd}. Fig. III.A.31 shows that there is a broad range of parameters where complex plasmas have the properties of one-phase fluids ν_{dd}/ν_{nd} >>1, and those of two-phase fluids ν_{dd}/ν_{nd} ~1. In the extreme limit of very small ν_{dd}/ν_{nd} we can also have "tracer particles" in the background medium.

The broad range of states that is accessible for complex plasmas and the possibility to study a variety of processes at the kinetic level makes these systems extremely attractive for further research. The obtained results are important for "engineering" experiments that aim to make use of special properties of complex plasmas.

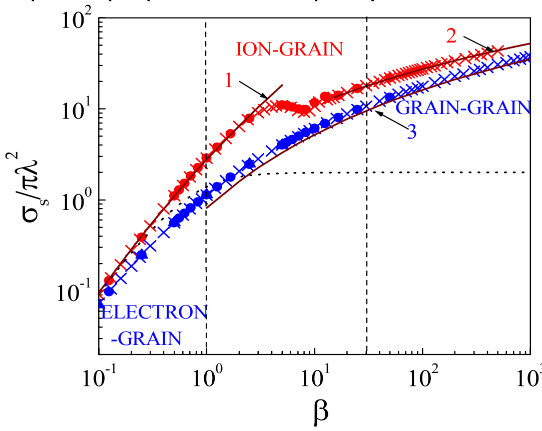

Fig. III.A.31: Momentum-transfer cross section, σ_S, normalized to $\pi\lambda^2$ (where λ is the plasma screening length), versus the scattering parameter β. Symbols correspond to numerical results: The upper (red) data are for attractive and the bottom (blue) data are for repulsive screened Coulomb potentials. Solid curves correspond to our analytical approximations. The dotted line corresponds to the Coulomb scattering theory. This underestimates the cross sections above β~1 considerably. Vertical dashed lines conditionally divide the β-axis into three regions: β<<1 is typical for electron-grain collisions; 1<β<30 is typical for ion-grain collisions; β>>1 is typical for grain-grain collisions.

Vertical oscillations of magnetized particles

We have studied the vertical oscillations of charged paramagnetic particles in a low temperature plasma sheath in an external magnetic field. For a single magnetized particle a novel type of vertical vibration is found. The vertical resonance frequency is independent of the particle mass, but is completely specified by the magnetic field profile inside the complex plasma and the magnetic properties of the grain material. A numerical estimate of the resonance frequency for typical complex plasma parameters in our magnetic experiments gives frequencies of ~10Hz. Such values can be easily measured and provide a tool for determining the complex plasma parameters.

In a one-dimensional particle string the magnetic force causes a new low-frequency oscillatory mode, which is characterized by inverse optic-mode-like dispersion when the wavelength far exceeds the intergrain distance. The characteristics of the mode are specified by the gradients of the external magnetic field and thus can be effectively controlled in experimental conditions. This opens new opportunities for the investigation of the particle behavior at the kinetic level as well as for stimulating phase transitions in the system, and for the study of self-organized structures in the experiments.

The Role of Negative Ions in Experiments with Complex Plasma

The influence of negative ions on the state of a rf gas-discharge dusty (complex) plasma containing electronegative gaseous impurities was investigated. A simple one-dimensional argon-discharge model allowing for the impurity-induced plasma chemical reactions was taken as an example to show that the addition of even a minor amount of molecular oxygen changes appreciably the plasma composition and plasma transport properties, as well as the microparticle charges. This has a strong effect on the microparticle force balance and the formation of various structures in the discharge.

The main results of the study can be summarized as follows: the addition of molecular oxygen to the argon plasma changes the composition and transport properties of the plasma substantially: the electron–ion plasma transforms to an ion–ion plasma. The appreciable decrease in the microparticle charge can also change the phase state (e.g., melt plasma crystals). The electric field also decreases in the discharge, thereby changing the force balance for the particles; in particular, the void size markedly increases. In addition, the metastable argon and oxygen states initiate heating of the neutral gas, and the corresponding induced thermophoretic force makes a considerable contribution to the force balance for dusty particles.

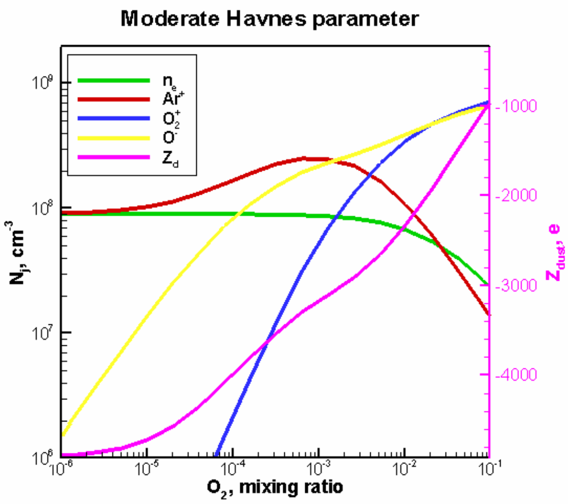

Fig. III.A.32: The composition of a rf discharge plasma in an O_2/Ar mixture and the charge Z of an individual microparticle as functions of the partial concentration $[O_2]/[Ar]$ of molecular oxygen.

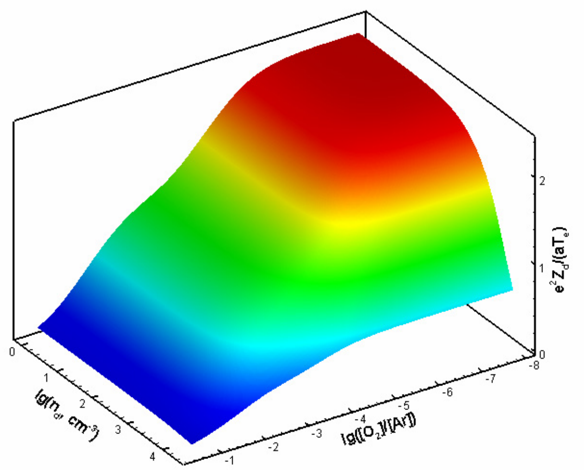

Fig. III.A.33: The charge of a microparticle of size 1 micron in a rf discharge in Ar/O_2 mixture vs. the partial concentration ($[O_2]/[Ar]$) of molecular oxygen and the dust particle concentration in units of cm^{-3}.

Strongly coupled plasmas in high energy physics

Recently first indications for a new state of matter, the so-called quark-gluon plasma, have been found in accelerator experiments at CERN (Geneva) and at the Brookhaven National Laboratory (USA). In energetic nucleus-nucleus collisions a hot and dense fireball (temperature about 10^{12} K) is created, which is expected to be in the quark-gluon plasma phase (see figure). Because of its extremely short life time and volume the quark-gluon plasma cannot be observed directly and its discovery relies on a comparison of theoretically predicted signatures and experimental data. Unfortunately, the theoretical description of a quark-gluon plasma from first principles is extremely difficult due to the strong interaction between the quarks and gluons. Therefore we proposed to use strongly coupled electromagnetic plasmas, such as complex plasmas, as model systems for the quark-gluon plasma. In this way, we were able to explain observed features of the quark-gluon plasmas, such as a cross section enhancement of the quark and gluon scattering, supporting the presence of the quark-gluon plasma in ultrarelativistic nucleus-nucleus collision experiments. Furthermore, adopting methods also used for complex plasmas, such as transport theory (Boltzmann equation), we were able to improve the theoretically predicted gluon dispersion relation and to describe the screening of a fast quark in the quark-gluon plasma. In the latter case we found a minimum in the screening potential which might have interesting consequences for the production of heavy mesons in high-energy nucleus-nucleus collisions. Finally, generalizing the theory of thermophoresis, as used for complex plasmas, to the relativistic case, we predict a strong thermophoretic flow in the fireball, which might be observable in future experiments.

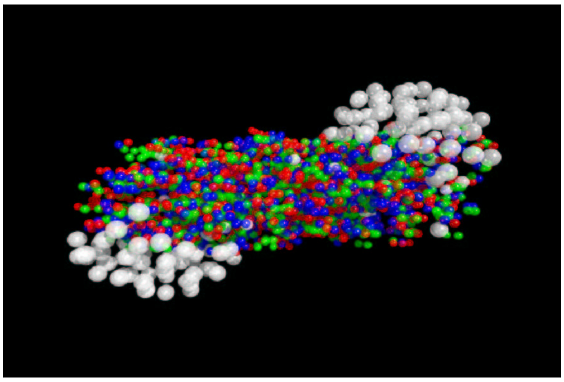

Fig. III.A.34: Numerical simulation of an ultrarelativistic nucleus-nucleus collision, based on transport theory, showing the formation of a quark-gluon plasma (colored spheres) from the protons and neutrons (white spheres) of the original atomic nuclei (www.th.physik.uni-frankfurt.de/~urqmd/).

4. Microgravity Research

As mentioned in the introduction complex plasmas consist of a “normal” plasma – electrons and ions – and an additional component of small solid particles, typically in the range of micrometers. This heavy component in the plasma makes it necessary to perform experiments under microgravity conditions although it is possible to levitate the particles in the laboratory as well. For instance, the charged microparticles can be levitated in a strong electric field. But this induces substantial stresses to the system of strongly interacting particles and implies that under gravity conditions only a small part of the parameter phase space of complex plasmas can be investigated. To complete the research on complex plasmas, investigations under microgravity conditions are mandatory.

Under gravity conditions only small complex plasma systems of limited extent in the vertical direction – as shown in Fig. III.A.35 (a) – can be investigated (in a region where gravity is compensated by a strong electric field). Under microgravity we observed large complex plasma systems extended in all three space co-ordinates (see Fig. III.A.35 (b)). It can be shown that under microgravity conditions much broader and different regions in the parameter phase space are accessible providing a means for researching new physics not attainable under gravity conditions.

a)

b)

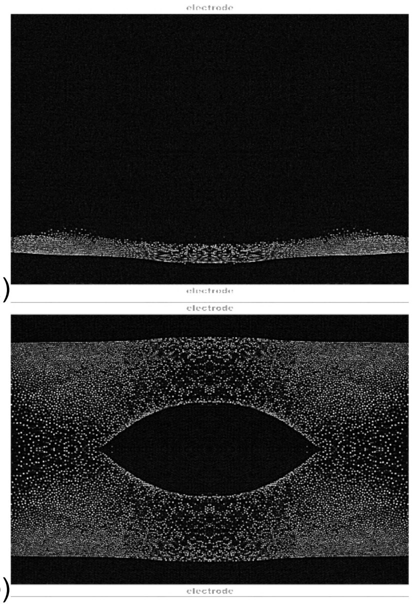

Fig. III.A.35: Microparticle (3.4 μm in diameter) distribution between the two electrodes under gravity (a) and microgravity conditions (b). Under gravity the charged particles sediment towards the lower electrode and can be levitated only by a strong electric field in the sheath. Under microgravity the particles are dispersed all over the experimental volume, forming large 3-dimensional complex plasmas.

The special conditions which Space provides for the investigation of complex plasmas are shown in the next paragraphs.

4.1 PKE-Nefedov

PKE-Nefedov, as a laboratory installed on the International Space Station, is operative since the beginning of 2001. In total 11 missions, 7 within the report period, with 36 separate experimental runs of 90 minutes each have been performed. It is the most actively used scientific apparatus on the ISS with a scientific outcome of more than 15 refereed publications.

Under microgravity conditions the typical static and dynamic behaviour of complex plasmas is illustrated in Fig. III.A.36. This figure shows a 3 second trajectory fragment of the microparticles, color coded from red to blue. The dominant features which can be investigated here are:

- a microparticle free “void” in the centre of the system for most experimental parameters.
- a sharp boundary between the void and the complex plasma.
- demixing of complex plasma clouds formed by microparticles of different sizes.
- crystalline structures along the central axis.
- vortices in different areas away from the central axis.

All of the above mentioned features have been investigated in detail over the last three years.

<u>The void</u>: The microparticle free centre between the electrodes can be explained by the equilibrium of all forces acting on the particles. Since the dominant force on earth, gravity, is reduced by orders of magnitude the weaker forces can be investigated in detail. These forces are the electrostatic force F_Q arising from an electric potential with a maximum in the centre, which decreases radially and axially, and the ion drag force F_{id}. The latter is due to the acceleration of the positive ions along this electric field out of the centre and the resulting friction force on the particles. According to the well known formula by Barnes et al., the ion drag force is too low to overcome the electrostatic force to form the void. A major result of the microgravity experiments has been the rederivation of the ion drag and the discovery of new processes that change the "classical" result by over a factor 10. The experimental results agree with the new theory. Since ion drag is of great importance in many physical situations and problems, the new insights gained from these experiments on the ISS have to be considered as a major achievement.

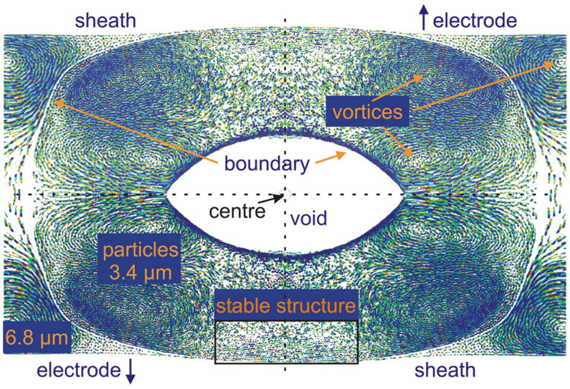

Fig. III.A.36: Structure and dynamics of a complex plasma containing particles of two different sizes (3.4µm and 6.8µm diameter) under microgravity conditions. The trajectories of the microparticles are shown colour coded from red at the beginning to blue at the end of the trajectory (over the rainbow colours) for an exposure time of 3 sec.

The void can be closed under special experimental conditions. These conditions are neutral gas pressures below 0.5 mbar and the lowest possible rf-voltages, close to the plasma-off condition. At these parameters the plasma density is so low and the electric field is so weak that finally the electrostatic force dominates over the ion-drag force, and the particles are pushed to the centre.

<u>Void/complex plasma boundary</u>: The equilibrium of the above mentioned (opposite) forces gives the radial position of an isolated microparticle. In a particle cloud, there are pressure forces, too. The sharp boundary cannot be explained by the equilibrium position alone. It was discovered that the complex plasma changes the potential distribution in such a way that a sheath with a so-called double layer is formed. This double layer produces a change in the sign of the electric field and can explain the sharp edge. This phenomenon, well known to occur in plasma-wall interactions, is apparently present, even if the "wall" is extremely porous (in our case only about 10^{-4} of the surface is "solid").

<u>Demixing of different particle sizes</u>: The forces are size dependent. $F_Q \propto a$ and $F_{id} \propto a^2$, where a is the radius of the particle. This results in an equilibrium position of smaller particles which is closer to the centre than that of bigger ones, easily explaining the observed demixing of the different sizes. The new physics is therefore not the fact of demixing – it lies in the way how de-mixing proceeds in strongly coupled plasmas. This topic is being actively pursued with new dedicated experiments on the ISS. For now it is sufficient to mention that the approach to final equilibrium can pass through a new universal process (a non-equilibrium coordinate space phase transition) not known previously – a process peculiar to strongly coupled systems.

<u>Crystalline structures</u>: In many crystallisation experiments with PKE-Nefedov, we observed crystalline order in a small area close to the sheath region. Even after several minutes the size of the crystal did not increase.

In one of the latest experiments, we injected particles with a diameter of 3.4 µm at a pressure of 0.24 mbar. A few minutes after the injection, when the complex plasma has reached a steady state, the pressure was reduced in little steps down to 0.14 mbar. Every step causes a little "puff" of gas, which disturbs the equilibrium position of the particles. These little kicks precipitate an annealing of crystal defects, so that a large crystalline region is formed, filling the whole area between void and sheath and between the vortices at the border of the complex plasma. This special condition made it possible, for the first time, to observe the crystal structure with the high resolution CCD camera. A scan in depth provided us finally with a 3-dimensional view of the crystal.

In contrast to crystals with similar particles under normal gravity it was found that in space the crystal planes where not mainly oriented parallel to the electrode. Using a vertical cut of the particle positions obtained from a scan with the high resolution camera through the crystalline area, one can see that the crystal consists of domains with different orientation and different crystalline structure (Fig. III.A.37).

This allows us to investigate the physics of 3-D domain boundaries, de-excitation of lattices, annealing etc. at the kinetic (individual particle) level.

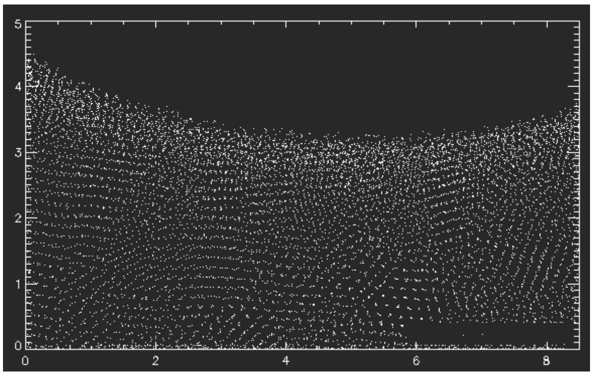

Fig. III.A.37: Superposition of the 3-D particle coordinates on a 2-D image. The crystal consists of crystalline domains with different structure and orientation. Tilted lattice planes and hexagonal areas can be seen.

<u>Vortices</u>: In the boundary regions the trajectories of the particles show a vortex like motion. This is caused by strong electric field inhomogeneities which occur at the edge of the electrodes and at the interface between the electrodes and the particle dispensers. These in turn affect the forces F_Q and F_{id}, causing the particle cloud to execute a convective-like motion. Although this motion is poorly controlled, it nevertheless provides interesting insights into the kinetics of shear flows – some of the phenomena observed will therefore become subject of special investigations in the future. For future experiments (see PK-3 Plus below) the plasma chamber and electrode assembly have been changed so that a much better symmetry and homogeneity of the electric field between the electrodes is achieved and therefore the vortex motion does not occur. In PK-4 (see below) the design criteria include special studies of controlled shear flows as a major goal.

Potential energy distribution inside the void

The formation of the so-called "void" in microgravity experiments has precipitated a number of theoretical explanations, including effect of the ion drag force, thermophoretic force, "plasma holes", etc. Whilst the ion drag mechanism of the void formation seemed most consistent with the observations, no direct experimental evidence was available previously. In one of the experiments we observed an instability of the particle cloud-void interface. The instability was accompanied by periodic contractions of the void volume and fast injection of a relatively small number microparticles from the cloud into the void. In the subsequent relaxation stage the injected grains were pushed from the void back into the complex plasma cloud. The relaxation stage was slow enough so that an accurate analysis of grain trajectories during this stage was possible. From this analysis the distribution of forces (and the equivalent potential energy) inside the void region was reconstructed. This distribution is shown in Fig. III.A.38. At the relatively low neutral gas pressure used in the experiments the direct comparison with theory, which a model of the ion drag force developed for collisionless ions was possible. Good agreement between theoretical and experimental results was found as shown in Fig. III.A.38. Hence the results may be considered as proof that the void formation in complex plasmas under microgravity conditions can be consistently explained by the ion drag mechanism.

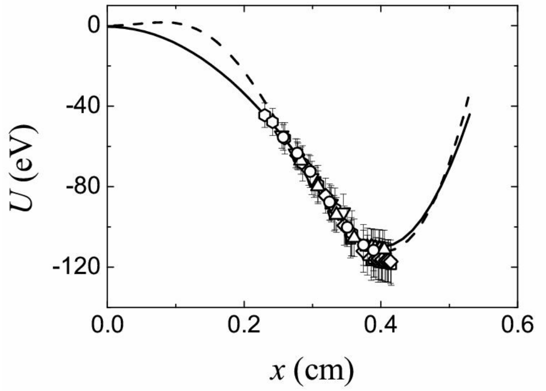

Fig.III.A.38. Potential energy distribution inside the void. Symbols correspond to the experiment, dashed line correspond to theory. The position x = 0 is at the void center.

Decharging of a complex plasma

In the "decharging experiment" the rest charge on the microparticles was measured after the plasma was switched off. To measure this, the particles were exposed to a sinusoidally varying electric field (at low frequencies around 0.5 Hz) and – if they remain charged – one can simply determine the charge from the oscillation amplitude shown in Fig. III.A.39.

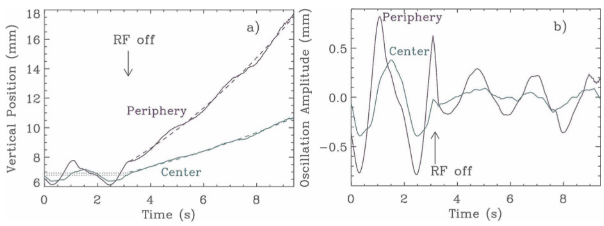

Fig. III.A.39. a) shows the particle motion upwards separately for particles in the periphery and the centre. The time when the plasma is switched off is shown in the graph. Subtracting the thermophoretic from the oscillatory motion we receive the oscillation amplitude in b).

On Earth such a measurement is practically impossible – the particles fall down too quickly and charge measurements are consequently very difficult to perform. This decharging experiment showed that the particles are not totally discharged after the plasma is turned off. They retain a "frozen" charge after the plasma electrons and ions have disappeared. This is a new insight from complex plasma physics and might be important for many other processes, including industrial applications.

Walking through walls

Sometimes it is observed that individual particles appear to simply pass through a strongly coupled complex plasma (even in the crystalline state). It is if these particles can "walk through a wall". We have studied this anomalous transport, a new phenomenon observed in ground-based laboratory experiments, in experiments under microgravity conditions and in parabolic flight experiments (Fig. III.A.40)

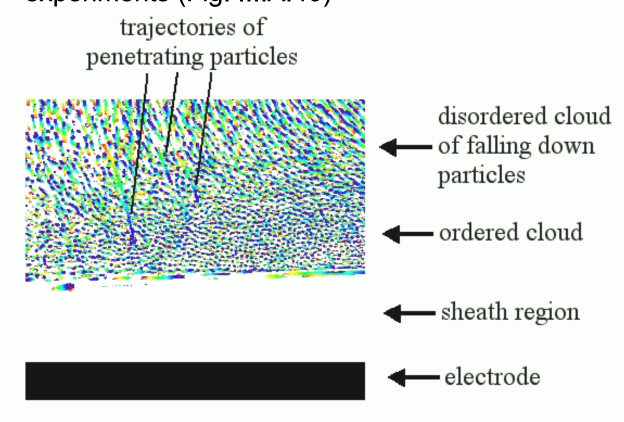

Fig. III.A.40: The trajectories of three penetrating particles are shown.

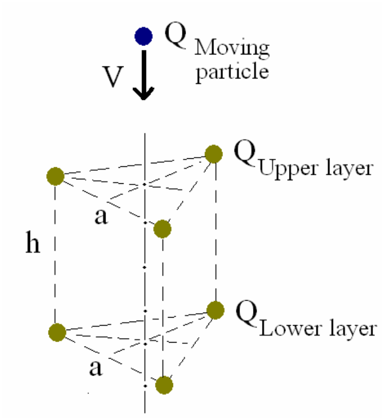

Fig.III.A.41: Geometrical model for charge variation of penetrating and crystal particles.

To explain the observations a "geometrical model for charge variation" of moving and crystal particles was proposed. The main assumption of the theory is that the new particle takes electrons away from crystal cell particles in proportion to the overlap of the Debye spheres (Fig. III.A.41). Since the sum of all charges remains constant inside a cell, the charge of an individual particle should decrease and the barrier for penetration will be lower. Theoretical predictions are in good qualitative agreement with observations and numerical simulations, and show that this extreme phenomenon can be considered as a consequence of the Non-Hamiltonian character of complex plasmas.

Low-frequency waves in complex plasmas

Under microgravity conditions the experimental investigation of weakly compressed three-dimensional complex plasmas is possible. One way to study these systems is by controlled excitation of low-frequency compressional waves. The waves were excited by modulating the voltage on the rf electrodes. The waves were either observed in almost the entire cloud of particles or in a specific wave channel (wave-guide). A typical picture of low-frequency waves propagating through a wave channel is shown in Fig. III.A.42. By varying the modulation frequency the dispersion relation was measured (see Fig. III.A.43). In order to compare experimental results with theory a self-consistent model of low-frequency waves in a collisional

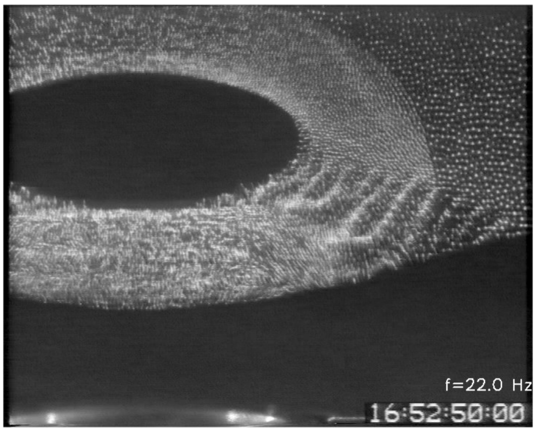

Fig. III.A.42: Experimentally observed typical plasma structures and the wave channel at excitation frequency f = 22 Hz.

complex plasma with ion drift was developed. We considered plasma conditions appropriate to the above wave experiment and took into account the following effects: ion-neutral, ion-dust and neutral-dust collisions, external forces acting on the microparticle component (i.e., electric force and the ion drag force), as well as particle charge variations in the presence of the wave. We then derived the linear dispersion relation. From comparison between the experimental and theoretical results we could estimate the particle charge and the plasma screening length, which are very important characteristics of complex plasmas. We found the dimensionless particle charge in the range from $z \sim 0.4$ to $z \sim 0.8$, which is considerably smaller than the collisionless orbital motion limited (OML) theory prediction, $z_{OML} \sim 2$. This difference was attributed to the important effect produced by ion-neutral charge exchange collisions, which increase the ion current to the grain surface and hence suppress the grain charge even when the ion mean free path is larger than the plasma screening length. Another important result of our "wave diagnostics" is that under microgravity conditions it is possible to create crystalline complex plasmas with intergrain spacing significantly larger than the plasma screening length.

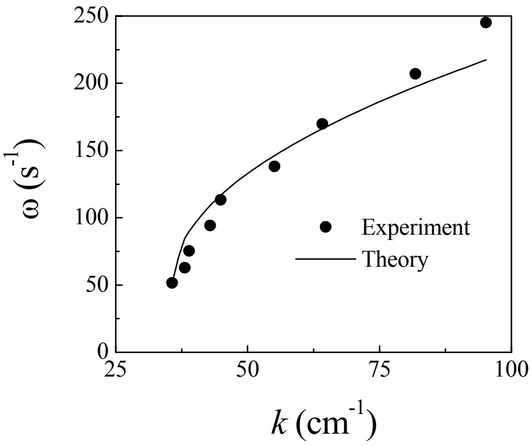

Fig. III.A.43. Comparison of the experimentally measured dispersion relation (symbols) with the theoretical one (solid line).

Agglomeration and gel transition

PKE-Nefedov was also used to perform coagulation experiments, where the plasma was switched off. Two experimental series of this kind have been analyzed so far. In some cases, the formation of a large agglomerate containing ~ 10% of the injected particle mass of the system's overall mass was observed. The agglomerate was formed during a very short time interval and coexisted with the ensemble of smaller particles of the system.

We use the light intensity of the particles as a measure for their cluster sizes and hence their masses. The intensity directly depends (via a fractal dimension) on the cluster cross section.

Whenever we observe the formation of a runaway agglomerate, the particle distribution exhibits an exponential power law (see Fig. III.A.44). In contrast, in the case when no runaway agglomerate is observed the particle distribution shows a cut-off towards the high intensity regime (Fig. III.A.44).

A theoretical model on the basis of coagulation theory was developed. According to this model, runaway growth sets in at the moment when the mass distribution exceeds a certain limit and is no longer bound exponentially. Hence a substantial fraction of the mass of the system decouples from its kinetic evolution and is transformed into a different phase (gel phase). Further analysis of the particle properties has shown that the particles were charged both positively and negatively, the overall charge distribution being neutral. Taking into account the charge induced interaction during the coagulation process it was shown that this increases the probability for runaway growth dramatically.

This process is of importance in several domains: particle growth in atmospheres, atmospheric pollution and, as an astrophysical application, the growth of planetesimals in the protoplanetray disk.

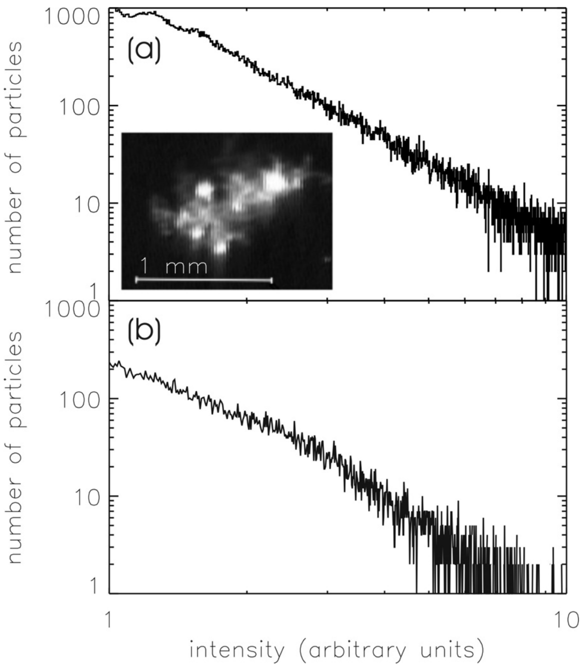

Fig. III.A.44: a) Powerlaw of intensity distribution and formation of large agglomerate, containing ~10% of the mass of the system. b) A cut off is observed at higher intensities. No runaway growth is observed.

Two-Stream-Instability

This experiment was performed with a special spherical plasma chamber on parabolic flights. Mixtures of particles with different particle radii have been shown to spatially separate within the plasma volume. The major reason for the separation is believed to be due to the size dependent ion drag force that pushes larger particles stronger to the plasma sheath boundary than smaller particles. This is the major "driving mechanism" for the complex plasma streaming experiments – where two kinds of particles are introduced into an inductively coupled radio-frequency discharge within a spherical plasma chamber. The particles are initially injected into an unstable situation, where the smaller particles of 3.4 µm diameter are closer to the sheath boundary than the 6.9 µm diameter particles. Due to the size dependent background force field the particles try to reverse their positions resulting in a counter streaming of strongly coupled complex plasmas.

As shown in (Fig. III.A.45) the small particles starts to penetrate the regime of the larger particles aligned in "lanes" of more than 10 particles each. Eventually, the spatial particle arrangement is reversed, the bigger particles are

close to the plasma sheath whereas the smaller particles occupy the centre plasma region.
Simulations have shown that in a long term counter-streaming process of the observed “lanes” of collectively streaming particles would merge to finally build up a two stream situation. To investigate the full dynamic of this instability we planed to set up a new experiment with circular boundary conditions with designed, known background force fields so that not only the instability onset will be observable.

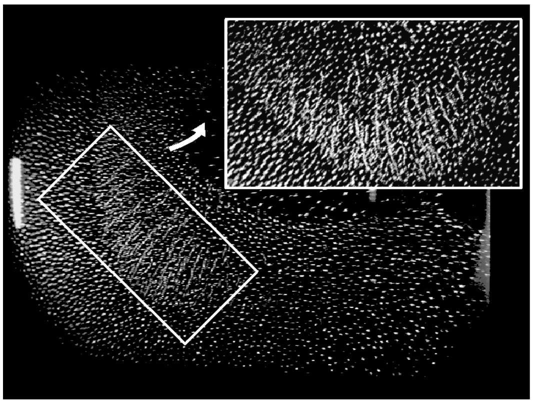

Fig. III.A.45: Counter streaming complex plasma liquids.

Conclusion
The observations and analyses of PKE-Nefedov described above show its great scientific use for fundamental research. It points to the importance of long-time experiments under microgravity conditions and on the ISS in particular. The investigation of complex plasmas under microgravity is an important pillar for the understanding of this young research field, besides the research in the laboratory and theory. For this reason we have established a long-term microgravity program, which will be described next.

4.2 PK3-Plus

PK-3 Plus shall replace PKE Nefedov on the International Space Station ISS end of 2005. Assembled in a safety container of 200 l., it has the same volume as the predecessor, however with vastly better performance. The plasma chamber is a novel design with particular attention given to minimum internal temperature gradients thus avoiding the thermophoretic effect. The new instrument gives the choice of two gases. Combining better vacuum technology with a novel gas-flow system, the gas purity could be enhanced 10 to 100 times. Experience teaches that gas purity is a decisive parameter in complex plasma research. Six rather than two microparticle dispensers provide a comprehensive choice of particle sizes and materials. Four progressive scan CCD cameras in place of two conventional cameras monitor both particles and the plasma glow in a calibrated brightness scale, improved resolution and twice the frame rate. In conjunction with hard disc video recording the overall performance of the video system is vastly improved with regard to image quality time resolution and storage volume.
The electronics, which controls the plasma diagnostics, the manipulation and other features, too many to enumerate them all, has been completely redesigned. It provides high precision measurements of a number of parameters, including the ionisation density and the RF discharge power, not measured in the previous payload.
Three models are being built for PK-3 Plus:

I. Science Model (in operation already for 18 months and tested in parabolic flights).
II. Qualification, Trainings and Flight Spare Model (also already in operation).
III. Flight Unit (assembled to 70%). This unit will be commissioned in summer 2005 and launched with a "Progress" transporter in Dec. 2005.

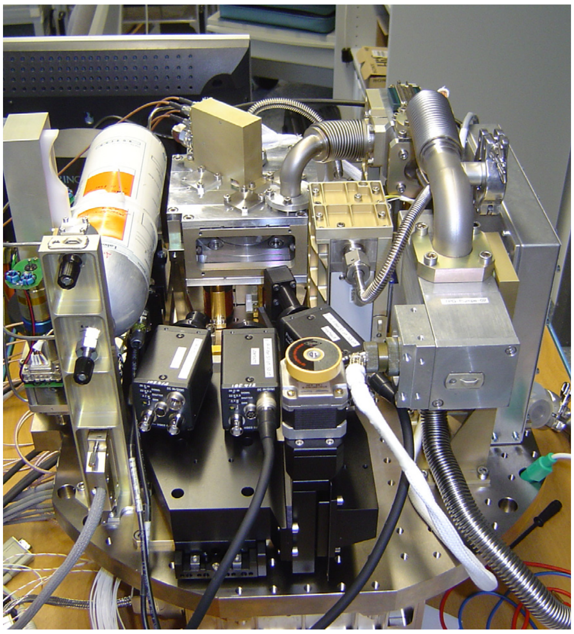

Fig. III.A.46: Image of the PK-3 Plus flight model.

PK-3 Plus, as its precursor PKE-Nefedov, is a joint Russian/German scientific project. The collaborating science teams are from the Russian Academy Institute for High Energy Densities in Moscow and from CIPS-MPE. The scientists and engineers from both institutions have been working since 2002 on the realisation of PK-3 Plus.
At the request of ESA, the Russian/ German science team agreed to make PK-3 Plus available for research to other scientists from ESA countries, thus providing much-needed

new science impulses to the community within ESA's interim ISS utilisation programme.

PK-3 Plus is an ideal laboratory for investigating complex plasmas on the ground and under microgravity conditions. The science model, which will stay at CIPS/MPE is fully functioning and equipped additionally with more diagnostics and other features. For example, it requires only slight changes to the plasma chamber and a temperature gradient can be established between the lower and the upper electrode allowing particle levitation of a certain size through the thermophoretic force. This opens up a broad field of interesting scientific observations, two of which are mentioned below.

The Crystallisation Process

The discovery of the crystallisation of complex plasmas triggered enormous interest in laboratory complex plasma research at the fundamental level. Plasma crystal features like defect migration, the melting but also wave propagation in the crystalline and liquid phase were investigated in detail and showed the special properties and possibilities of complex plasmas mentioned above.

Under special conditions (e.g. very small microparticles) it was found that the small microgravity plasma chamber can be used to produce significant 3-dimensional plasma crystals even under gravity conditions. The special field lines, the symmetry and the direct symmetrical coupling of the rf-voltage to both electrodes are responsible for that. In the first example we studied the kinetics of the crystallisation process in real time. A plasma crystal is first melted into a disordered liquid-like phase (by a short pulse of increased discharge power). Afterwards, the system starts re-crystallizing. Sometimes, this results in homogeneous nucleation, but often it occurs in the form of a crystallization front. Fig. III.A.47a shows colour-coded particle traces observed in the experiment during $\approx$ 1 s (side view), which give an impression of the particle temperature. The crystallization front is fairly narrow (about 3-4 interparticle distances). The temperature of the liquid phase is about twice that of the crystalline phase, indicating that the observed condensation is non-equilibrium. One can also see the interface between different crystalline domains, which has a narrow width (2-3 lattice planes) and a substantially higher temperature than the crystal domains themselves – direct observation of interfacial melting. Fig. III.A.47b shows molecular dynamics simulations of the crystallization front, also revealing the qualitative features observed in experiments. The front has a well developed fractal structure, with an abrupt temperature drop within the transition layer (blue) from the liquid/gaseous (green-yellow) to the crystalline (black) phase.

Fig. III.A.48 (molecular dynamics simulations) shows how the temperature (kinetic energy, red line) of microparticles decays with time during the crystallisation.

Initially, when the system is in a weakly coupled phase, the temperature T exceeds or is about equal to the energy of electrostatic interaction. At this stage, T decreases rapidly due to neutral gas friction, and the slope of the decay obeys the pure Epstein drag law for an individual particle. However, as T decreases further and consequently the coupling parameter Γ_{ES} grows, the decay becomes much slower. In the crystalline regime, when Γ_{ES} exceeds the critical value corresponding to the "solid-liquid boundary" (see phase diagram shown in Fig. 3), the sequence of transitions from one (metastable) configuration of particles to another (lower energy level) can take from a few seconds to dozens of minutes. Energy and structure relaxation at this stage is solely

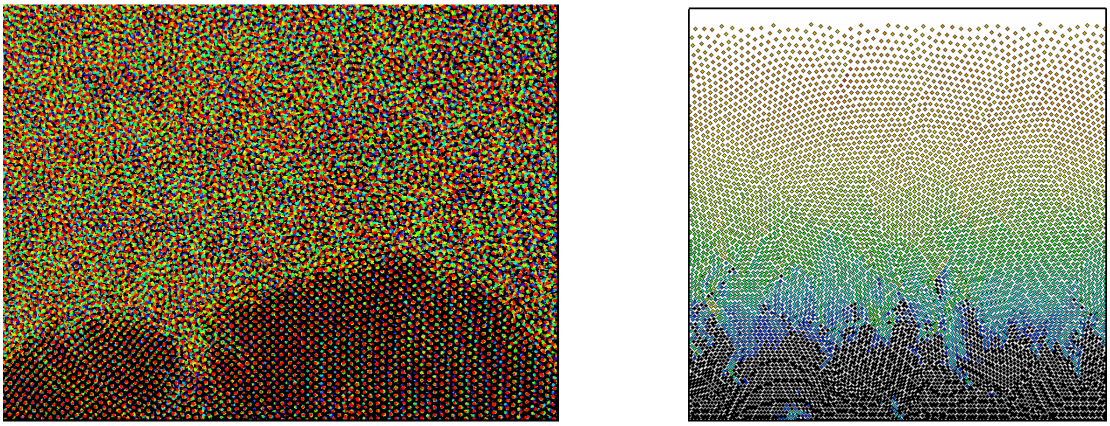

Fig. III.A.47: (a) Crystallization wave observed in the experiment (particle positions are colour-coded from green to red, i.e., cooler particles appear redder, hotter are multicoloured). (b) Crystallization wave in molecular dynamics simulation (particle temperature is colour-coded, temperature rises from black to yellow).

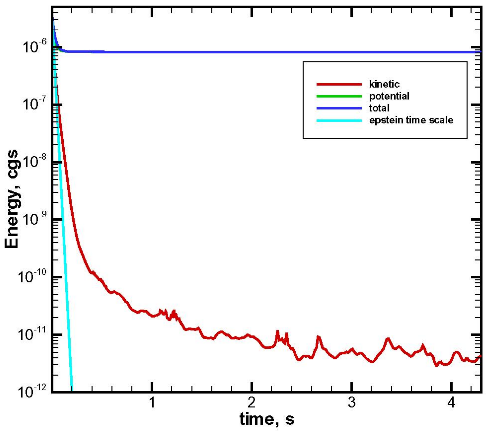

Fig. III.A.48: Decay of the particle temperature during the crystallisation (molecular dynamics simulation).

governed by transport properties of the crystal itself.

Liquid plasma flow

The second experiment presented here was performed in a slightly modified PKE chamber, with a temperature gradient producing a thermophoretic force capable of lifting the microparticles against gravity in an outer ring and introducing a toroidal flow pattern of the complex plasma. (The importance of the thermophoretic force and its quantitative effect was discovered in experiments performed on the ISS.) Fig. III.A.49a shows the steady axially symmetric flow of the complex plasma around an obstacle (void). Surrounding the void upstream, a laminar boundary layer is formed. Downstream is a wake region. The boundary layer covers most of the void surface, the detachment line is remarkably stable. In the wake, there exist two toroidal vortex regions (1) and (2), a compressed quasi-crystalline layer (3), and a "buffer zone" between the vortices (4). The wake and the laminar flow regimes downstream are separated by a mixing layer. Fig. III.A.49b is a zoomed snapshot, which shows that the boundary becomes unstable on kinetic (particle) scales. The microscopic driving mechanism for the observed instability is identified as a Rayleigh-Taylor instability inertially driven by (large-angle-scattering) collisions between particles. This also has been confirmed by molecular dynamics simulations. A numerical simulation of the mixing layer is shown in Fig. III.A.49c. Particle velocities are color coded, increasing from blue to red. The numerical parameters are similar to those in the experiment. The traces show particle displacements during 0.06 s which corresponds to the exposure time in the experiment.

4.3 PK-4

PK-4 is a follow-up project of PKE-Nefedov and PK-3Plus. Other than its predecessors, PK-4 utilizes mainly a DC discharge plasma, which can optionally be combined with one or two RF inductive discharges. This offers in particular the capability to perform kinetic studies of a great variety of dynamical phenomena in complex plasmas, such as laminar shear flows and their transition into the turbulent regime, formation of waves and their propagation, collision experiments and shock wave generation, flow through nozzles and so on.

PK-4 is planned to succeed PK-3 Plus on the ISS around 2007. A science insert of the PK-4 type is also scheduled to be included in the planned ESA cornerstone facility IMPACT, which contains a Plasma Laboratory, the "International Microgravity Plasma Facility" (IMPF) and could be launched (to the ISS) in 2009.

Within a DLR funded predevelopment phase, which started in August 2002, three identical prototype PK4 discharge chambers were developed and their functional properties investigated (Fig. III.A.50). One of these chambers is used by our collaborating group at IHED in Moscow, the second serves as laboratory chamber in the MPE lab. Both lab chambers can be operated in any orientation with respect to the gravitational force. The third

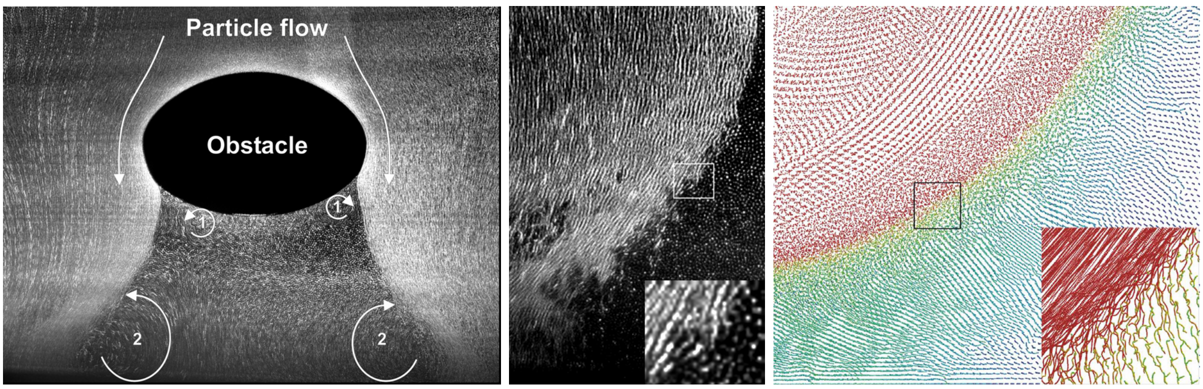

Fig. III.A.49: (a) Flow of liquid complex plasmas around an obstacle, (b) zoom at the mixing layer, and (c) numerical simulation of the mixing layer.

chamber forms the central part of the PK4 parabolic flight rack (Fig. III.A.51). Up to now, the latter has been operated under microgravity conditions on two ESA parabolic flight campaigns onboard the A300 ZERO-G airplane with a total of 180 parabolas, each 20 seconds in duration.

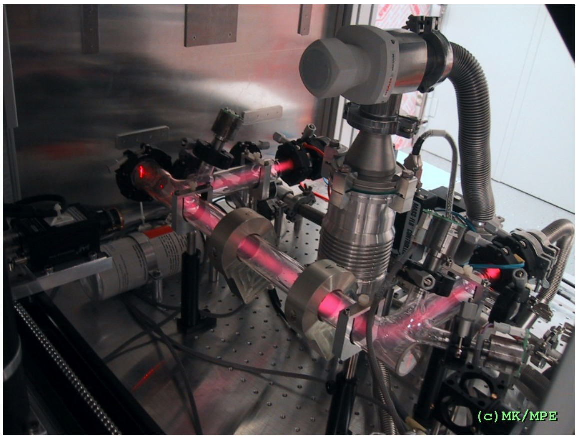

Fig. III.A.50: The PK4 plasma chamber, mounted inside the parabolic flight rack, tube diameter is 30 mm.

Fig. III.A.51: PK4 parabolic flight rack inside the ZERO-G airplane in the front and PK-3 Plus science model in the back of the image.

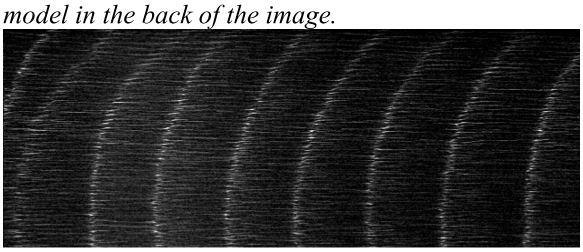

Fig. III.A.52: The transition to unstable flow with a clear wave behaviour occurs at a certain threshold pressure. The transition is a manifestation of the ion-dust streaming instability, caused by the relative drift between the dust and the ion component. This transition allows the estimation of dust charge from a linear dispersion relation, which describes the transition of the particle flow to the unstable regime at the experimentally found pressure threshold.

So far PK-4 activities were dominated by basic development tasks, but nevertheless have already led to several publications. An impression of the variety of studied phenomena can be obtained from a few selected images Fig. III.A.52 to Fig. III.A.56. Note that the first three pictures shown (Fig. III.A.52 to Fig. III.A.54) were taken in the lab while Fig. III.A.55 – 56 were obtained under microgravity conditions.

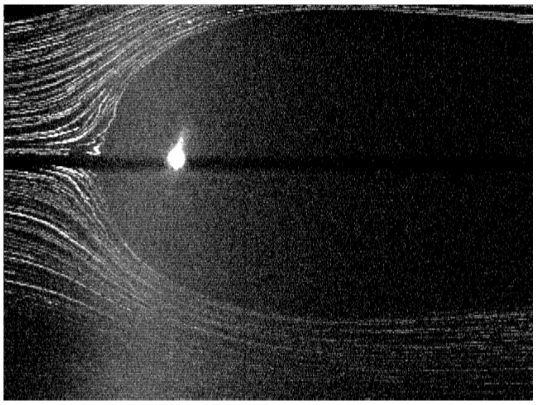

Fig. III.A.53: Laminar flow around an obstacle (charged wire). Superposition of 10 images, covering a time of 83 msec. Note that the stagnation "point" really is pointlike (dimension ~r^{-2} particle separations).

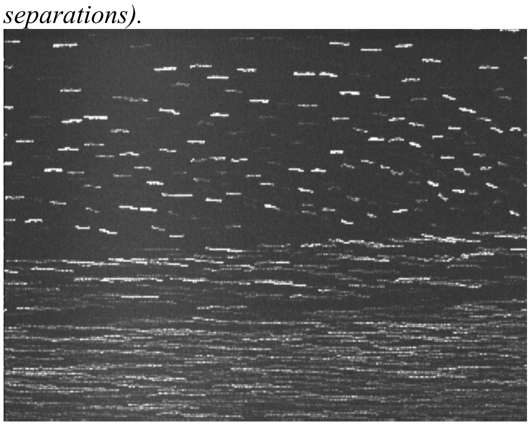

Fig. III.A.54: Example of laminar shear flow. Superposition of several consecutive images reveal that the flow velocity does not vary continuously across the shear - instead it breaks up into 3 distinct regimes with different flow velocities (top to bottom) 2.6, 5.4 and 8.7 mm/sec.

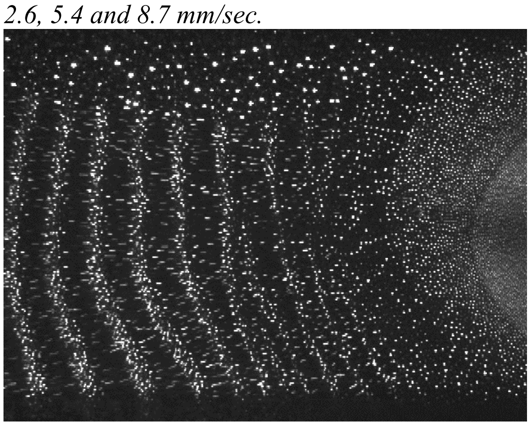

Fig. III.A.55: Oscillations of 6 micron particles close to particles is confined in the rf induced discharge to the right (1.2 and 3.4 micron).

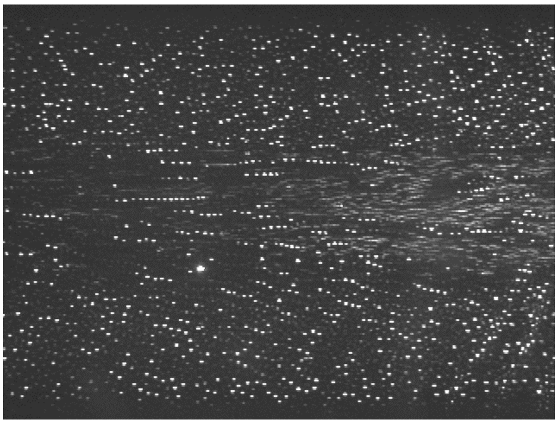

Fig. III.A.56: Particle chain formation in a counterstreaming complex plasma – a non-equilibrium phase transition.

Measurements of the particle charge

The particle charge is one of the most important characteristics of complex (dusty) plasmas, which determines the interaction of particles with the plasma electrons and ions, electromagnetic fields, interaction between the particles themselves, etc. Not surprisingly, the charging of dust particles is actively investigated both theoretically and experimentally. We determined the dust particle charge experimentally in a bulk dc discharge plasma using the PK-4 facility. The experiments were performed in a wide pressure range from ~20 up to ~150 Pa. The charge was obtained by two independent methods: One based on analysis of the particle motion in a stable particle flow (force balance condition) and another on transition to unstable flow (solution of the dispersion relation). The experiments with relatively small dust particles (0.6 μm in radius) were performed in ground-based conditions. Some experiments with larger particles (1.7 and 3.4 μm in radius) were also performed in microgravity conditions during the 36th ESA parabolic flight campaign (March, 2004). To have an independent verification of the charge estimated from experiments, molecular dynamics (MD) simulations of particle charging for conditions similar to those of the experiment were performed. The results of two experimental methods and MD simulations show good agreement (see Fig. III.A.57). The charges obtained are considerably smaller than those predicted by the collisionless orbit motion limited (OML) theory (especially, at higher pressures). This serves as an experimental confirmation that ion-neutral collisions significantly affect particle charging in the regime when the ion mean free path is comparable to the plasma screening length.

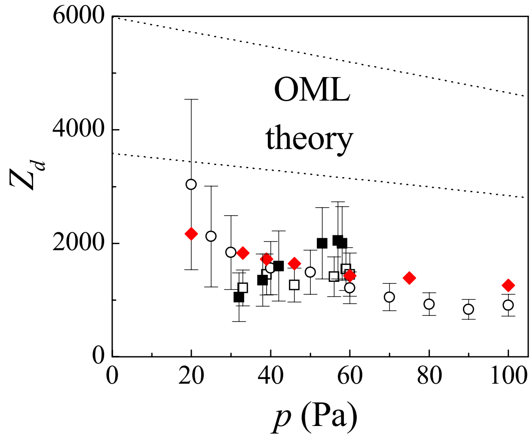

Fig. III.A.57: The particle charge obtained from experiments [force balance for low number of injected particles (open circles); force balance for pressures above the threshold (open squares), solution of dispersion relation (solid squares)], and from MD simulations (red diamonds). The area between the two dotted lines corresponds to the charge given by the OML model for Havnes parameters between P = 0.2 (upper line) and P = 3 (lower line)

Nanofluidics in PK-4

The PK-4 chamber makes it possible to study fluids at the kinetic level. If one compares the dimensions and parameters of such a fluid with water, one finds that streams of complex plasmas are similar to water streaming at high speeds, visualized at the molecular level. In the nanofluidic experiments in PK-4 we force particles through a Laval-nozzle. In this experiment we are able to distinguish between single particle movement through the nozzle and the collective effect that is well-known in rocket-engines technology. In a first step we simply built a "nozzle" by forming a plasma with a central narrow opening using pairs of copper electrodes with applied rf-voltage (Fig. III.A.58).

Fig. III.A.58: PK-4 chamber in vertical position with two pairs of copper electrodes working as "nozzle".

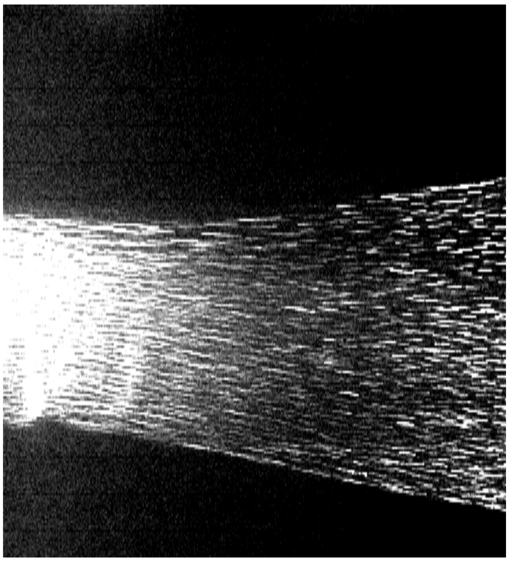

Fig. III.A.59: Particles flowing from right to left through a Laval-nozzle with the nozzle centre at the narrrowest point at the left side of picture (Gravity is pointing to the left).

The flow of particles through this nozzle can be seen in Fig. III.A.59. From the video data we obtained the velocity of the particles. We compared the mean velocity of a stream containing of the order of 1000 particles in the flow cross section with a single particle going through the nozzle. Fig. III.A.60 shows, as one would expect, that the velocity of a single particle remains almost constant as it passes through the nozzle, whereas the mean velocity of the particle cloud increases substantially by almost a factor 2. This is a strong evidence of a collective acceleration process. In addition, the feature at z=15 mm suggests the formation of a weak reverse shok.

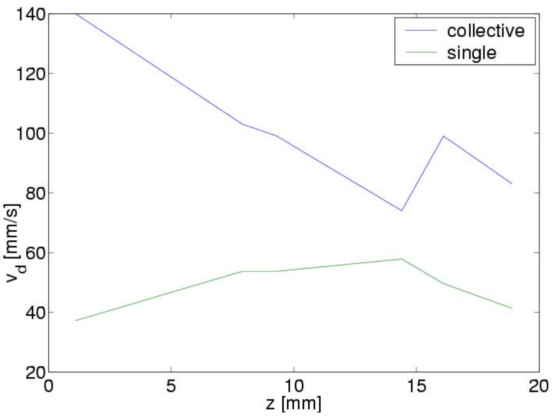

Fig. III.A.60: Comparison of velocities of a single particle with a particle cloud while passing through the nozzle.

More experiments have to be performed to find the transition between single particle movement and collective behaviour.

4.4 IMPF/IMPACT

The International Microgravity Plasma Facility is one of the two facilities of the ESA cornerstone Laboratory IMPACT (International Microgravity Plasma, Aerosol and Cosmic dust Twin). It is designed as a modular facility consisting of sub-units for easy accommodation. IMPACT, as the master facility, delivers the rack structure, power, vacuum, cooling, experiment control via laptop and/or telescience, data storage etc. The experimental inserts are defined by the scientific community on evaluated proposals. For IMPF two kinds of different plasma chamber inserts are foreseen: an rf-IMPF insert and a dc/rf combined insert, both very different in their set-up and scientific goals. The rf-IMPF insert consists of a parallel plate plasma discharge, similar to the PKE-Nefedov and PK-3 Plus experiments. This insert is designed to investigate strongly coupled plasmas – mainly in the crystalline state including the solid-liquid phase transition. The second insert consists of a long dc-tube discharge with rf-coils or electrodes used for manipulation and trapping. This set-up will open up a new field of research under microgravity, liquid complex plasmas.

The IMPF facility proposal was selected following an ESA Announcement of Opportunities AO 1998 (Principal Investigator or Team Coordinator G. Morfill, with participating scientific groups from 13 international institutions). In the subsequent review process, the proposal was given the highest rating "outstanding". Since then the Institute (MPE) has been working on the implementation, partly financed by DLR and ESA, supported by an international advisory board and the space industry.

In a second International AO 2000, the ISS related agencies called for experiment proposals for existing or planned facilities. From a total of over 100 proposals world wide, five received the top grade "outstanding", of those three IMPF proposals took the first three places.

In May 2002 it was recommended by the facility science teams to combine IMPF with another outstandingly rated facility ICAPS (Interactions in Cosmic and Atmospheric Particle Systems) into one microgravity research facility – IMPACT. Since then IMPACT has become an ESA cornerstone project.

The IMPACT Laboratory consists of an electronic and mechanical support system which delivers the rack structure, power, gas and vacuum, cooling, control, data storage etc. and two experiment inserts, one for the scientific field of complex plasmas and the second one for the field of dust and aerosol physics (see Fig. III.A.61, which shows the sketch of the IMPACT

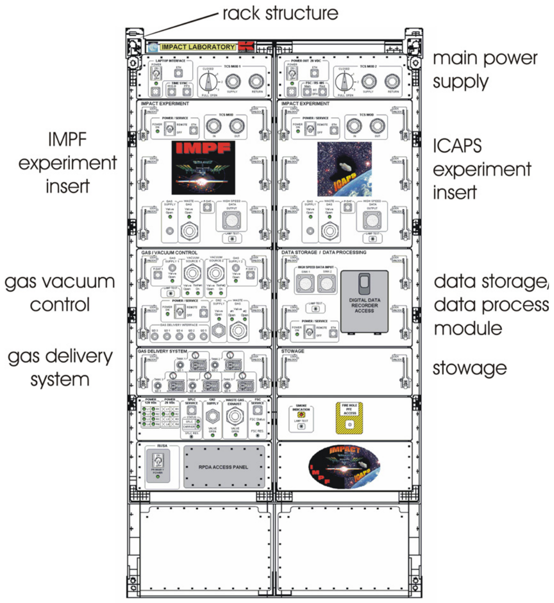

Fig. III.A.61: The IMPACT laboratory with the different modules. The major parts are mentioned in the Figure.

laboratory). For further information, see http://www.mpe.mpg.de/theory/plasma-crystal/.

The projects PKE-Nefedov (grant no. 50WM9852), PK-3 Plus (grant no. 50 WB 0203), PK-4 (grant no. 50 WP 0204) und IMPF-pre development (grant no. 50WM0038) have been supported by DLR (BMBF) within „Research under Microgravity" and the Adaptive Electrodes (grant no. 50TK0001 and 50 RT 0207) within the "First Chance Program". A Topical Team is founded by ESA to keep the IMPF scientific advisory board in operation.

III. B. Low Temperature Plasma Science

The Low-Temperature Plasma Physics group (LTPP group) at IPP is concerned with the application of low-temperature plasmas for surface treatment, such as deposition of thin films, erosion, and surface modification. The main focus is on the investigation of plasma-surface interaction processes of hydrogen and hydrocarbon plasmas (e.g. CH_4) with hydrocarbon films. These processes play an important role in the transport of carbon in the boundary layers of fusion experiments.

Summary of Previous Work (Period 2000 till 2001)

In the field of thin film characterisation an improved theoretical description of infrared spectra was developed and applied to the analysis of amorphous, hydrogenated carbon films (a-C:H). It was shown that the infrared absorption spectra and the resulting k spectra in the range of the CH vibrational bands around 3000 cm^{-1} are quite sensitive to the film structure. These k spectra can be considered as fingerprint of the type of a-C:H film.
Interaction of hydrocarbon radicals, atomic hydrogen, and ions with a-C:H surfaces was studied in a dedicated UHV particle-beam experiment (MAJESTIX) which is unique in the world. The experiment is equipped with two independent radical sources and an ion source for a mass-selected ion beam. These radical beam sources have previously been developed and characterised in the LTPP group. Growth or etch rates during exposure of a sample to the radical beams are measured by in-situ real-time ellipsometry and the chemical structure of the surface is measured by in-situ real-time infrared spectroscopy. One topic that was thoroughly studied is the interaction of thermal radicals with a-C:H surfaces. The temperature dependence of CH_3 sticking was measured in the temperature range from 300 to 800 K. The synergistic interaction of atomic hydrogen and CH_3 radicals leads to an enhancement of the sticking of CH_3 by up to about two orders of magnitude if the surface is exposed to a flux of H simultaneously to CH_3. It was shown that a key step for the growth of polymer like a-C:H films is the hydrogen elimination due to interaction of the surface with atomic hydrogen. A rate equation model was developed to describe the flux dependence and dynamics of a-C:H film growth from radical beams. The parameters of the model were estimated applying Bayesian probability theory (collaboration with the data analysis group).

The MAJESTIX device was also employed to investigate the erosion of a-C:H films due to combined irradiation with Ar^+ ions and atomic hydrogen. The simultaneous interaction of energetic species (ions) and thermal H radicals causes a significantly enhanced erosion rate which is much higher than the simple sum of the rates of the individual processes. This synergistic interaction process is termed *Chemical Sputtering*.
A new low-temperature plasma experiment was constructed (PAUKE). The plasma is produced by inductive coupling at a frequency of 13.56 MHz. The experiment is equipped with a number of surface and plasma diagnostics. A commercial Langmuir probe is applied to measure electron temperature and density and a plasma monitor (= energy and mass analyser) is used to determine charged and neutral fluxes reaching the substrate surfaces. Growth and erosion of layers are investigated by real-time, in-situ ellipsometry and in-situ infrared spectroscopy.

New results from the period 2001 to 2004 will be presented in the following sections.

1 Basic Studies of Thin-film Erosion Processes

1.1 Synergistic erosion of C:H surfaces by energetic argon ions and thermal hydrogen atoms

Erosion of hard a-C:H films by simultaneous exposure to an Ar^+ ion beam and a beam of thermal, atomic hydrogen (*chemical sputtering*) was investigated by in-situ real-time ellipsometry in the MAJESTIX device. Experiments were performed at room temperature, where erosion by atomic hydrogen is negligible. The energy of the Ar^+ ions was varied between 20 eV and 800 eV. Bombardment of the film with Ar^+ ions alone yields physical sputtering at energies higher than about 100 eV (Fig. III.B.1). Below this energy no physical sputtering is observed. The observed energy dependence of physical sputtering is in agreement with TRIM.SP computer simulations assuming a surface binding energy of 3.0 eV (typical of rough graphite surfaces is 4.5 eV). However, if both beams are switched on, a strong increase of the erosion rate by a factor of more than 5 is observed at an ion energy of 800 eV, and even at 20 eV substantial erosion occurs which significantly exceeds that due to atomic hydrogen alone.
In the literature low-energy erosion of carbon at room temperature due to hydrogen ions is explained by so-called *kinetic hydrocarbon emission*: Chemical reaction of hydrogen leads

to creation of hydrocarbon groups which are weakly bound to the surface and, hence, sputtered even at energies below the threshold for physical sputtering of the original material. To test the consistency of this explanation with our results, TRIM.SP calculations were performed for different surface binding energies of carbon. In order to simulate erosion yields of the order of those found experimentally, a surface binding energy of ≈0.1 eV has to be assumed (see pink line in Fig. III.B.1), which is unreasonably low. Consequently, kinetic hydrocarbon emission was discarded as explanation for the observed chemical sputtering process.

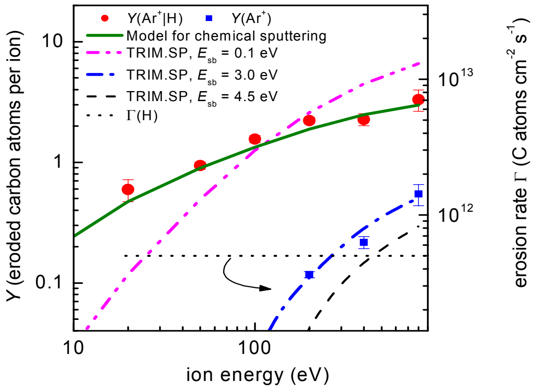

Fig. III.B.1: Physical and chemical sputtering of a-C:H layers due to interaction with atomic hydrogen and argon ions as a function of the ion energy. Blue squares show the physical sputtering yield due to argon ions alone. The black and blue lines are TRIM.SP simulations for a surface binding energy of 4.5 and 3.0 eV, respectively. The black dotted line is the erosion rate (right hand scale) for atomic hydrogen alone. Red circles are the chemical sputtering yields for the combined interaction of atomic hydrogen and argon ions (flux ratio (H/ion flux) = 400). A TRIM.SP simulation with a surface binding energy of 0.1 eV cannot describe the measured energy dependence. The green line is the result of the chemical sputtering model.

Alternatively, the following mechanism of *chemical sputtering* was proposed: Incident ions break C—C bonds within their penetration range. Atomic hydrogen, which is known to permeate a few nanometres into a-C:H, passivates the broken bonds. By repeated bond breaking by ions and passivation by hydrogen, volatile molecules are formed at and underneath the surface which thermally diffuse out of the film. The proposed mechanism is in agreement with various experimental observations reported in the literature.

Based on this microscopic mechanism we devised a framework for understanding chemical sputtering of carbonaceous surfaces, which allows a quantitative description of the ion energy and ion species dependence of chemical sputtering in the presence of atomic hydrogen (see green model curve in Fig. III.B.1). This model is extrapolated to other ion species relevant to plasma surface interaction in nuclear fusion devices such as He^+, Ne^+, H^+, D^+, T^+, and N^+. Some results of these model calculations are presented in Fig. III.B.2.

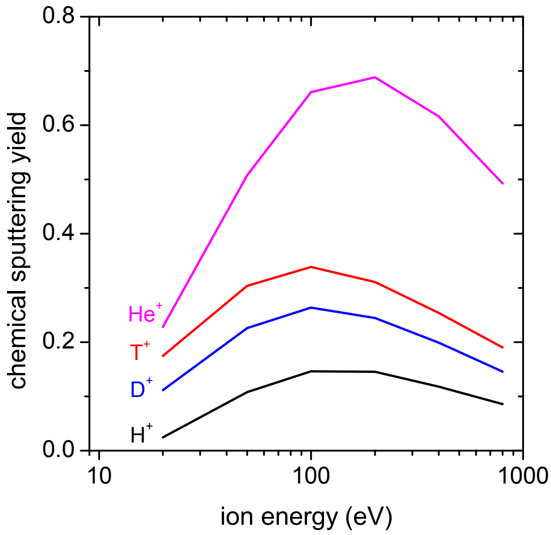

Fig. III.B.2: Modelling results for the erosion yield (eroded carbon atoms per incident ion) as a function of ion energy for the erosion of a-C:H layers due to a simultaneous bombardment with ions and a flux of atomic H for different ion species (He+, H+, D+, T+). A flux ratio of 400 (H/ion flux) as for the argon experiment shown in Fig. III.B.1 was assumed.

In addition, the flux dependence, i.e. the dependence of the chemical sputtering yield, Y(Ar|H), on the H atom to Ar^+ ion flux ratio R (= j_H/j_{Ar}), was investigated for an argon ion energy of 200 eV. Y decreases with decreasing R. The data can be well described by a simple rate equation model. The model suggests that saturation of Y occurs only for very high values of R (R > 1000, saturation value of Y ≈ 3).

1.2 Synergistic erosion of C:H surfaces by energetic neon ions and thermal hydrogen atoms

Similar to the experiments presented in the preceding section, new experiments with neon ions were performed. The data are shown in Fig. III.B.3. In general, the same observations as for argon are made. Interaction of the ions alone (physical sputtering) is well described by the TRIM.SP calculations. The combined interaction of ions and H causes an erosion rate that is much higher than the sum of the individual processes. The model curve shown in Fig. III.B.3 is a prediction that is solely based on the model parameters fitted to the Ar data. The good agreement of the data with the model predictions is quite remarkable l. It is further interesting to note that the rates for Ar and Ne are very similar although the masses of both species differ significantly. This is a consequence of the change in the collision cascade due to differences in stopping power, penetration range, and cross section for nuclear collisions. These effects are inherently included in the model due to the simulation of the collision physics by the TRIM.SP computer code. These new neon data represent an excellent confirmation of the devised chemical sputtering model.

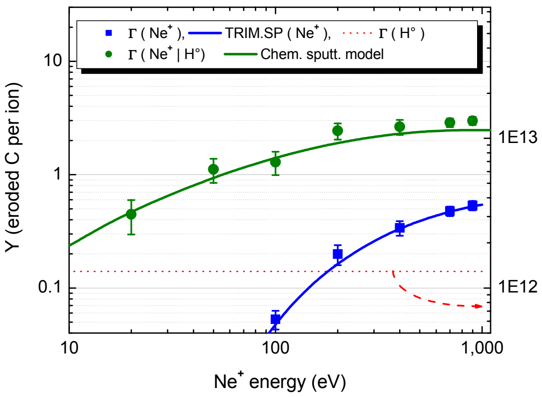

Fig. III.B. 3: Physical and chemical sputtering of a-C:H layers due to interaction with atomic hydrogen and neon ions as a function of the ion energy. Blue squares show the physical sputtering due to neon ions alone. The blue line is a TRIM.SP simulation for a surface binding energy of 2.8 eV. The red dotted line is the erosion rate (right hand scale) for atomic hydrogen alone. Green circles are the chemical sputtering yields for the combined interaction of atomic hydrogen and neon ions. The green line is the result of the chemical sputtering model. H-atom-to-ion flux ratio ≈ 250.

1.3 Synergistic erosion of C:H surfaces by energetic nitrogen molecular ions and thermal hydrogen atoms

In addition to the experiments with noble gas ions, where the energetic species are chemically unreactive, we started first experiments using chemically active ion species. Some initial measurements using molecular H_2^+ ions showed reasonable agreement with the chemical sputtering model predictions. Very recently, new experiments with molecular nitrogen ions (N_2^+) were performed. These data are presented in Fig. III.B.4. In contrast to the case with noble gas ions, the erosion due to N_2^+ ions alone cannot be explained by TRIM.SP calculations. The erosion yields for N_2^+ ions are significantly higher than the predicted physical sputtering yields and show in contrast to them no clear energy dependence over a wide energy range (50 to 900 eV). This is a clear signature of chemical sputtering. We assert, interaction of N_2^+ ions with a-C:H surfaces causes chemical sputtering similar to H_2^+ ions alone. In principle, this effect is known from literature. In ion beam irradiation of a-C:H surfaces with nitrogen ions, $C_xH_yN_z$ species have been identified as erosion products by mass spectroscopy. This is a clear indication of a chemical reaction at the surface. Similar observations have been made in the plasma erosion of a-C:H layers using nitrogen containing plasmas. So far, there has, however, been no systematic investigation of the energy dependence of this process. If the a-C:H surfaces are exposed to a simultaneous flux of N_2^+ ions and atomic hydrogen, we again find a significantly enhanced erosion. The agreement of the data with the chemical sputtering model is acceptable, but the measured yield is systematically higher than the model predictions. This deviation might be due to the chemical activity of nitrogen.

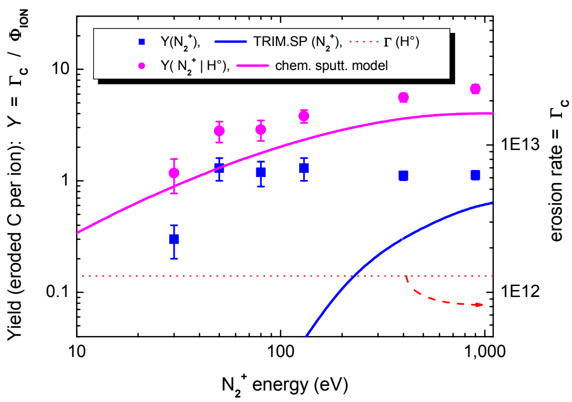

Fig. III.B.4: Sputtering of a-C:H layers due to interaction with atomic hydrogen and nitrogen ions as a function of the ion energy. Blue squares show the sputtering due to N2+ ions alone. The blue line is a TRIM.SP simulation for a surface binding energy of 2.8 eV. The red dotted line is the erosion rate (right hand scale) for atomic hydrogen alone. Magenta circles are the chemical sputtering yields for the combined interaction of atomic hydrogen and N2+ ions. The magenta line is the result of the chemical sputtering model. H-atom-to-ion flux ratio ≈ 250.

In summary, we can state that the combined interaction of atomic hydrogen and energetic ions leads to a synergistic enhancement of the sputtering yields called chemical sputtering. In addition to the enhanced yields, the energy threshold for chemical sputtering is much lower than for physical sputtering. A microscopic mechanism for chemical sputtering was developed. Based on this microscopic mechanism we devised a mathematical model, which allows a quantitative description of the ion energy and ion species dependence of chemical sputtering in the presence of excess supply of atomic hydrogen. The agreement of this chemical sputtering model with experimental results is excellent for the case of noble gas ions (Ar, Ne) and reasonable for the case of chemically active species (H_2^+, N_2^+).

2 Plasma Studies

2.1 Inductively-coupled plasma device for in-situ growth studies (PAUKE)

In a new plasma experiment set up in 2001 the plasma is produced by inductive coupling at a frequency of 13.56 MHz. In this device, the deposition of a-C:H layers from pulsed discharges is investigated. One aim of this work is to identify the main growth precursors that contribute to the growth of amorphous hydrocarbon (a-C:H) films in pulsed methane discharges. To control the energy of the impinging ions a self-bias voltage can be applied to the substrate holder with a second rf generator. Growth and erosion of layers are investigated by real-time, in-situ ellipsometry. In addition to the plasma monitor that allows detecting ions and neutrals impinging on the substrate surface a molecular beam mass spectrometer setup was developed to determine the fluxes of reactive radicals to the chamber walls. A multi channel scaler allows the time-resolved monitoring of the fluxes. As far as possible all measurements were quantified.

Measurements were performed in different hydrocarbon precursor gases with a plasma on-time τ_{on} = 3 ms and varying plasma off-times τ_{off}. To change the deposition conditions the following experimental parameters were changed: plasma off-times τ_{off}, source gas fluxes, pressures, and self-bias voltages at the substrate. The measured thickness gain per pulse can be converted into the number of carbon atoms incorporated per pulse.

The parameter that governs the plasma chemistry and with it the whole deposition process, is the mean energy per source gas molecule E_{mean}. It is determined by the absorbed rf power, P_{ICP}, the duty cycle, *d.c.* = $\tau_{on}/[\tau_{on} + \tau_{off}]$, and the flux of the source gas, Φ_{source}:

$$E_{mean} / molecule = P_{ICP} \cdot d.c. / \Phi_{source} .$$

Some results for the number of carbon atoms incorporated per pulse are plotted in Fig. III.B.5. The plot contains data from a large variety of experiments where different process parameters were changed over a wide range. It is quite remarkable that in spite of this large variation all measurements for a certain pressure lie on the same curve. This is at least an indication that E_{mean} is a useful parameter to characterise these types of plasmas. Experiments for 2 and 3 Pa fall on one common curve. In this case, the carbon incorporation shows a maximum around 20-30 eV/molecule The results for 10 Pa deviate clearly. This is an indication of a different plasma chemistry at increased pressures.

Densities of the majority of the species in the plasma were measured by quantitative mass spectrometry (see Sect. 3 below). Fig. III.B.6 shows the measured densities of hydrogen and hydrocarbon molecules with up to 4 carbon atoms. Since pure methane is introduced into the chamber, all other species are produced in the plasma or at the surface. With increasing E_{mean} we find an increasing consumption of the precursor gas methane (CH_4) and accordingly a significant production of hydrogen. All measured heavier hydrocarbon species (C_xH_y, x>1) show a very similar behaviour: For low E_{mean} they rise steeply with increasing E_{mean}. Then they exhibit a maximum around 20-30 eV/molecule and decrease again for higher values of E_{mean}. This maximum in the density of heavier hydrocarbon species (C_xH_y, x>1) coincides with the maximum of the number of incorporated carbon atoms as shown in Fig. III.B.5. The decrease following the maximum is caused by the depletion of the source gas.

Quantitative measurements of the ion and methyl radical fluences to the substrate show that these species contribute only about 10% to the growth. The observed growth can only be explained by highly reactive radicals, which do not need any surface activation of the film for incorporation. These species can either be formed directly from the source gas (preferentially for low <E>/molecule, where the source gas density is still high) or from heavier hydrocarbons (C_xH_y, x>1). The highly reactive radicals C and CH have, however, also a high reaction rate coefficient for gas phase recombination with CH_4. which produces either stable or less reactive species. One should therefore expect substantially lower growth yields at low E_{mean} for higher pressures. This can also be clearly seen in Fig. III.B.5.

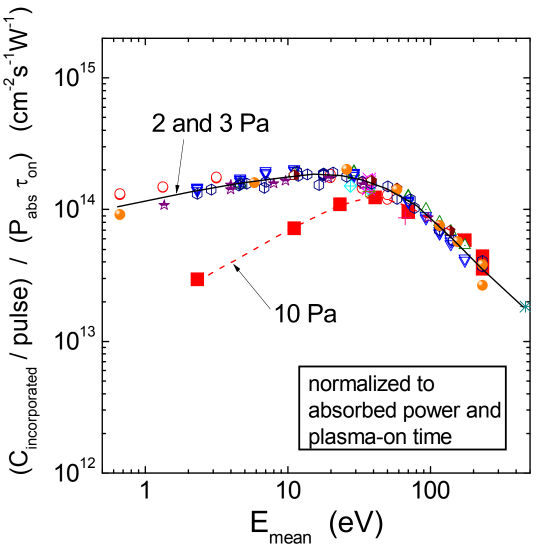

Fig. III.B.5: Number of incorporated carbon atoms per pulse normalized to the absorbed power and plasma-on time for a variety of different plasma parameters. Different symbols indicate series in which different parameters were changed. Process parameters: gas flow 10 – 70 sccm, pressure = 2,3, and 10 Pa, absorbed rf power = 250 – 400 W, τ_{on} = 0.25 – 20 ms.

In addition to the densities of the stable C_xH_y molecules with $0 \le x \le 4$ shown in Fig. III.B.6, the radicals CH_3 and CH_2, and the ion fluences per pulse are measured. Comparing the absolute gas densities with growth rates global carbon and hydrogen balances are drawn. From the measured CH_3 density the fluences per pulse to the substrate of the radicals C, CH, CH_2 and CH_3 are deduced. From the gas densities of C_2H_2, C_2H_4, and C_2H_6 the fluences to the substrate of the radicals C_2H, C_2H_3 and C_2H_5 are estimated. The growth contributions of the ions and the different radicals are obtained by multiplying the fluences with the corresponding sticking coefficient. These growth contributions for the various species are presented in Fig. III.B.7 and compared with the film growth per pulse.

The growth contributions of CH_3 and CH_2 are negligible over the whole investigated process parameter range. The main growth precursor changes with E_{mean}: for E_{mean} < 10 eV growth is mainly caused by CH; hydrocarbon ions contribute here only about 10%. In the range of 10 eV < E_{mean} <100 eV the contribution of C_2H and C_2H_3 is dominant and only for E_{mean} > 100 eV C_xH_y ions come to play an important role.

Furthermore, the dependence of the film properties on the process parameters was investigated. The properties do not depend solely on the energy of the impinging ions, but also on the value of E_{mean}. The film properties are determined by the dissipated energy per incorporated carbon atom.

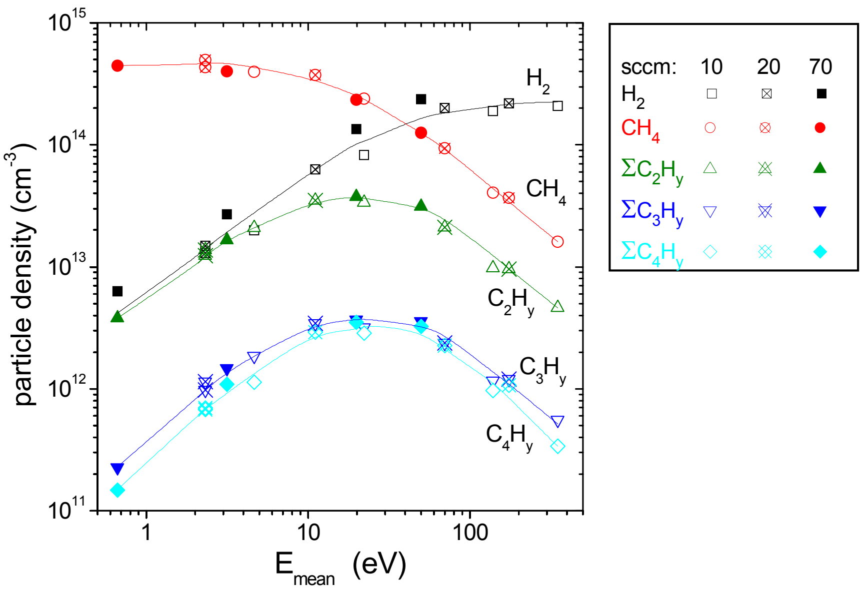

Fig. III.B.6: Neutral gas density of hydrogen and hydrocarbon species in methane plasmas. Hydrocarbon molecules with 2, 3, and 4 carbon atoms are always combined to one group. Lines are only a guide to the eye. Plasma parameters: gas flow = 10 – 70 sccm, pressure = 2 Pa, absorbed rf power = 300 W, τ_{on} = 3 ms.

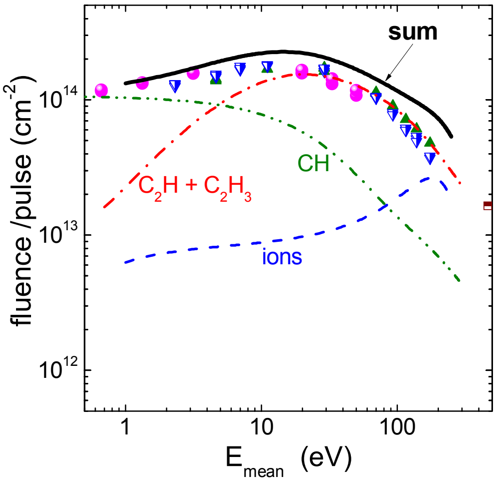

Fig. III.B.7: Contribution of different species from the plasma to the growth of a-C:H layers. The sum of the individual contributions is in good agreement with the measured growth per pulse. Symbols show measured deposition rate and lines the contributions of different species.
Plasma parameters: gas flow 10–70 sccm, pressure = 2 Pa, absorbed RF power = 300 W, τ_{on} = 3 ms.

2.2 Inductively-coupled plasma device for plasma diagnostics (PUMA)

A new low-temperature plasma device was installed. Following the development of an inductively-coupled plasma device for in-situ growth studies in 2001 this setup is mainly devoted to plasma diagnostics. The device is designed as an all-metal UHV experiment. An energy-dispersive mass spectrometer (Plasma Process Monitor PPM 422, Pfeiffer, Germany), a multi-grid retarding field analyzer (home-made), and a Langmuir probe are the main diagnostics applied to measure the fluxes of ions, stable neutrals, and radicals reaching the electrode surface as well as the particle energy distributions. The chamber and electrode geometry resemble the GEC (gaseous electronic conference) reference cell and are identical to the PAUKE setup. The plasma device as well as the diagnostics were installed and first experiments to characterize the Plasma Process Monitor were performed. The final aim is to combine the quantitative results obtained from both experiments to develop a well-founded description of the processes during growth and erosion of a-C:H films.

3 Quantitative Mass Spectrometry

An advanced method was developed in collaboration with the data analysis group that allows decomposing complex multi-component mass spectra based on Bayesian probability theory. In addition to the successful disentanglement of the thermal decomposition of azomethane discussed in the last report, the method was applied to further demanding examples. The decomposition of an artificial gas mixture clearly showed the capability of the method to handle incomplete data sets. It also demonstrated the knowledge gain that is achieved when calibration measurements are incorporated consistently. Applying the algorithm to the decomposition of mass spectra of low-temperature methane plasmas radicals could be identified with standard low-resolution mass spectrometry for the first time.
In addition to the above mentioned examples the algorithm was extended with a so-called model comparison module. It now allows one to decompose even mixtures containing an unknown number of constituents. Applying the principle of Occam's razor, the method penalizes complicated models for increasing the number of species unless they are supported by the data. As a result, it provides not only the point estimates for the species concentrations and improved values of the cracking coefficients together with their margin of confidence, but also the actual number of species reflected by the data. This feature makes it superior to all existing algorithms. The method was applied to disentangle mass spectra for methane, ethane, and acetylene plasma discharges (see, e.g., Fig. III.B.6). Signals of 34 mass channels produced by 10 different stable species were considered, ranging up to 60 amu. Uncommon species such as C_4H_2 were identified. In this example, Bayesian model comparison proved its power to extract information about trace gas elements in the overwhelming parent gas atmosphere.

4 Particle Growth Experiment (PAGE)

The behavior of particle clouds and particle growth in reactive plasmas is studied in a capacitively-coupled rf discharge. We use a three electrode assembly with the electrodes, 10 cm in diameter, being oriented horizontally. The rf power is applied to the upper electrode. To change the plasma conditions in the levitation region, a grided electrode is placed between the two lower rf electrodes. The particles are levitated between this grided and the lower electrode. To collect the particles directly from the particle clouds, we use a NFP (negatively charged fine particle) collector.

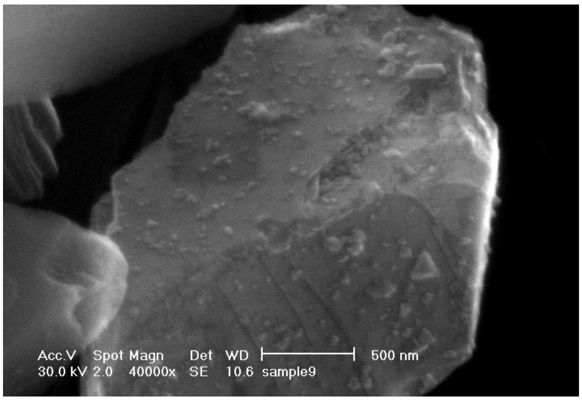

Fig. III.B. 8: SEM image of diamond particle.

Particles generated in the plasma without introducing seed particles are mainly amorphous carbon. Most of the particles levitated are flakes, delaminated from the surface of the upper two electrodes. However, we also find a few nano-diamond particles for the following growth condition, CH_4: 1 sccm, H_2: 20 sccm, temperature of electrodes: 800 K. If we pour diamond seed particles (average size ~2.8 micron) into the apparatus, we observe nucleation of new particles on their surface as shown in Fig. III.B.8 (size up to 100 nm after 8 hours plasma exposure at 800 K).

In order to increase the growth rate of diamonds and improve the quality, we have installed a tungsten hot filament between the grided electrode and the lower electrode. Inserting the W hot filament, three effects are expected. The first is to heat the particles more efficiently. The second is to produce atomic hydrogen more efficiently. The third is to decrease the electron temperature. Energetic electrons from the plasma are absorbed by the filament and replaced by low-energy electrons emitted from the filament because the hot filament system is electrically floating. First tests of this setup allowed levitation and treatment of diamond seed particles at filament temperatures of 2300 K.

IV. ANALYSIS, TECHNIQUES AND APPLICATIONS

A. Bayesian Probability Theory

1. Summary of Previous Work

Modern techniques of data analysis have to be applied whenever the inferential problem is ill-posed, different sources of information have to be combined, or model choice or model uncertainty is an issue. Scientific reasoning is always based on uncertain measurements and (vague) prior information from previous knowledge about the system of interest. Bayesian probability theory (BPT) provides a general and consistent frame for combining various kinds of information taking into account the degree of uncertainty of data, parameters and models.

The probabilistic method was applied to solve ill-conditioned inferential problems in plasma physics, surface science and astrophysics. The problems solved in time period 2000/2001 are summarized in this chapter whereas problems continued until 2004 will be discussed in the following sections.

An ubiquitous ill-posed problem is given by the deconvolution of a transfer function from measured data. Measured data are often deteriorated by a low temporal, spatial or energy resolution. The deconvolution was performed with the adaptive kernel method in the framework of BPT allowing for local smoothness properties. In unstructured regions of the spectrum the smoothness level is high whereas in regions where structures arise the smoothness level is low. This powerful multi-resolution technique for adaptively reducing the number of degrees of freedom of a form-free reconstruction effectively reduces noise fitting.

An increase of the temporal resolution of a sniffer probe for measuring the temporal development of hydrogen and deuterium fluxes at the plasma edge was achieved. A temporal transfer function was determined by deconvolving the signal of the sniffer probe in Wendelstein 7-AS with the known time distribution of the hydrogen pressure in the torus. The deconvolution of the obtained transfer function from a measured data set resulted in addition to a significant improvement of the temporal resolution also in the reduction of the time lag introduced by the retarding property of the sniffer probe volume.

Energy resolution is a permanent issue in accelerator-based solid state analysis. It is closely related to the reconstruction of the depth profiles from ion-beam experiments. The limited energy resolution of the ion-beam and the detector as well as energy-loss straggling and small-angle scattering effects restrict the mass and depth resolution. The adaptive kernel method was applied to enhance the resolution as well as to study the growth process of tetrahedral amorphous carbon (ta-C). Thin-film growth of ta-C is only possible with techniques involving energetic ions. ^{13}C depth profiles from various growth scenarios were derived from high-resolution elastic recoil detection (ERD) data measured with the Munich Q3D magnetic spectrograph (TU München, G. Dollinger), which allows to resolve single monolayers using heavy ion beams.

Plasma-wall interaction is one of the major sources for impurities found in magnetically confined plasmas. The proper modeling of these interactions is therefore crucial for the correct choice of a first wall material. Monte-Carlo-Code simulations of a carbon surface bombarded with 100 keV tungsten ions predicted an oscillatory time varying carbon concentration profile. Rutherford backscattering spectroscopy (RBS) profiles measured at carbon samples irradiated with increasing amounts of tungsten were deconvoluted with the known energy resolution function. The depth profile of a carbon surface shows an oscillatory time varying carbon concentration profile. The depth profiles are in good agreement with the results from a TRIDYN simulation.

In many areas of physical research the measured spectra consist of a collection of \`peaks' from some parametric family. For an unknown number of components the technique of reversible jump Markov Chain Monte Carlo (RJMCMC) allows jumping between the parameter subspaces corresponding to different numbers of components. The number of components supported by the data and the parameters of the individual component are estimated by RJMCMC sampling of the posterior probability distribution with variable dimensions. The method was applied to data from RBS and High-Resolution Electron Energy Loss Spectroscopy.

A Bayesian parameter estimation problem was solved for understanding the magnetic island dynamics of tearing modes in ASDEX Upgrade. The dynamics of neoclassical tearing modes is theoretically described by the generalized Rutherford equation for the magnetic island width -a first order differential equation. It contains three free parameters which are assigned to three terms describing the destabilizing bootstrap effect, the stabilizing effects of shaping and toroidicity (Glasser-Greene-Johnson effect) and finally the polarization currents induced by the motion of the island through the plasma. The knowledge of these free parameters is of crucial importance for the determination of the microwave power in order to perform electron cyclotron current drive stabilization of tearing modes. However, they can hardly be calculated theoretically and have to be determined from experiment. Nevertheless, prior information about the parameters was derived from ECE measurements and from ideal plasma configurations, and combined with the data according to the Bayesian theorem.

A generalized maximum-entropy-based approach (GME) was applied to the tomographic reconstruction of the soft X-ray emissivity of the hot fusion plasma. In this generalized method, instead of employing a regularization parameter, each unknown parameter is redefined as a proper probability distribution within a certain pre-specified support. Then, the joint entropies of both, the noise and the signal probabilities, are maximized subject to the observed data. This method was contrasted with other approaches and includes the classical maximum-entropy formulation as a special case. Subsequently, the GME approach was extended and applied to the mass spectroscopy problem.

Another ubiquitous problem is given by the presence of outliers or unknown signal contributions to measured data. Temperature measurements in tokamak edge plasmas suffer frequently from outliers of unknown origin. Such outliers have an important unwanted influence on the estimation of parameters for edge temperature model functions in conventional least-squares fits. BPT is applied to deal with such outliers and to develop a robust procedure. The method to tackle outliers is closely related to the determination of the background or to estimate a signal in the presence of background intensity which will be addressed in the next section.

The following sections are devoted to results which were obtained since the last meeting of the Fachbeirat.

2 Background Estimation

Quantitative spectral analysis often relies on being able to subtract from the data the contribution from the background. A general probabilistic model for estimating background contributions to measured spectra is developed on the defining characteristics, namely that the background is smoother than the signal and that each rapidly varying signal peak is confined to a well-defined interval. The coexistence of background and sources is described with a probabilistic two-component mixture model where one component describes background contribution only and the other component describes background plus signal contributions.

2.1 PIXE and Auger

The methods of particle induced X-ray emission (PIXE) and Auger spectroscopy frequently suffer from complex background contributions which are difficult to specify theoretically. The background is represented in terms of a cubic spline basis. A variable degree of smoothness of the background is attained by allowing the number of knots and the knot positions to be adaptively chosen on the basis of the data. The Bayesian approach provides a straightforward way to deal with this adaptivity by marginalizing over the knot positions. The effect of Ockham's factor is to produce a minimum number of knots sufficient for fitting the significant information in the data, but to avoid overfitting of the noise.

2.2 Spectroscopic bremsstrahlung measure ments at ASDEX Upgrade and Wendelstein 7-AS

The bremsstrahlung spectra measured by the ZEB and CXRS diagnostics at ASDEX Upgrade and by the UV-NIR spectrometer at Wendelstein 7-AS normally show contributions of spectral line emission. Nonetheless, there remain always enough regions of the spectra which exhibit line-free bremsstrahlung background of the plasma. The Bayesian mixture model was applied to separate the line emission from the background which is proportional to $1/\lambda^2$. This approach provides a natural way to reliably determine the bremsstrahlung emission irrespective of the fraction of line radiation while including all uncertainties of the measurements. An example for the fit of the bremsstrahlung background to one line-of-sight of diagnostic ZEB is shown in Fig. IV.A.1.

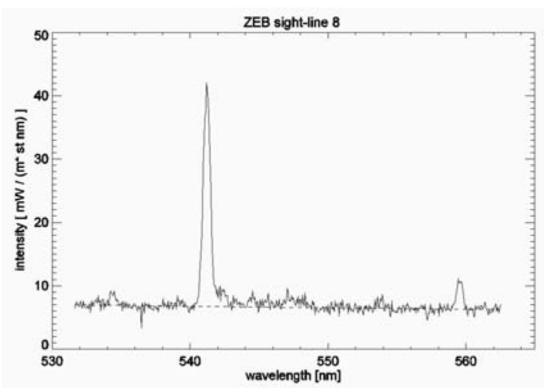

Fig. IV.A.1: Fit of the bremsstrahlung background (dashed line) to sight line 8 of the ZEB diagnostic in case of a background plasma with relatively strong spectral lines (#18468, t=3.5s).

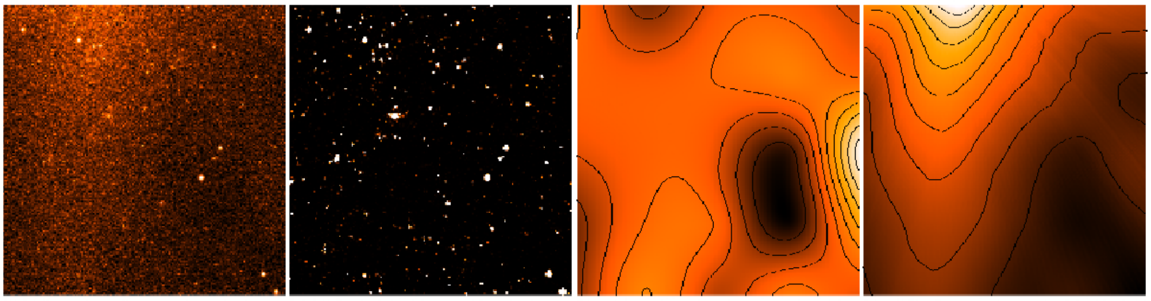

Fig. IV.A.2: Images are described from left to right. (1) RS930625n00 field from ROSAT PSPC in Survey Mode, broad energy band (0.1-2.4 keV), is located in the vicinity of the north ecliptic pole. The field of view corresponds to 6.4° x 6.4° in the sky. The observatory's exposure time ranges from 1.7 to 14 ksec. (2) Source probability map for the combined soft (0.1-0.4 keV) and hard (0.5-2.0 keV) energy bands. The map accounts for the width of the instrumental point spread function. (3) The thin-plate spline map, shown for the broad energy band, models the background rate. (4) The corresponding background map, which is the estimated background intensity, is obtained from the thin-plate spline multiplied by the observatory's exposure time (compare with image 1).

Each measured data point is classified with a probability of consisting of bremsstrahlung only or if line emission contributes. The robust technique does not need censored data where data points have to be excluded. Every data point contributes to the estimation of the bremsstrahlung amplitude according to the probability of consisting of background only.

2.3 ROSAT

BPT is employed for the joint estimation of background and sources detected by the X-ray space telescope satellite ROSAT. A background map for the complete field data of the ROSAT PSPC (0.1-2.4 keV) in survey mode is inferred simultaneously with a probability map for having source intensities in pixel cells or domains. We assume that the background is smooth, e.g. spatially slowly varying compared to source dimensions. To allow for smoothness the back-ground rate is modeled with a two-dimensional Thin-Plate spline.

Each pixel cell (or domain) is characterized by the probability of belonging to one of the two mixture components. The mixture model technique allows to consider all pixels for the background spline estimation even those containing additional source contribution. The source probability is evaluated also by correlating information with neighboring pixels in order to enhance the detection of weak and extended sources. The probabilistic method allows for detection improvement of faint extended celestial sources compared to the Standard Analysis Software System (SASS) used for the generation of the ROSAT All-Sky Survey (RASS) catalogues (see Fig. IV.A.3).

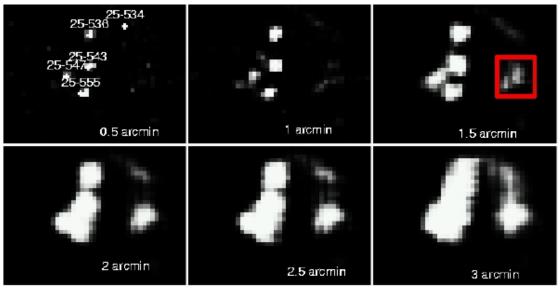

Fig. IV.A.3: Example of source detections at different correlation lengths (arcmin), covering a field of view of nearly 30 arcmin at the side. On the first image, the SASS sources are overplotted to the source probability map. The SASS source indicated with 25-534 is recovered at a correlation length of 2 arcmin. The red box guides the eyes to a new source detection which has been missed by SASS. A search in the NASA/IPAC Extragalactic Database reveals several galaxies close to the position of this source, indicating that this emission is due to a group or a cluster of galaxies.

3 Discordant Data Sets

Experimental data from different sources often suffer from discordant calibration and cover different regions. A model function spanning the complete range has to take advantage of all available data. This ubiquitous problem had to be solved in two different fields of physics. The first dealt with the evaluation of chemical erosion data for carbon materials at high ion fluxes, the second with cross-sections for partial electron impact ionization of methane and hydrogen. In both problems one of the data sets was taken as correct on the absolute scale, while the other data sets were equipped with scale factors. BPT was employed to evaluate the unknown scale factors and the model parameters. Finally, a model comparison showed in both problems which of the physically possible explanations is best supported by the data. The established procedure was further applied to recent data sets of the erosion yield at high ion fluxes from various experiments (see Fig. IV.A.4). The result predicts an order of magnitude lower erosion than previously assumed for ITER, the planned international fusion reactor.

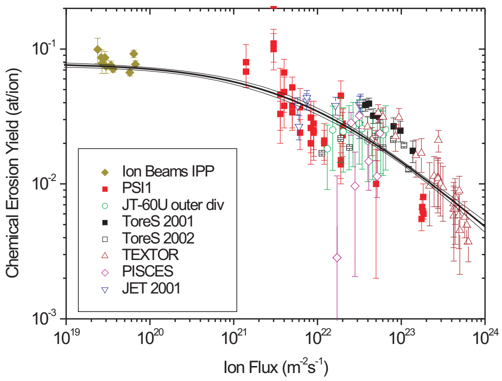

Fig. IV.A.4: Dependence of the chemical erosion yield on ion flux with an ion energy of 30 eV. The data stem from spectroscopic measurements in different fusion devices and plasma simulators. The Bayesian result for the yield is given by the solid line, accompanied by lines representing the confidence range.

4 Quantitative Analysis of Multicomponent Mass Spectra

Identification and quantification of components in a gas mixture from quadrupole mass spectra are difficult due to the fragmentation of molecules in the ionization source. Though every molecule produces a particular spectrum characteristic for both the molecule and the mass spectrometer (referred to as cracking pattern) the pattern of various species in a gas mixture may overlap and have to be disentangled. Since the data is noisy and the cracking pattern itself originates from a noisy calibration measurement, a method for the decomposition of mass spectra based on BPT was successfully developed and applied. The developed algorithm is computational demanding and therefore not suited for online monitoring purposes, e.g. in low-temperature process-plasma diagnostics. Therefore, a different method based on an information-theoretic measure called generalized maximum entropy (GME) was developed for decomposing the mass spectra. In this approach, the joint entropies of concentration, cracking, and noise probabilities are maximized subject to the measured data. This provides a robust estimation of the unknown cracking patterns and the concentrations of the contributing molecules. The method has been applied to mass spectroscopic data of hydrocarbons. The estimates were compared with those obtained from the Bayesian approach. The GME results provide good approximations to the elaborate Bayesian results using MCMC techniques. The GME method is fast enough to allow online monitoring of the plasma composition.

Another important problem frequently occurring in the application of mass spectrometry is given by the choice of the number of species used for disentangling the spectra. Is there evidence for other molecules? The recently developed Bayesian algorithm for mass spectrometry has been extended to model comparison capabilities. This allows the quantification of the probability of different models. The method is now routinely applied for plasma diagnostic purposes (for further details see also the section 'Low temperature plasma science').

5 Neural Networks

Neural Networks are a very powerful tool for parameter-free estimation if there is only sparse information about a system (i.e. very complex systems). The large number of degrees of freedom usually used for those networks implies a tendency for overfitting of the data. Bayesian regularization of neural networks based on hyperplane priors has proven to be a successful approach to solve this problem.

5.1 Speckle interferometry

In fusion devices plasma-wall interaction causes erosion and redeposition. Determination of erosion depths is of high importance since erosion limits the lifetime of plasma facing materials and eroded particles from the wall contaminate the plasma, increase radiation losses and, therefore, degrade the performance of fusion devices. An in-situ technique for the detection of surface changes with µm-resolution is a necessary prerequisite to study the influence of different plasma regimes on the plasma-wall interactions. Furthermore, the large amount of data requires an automated data evaluation. Speckle interferometry has already shown its potential for erosion and redeposition measurements in fusion experiments. However, the automated reconstruction of phase maps and erosion profiles from noisy speckle data (see Fig. IV.A.5, left panel) still requires considerable operator interaction which is not

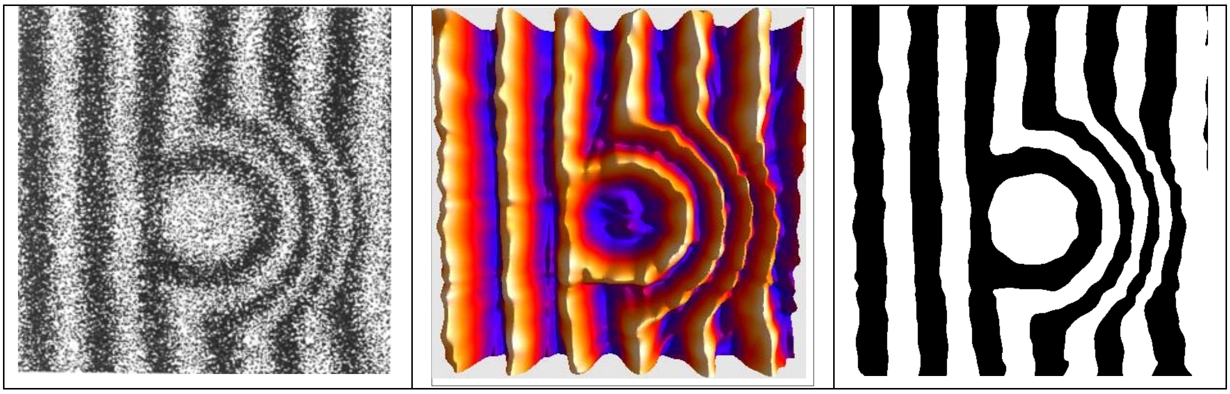

Fig.IV.A. 5: Left panel: Binary (0,1)-speckle image with 512 x 512-pixels obtained by subtracting two phase-shifting images with a bias step of π of a rough test surface. Middle panel: Probability map for each pixel to be either a black or white pixel. Right panel: Reconstructed fringe pattern.

feasible for routine measurements at large fusion devices like ITER. We developed a method for the evaluation of fringe patterns based on BPT and neural networks, bridging the gap from noisy speckle data to a denoised fringe pattern for subsequent automated unwrapping. The probability distribution for each pixel being 1 or 0 is shown in Fig. IV.A.5. If each pixel is assigned it's most likely value a clear and denoised fringe pattern is obtained (Fig. IV.A.5, right panel).

5.2 Online evaluation of Soft-X-ray diagnostics

The long-pulse operation (up to 30 minutes) of the fusion experiment W7-X requires continuous monitoring of the plasma. A multi-camera X-ray tomographic system with 400 viewing chords will be installed inside the vacuum vessel of W7-X to obtain information about plasma temperature, impurities and plasma equilibrium and stability. All presently available algorithms are unable to solve the inverse problem of the 2-dimensional reconstruction of the emission intensities fast enough for monitoring. For this purpose a Bayesian Neural Network has been developed and integrated into the framework of the data processing system of W7-X. Special care is dedicated to the error estimation of the Bayesian Neural Networks and robustness with respect to sensor failures. An example of the reconstruction is shown in Fig. IV.A.6.

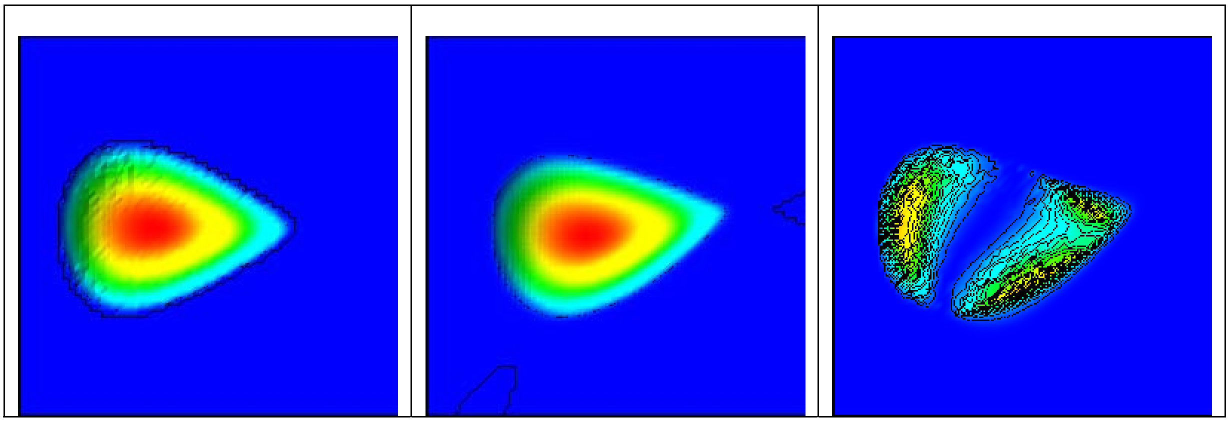

Fig. IV.A.6: Left panel: Modelled intensity distribution of W7-X in the triangular plane. Middle panel: Reconstruction of the intensity distribution by a neural network using the line integrated sensor data. Right panel: Deviation between original distribution and the reconstructed data.

6 Integrated Data Analysis of Fusion Diagnostics

Integrated data analysis (IDA) of fusion diagnostics is the combination of heterogeneous diagnostics in order to improve physics knowledge and increase the reliability of results. Instead of evaluating every diagnostic separately all the gathered information will be used simultaneously exploiting the implicit interdependencies of the

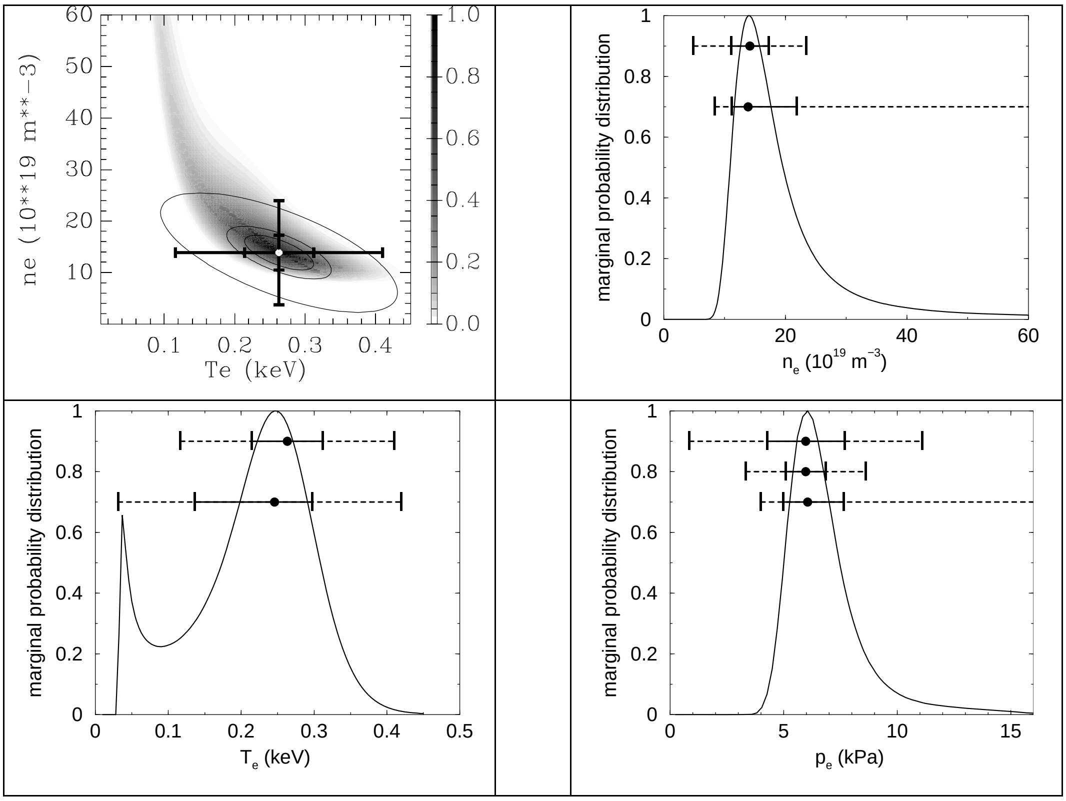

Fig. IV.A.7: Contour plot of the marginal posterior distribution for the electron temperature and electron density of the Thomson scattering data of the Wendelstein 7-AS discharge #56123 at t = 526 ms. The error bars refer to a 3σ (large error bars) and a 1σ confidence interval. The other 3 panels show marginal posterior distributions (normalized to maximum value) for the electron density ne, electron temperature Te, and electron pressure pe. The upper error bars are derived from the Gaussian approximation of the full posterior pdf. The lower error bars depict confidence intervals from the marginal distributions. For pe the middle error bar corresponds to an error propagation law taking into account first order correlations between ne and Te.

different measured plasma parameters. One example is the validation of profiles of plasma quantities. A joint automatic evaluation of experimental data from different plasma diagnostics to derive reliable spatial profiles of plasma quantities (n_e, T_e, T_i, Z_{eff}, …) suffers from the lack of a systematic statistical modeling of the uncertainties involved. Hence, integration of different diagnostics requires systematic and formalized error analysis for all statistic and systematic uncertainties involved. BPT allows systematic combination of all *Integrated data analysis* (IDA) of fusion diagnostics is the combination of heterogeneous diagnostics in order to improve physics knowledge and increase the reliability of results. Instead of evaluating every diagnostic separately all the gathered information will be used simultaneously

exploiting the implicit interdependencies of the different measured plasma parameters. One example is the validation of profiles of plasma quantities. A joint automatic evaluation of experimental data from different plasma diagnostics to derive reliable spatial profiles of plasma quantities (n_e, T_e, T_i, Z_{eff}, …) suffers from the lack of a systematic statistical modeling of the uncertainties involved. Hence, integration of different diagnostics requires systematic and formalized error analysis for all statistic and systematic uncertainties involved. BPT allows systematic combination of all information entering the measurement descriptive model that considers all uncertainties of the measured data, calibration measurements, physical model parameters, and measurement nuisance parameters.

6.1 ECE

One of the most important quantities in fusion experiments is the electron temperature distribution. Therefore, a variety of different diagnostics have been developed to measure the electron temperature. Using electron cyclotron emission (ECE) for this purpose has several advantages. The theory of ECE is well established and takes into account, at least in principle, all relevant physical effects. Furthermore, experience with different experimental realizations and cross-validations have uncovered most of the pitfalls. Therefore, ECE is considered as a main diagnostic for electron temperature measurements at the stellarator experiment W7-X. The IDA concept at W7-X requires a systematic assessment and quantification of the uncertainty of all measured data sets. A careful analysis of ECE is a step towards a fully integrated data analysis for the fusion experiment W7-X. The uncertainties of the ECE results can be split into two major contributions. The first contribution is due to the use of a simplified, linear model for the relationship between electron temperature and emitted radiation intensity. This model provides a good approximation under many operational regimes in modern fusion experiments but, nevertheless, there can be large deviations depending, e.g., on a non-Maxwellian velocity distribution of the electrons, a reduced optical thickness of the plasma and relativistic broadening. Those so called systematic errors can be reduced using more sophisticated ray-tracing codes for beam propagation. In a first step a comprehensive statistical description of the calibration procedure of the ECE diagnostic and the measurement uncertainties of the ECE measurements was derived. Bayesian parameter estimation provide electron temperatures (and its uncertainty) from the ECE measurements. Consideration of parameter correlations allows one to quantify the relevance of various improvements of the calibration procedure. Furthermore, nuisance parameters were marginalized, which provides the correct error propagation of their uncertainties into the results for the electron temperature. At the same time, we get rid of the cumbersome explicit dependence.

6.2 Probabilistic modeling of Thomson scattering diagnostics

Systematic error analysis was performed at the Nd:YAG Thomson scattering diagnostics (see Fig. IV.A.7). The statistical modeling includes statistical errors of the Thomson scattering data, the Thomson scattering background data, the Raman calibration data, the Raman calibration background data, and the systematical uncertainties of the polarization factors and of the scale factors of the spectral sensitivities.

The complete statistical model of the diagnostics allows the experimentalist to quantify the influence of different error sources on the reliability of the results, which has an impact on both diagnostic improvement and design. The reliability of the profiles can be studied by eliminating selected error sources or assuming exact calibration measurements. The error sources are of different importance for the various quantities of interest. Hence, the diagnostic improvement is strongly related to physics goals, i.e. one has to specify if n_e or T_e measurements are to be preferred in terms of accuracy. Diagnostics improvement can be achieved by reducing crucial uncertainties and by hardware upgrades, e.g. with additional spectral channels. The complete statistical description allows one to find the best operational settings for existing hardware and hardware upgrades. In addition, the Bayesian framework allows easy adaptation of the analysis to changes in the diagnostics due to new operational plasma regimes.

6.3 Integrating heterogeneous diagnostics

First steps towards an IDA were achieved by combining different heterogeneous data (see Fig. IV.A.8).

The result of combining different diagnostics within the Bayesian framework affords a gain in information, since it contains all the correlations between different parameters. For example, the combination of a diagnostic allowing information only about T_e (soft X-ray) with a diagnostic containing information about T_e and n_e (Thomson scattering) yields more reliable results for n_e compared with the results from the second diagnostic only. The probabilistic description contains the full correlation structure of parameters.

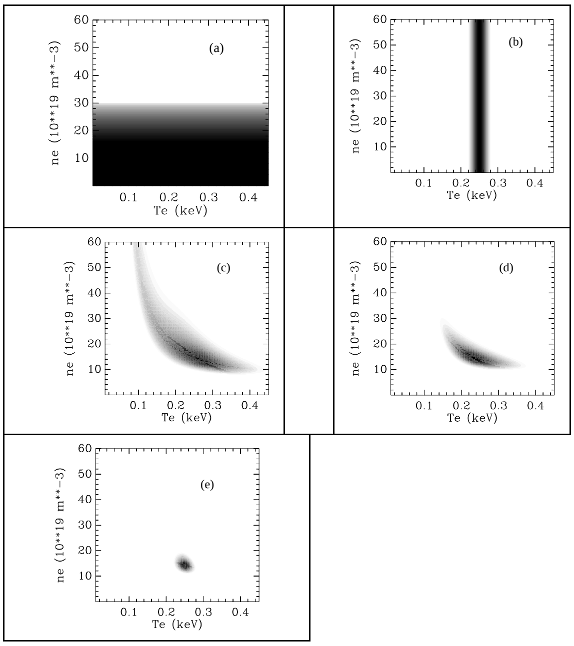

Fig. IV.A.8: Posterior probability distributions for the electron temperature and electron density exploiting information from (a) the cut-off density from the operational regime of the μ-wave interferometer, (b) the soft X-ray diagnostic containing only information about Te, (c) the Nd:YAG Thomson scattering diagnostic, (d) monotonicity constraints on neighbouring spatial channels of the Nd:YAG Thomson scattering diagnostic, (e) the result from the integrated information.

6.4 Experimental design of fusion diagnostics

It is of major concern for any scientist planning experiments to optimize the design of a future experiment with respect to best performance within expected experimental scenarios. The design of fusion diagnostics is essential for the physics program of future fusion devices such as Wendelstein 7-X. We introduced a probabilistic framework for quantified experimental design of fusion diagnostics and applied it to a Thomson scattering experiment.

Best performance has to be defined with respect to the goals of the experiment and cannot be a derived from first principles. The goal is to maximize the information gain of a future experiment with respect to various constraints. A measure of information gain is the mutual information between the posterior and the prior distribution. A utility function has to be defined specifying the desired benefit of the experimental outcome and to evaluate different designs. The Kullback-Leibler distance is used as a utility function to calculate the expected information gain marginalizing over data and parameter space. The optimal design parameters of the experiment are obtained by maximizing the expected utility function.

A design parameter of a future Thomson scattering experiment is the position of the spectral bands. The left panel of fig. IV.A.9 shows shifts of the filter closest to the laser line in the direction to the laser line. The right panel shows the information gain in units of bits as a function of the shift of one spectral curve. For two extreme experimental scenarios it is favorable to chose one spectral filter close to the laser line. In order to obtain reliable results for small T_e values (constant prior) one spectral band should be very close to the laser line. Other design parameters are the number and widths of the spectral bands.

7 First Principle Priors

The problem of assigning probability distributions which objectively reflect the prior information available about experiments is still an open problem. We employed the method of Maximum Entropy in order to translate the information contained in the known form of the likelihood into a prior distribution for Bayesian inference. The resulting entropic prior showed differences to the standard results from statistic, which, however, disappeared with increasing sample size.

8 Sputtering Yield

Bayesian parameter estimation was employed to determine the parameters of empirical fit formulae for the energy and angular dependence of the sputtering yield. In fusion devices most of the particles hitting the first wall have low energy attracting interest on the behavior of the sputtering yield close to the threshold energy. While former formulae failed in that respect the new approach gives a good description in the whole energy (and angular) range. With this method the full variety of ion-target combinations will be treated to facilitate a consistent view on the sputtering properties.

9 Reaction Cross Sections

Reaction cross sections and rate constants are parameters of a rate equation model for the interaction of CH_3 and H with amorphous hydrocarbon surfaces. Instead of stating the result of the parameter estimation traditionally as single numbers with uncertainties, it was much more informative to have a look at the Bayesian posterior distributions for the model parameters. The comparison of the posterior with the prior distributions revealed the amount of information that was contained in the analyzed data set.

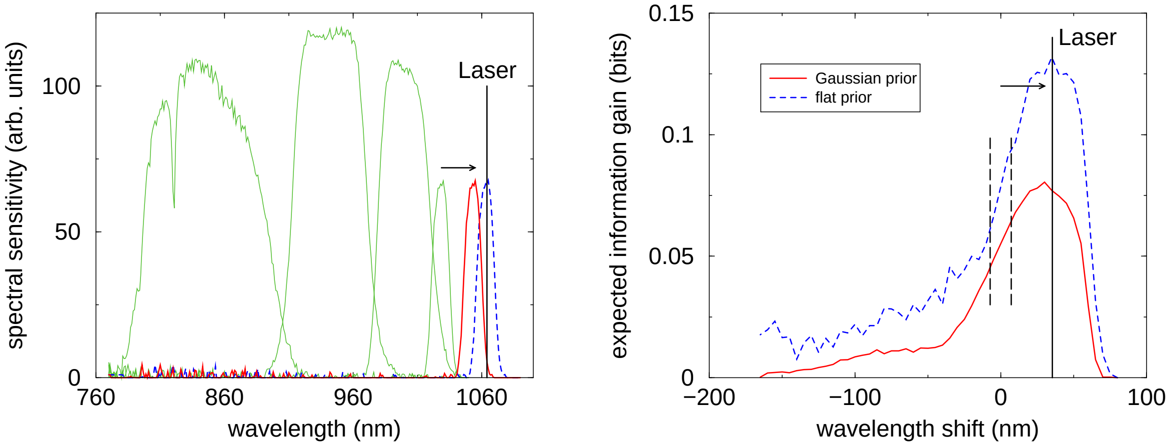

Fig. IV.A.9: Information gain (right panel) as a function of the shift of one spectral curve (left).

10 Bayesian Group Analysis of Plasma-enhanced Chemical Vapor Deposition Data

A ubiquitous goal in plasma-enhanced chemical vapor deposition (PECVD) is to describe the correlation between film properties and categorical and quantitative input variables. To gain insight into the underlying theoretical description, without having an established theory, it is important to reveal the interrelationship among the data. Bayesian group analysis is employed to find and describe the underlying data structure in high-dimensional parameter space. The parameter space consists of the combination of the input and response variables. The correlations within the high-dimensional parameter space are described with a multivariate model. The measured (response) data for a set of input quantities are grouped in different ways according to ``natural'' characteristics such as the type of the source gas and the bias voltage applied in plasma deposition. The goals are to find groups of objects that have a small within-group variability relative to the between-group variability and to decide if the preformed groups form genuine groups or if they can be pooled into larger meta-structures (groupings) without loss of information.

The approach allows for arbitrary covariance matrices for different groups and to handle missing data. Outliers can be identified by the necessity to form a separate group. The grouping probabilities are compared with classical approaches of likelihood ratio tests and the Akaike information criterion and a Bayesian variant called Bayesian information criterion. The method was applied to PECVD data of rare-earth oxide film deposition and hydrocarbon film deposition to study the evidence for grouping structures attributed to categorical quantities such as rare-earth components or source gases and quantitative variates such as bias voltage.

11 Know-how Transfer

11.1 Cell migration

Cell migration plays a key role in many medical questions, as for example during wound healing and the transmigration of leukocytes or tumor cells. However, it turns out to be a highly complex process involving the cooperative interaction of a large variety of biomolecular components. Up to now migration models were mainly developed on two scales of description: either on the molecular scale being far too complex or, in a more abstract way, it is focused on the movement of the center of mass of the cell being too crude to allow for differentiated statements about the cell behavior. In our approach we analyze experimental time series from phase contrast microscopy of cells moving on a 2D substrate. These data do not allow to give insight on the microscopic level, but deliver far more information than only the center of mass, e.g. they take account of sub-cellular processes like the dynamics of protrusions and adhesion releases. Considering this information content a model is developed which allows to characterize cell migration with a few parameters. Within this model one has to solve a differential equation of second order which can easily be transformed into two differential equation of first order. The same program as above was used for the computation of the expectation values of the model parameters.

11.2 Climate change impacts in phenology

The identification of changes in observational data relating to the climate change hypothesis remains a topic of paramount importance. In particular scientifically sound and rigorous methods for detecting changes are urgently needed. In this work we present a Bayesian approach to nonparametric function estimation. The method is applied to blossom time series of sweet cherries. The functional behavior of this series is represented by three different models: the constant model, the linear model and the one change point model (two section polygon). Model comparison results are shown in the table.

In addition to the functional behavior, rates of change in terms of days per year were also calculated. We obtain also uncertainty margins for both the function estimates and the rates of change. Our results provide a quantitative representation of what was previously inferred from the same data by essentially qualitative arguments.

	$p(M_j \mid \vec{d},\vec{x},I)$	residue	DOF
constant model	0.074	8874	1
linear model	0.104	8710	2
one change point	0.822	8118	4

11.3 Rheology of snow

Despite considerably research efforts, the rheology of snow is still not well understood, though many empirical and theoretical attempts have been made to describe the flowing behavior of avalanche-like flows. The nature of the internal flow dynamics of snow avalanches remains a subject of debate. Without a verified snow rheology it is impossible to develop

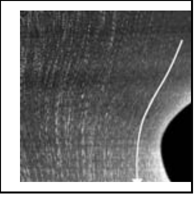

predictive avalanche models and subsequent avalanche hazard zoning. In collaboration with the Eidgenössischen Institut für Lawinenforschung data obtained from mesoscale chute flows of snow were analyzed with Bayesian methods. Of special interest is the question if a model based on the empirical constitutive law of Bingham is supported by the observed flow behavior or if more complex descriptions of the rheology of snow are required. The presently available data result in a weak evidence against the Bingham model.

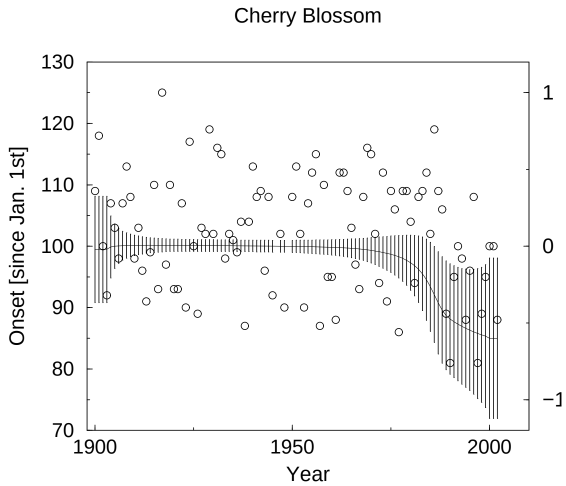

Fig. IV.A.10: Cherry blossom: open circles are the observations. The continuous line with error bars is the prediction for the one change point model.

IV. B. Nonlinear Methods

Introduction

Nonlinear data analysis methods in our sense are based on the state-space concept together with the assigned measures, such as dimensions or information entropies. The development of methods, measures and procedures are oriented to the requirements of the data analysis problems.
In this context, one of our main objectives is the characterization of the scaling properties of point distributions in high-dimensional state-spaces. From a theoretical point of view this is connected with the information content of a measurement.
The existence of nonlinear correlations in data sets determines the class of physical models of the underlying generating process. To proof the existence of (weak) nonlinearities, sophisticated statistical methods, involving resampling and surrogate data techniques are employed.
The data analysis instruments are completed by elements from graph theory.

Summary

The scaling-index-method (SIM), developed at the MPE, is a realization of the distribution of pointwise dimension and allows a structural characterisation of point distributions of any dimensionality. Local as well as global measures can be derived with the help of the scaling-indices α and with their frequency distribution, the so-called $N(\alpha)$-spectrum. The basic formulation of SIM, the so-called binary SIM is based on the scaling properties of the local cumulative point distribution, which is computed using the Heaviside-function. Drawbacks of this approach are that due to the non-differentiability of the Heavside-function the difference quotient has to be used instead of the derivative and two radii have to be supplied for the definition of the scaling range. We have generalised the SIM approach by using differentiable shaping functions like e.g. a Gaussian or a Lorentzian function that can remedy these disadvantages. According to the theory of fuzzy sets we call this generalisation fuzzy SIM (fSIM). One can show that the scaling-index defined in this manner is equivalent to SIM in the limit of small scaling radii. We pointed out that fSIM is in many cases superior to the basic formulation in particular with respect to pattern recognition, since it allows to incorporate pre-knowledge about e.g. the noise characteristics. Moreover, the differentiability achieved by the “fuzzification” of the shaping function facilitates the formulation of the scaling-index-method as a neural network as well.
SIM and its derivatives (fSIM/SVM) are used in many projects as a method for structural decomposition, pattern recognition or textural characterisation.
They are also powerful methods in the investigation of astrophysical data sets. One additional focus of our interest in this context was the development and application of surrogate data techniques. With the method of ‘constrained randomisation’ an ensemble of surrogate data sets, which share properties of given data, is generated. The analysis of the original and surrogate data sets with measures, which are sensitive to nonlinearities, yields statistical information about the significance of nonlinear correlations in the data. In addition, one can test whether given statistical measures are able to account for higher order or nonlinear correlations by applying them to original and surrogate data sets.
We used the surrogate data techniques to test for nonlinearities in the light curves of Active Galactic Nuclei (AGN) and to investigate the properties of different (non)-linear statistical measures for the analysis of the Large Scale Structure of the Universe:
Active Galactic Nuclei (AGN), the central regions of galaxies with a massive black hole surrounded by an accretion disc, show X-ray light curves with variability on time scales shorter than in any other energy band. A study of the X-ray variability gives insights to the extreme physical processes operating in the very inner parts of the accretion flow, close to the accreting black hole. The understanding of the nature of the time variability of these processes is essential for modelling the X-ray source. In this context we tested for nonlinearities in the X-ray time series of the AGN Ark564, the brightest Narrow Line Seyfert I (NLSI) galaxy. Since the observational data are not evenly binned for generating surrogates, we had to rely on simulated annealing techniques instead of Fourier techniques. By calculating the nonlinear prediction error, it is possible to discriminate between the surrogates and original data, which indicates that there might be nonlinearities involved in the physical processes governing the emission of X-ray light.

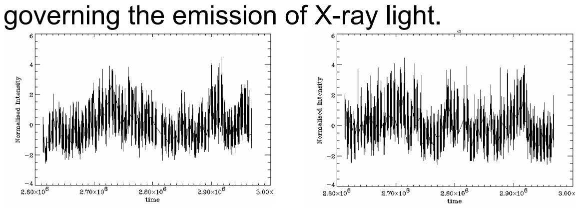

Fig. IV.B.1: X-ray light curve of Ark 564 (left) and respective surrogate data set.

One of the important issues in cosmology today is to characterise the nature of the large scale structure as revealed by observations and to compare the results with those of the various cosmological models.

Among the first and most frequently used statistical measures are the 2-point correlation function and the power spectrum, which have the advantage of being directly related to simulations of different cosmological models. However, they are linear global measures, which cannot provide any information about higher order and nonlinear correlations in the data. Therefore it is necessary to define more refined statistical descriptors, which go beyond the linear 2-point correlations. We tested whether the scaling indices as nonlinear descriptors can distinguish between structural properties resulting from model calculations (Open Cold Dark Matter) and their surrogates with the same two-point correlation function. Comparison of the resulting $N(\alpha)$-spectra, the distribution of scaling indices, reveals significant differences.

Complementary to this investigation we analysed the cluster properties of the same data sets with minimal spanning tree techniques and hierarchical clustering algorithms. Hereby, the galaxy distribution is described by a tree-like structure and the ultrametric distances between all galaxies are used for generating a hierarchical tree. For the quantification of the cluster properties we developed a method that combines hierarchical clustering techniques with measures of the information entropy. Fig. IV.B.2 shows a cluster profile expressed with the help of information measures that can also explain at which scale original and surrogates differ most significantly.

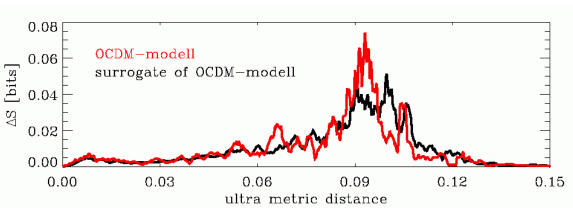

Fig. IV.B.2: Characteristic hierarchical clustering profiles are shown for the original data (red line) and the surrogates (black line). ΔS gives the growth rate of the entropy measure applied on the density distribution of clusters with decreasing ultrametric distance between the clusters.

The following subsections are devoted to results which were obtained since the last meeting of the FBR:

Self-organising Approaches

Methods that are motivated by nature like e.g. neural networks or genetic algorithms have been applied successfully in many tasks. These principles have been used with the aim to solve segmentation and optimisation problems in the context of the investigation of the plasma crystal experiments. This requires the knowledge of both the positions and the trajectories of the particles in the crystal. Detection based on grey-value thresholding may lead to unsatisfying results due to complicated light scattering properties on the particle surface, digitalisation effects and optical superposition phenomena from adjacent crystal layers. The determination of the particle trajectories is difficult in the presence of hundreds of particles which may flow in and out of the focus of the camera and may cross in the visible plane. In the turbulent or chaotic regime this task becomes even more difficult. This problem may be approached by applying heuristic methods that optimise several properties.

Segmentation using the scaling index method can be improved by its neural formulation. Fig. IV.B.3 illustrates the detection of the particles from the upper image. Almost all particles were detected and furthermore some particles could be identified, which were not found with the reference method, but could be verified by a subsequent visual inspection. The robustness of this approach was investigated by subsequently allowing only particles with increasing grey-values in the training phase of the neural nets. It turned out that the detection rate depends only weakly on these variations. This indicates that the method aims at structural properties. In the experiments, the particle detection based on this neural formulation of a structural complexity measure revealed a high degree of reliability and robustness.

Genetic algorithms or evolutionary strategies mimic biological phenomena like mutation, genetic recombination and selection in order to solve multi-objective optimisation problems. For that purpose a pool of “individuals” is generated, of which each represents a possible solution. In each iteration step, descendents are created based on this parent generation by recombination and mutation. The quality of a solution by an individual is evaluated using a fitness function. A selection mechanism guarantees that only the “fittest individuals” (i.e. the best approximation to solutions of the problem) attain the next generation. These methods, which are motivated by nature, are an interesting alternative to other optimisation procedures as for example simulated annealing.

Applied to particle tracking in the analysis of plasma crystal experiments, an individual consists of a set of paths. Recombination can be

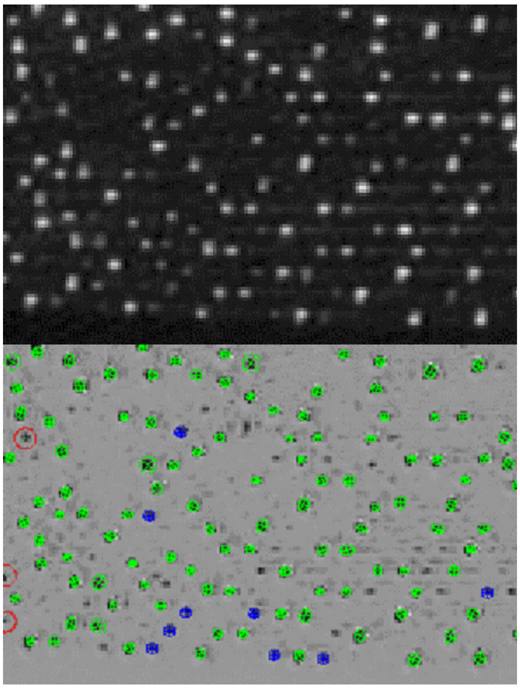

Fig. IV.B.3: The upper image shows a cutout of an image from the plasma crystal experiments. The result of the particle detection using the neural formulation of the scaling-index-method is shown in the lower image. Both the reference algorithm and the newly developed method were able to detect the green marked particles. The neural net has not identified the particles labelled in red, while the reference algorithm has not spotted the blue marked particles.

implemented e.g. by mixing two different paths and mutation is imitated by randomly changing an element of a path. The fitness of each individual is assessed with respect to the properties of the single trajectories: the length of the path is evaluated as well as the constancy in direction and speed.

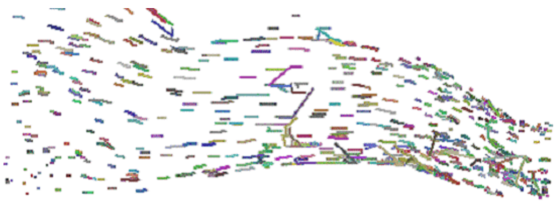

Fig. IV.B.4: Trajectories of particles determined by an evolutionary approach. Starting point of the analysis are the particle positions in five consecutive time steps. The algorithm joins this unordered set of particles to trajectories, which were colour marked for better distinction here. The errors in the result can be corrected by suitable post-processing.

In numerical experiments good results could be obtained. However the multiplicity of free parameters appears problematic because of the high computation time needed. In order to reduce the dimensionality of the problem, a more compact description of the individuals is necessary. The computational effort can substantially be reduced by parallelisation of the algorithm. However, this technique seems to be a promising approach for analysing the plasma crystal experiments.

Analysis of the Observed Large Scale Galaxy Distribution

The well-known two-point correlation function $\xi(r)$ estimates the excess of clustering relative to a uniform random distribution. $\xi(r)$ provides a mean and global scaling behaviour of a point distribution for each distance range r.

Instead of an averaged, global scaling behaviour, the scaling index α offers the possibility to characterize the geometry of the local environment around each point. This classification is more sophisticated than density measures or the correlation function because it is sensitive to structural elements (filaments, walls, etc.).

Having proved the usefulness of this geometrical classification with the help of simulated data and surrogates in previous work, we now apply the SIM to latest observational data (Sloan Digital Sky Survey, SDSS).

It is well known that galaxies are not randomly and uniformly distributed but are arranged in structures like clusters, filaments, walls, etc. Their affiliation to these specific structural components is supposed to be reflected in intrinsic properties like colour and morphology (spirals, ellipticals).

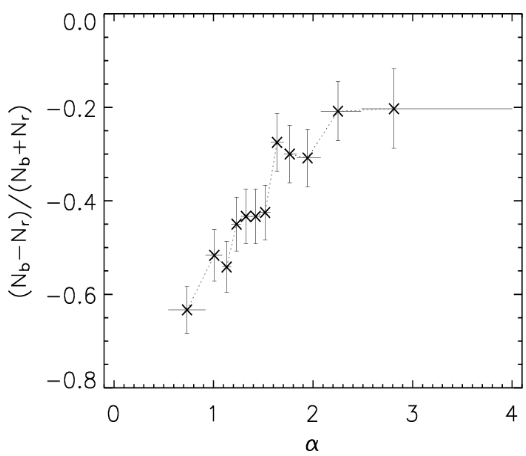

Fig. IV.B.5: Galaxy colour ratio versus scaling indices that characterise local topological properties. There is a significant excess of red galaxies in clusters and filaments.

Using scaling indices, we connect these properties and find a significant colour-geometry-relation: clusters are mainly populated with red galaxies, voids with blue galaxies and filaments consist of both. This relation is the result of well-known processes in the galaxy evolution. In high density regions like clusters, different interactions between galaxies change their physical properties, e.g. from a red to a blue colour. The probability of these interactions decreases with the local galaxy density. The scaling index improves this picture because it quantitatively relates the colour evolution of a galaxy with a change of its environment. One possible scenario is that a blue galaxy is formed in a low density region (void), falls into a filament and ends with a red colour in a cluster.

A Search for Non-Gaussian Signatures in CMB Maps

The identification of non-Gaussian signatures in cosmic microwave background (CMB) maps is one of the main cosmological challenges today, because it allows us to discriminate between different cosmological models (e.g. inflationary or cyclic processes, moving cosmic strings etc.), which explain the evolution of the very Early Universe. We applied techniques developed in the field of nonlinear time series analysis to CMB maps in order to design highly significant statistical tests for non-Gaussian signatures. With the method of constrained randomisation so-called surrogate maps are generated which mimic both the power spectrum and the amplitude distribution of simulated CMB maps containing non-Gaussian signals while all higher order correlations are wiped out (see Fig. IV.B.6). Analysing all maps with measures sensitive to higher order correlations (e.g. weighted scaling indices, Minkowski functionals) leads to a statistically significant discrimination between the surrogate and original maps (see diagram in Fig. IV.B.6). Thus a clear detection of non-Gaussian signatures becomes possible. We could also show that this approach is very robust with respect to superimposed noise and that one can detect non-Gaussianity at higher noise level than with other techniques commonly used.
In a further study we compared the relationship between Minkowski functionals and estimators for local scaling properties with respect to their sensitivity to (different) non-Gaussian signatures in the images shown above. Therefore we extended the formalism of constrained randomization to spatial patterns and showed the feasibility to generate surrogates for two-dimensional images preserving more complicated (non-linear) constraints, namely the Minkowski functionals using simulated annealing techniques. By analysing the original and surrogate image with scaling indices a clear discrimination between original and surrogates is found. Therefore these two statistics complement each other in the sense that they are sensitive to different aspects of non-Gaussian features in the image. These findings suggest that for a comprehensive test for non-Gaussianities in CMB maps it is advisable to use a variety of statistics sensitive to non-Gaussian signatures so that none of these remain undetected. In current research activities we apply these newly developed methodologies to the analysis of the data from the WMAP-satellite.

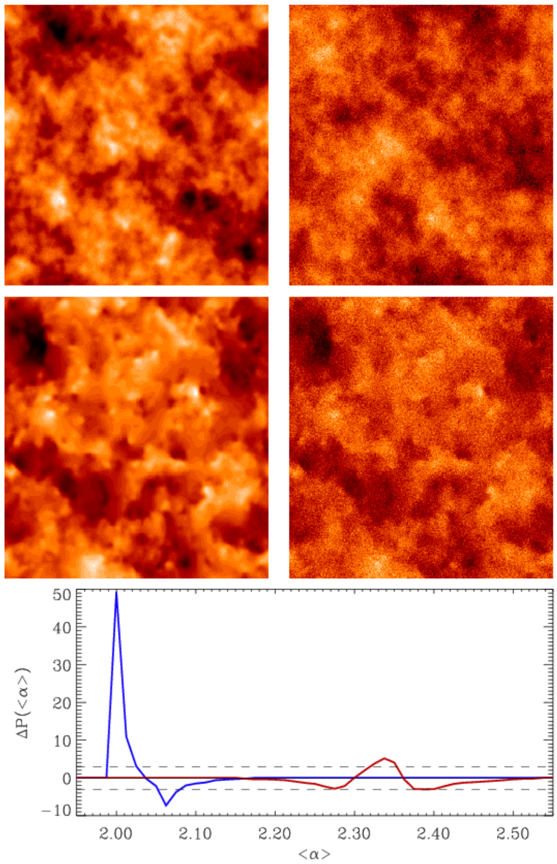

Fig. IV.B.6: Lower left image: Simulated CMB map containing non-Gaussian signatures. Lower right image: Same CMB map with additive noise (SNR=2). Upper images: one realisation of the corresponding surrogate images. The diagram shows the deviation of the weighted scaling indices for the CMB maps from the mean surrogate distribution. Blue: no noise, red: SNR = 2. Even for the noisy image a clear 3σ signal is detectable.

Unveiling Weak Nonlinearities Analysing Fourier Phases

Besides the power spectrum the Fourier phases are powerful indicators of the structure of a data set. The phase information can be represented as a phase map, which is a two-dimensional set of points that is spanned by the phases of mode k and the phase of mode k+Δ, where Δ is a mode shift. Studies of phase coupling involving phase maps are found in astrophysics to test for non-Gaussian signatures in the Cosmic Microwave Radiation Background (CMB). We developed a method to detect non-linearities, which uses the method of surrogates. Next, we create for both the original and the surrogate data phase maps, which are subsequently characterized by means of the spectrum of weighted scaling indices. We applied the method to two different time series, namely the *z*-component of the Lorenz system in a chaotic regime and the logarithmic daily returns of the Dow Jones for the period 1930-2003.

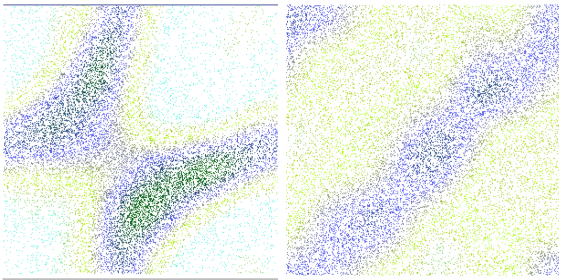

Fig. IV.B.7: Representative phase maps of the Lorenz-system (left) and of one corresponding surrogate (right). The colour-coding represents the value of the scaling index of the points.

As expected, the Lorenz system showed signatures of non-linear behavior represented as a highly non-uniform distribution of the points in the phase maps at all scales Δ (see Fig. IV.B.7). However, for the Lorenz system surrogates are not always free from phase coupling. Then, our method can assess the quality of surrogate data. We already improved commonly used methods for generating surrogates in this respect.
For the Dow Jones data our results indicate that a novel characteristic scale of non-linearities exists. These findings may help to better understand the financial-price dynamics.

Information Content of an Image

In many applications of image analysis a rescaling of the grey level scale or the colour values is a first and important step for subsequent image processing tasks. It is therefore relevant for e.g. image enhancement, scene processing or segmentation, optical character recognition (OCR), classification or quality assessment of surfaces, morphological filtering etc. It is in particular necessary for all methods that use e.g. thresholding or the characterization by means of its fractal or multiscaling properties.

In the context of the latter approach, an image is seen as a point distribution embedded in a multidimensional state space, that is made up by the pixel and the colour coordinates. Based on this concept, a method for the characterization of the structural content is the above mentioned scaling index method and its derivatives. However, this approach implies a relation between spatial and colour scales, which is not given a priori. To overcome this problem, we consequently studied possibilities to objectify and to optimize the scaling and partitioning of the state space.
We developed a new method of a nonlinear colour value rescaling based on information theoretical considerations, that can not only significantly improve image processing techniques based on scaling properties, but allows also for image enhancement in general. The basic idea herein is that the structural or textural elements of an image recognised by its locally increased correlation function.
To quantify the local structural information content, the surrounding of each pixel is scanned by applying a two-dimensional shift operator. As a result of this procedure one obtains a two-dimensional distribution of colour-colour transitions associated with structural elements of the image. This two-dimensional distribution is evaluated using mutual information which results in a specific averaged information content of each colour value. In this way the specific contribution to the total information content of the image can be assigned to each colour value. Finally a non-linear rescaling of the colour values is achieved by an homogenous partitioning of the respective information space.
The examples show applications of this method for a classification problem and image enhancement. Fig. IV.B.8 displays three different Brodatz textures (A, B, C) with equal mean and standard deviation. The classification relies primarily on the different structural properties. After rescaling of the colour scale, local scaling properties are computed using the scaling index method. The classification performance as a function of the size of the texture probe is plotted for three different cases: The black curve denotes a simple grey value-based thresholding procedure. The two other curves represent the classification based on the scaling index method: The texture classification using the information-optimized images (red curve) is superior to the original images (blue curve) as input. In Fig. IV.B.9 the effect of this method on an image of a skin lesion is demonstrated: The structure of the lesion is enhanced (right image) compared to the original image (left).

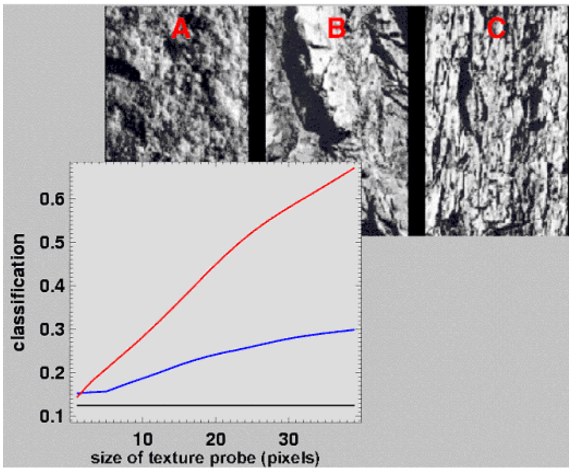

Fig. IV.B.8: The curves show the classification performance as a function of texture probe size for a simple grey value thresholding procedure (black curve) and for an analysis based on the scaling index method (red and blue curve). The scaling indices applied to the enhanced images (red curve) yields better classification results compared to the scaling index method executed on the original images (blue curve).

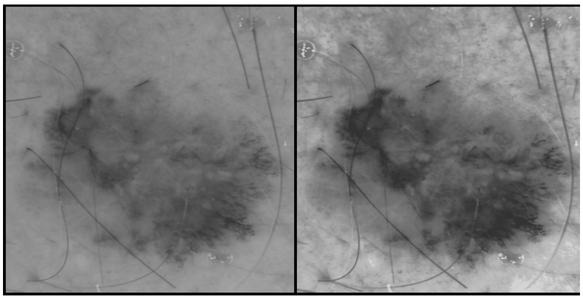

Fig. IV.B.9: Information based enhancement applied to an image of a skin lesion (left: original, right: structure enhanced version)

IV. C. Know-How Transfer

Introduction

The working group deals with the analysis of complex systems in a number of projects within the institute (MPE/IPP), considering e.g. astrophysical questions and specific data analysis aspects in the context of complex plasmas. The development of analysis techniques, procedures and complexity measures is mostly inspired by the demanding questions that arise there. This section, however, is devoted to those cooperations with external partners mainly at scientific institutes in other fields of science.

The term “Know-How-Transfer” is therefore used in this context for knowledge transfer in collaborations of interdisciplinary nature. In some cases, the know-how is transferred directly from basic science into industrial applications in a “pre-competitive” phase. Beyond this level a transfer is managed and promoted by “Garching Innovation GmbH” on behalf of the Max-Planck-Society.

The expertise of the group is in particular the model-free description of complex systems based on the measurements of arbitrary modality, e.g. univariate or multivariate time series, images, tomographic data or multidimensional sensor data.

Since the methods are motivated from the study of nonlinear dynamics, the methodological approach starts very often with searching for an appropriate representation of the available data in high-dimensional state-spaces. Already in this phase it is worth to include arguments from information theory (e.g. redundancy measures) in order to reduce the dimensionality. In many cases the underlying process that “generates” the data can then be unmasked by patterns that are detectable in the resulting point distribution. Information measures or the description by means of the scaling properties are very helpful for this kind of pattern recognition.

Usually these patterns are contaminated by noise, systemic noise or measuring noise. The effect of noise is at least twofold: first, it conceals existing structures in state space, and second, it makes a pretence of structure that is actually not in the data. The second case is of particular importance when nonlinear properties for the characterization of data sets and the underlying processes are considered. For that reason, data analysis commonly goes beyond pattern recognition, characterization or classification. An important aspect is hypothesis testing and, if possible, the reconstruction of the data by modelling or the explanation of noise and artefacts in the data sets. For hypothesis testing, we apply advanced surrogate techniques (e.g. “Iterative Amplitude Adjusted Fourier Transformation”) that preserve specific properties. Very frequently, the task in data analysis is to describe the relation between objects or items represented by the respective data sets. These questions are within the field of data mining. From our experience with astrophysical data concerning the large scale structure of the Universe we developed clustering algorithms that can be applied to a wide range of data modalities. The combination of nonlinear correlation measures with elements from graph theory provides new strategies for the purpose of classification or generating taxonomies.

Summary

The activities can be ordered in several ways: With respect to the field of application, to the data modalities and with regard to the data analysis task. In this sense, the know-how transfer includes applications in biosciences, medicine, engineering, economy, and nano science. Due to the generic formulation of the analysis techniques the range of data modalities covers time series, conventional images, scanning probe microscopic images, and tomographic data sets, as well as spectra of different kind (e.g. light spectra or mass spectra). According to the data analysis task typical questions are noise reduction, segmentation, structural determination, classification, and cluster analysis.

From all projects carried out only a selection can be presented here:

In cooperation with the Department for Geosciences of the University of Munich we have developed new techniques for the analysis and structure determination of scanning probe microscopic images. The images were recorded using either a scanning tunnelling microscope (STM) or an atomic force microscope (AFM).

The structure determination of mono-molecular adsorbates plays an important role in the understanding of processes on the nano-metre scale. Several ordered mono- and bi-layer substrates have been investigated using STM and the results have been interpreted with the help of image processing and numerical molecular simulations. Combining the results from the numerical simulations and the experimental data after image processing yields very accurate structure determinations for several organic molecules.

Trimesic-acid (TMA) is an example which can form a mono-molecular layer on graphite, which can be used as a host system for other molecules. By calculating the structure of the layer using a molecular mechanics simulation it has been found, that although the interactions of the molecules with the substrate are predominantly governed by van der Waals forces, hydrogen bonds play an important role in the stability of the layer and the absorption of guest molecules.

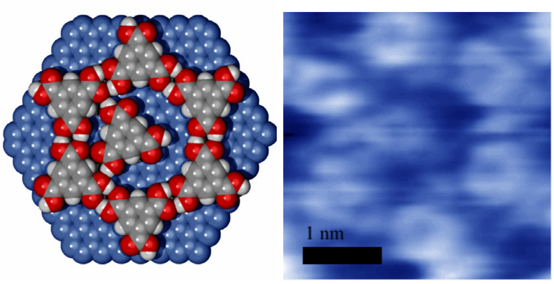

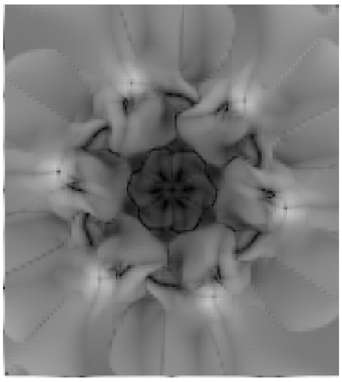

Fig. IV.C.1: Upper left panel: Molecular mechanics simulation of a mono-layer of TMA ($C_9H_6O_6$) on graphite. The TMA-molecules (carbon-grey, hydrogen-white, oxygen-red) form a hexagonal grid on the graphite surface (blue) in which an additional molecule can take the place of a guest molecule. Upper right panel: STM image of one hexagonal cell of TMA with an additional TMA guest molecule. The colour represents the height of the structure. The guest molecule is located on the left side of the void. Lower panel: Differential image of the energy surface of the guest molecule in the hexagonal void. The image was calculated by moving the molecule inside the void and performing an energy minimization.

Our nonlinear image processing techniques have been applied to several modalities of medical images for diagnostic purposes:
In an interdisciplinary team (together with partners from the Universität Regensburg, Technische Universität München and Fachhochschule München) a prototype of a dermatoscopic workplace has been completed, which consists of defined procedures for standardized image acquisition and documentation, components of data pre-processing (e.g. shading- and colour-correction, removal of artefacts), segmentation, quantification, visualization algorithms and classification routines. Our main contribution to the system is the reproducible and quantitative characterization and visualization of object properties based on the dermatoscopic ABCD-rule by means of nonlinear and information measures.

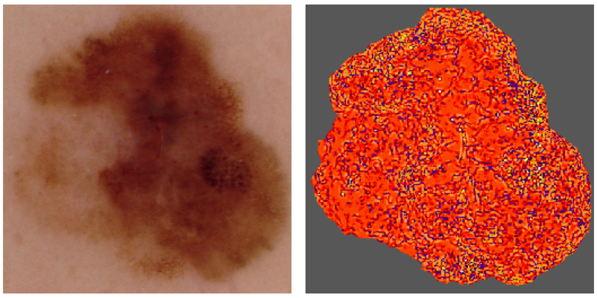

Fig. IV.C.2 The scaling-index method enables a structural decomposition of the lesion. The colour-coded scaling-indices (right) indicate the content of different structural elements of the malignant skin lesion (left) and contribute to our system of diagnostic parameters.

In a large study of more than 700 images of melanocytic skin lesions an overall accuracy of more than 90% could be achieved. The developed prototype was transferred to industry and has been marketed by Linos AG for use in medical practice and hospitals.
A four-dimensional representation is the starting point in the analysis of 3D tomographic images as they are typical in radiology. A number of segmentation algorithms with nonlinear image processing steps have been developed and tested for segmentation, detection and volumetry of tumours.
In a clinical study the response of patients with oesophagus cancer to (chemo-) therapy using different imaging techniques - 3D X-ray computer tomography (CT) vs. the positron emission tomography (PET) - has been investigated. It could be shown that the measurement of the activity with PET yields a higher sensitivity but a lower specificity compared to CT-volumetry. The combination of both methods yields the best diagnostic accuracy. Furthermore it could be demonstrated that a much higher diagnostic accuracy can be reached by a refined volumetric analysis of the tumor size.
In a related morphology-based study, a method has been developed for detecting lung (micro-) nodules in high resolution thoracic CT images. It makes use of the quantitative description of the main morphological features. In configuration space the local scaling properties are determined for each point by calculating the fuzzy scaling-indices α. Point-like nodules could clearly be discriminated from voxels in the tubular bronchovascular structures and voxels belonging to the lung tissue.

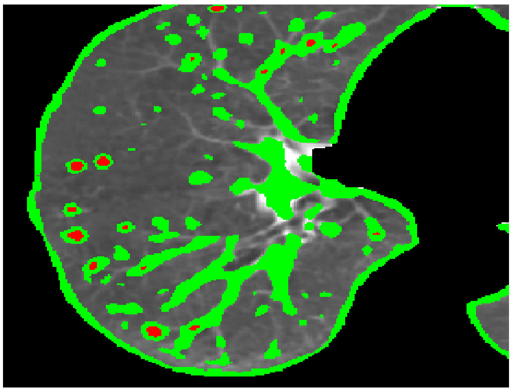

Fig. IV.C.3: Lung image with detected bronchovascular structures (green) and possible pulmonary nodules (red).

The characterization of different morphological features in images by estimating the local scaling properties has been used for the analysis of bone structures as they are present in high resolution tomographic nuclear magnetic resonance (NMR) images. The goal was the early recognition of osteoporosis, which manifests itself in the reduction of bone mass and in the destruction of the trabecular bone structure. First in vitro studies have been conducted with the aim to correlate structure parameters, which characterize the morphological content in the images, with macroscopic mechanical parameters of the bones e.g. bone strength.
Time series can be treated very similar to images after embedding them in appropriate state spaces, using for example delay coordinates.
In cooperation with the research department of a large German banking corporation we investigated the influence of nonlinear correlations between time series of the daily market price fluctuations on the definition of business sectors. Comparison with surrogate data sets (preserving the cross-correlation), which are obtained by a combinatorial minimization method (simulated annealing) indicated, that at least small nonlinear correlations are present and that the use of nonlinear measures leads to a better agreement with the so-called “Standard Industrial Code” than the linear measures. The agreement was assessed by clustering methods employing hierarchical tree techniques.

The following subsections are devoted to results which were obtained since the last meeting of the FBR:

Nano-Structures

The analysis and structure determination of scanning probe microscopic images has been continued with growing intensity. The activities can be divided in three major parts: Study of monomolecular layers, processing of AFM images and investigations of the AFM as a non-linear system.
A main focus became the self-organization of organic molecular systems on semi-conducting surfaces, which lead to a model for the natural emergence of DNA-protein complexes at the origin of life, as well as from the technological point of view to a "lab-on-a-chip" system of a polypeptide library. The generated structures can be used as templates for the nano-structuring of surfaces, which, together with the semi-conducting properties of the used molecules, are the building blocks for self-assembled nano-electronic circuits.

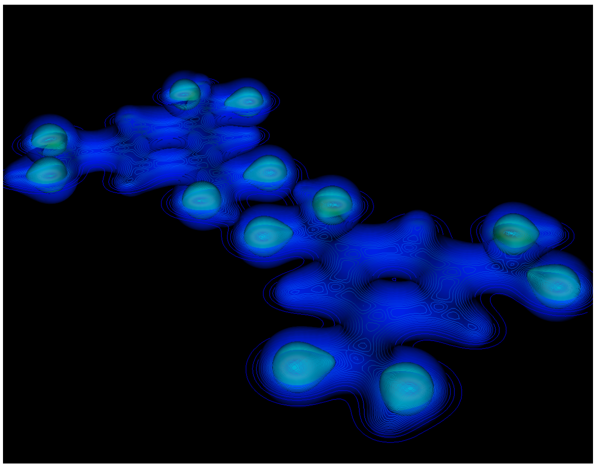

Fig. IV.C.4: Density functional simulation of two trimesic acid molecules TMA on a graphite layer. Shown is the electron density of the LUMO (Lowest Unoccupied Molecular Orbital) of the two TMA molecules.

The underlying experiments generate arrays of molecular nano-wires on a crystal surface by dynamic self-assembly. The one- and two-dimensional nano-structures are simulated using molecular-mechanical simulations (force field calculations) and quantum mechanical simulations (density functional simulations). The single atoms are described by individual particles, which interact by potentials. The potential functions are computed by summation of two-, three- and four-body potentials.
The force field simulations are able to describe the dynamical modification of the nano-structures during the manipulation using a STM tip.
An example is the manipulation of single C60 molecules (Buckminsterfullerene) with a carbon nano-tube. The buckyball acts as a guest molecule inside a cavity which has been generated by self assembly of a trimesic acid monolayer. This localization makes a controlled manipulation with the carbon nanotube possible which will eventually result in the assembly of active components using single molecules.

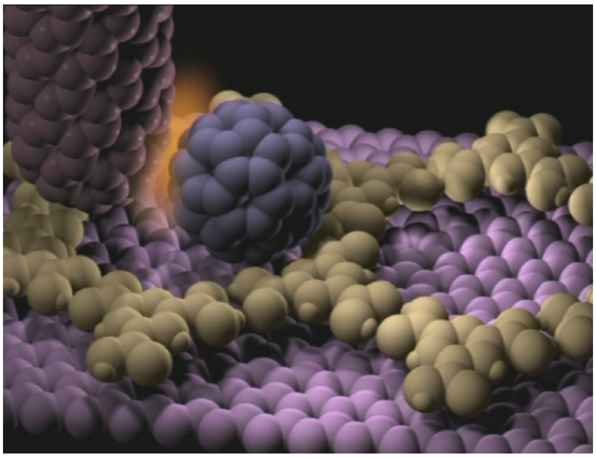

Fig IV.C.5: Dynamical force field simulation of a manipulation of Buckminsterfulleren molecules, which are embedded into a template of molecules of trimesic acid. The bucky balls are moved using a carbon nano-tube. The simulations have been conducted in order to clarify the scanning probe recordings.

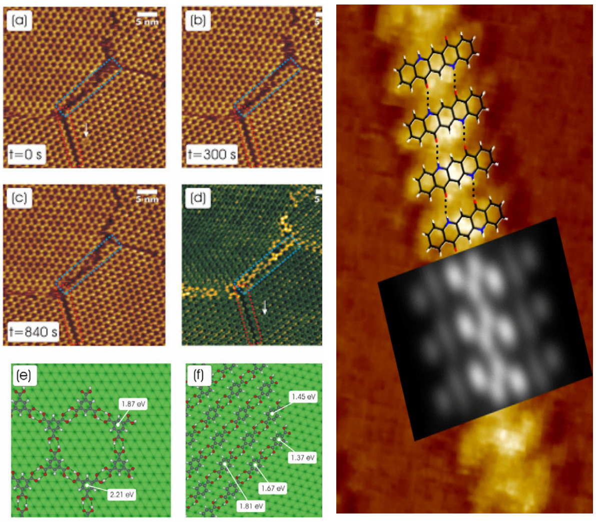

Fig. IV.C.6 a-c: Selected snapshots of a series of 47 STM images of TMA domain boundaries (40x40 nm²). Only slight changes happen directly at the domain edge and the domain size and shape is mainly preserved. (d) Standard deviation of all 47 images of the series.

Lower left panel: Molecular mechanics simulations of finite islands of (e) TMA and (f) TPA were utilized to obtain a estimate for the binding energy of edge molecules. Two adjacent carboxylic groups form two H-bonds, symbolized by black dotted lines. Right panel: Scanning probe microscopic image of the organic dye molecule Quinacridon (QAC). Overlaid on the image are the results of a force field calculation (upper) and a density functional simulation (lower).

A further example are molecular mechanics simulations of finite islands of TMA and TPA which were utilized to obtain an estimate for the binding energy of edge molecules. Two adjacent carboxylic groups form two H-bonds, symbolized by black dotted lines in Fig. IV.C.6. The corresponding binding energies of non-equivalent edge-molecules are indicated within the models. TPA islands show two substantially different facets where the molecules being bound by either two or four H-bonds, which results in a significant difference in the binding energy.

It is well known that the organic dye molecule quinacrodone (QAC) forms monomolecular layers on highly ordered pyrolytic graphite (HOPG). These mono-layers exhibit a variety of configurations and are candidates for organic semi-conductors which would open up the way for a new kind of electric circuits on the nano-meter scale.

In order to understand the self-assemblation of different structures, the hetero-epitaxial growth of QAC mono-layers on graphite has been simulated by using molecular mechanics simulations, density functional simulations (Fig. IV.C.6) and a probabilistic cellular automaton. In Fig. IV.C.7 the phase diagram for the simulated system is shown. Three different phases of the crystal can be differentiated. Phase I corresponds to an unordered random phase, while Phase II shows large domains of ordered structures with a spontaneously broken symmetry. Phase III corresponds to a checker-board like configuration of the molecules. Phase II has been experimentally observed and the predicted phase transition from phase I to phase II is now experimentally investigated.

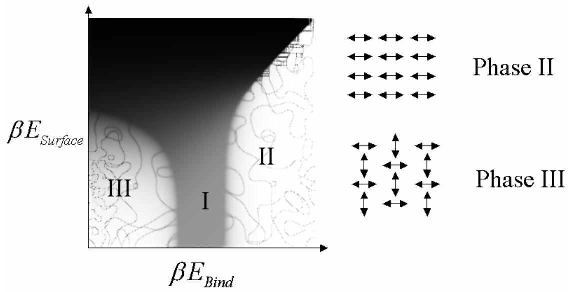

Fig. IV.C.7: Phase diagram of a probabilistic cellular automaton describing the hetero-epitaxial growth of QAC mono-layers on HOPG. The probability for the horizontal phase is shown as gray scale plot.

Search for Water on Mars

In the search for aqueous habitats on Mars direct proof for (ancient) flowing water is still lacking although remote sensing has provided indications for young fluvial systems. In collaboration with the Department for Geo- and Environmental Sciences of the University Munich a classification scheme was developed in order to demonstrate that such proof can be given. Surface marks on recent terrestrial sand grains have been examined with the atomic force microscope (AFM) and a quantitative 3d-analysis that can numerically distinguish between aeolian and aquatic transport in sedimentary deposits on Earth has been applied. The surfaces of natural quartz grains as well as olivine, feldspar pyroxene and monazite sands of known origin have been imaged, each image providing a 3d map of the mineral surface. A fully automated analysis of distribution patterns of the structural elements that build up the grain surfaces shows that wind transported quartz grains have linear segments that are short and distributed irregularly on the surface, whereas the linear segments on water transported grains are longer with orientations that reflect the mineral symmetry. Because the surface patterns found on aqueous grains are due to anisotropic etching, they can be used as diagnostic fingerprints for the existence of aqueous transport systems in present or past.

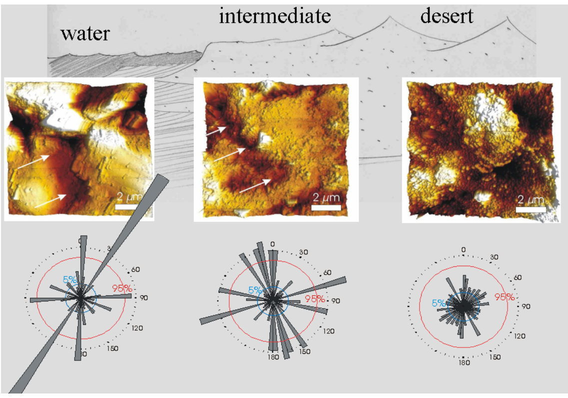

Fig. IV.C.8: Comparison of aeolian and aquatic quartz sand. (a,d,g) AFM images of a sand grain typical for aquatic (a,d) and aeolian transport (g). (c,f,g) Edge detection of the AFM images, (b,e,h) Distribution of linear segments.

A cluster analysis of the cross-correlation-distance of distribution patterns in the structures of aeolian and aquatic sand grains has been used in order to build a minimal spanning tree, that provides a map for the relationship of the various sediments found on earth. The analysis shows that the method is highly significant and that water and wind transport can clearly be differentiated. In particular, feldspar and olivine sands contribute even more to the discrimination than quartz grains, indicating that the method is promising for its application on future Mars missions, assuming that Martian aqueous sand grains exhibit similar erosional patterns as mineral grains on Earth.

The algorithm has now been implemented in a distributed computing environment using a database server where the images are stored and clients computers which access this database in order to process the data. Therefore it is possible to extend the database while processing and testing different analysis methods.

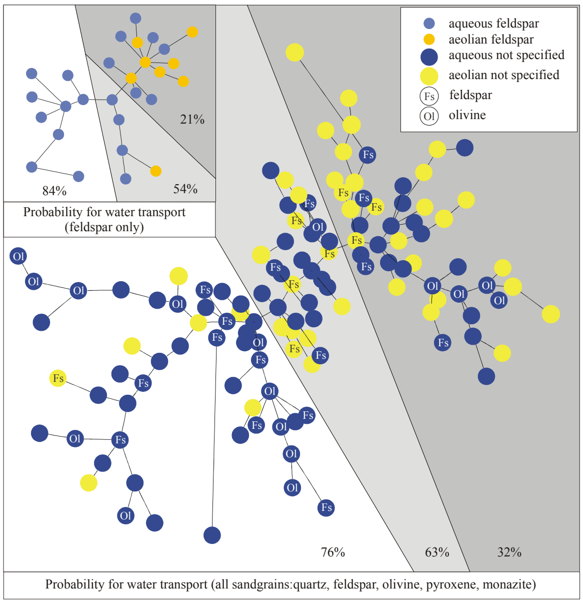

Fig. IV.C.9: Minimal spanning tree showing the similarity of 129 measure points taken from 51 specimens. The degree of affinity of two measurements is indicated by the length of the connecting line. The positive predictive value (PPV) for water transport in each portion of the trees is given in percent.

Chaotic Modes of the AFM

The so called Duffing Oscillator is a prominent example exhibiting chaotic dynamics. While it is numerically well investigated only very few experimental realizations are studied. The dynamics of an AFM-tip can be idealized as a Duffing Oscillator and is governed by very complex dynamics. In collaboration with the Max-Planck-Institut für Biochemie and the Dept. for Geo- and Environmental-Sciences of the University Munich experiments have been conducted in order to explore the route to chaotic behavior in the AFM.

In order to characterize a complex system the so-called correlation dimension can be used. It serves as a dimensionality parameter for an embedded trajectory in phase space and is closely related to the scaling indices.

Within the regular regime the system has a correlation dimension near unity while in the chaotic region values beyond 2 are obtained. The aim of this work was an improvement of the signal-to-noise ratio for AFM-images.

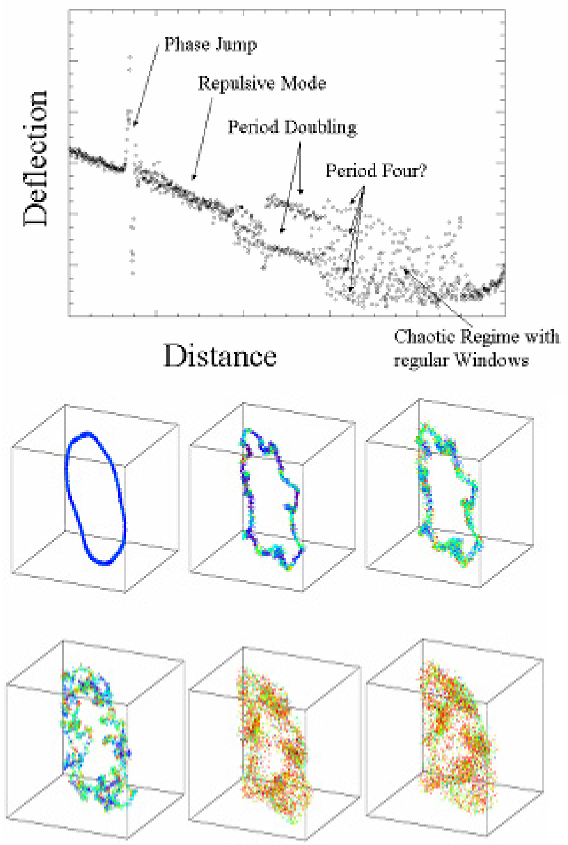

Fig. IV.C.10: Bifurcation Diagram for the experimentally recorded AFM data. The large panel shows a close-up for the transition from regular to chaotic behaviour. After a transition from the attractive to the repulsive mode the system undergoes a period-doubling and finally ends in a chaotic regime.

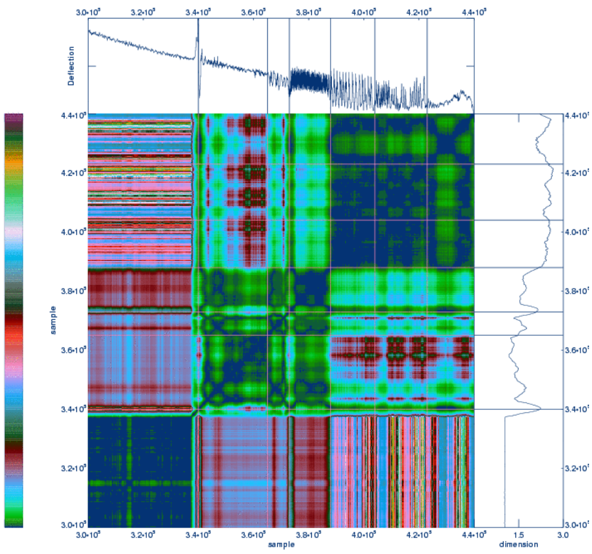

Fig. IV.C.11: Colour coded distance matrix of the pointwise dimension, using a distance measure related to the Kullback-Leibler contrast. For comparison the fractal dimension (on the right) and the deflection signal (upper diagram) are shown.

Medical image processing

In the field of cancer research the possibilities of detection and quantification of early necrosis in breast cancer by MR imaging were investigated. We evaluated the ability of the contrast agent 'Gadophrin' to detect and quantify early necrosis in breast cancer. Therefore breast tumours, which were implanted in mice, underwent MR imaging with and without the injection of Gadophrin. The extent of the tumour necrosis was quantified by applying segmentation algorithms developed at the MPE during the last years, and was correlated with the histological findings. We found that the detection of early necrosis is enhanced by using the contrast agent Gadophrin. These findings improve the assessment of early tumour response on chemotherapy in the future.

The main focus of our studies in medical image processing using non-linear techniques during the last two years was the analysis of bone structures as displayed in high resolution three-dimensional tomographic MR images in order to better assess osteoporosis and the risk of fractures for (mainly) elderly persons. All these studies were conducted within the framework of a so-called 'TANDEM-project' in collaboration with the Institute of Radiology of the Technical University of Munich and the University of California San Francisco (UCSF).

According to the world health organisation (WHO) osteoporosis, which is characterised by low bone mass and structural deterioration of bone tissue leading to fractures of the hip, spine and wrist is among the ten most important diseases worldwide. As populations age the incidence of osteoporosis and subsequent fractures is increasing. In the Western civilization, osteoporosis is already the most prevalent bone disease and will in the future generate major problems for public health institutions.

Besides the application of conventional techniques of measuring the bone mineral density (BMD), high resolution imaging techniques (CT and MR) for the visualisation of the complex, three-dimensional bone structures are optimized. Nowadays it is possible for MR imaging to achieve an in-plane resolution up to 150 µm with a slice thickness of 300 µm. Such high resolutions are obtained for the distal radius and the calcaneus in vivo.

The subsequent application of structure measures offers new diagnostic perspectives in the diagnosis of osteoporosis.

Different linear and non-linear statistical measures for the quantitative characterisation of bone structures were evaluated by using the method of surrogates. It could be shown that for both healthy and osteoporotic bones, surrogates preserving linear correlations in the images can

be generated. By applying non-linear statistical measures such as the spectrum of scaling indices a clear discrimination between the original and surrogate data was possible. We conclude that bone structure contains non-linearities and it is therefore mandatory to use non-linear statistical measures to enable an appropriate description of the data sets.
We used Minkowski-functionals and estimators for the local scaling properties of the data, i.e. scaling index method (SIM) and scaling vector method (SVM). Furthermore it was shown that for both healthy and osteoporotic bones, the generation of surrogates, which preserve the Minkowski functionals, is possible by applying simulated annealing. Using SIM a discrimination between the original and surrogates was possible indicating that the Minkowski functionals and the scaling indices complement each other.
In in vitro studies we investigated the correlation of newly defined statistical measures that quantify the microscopic properties of the trabecular bone structures with macroscopic biomechanical properties (e.g. maximal contraction strength (MCS)).

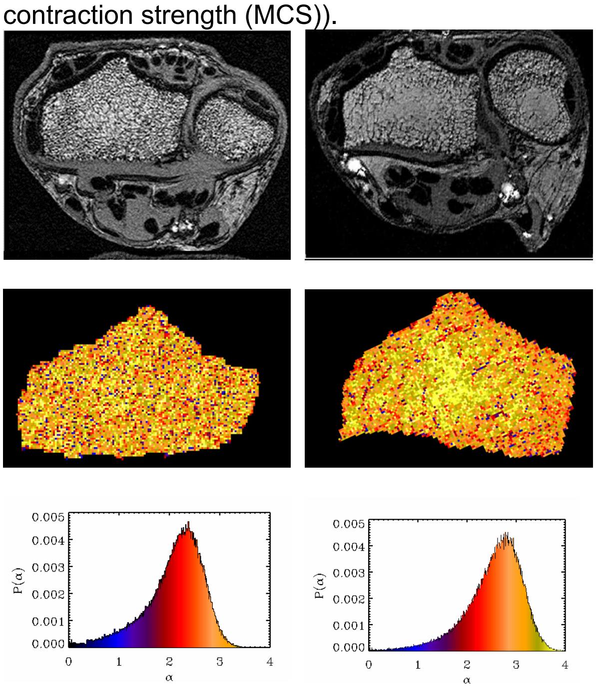

Fig. IV.C.12: Upper row: HR-MR image of the distal radius for a healthy patient (left) and a patient with osteoporotic spine fracture (right). Middle row: the respective segmented distal radius for the images shown in the upper row. Lower row: Spectrum of the scaling indices for the segmented part of the images. The shift of the P(α)-spectrum towards higher values for osteoporotic bones with rarefied trabecular structure is clearly visible.

From the spectrum of scaling indices, which quantifies the local scaling properties in an image, we derived a structural measure $\Delta P(\alpha)$ using a filtering procedure which considers sliding windows of variable width. Thus $P(\alpha)$ represents a part of the bone structure as measured with the scaling indices. For specimen taken from the spine a correlation coefficient R=0.93 between $P(\alpha)$ and MCS was achieved. This result is significantly better than the correlation between the commonly used bone mineral density (BMD) and MCS (R=0.73).
A comparable improvement was obtained for femur specimen, where we obtained a correlation coefficient of R=0.91 using anisotropic scaling indices. The correlation with BMD was only R= 0.72. In this case the conventional measures performed even worse (R=0.6 for BV/TV (=bone volume/ trabecular volume) and R=0.52 for Tr. N. (= trabecular number)).

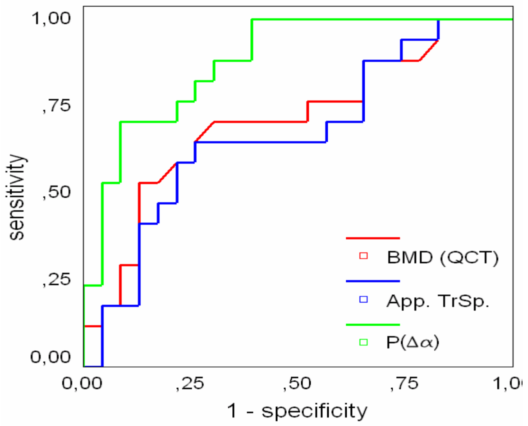

Fig. IV.C.13: ROC-curves, comparing the results of an in vivo study. We show the sensitivity of the BMD (red), of a conventional two-dimensional measure (blue) and of the newly developed structure parameter P(Δα) (green) as a function of the specificity.

A large clinical study is now conducted in order to assess how well the structure measures can predict the risk of spine fractures for postmenopausal women (Fig. IV.C.12). The structure measures $\Delta P(\alpha)$ has been determined in the same way as in the in vitro study. By means of a Receiver Operator Characteristic (ROC) analysis we searched for parts of the $P(\alpha)$-spectrum, or equivalently the part of the bone structure, which are optimal to discriminate between patients with fracture and patients without fracture. The degree of discrimination is quantified by calculating the area (A) under the ROC curve. Our best result is A = 0.86 (see Fig. IV.C.13). To our best knowledge, such a degree of discrimination has never been achieved using other methods.
Bone remodelling processes are governed by two opposite processes namely bone resorption by osteoclasts (spatially random) and bone formation by osteoblasts (stress dependent). These processes can be described by non-linear partial differential equations, which model the effects of osteoclasts and osteoblasts on the local change of the relative bone density. A

possibility to solve partial differential equations numerically is the use of cellular automata. We demonstrated the feasibility of modelling trabecular changes using cellular automata. We showed that trabecular structures emerge from a uniform distribution whereas the alignment of the trabeculae follows the direction of the forces acting on the bone (Wolff's law). The configuration remains stable. Slightly decreasing the sensitivity of osteoblasts to local strain results in a new stable configuration with lower bone density and rarefied trabecular structure (Fig. IV.C.14). The texture measures (e.g. scaling indices and Minkowski functionals) can account for the structural changes. These variations are comparable to those observed in vitro and in vivo (Fig. IV.C.12). In the future we will extend the model to three dimensions, optimize its rules and the choice of parameters.
Investigations of drug effects in silicio as well as a systematic analysis of the sensitivity of texture measures to slight changes in the bone structures will become possible.

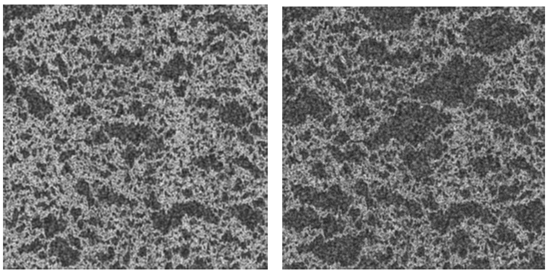

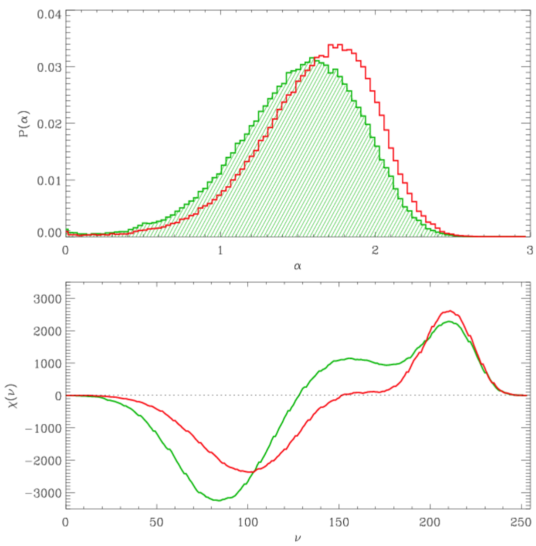

Fig. IV.C.14: Upper left: Image of a simulated two-dimensional trabecular bone structure. Upper right: Configuration after changing a parameter controlling the action of the osteoblasts. Spectrum of the scaling indices (upper diagram) and for the third Minkowski-functional, i.e. Euler characteristic (lower diagram), for the left image (green) and right image (red).

These new methods may well be suited to monitor (drug-induced) changes in the trabecular bone structure, so that a better assessment of the patient's response to a drug-therapy will become available. Future research activities will go into this direction.

EEG Analysis

In a cooperation with the Heckscher Klinik für Kinder- und Jugendpsychiatrie (München) methods were developed, which characterize brain activity in infantile epileptic patients. The analyses base on surface encephalograms (non-invasive EEGs), which were recorded according to the 10-20-International System of Electrode Placements, that means that 21 EEG channels were recorded simultaneously. Hence, additional information could be achieved from the interaction of the different EEG-channels: a spatio-temporal analysis of brain activity is feasible.
In interictal periods, between epileptic attacks (seizures), visual inspection often yields no indications for epileptic patterns. Therefore a method is desired which is sensitive for epileptic signatures even if typical pathological patterns are missing in the EEG. The interaction of the different brain regions is assessed by applying a number of correlation measures on synchronous time segments (1-2 s) of pairs of EEG-channels. It turns out, that the most suitable measure to distinguish between epileptic and normal patients is mutual information. The working hypothesis, that the correlation between the different brain regions during epileptic attacks is high holds even during interictal periods. In Fig. IV.C.15 the effect of medical therapy, which moves the patient in the region of normal brain activity is demonstrated.

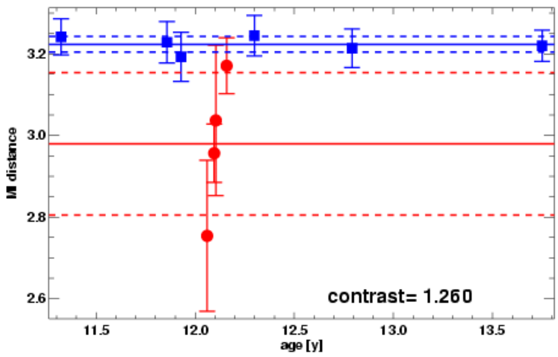

Fig. IV.C.15: Mean mutual information distance for patient A (red) and B (blue). The filled circles denote the mean mutual information distance, the vertical lines indicate the standard deviation of the single EEG-recordings. The horizontal lines label the mean mutual information for patient A and patient B, the dashed lines mark the respective standard deviations. As a consequence of medication patient A "approaches" the region where patient B resides during a longer time of observations.

In some cases the functional deficits stemming from epilepsies are therapy resistant. In these cases even a surgical intervention and removal of the epilepsy triggering brain region is an option. This demands for a very high sensitivity and specificity in selecting the right region.
To get some hints for the localisation of pathological abnormalities a hierarchical tree is generated based on distances constructed from these correlation measures. Up to now, candidates for pathological brain activities could be localised but the exact localisation of the origin of epileptic seizures could not be pinpointed.

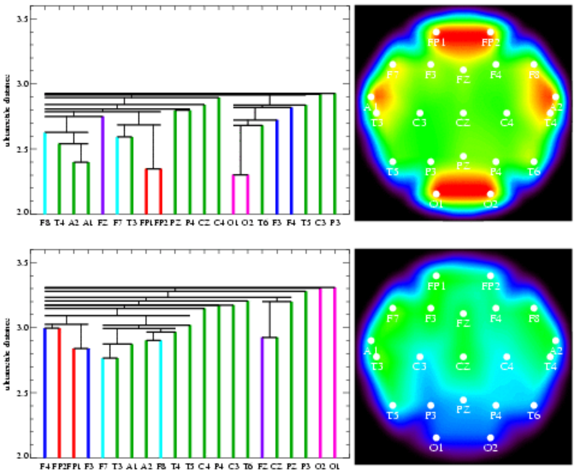

Fig. IV.C.16: Characterization of clustering behaviour of patient A during an epileptic seizure (a) and patient B as a reference (b). In the left part of each panel the exact hierarchical tree is shown, while at the right side a two dimensional approximation (topogram) of the cluster behaviour is displayed. High synchronisation is colour coded in red, low in blue.

The long term goal of this project is, of course, the precise determination of the region of the epileptic focus.

Low-Temperature-Plasma for in vivo-sterilization

In collaboration with ADTEC Plasma Technology Co., Ltd. (Japan) and the Ludwig-Maximilians-University (Prof. Stolz), very recently a new study for the biomedical applications of atmospheric pressure discharge plasmas has been started. The objective is the development of an innovative low temperature plasma for in-vivo sterilisation in medical every-day routine. In order to utilize the expected benefits, this technique will be applied at first to the therapy of chronic foot and leg ulcers.
Fig. IV.C.17 shows the plasma flame which is generated by microwaves. For applications in health care, a non-thermal atmospheric pressure plasma, especially at low gas-temperature, is necessary. In first experiments, the conditions of the low gas-temperature device have been investigated. As a result, a parameter set concerning gas composition and rates, microwave power, and gas temperature has been identified, which fulfils major requirements for the treatment of living tissue. First biological experiments indicate the desired sterilising effect on bacteria. The efficiency of the sterilising process will be evaluated on microbiological level and its effect on the wound healing progress will be quantified using image processing. The latter will benefit from the experience gained in the project concerning the early recognition of skin cancer. Beside standard biomedical techniques, also AFM microscopy will be employed in this study. Fig. IV.C.18 shows an AFM-image of Escherichia coli bacteria after plasma treatment.

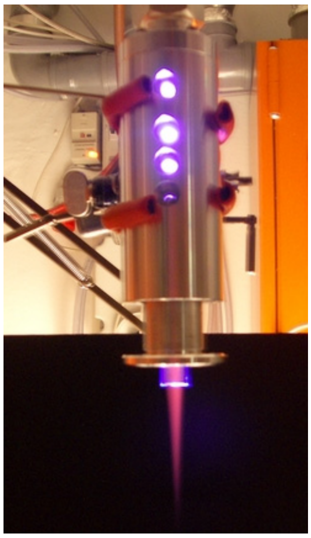

Fig. IV.C.18: First experimental setup of a low-temperature plasma device for in-vivo sterilisation of chronic wounds.

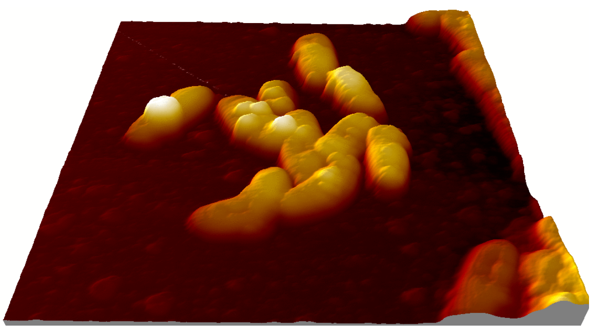

Fig. IV.C.17: AFM-images of Escherichia coli bacteria after treatment with the low-temperature plasma torch.

V. ORGANISATION

Directors

Prof. Dr. Dr. h.c. V. Dose, IPP
Prof. Dr. Dr. h.c. G. Morfill, MPE

Scientific Secretary

Dr. W. Brinkmann

Scientific Advisory Board (CIPS)

Prof. Dr. O. Havnes, University of Trømsø (Norway)
Prof. Dr. J. Honerkamp, Universität Freiburg (Deutschland)
Prof. Dr. K. H. Spatschek, Universität Düsseldorf (Deutschland)

CIPS Associates

Dr. H. Atmanspacher, Institut für Grenzgebiete der Psychologie und Psychohygiene e.V.
Prof. Dr. Peter Awakowicz, Technische Universität, München
Prof. Dr. Dietrich Habs, Ludwig-Maximilians Universität, München
Prof. Dr. Wolfgang Heckl, Ludwig-Maximilians-Universität, München
Prof. Dr. Rainer Hippler, Institut für Physik der Ernst Moritz Arndt Universität Greifswald
Dr. Holger Kersten, Institut für Physik der Ernst Moritz Arndt Universität Greifswald
Prof. Dr. Harald Lesch, Institut für Astronomie und Astrophysik der Univ. München
Prof. Dr. A. Lunk, Institut für Plasmaforschung, Stuttgart
Prof. Dr. Jürgen Meichsner, Institut für Physik der Ernst Moritz Arndt Universität Greifswald
Prof. Dr. Alexander Piel, Christian-Albrechts-Universität Kiel
Prof. Dr. Padma Shukla, Institut für Theoretische Physik, Ruhr-Universität Bochum
Prof. Dr. med. W. Stolz, Dermatologische Klinik und Poliklinik, Klinikum der Universität Regensburg
Prof. Dr. J. Winter, Institut für Experimentalphysik II, Ruhr-Universität Bochum

Personnel (CIPS)

Annaratone, Dr. B. (Complex Plasmas)
Aschenbrenner, Dr. T. (Data Analysis)
Bauer, Dr. M. till 30.09.04 (Complex Plasmas)
Biskamp, Dr. D. (Plasma Theory)
Böhringer, Dr. H. (Extragalactical Astrophysics)
Brinkmann, Dr. W. (Plasma Theory)
Bryant, Dr. P. till 31.08.04 (Complex Plasmas)
Bunk, Dr. W. (Medical Research, Data Analysis)
Collmar, E. (Secretary Projects)
Dum, Dr. C. till 30.06.04 (Plasma Theory)
Fischer, Dr. R. (Data Analysis)
Hallatschek, Dr. K. (Plasma Theory)
Höfner, Dipl. Phys. H. (Complex Plasmas)
Hopf, Dr. Ch. till 31.07.04 (Complex Plasmas)
Ivlev, Dr. A. (Complex Plasmas)
Jacob, Dr. W. (Complex Plasmas)
Jamitzky, Dr. F. (Data Analysis)
Kang, Dr. H. till 31.01.04 (Plasma Theory)
von Keudell, Dr. A. till 28.02.03 (Complex Plasmas)
Khrapak, Dr. S. (Complex Plasmas)
Klumov, Dr. B. (Complex Plasmas)
Konopka, Dr. U. (Complex Plasmas)
Kretschmer, Dr. M. (Complex Plasmas)
Langer, A. (Secretary Management)
Leinthaler, A. till 30.09.03 (Administration)
Matsukiyo, Dr. S. till 18.06.04 (Plasma Theory)
Matsushita, Dr. K. till 31.05.03 (Extragalactical Astrophysics)
Meier, Dr. M. till 31.12.03 (Complex Plasmas)
Monetti, Dr. R. (Data Analysis)
Müller, Dr. W.-Ch. till 31.03.03 (Plasma Theory)
Nanuomura, Dr. S. till 31.12.03 (Complex Plasmas)
Pilipp, Dr. W. till 30.06.04 (Complex Plasmas)
Pompl, Dr. R. (Data Analysis)
Preuss, Dr. R. (Data Analysis)
Quinn, Dr. R. till 29.02.04 (Complex Plasmas)
Ratynskaia, Dr. S. (Complex Plasmas)
Räth, Dr. Ch. (Complex Systems)
Retzlaff, Dr. J. till 30.1.03 (Extragalactical Astrophysics)
Rubin-Zuzic, Dr. M. (Complex Plasmas)
Samsonov, Dr. D. (Complex Plasmas)
Scheingraber, Dr. H. (Complex Dynamics)
Scholer, Prof. Dr. M. (Plasma Theory)
Schuecker, Dr. P. (Extragalactical Astrophysics)
Schwarz-Selinger, Dr. Th. (Complex Plasmas)
Sidorenko, Dr. I. till 30.09.04 (Plasma Theory)
Shimizu, Dr. T. till 31.07.04 (Data Analysis)
Shinohara, Dr. I. till 30.9.01 (Plasma Physics)
Stark, St. till 31.05.02 (Administration)
Sugiyama, Dr. T. till 01.12.02 (Plasma Theory)
Thoma, Dr. M. (Complex Plasmas)
Thomas, Dr. H. (Complex Plasmas)
von Toussaint, Dr. U. (Data Analysis)
Treumann, Prof. Dr. R. (Plasma Astrophysics)
Uchida, Dr. G. since 01.04.03 (Complex Plasmas)
Venus, Dr. G. till 30.06.02 (Data Analysis)
Wiechen, Dr. H. till 31.07.03 (Plasma Astrophysics)
Xue, Dr. Y. till 30.03.04 (Extragalactical Astrophysics)
Yaroshenko, Dr. V. (Complex Plasmas)
Yoon, Dr. J.-S. till 31.01.03 (Data Analysis)
Zeising, I. (Administration)
Zhdanov, Dr. S. (Complex Plasmas)

PhD and Diploma students

(Topic and supervisor in brackets)
Antonova, Dipl. Phys. T. since 04.03.04 (Complex Plasmas; Annaratone)
Ferrero, Dipl.-Phys. E. till 30.08.04 (Extragalactic Astrophysics; Brinkmann)
Fink, Dipl. Phys. M. since 01.04.03 (Complex Plasmas; Morfill)
Goldbeck, Dipl.-Phys. D. till 31.03.04 (Complex Plasmas; Morfill)
Gonzales, E. since 01.04.03 (Complex Plasmas, Morfill)
Guglielmetti, Dipl.-Phys. F. (Data Analysis; Fischer)
Huber, M. till 29.2.2004 (Extragalactical Astrophysics; Schuecker)
Huber, Dipl. Phys. P. since 10.05.04 (Complex Plasmas; Morfill)
Jaroschek, Dipl.-Phys. C. till 30.04.04 (Plasma Astrophysics; Treumann)
Johnson, L. since 01.10.04 (Complex Plasmas, Morfill)
Kompaneets, R., since 01.09.04 (Complex Plasmas, Morfill)
Knapek, Dipl. Phys. C. since 01.06.04 (Complex Plasmas, Morfill)
Mimica, Dipl.-Phys. P. till 30.08.04 (Plasma Astrophysics; Brinkmann)
Mokler, Dipl. Phys. F. (Complex Plasmas, Morfill)
Nodes, Dipl.-Phys. Ch. till 31.08.04 (Plasma Astrophysics; Morfill)
Schlüter, Dipl.-Phys. M. since 01.09.03 (Complex Plasmas; Jacob)
Sütterlin, Dipl.-Phys. R. (Complex Plasmas; Morfill)

Guests

Abelson, Prof. J.R., Univ. of Illinois at Urbana, USA (Data Analysis)
Arkhipov, Dr. I., Moscow, Russia (Complex Plasmas)
Aslaksen, Dr. T. (Complex plasmas)
Atmanspacher, Dr. H., Freiburg, Germany (Analysis Techniques)
Babkina, T., Ruhr-Univ. Bochum, Germany (Complex Plasmas)
Bernardo, Prof. Dr. J., Univ. de València, Spain (Data Analysis)
Caticha, Dr. A., Univ. at Albany-SUNY, USA (Data Analysis)
Daghofer, M., Technical Univ. Graz, Austria (Data Analysis)
D'Agostini, Prof. G., Univ. La Sapienza Rome, Italy (Data Analysis)
Dieterich, Dr. P., TU Dresden, Germany (Data Analysis)
Drake, Prof. J.F., Univ. of Maryland, USA (Plasma Theory)
Durand-Drohin, O., Univ. of Amiens, France (Complex Plasmas)
Edelmann, Dr. E., Univ. of Helsinki, Finland (Data Analysis)
Fedosenko, Dr. G,, Forschungszentrum für Mikrostrukturtechnik Wuppertal, Germany (Complex Plasmas)
Giudici, Prof. P., Univ. di Pavia, Italy (Data Analysis)
Gozadinos, Dr. Y., Univ. P. Sabatier, Toulouse, France (Complex Plasmas)
Hoshino, Prof. Dr. M., Univ. of Tokyo, Japan (Plasma Theory)
Joyce, Prof. G., George Mason University Fairfax, VA, USA (Complex Plasmas)
Jovanovich, Dr. D. University of Warschaw, Poland (Complex Plasmas)
Khrapak, Prof. A, IHED, Moscow (Complex Plasmas)
LaBelle, Prof. J., Dept. Phys. Astron., Dartmouth College, New Hampshire, USA (Plasma Theory)
Loredo, Dr. Th., Cornell Univ., Ithaca, USA (Data Analysis)
Mamun, Prof. A. Tata Institute, Bombay India (Complex Plasmas)
Polozhiy, Dr. K., Kharkov State Univ., Ukraine (Complex Plasmas)
Rodriguez, Prof. C., Univ. at Albany, USA (Data Analysis)
Salonen, Dr. E., TU Helsinki, Finland (Data Analysis)
Shinohara, Dr. I., ISAS Tokyo, Japan
Steinberg, Prof. V., Senior Humboldt Fellow 2001, Weizman Institute, Rehovot, Israel (Complex Plasmas)
Sun, C. Dalian University of Technology, P. R. China (Complex Plasmas; Jacob)
Swisdak, Dr. M., Univ. of Maryland, USA (Plasma Theory)
Thomas, Dr. E., Auburn Univ., USA (Complex Plasmas)
Tsytovich, Prof. V., General Physics Institute, Moscow (Complex plasmas)
van der Linde, Prof. Dr. A., Univ. Bremen, Germany (Data Analysis)
Vladimirov, Dr. S., Univ. of Sidney, Australia (Complex Plasmas)
Zaslavsky, Prof. G., Courant Institute, New York, USA (Data Analysis)

Engineering

Biglmayr, Dipl.-Ing. (FH) B. since 01.09.02 (Complex Plasmas)
Deutsch, R. till 31.04.2004 (Complex Plasmas)
Deysenroth, C. since 01.01.04 (Complex Plasmas)
Dürbeck, Th. since 01.02.01 (Complex Plasmas)
Gori, S. (Data Analysis)
Hagl, Dipl.-Ing. (FH) T. (Complex Plasmas)
Huber, H. (Complex Plasmas)
Lieb, W. (Complex plasmas)
Plöckl, B. (Complex Plasmas)
Rothermel, Dr. H. (Complex plasmas)

Steffes, H. (Complex plasmas)
Stöcker, Dipl. Ing. J. (Complex plasmas)
Tarantik, Dipl. Ing. K. (Complex Plasmas)

Science Project Teams

Experimental Plasma Science
Annaratone, Antonova, Bauer, Fink, Goldbeck, Gonzales, Hadziavdic, Höfner, Hopf, Huber, Ivlev, Jacob, Johnson, Kang, Khrapak, Klumov, Knapek, Kompaneets, Konopka, Korobkov, Kretschmer, Meier, Mokler, Nanomura, Pilipp, Quinn, Ratynskaia, Rothermel, Rubin-Zuzic, Samsonov, Schlüter, Schwarz-Selinger, Shimitsu, Sütterlin, Thoma, Thomas, Uchida, von Keudell.

Analysis Techniques and Applications
Aschenbrenner, Bunk, Fischer, Gori, Guglielmetti, Jamitzky, Preuss, Pompl, Räth, Scheingraber, von Toussaint, Venus, Yoon.

Theoretical Plasma Science
Ambros, Biskamp, Böhringer, Brinkmann, Chen, Dum, Ferrero, Hallatschek, Lynam, Matsushita, Müller, Nakamura, Popesso, Scholer, Schuecker, Sidorenko, Treumann

Scientific Collaborations in Projects

Austria
Technische Universität Graz: Analysis Techniques

Brazil
Universidade Federal do Rio de Janeiro: Plasma Science

France
GREMI-Lab, Orleans: Complex Plasmas; Plasma Kristall Experiment (PKE)
Université Denis Diderot: Analysis Techniques
University Amiens: Plasma Science

Germany
DLR-Köln Porz: Plasma Kristall Experiment (PKE)
Universität Bochum: Complex Plasmas
Universität Kiel: Complex Plasmas
TU München: Analysis Techniques
Universität Stuttgart: Analysis Techniques
FHI Berlin: Analysis Techniques
TU Dresden: Analysis Techniques
Universität Würzburg: Analysis Techniques
EMA Universität Greifswald: Analysis Techniques
Universität Münster: Analysis Techniques
MPQ Garching: Complex Plasmas

Great Britain
Rutherford Appleton Laboratory: Complex Plasmas
University Oxford: Complex Plasmas
Cambridge University: Complex Plasmas

Italy
University Naples: Complex Plasmas
Univ. La Sapienza Rome: Analysis Techniques

Japan
Tohuko University: Complex Plasmas

The Netherlands
University Eindhoven: Complex Plasmas

Norway
University Tromsø: Complex Plasmas

Portugal
University Lisbon: Complex Plasmas

Russia
Institute for High Energy Densities of the Russian Academy of Science, Moscow: Plasma-Kristall-Experimente (PKE-Nefedov, PK-3 Plus, PK-4).

USA
Naval Research Laboratory, Washington: Complex Plasmas – numerical simulations
University of Iowa, Iowa City: Complex Plasmas
American University Washington DC: Analysis Techniques, Maximum Entropy
University of Illinois, Urbana: Plasma Science

Multinational Collaborations

Plasmakristall Experiment PKE: IHED Moscow, Russia; GREMI-Lab, Orleans; University of Iowa, USA; DLR-Köln, Germany.

Industrial Collaborations

Kayser-Threde GmbH, München;
- Plasmakristall-Experimente (PKE) on board of the ISS
- Development of adaptive electrodes

Adtec, Japan:
- Plasma Medicine

Research cooperations (partially) financed by industry

DZ Bank, Deutsche Zentralgenossenschafts-bank, Frankfurt:
Physics of financial markets
Knoll AG, Ludwigshafen: Analysis of long term cardiograms
Linos AG / Rodenstock Präzisionsoptik,

München: Detection of malignant melanoma.
Focus GmbH, Hünstetten-Görsroth
'Characterisation of atomic hydrogen source'

Licenses

Knoll AG, Ludwigshafen: Pharmacology.
Linos AG / Rodenstock Präzisionsoptik, München: Detection of malignant melanoma.
Gany Med AG: Heart Disease
Licensing agreements pending
Kayser-Threde GmbH, München: Complex Plasmas.

Cooperation with Universities (contracts)

Analysis of complex systems:
Institut für Werkstofftechnik und Strukturforschung, Universität Bremen.

Anaesthesiology:
Klinik für Anästhesiologie, Klinikum Rechts der Isar, TU München.

Dermatology:
Dermatologische Klinik, Universität Regensburg;
Fachhochschule München, Institut für Informatik und Mathematik;
Institut für med. Statistik und Epidemilogie, TU München.

Prenatal studies:
Frauenklinik und Poliklinik, Klinikum Rechts der Isar, TU München.

Rastersonden Mikroskopie:
Institut für Kristallographie und Angewandte Mineralogie, LMU, München.

Radio diagnostics:
Institut für med. Statistik und Epidemilogie, TU München;
Institut für Röntgendiagnostik, TU München

Patents

Verfahren und Einrichtung zur Raumfilterung (D, Eu, USA, J); Pat. 700 544

Verfahren und Vorrichtung zur Mustererfassung (D, Eu, USA, J); Pat. 825 543

Teilchenmanipulierung (D, Eu, USA, Japan, Russland); Pat. pending 197 13 637.0

Melanomerkennung (D);
Pat.: # 197 54 909

Verfahren und Vorrichtung zur Segmentierung einer Punkteverteilung (D);
Pat. pending: # 199 28 231-5

Method for Producing Particles with diamond Structure (Pat. Appl. For)

Awards

Schwarz-Selinger Th., 2000: Best Poster Award,
14th International Conference on Plasma Surface Interaction, Rosenheim, Germany

Meier M., 2001: Best Paper Award,
15th International Symposium on Plasma Chemistry, Orelans, France

von Keudell A., 2001: Akademiepreis awarded by Berlin-Brandenburgische Akademie der Wissenschaften

Appointments

Dr. W. Jacob, C3, IPP
Dr. A. von Keudell, C3, University of Bochum
Dr. H. Thomas, C3, MPE

VI. PUBLICATIONS 2000 - 2004

Amin, M.R., G.E. Morfill: Effects of dust on amplitude modulation of kinetic Alfven waves, Physica Scripta **63**, 391-394 (2001).

Annaratone, B.M.A., A.G. Khrapak, A.V. Ivlev et al.: Levitation of Cylindrical Particles in the Sheath of an rf Plasma. Phys. Rev. (E) **63**, 36406-36412 (2001).

Annaratone, B.M.A. and J.E. Allen: A Radiofrequency sustained double layer in a plasma reactor. J. Appl. Phys. **91**, 6321-6324 (2002).

Annaratone, B.M.A., S.A. Khrapak, P. Bryant, G.E. Morfill, H. Rothermel, H.M. Thomas, M. Zuzic, V. E. Fortov, V. I. Molotkov, A.P. Nefedov, S. Krikalev and Yu.P. Semenov. Complex-plasma boundaries. Phys. Rev. E **66**, 056411 (2002).

Annaratone, B.M.A. and G. Morfill: On the motion of particles in plasma in absence of external forces. J. Phys. D: Applied Physics **36**, 2853-2858 (2003).

Annaratone, B.M.A., M. Glier, M. Raif, T. Stuffler, H. Thomas and G.E. Morfill: The plasma sheath in front of an adaptive electrode. In: International Conference on Plasma and Ionised Gases. (Ed.) J. Meichsner, Greifswald, 1-2 (2003).

Annaratone, B.M.A., M. Glier, T. Stuffler, H. Thomas, M. Raif and G.E. Morfill: The plasma-sheath boundary near the adaptive electrode as traced by particles. New Journal of Physics **583**, 3, 92.1-92.12 (2003).

Annaratone B.M., T. Antonova, H.M.Thomas, et al.: Diagnostics of the electronegative plasma sheath at low pressures using microparticles Phyiscal Review Letters **93** (18): 185001 OCT 29 (2004).

Annaratone, B.M. and J. E. Allen: A note on the potential acquired by a dust particle in an electronegative plasma, J. Phys. **38**, 26 (2005).

Arzner, K. and M. Scholer: Kinetic Structure of the Post Plasmoid Plasma Sheet during Magnetotail Reconnection. Journal of Geophysical Research **106**, 3827-3844 (2001).

Arzner, K. and M. Scholer: Magnetotail Reconnection: Simulation Predictions on Magnetic Time Series. Earth Planets Space **53**, 655-661, (2001).

Arzner, K., M. Scholer and R.A. Treumann: Percolation of Charged Particle Orbits in Two-dimensional Irregular Magnetic Fields and its Effect in the Magnetospheric Tail. Journal of Geophysical Research **107**, SMP 5-1-5-15 (2002).

Atmanspacher, H. and H. Scheingraber: Investigating Deviations from Dynamical Randomness with Scaling Indices. Journal of Scientific Exploration **14**, 1-18 (2000).

Atmanspacher, H., W. Ehm, H. Scheingraber and G. Wiedenmann: Statistical Analysis of Time Series with Scaling Indices. Discrete Dynamics in Nature and Society **5**, 297-309 (2001).

Atmanspacher, H. and H. Scheingraber: Stabilization of causally and non-causally coupled map lattices. Physica A **345,** 435-447 (2005).

Bandyopadhyay, M., A. Tanga, P.C. McNeely, V. Yaroshenko: Comparative measurements between Langmuir probe and ion-acoustic wave detection in a radio-frequency source, Contrib. Plasma Phys., **44,** No 7-8, 624-628 (2004).

Bauer, T.M., G. Paschmann, N. Sckopke et al.: Fluid and Particle Signatures of Dayside Reconnection. Annales Geophysicae **19**, 1045-1063 (2001).

Bauer, T.M., R.A. Treumann and W. Baumjohann: Investigation of the Outer and Inner Low-latitude Boundary Layers. Annales Geophyiscae **19**, 1065-1088 (2001).

Behrisch, B., M. Mayer, W. Jacob et al.: Quantitative Analysis of Deuterium in a-C:D Layers, a Round Robin Experiment. Journal of Nuclear Materials **281**, 42-56 (2000).

Birk, G.T. and H. Wiechen: Resistive Tearing Mode Instabilities in Partially Ionised Dusty Plasmas. Proceedings of ISSS, 6222-225 (2001).

Birk, G.T. and H. Wiechen: Radiative Condensation Modes in Dense Dusty Plasmas. Physics of Plasmas **8**, 5057-5060 (2001).

Birk, G.T. and H. Wiechen: Shear Flow Instabilities in Magnetized Partially Ionized Dense Dusty Plasmas. Physics of Plasmas **9**, 964-970 (2002).

Biskamp, D. and E. Schwarz: Localization, the Clue to Fast Magnetic Reconnection. Physics of Plasma **8**, 4729-4731 (2001).

Biskamp, D. and W.Ch. Müller: Scaling Properties of Three-dimensional Isotropic Magnetohydrodynamic Turbulence. Physics of Plasmas **7**, 4889-4900 (2000).

Biskamp, D. and E. Schwarz: On Two-dimensional Magnetohydrodynamic Turbulence. Physics of Plasmas **8**, 3282-3292 (2001).

Biskamp, D., K. Hallatschek and E. Schwarz: Scaling Laws in Two-dimenisonal Turbulent Convection. Physical Review E **63**, 045302-1–045302-4 (2001).

Biskamp, D.: Response to "Comment on 'On Two-dimensional Magnetoyhydrodynamic Turbulence' "[Phys. Plasmas 9, 1484 (2002).]. Physics of Plasmas **9**, 1486 (2002).

Blum, J., G. Wurm, S. Kempf, G.E. Morfill et al.: Growth and form of planetary seedlings: Results from a microgravity aggregation experiment, Physical Review Letters **85**, 2426-2429 (2000).

Böhm, H., C. Räth, G. Morfill, S. Majumdar, E. Rummeny and T.M. Link: Comparison of local 3D scaling properties extracted from high resolution MRI of human trabecular bone and BMD with respect to predict mechanical strength in vitro. Radiol., **225** (Suppl. S), 419 (2002).

Böhm, H., C. Räth, R.A. Monetti, D. Müller, D. Newitt, S. Majumdar, E. Rummeny and T.M. Link: Application of the standard Hough-transformation to high resolution MRI of human trabecular bone to predict mechanical strength, Proc. of the SPIE: Medical Imaging: Image Processing, **5032**, 470-479 (2003).

Böhm, H., C. Räth, R. Monetti, D. Müller, D. Newitt, S. Majumdar and T. Link: Prediction of the biomechanical strength of bone by analysis of local 3D scaling properties extracted from high resolution MRI of human trabecular bone in comparison with bone mineral desity in vitro, Bone, **32**, S78 (2003).

Böhm, H., C. Räth, R. Monetti, D. Müller, S. Majumdar and T. Link: Predicting the Mechanical strength of human trabecular bone specimens in vitro by application of non-linear structural parameters based on topological properties (Minkowski Functionals) to high resolution magnetic resonance images, Radiol., **229** (Suppl. S), 517 (2003).

Böhm, H.F., C. Räth, R.A. Monetti, D. Mueller, D. Newitt, S. Majumdar, E. Rummeny, G. Morfill and T.M. Link: Local 3D scaling properties for the analysis of trabecular bone extracted from high-resolution magnetic resonance imaging of human trabecular bone. Investigative Radiology **38**, 269-280 (2003).

Böhm, H., T. M. Link, R. A. Monetti, D. Müller, E. J. Rummeny, D. Newitt, S. Majumdar and C. W. Räth: Application of the Minkowski functionals in 3D to high resolution MR images of trabecular bone: prediction of the biomechanical strength by non-linear topological measures, Proc. of the SPIE: Medical Imaging: Image Processing **5370**, 172-180 (2004).

Böhm, H., T. M. Link, R. A. Monetti, D. Müller, E. J. Rummeny, G. Morfill and C. W. Räth: Assessment of Vertebral Fractures in Post-Menopausal Women by Topological Analysis of High Resolution MRI of the Distal Radius in 2D and 3D Using Bone Mineral Density and Linear Texture Measures as a Standard of Reference, J. Bone Min. Res., **19**, S371 (2004).

Böhm, H., C. Räth, R. Monetti, D. Newitt, S. Majumdar, E. Rummeny, G. Morfill and T. Link: Nichtlineare Texturmaße basierend auf den Minkowski-Funktionalen in 3D: Vorhersage der Bruchlast trabekulärer Knochenpräparate durch Strukturanalyse hochauflösender MR-Aufnahmen, in: Bildverarbeitung für die Medizin, T. Tolxdorff, J. Braun, H. Handels, A. Horsch, H.-P. Meinzer (Eds.), Springer Verlag, Berlin, 140-144 (2004).

Böhm, H., T.Link, R. Monetti, D. Müller, E. Rummeny, D. Newitt, S. Majumdar and C. Räth: Application of the Minkowski functionals in 3D to high resolution MR images of the trabecular bone for the prediction of the biomechanical strength, Proceedings of Microscopy and Microanalysis, 714-715 (2004).

Böhringer, H., G. Soucail, Y. Mellier, Y. Ikebe and P. Schuecker: The X-ray Morphology of the Lensing Galaxy Cluster Cl0024+17. Astron. Astrophys. **353**, 124-128 (2000).

Böhringer, H., E. Belsole, J. Kennea et al.: XMM-Newton Observation of M87 and its X-ray Halo. Astron. Astrophys. Lett. **365**, L181-L187 (2001).

Böhringer, H., P. Schuecker, L. Guzzo et al.: The ROSAT-ESO Flux Limited X-Ray (REFLEX) Galaxy Cluster Survey I: The Construction of the Cluster Sample. Astron. Astrophys. **369**, 826-850 (2001).

Böhringer, H., C.A. Collins, L. Guzzo et al.: The REFLEX Galaxy Cluster Survey IV: The X-ray luminosity function. Astrophys. J. **566**, 93-102 (2002).

Böhringer, H., P. Schuecker, L. Guzzo et al.: The ROSAT-ESO Flux Limited X-ray (REFLEX) Galaxy Cluster Survey V. The cluster catalogue. Astron. Astrophys. **425**, 367-383 (2004).

Boller, Th., M. Gliozzi, G. Griffiths et al.: XMM-Newton Observations of the BL Lac 0737+7441. Astron. Astrophys. Lett. **365**, L158-L162 (2001).

Bornhausen, M. and H. Scheingraber: Prenatal Exposure to 900 MHz, Cell-phone Electromagnetic Fields had no Effect on Operant-behavior Performances of Adult Rats. Bioelectromagnetics **21**, 566-574 (2000).

Brinkmann, W., S.A. Laurent-Muehleisen, W. Voges et al.: Radio and X-ray bright AGN: The ROSAT – First correlation. Astronomy and Astrophysics **356**, 445-462 (2000).

Brinkmann, W. and N. Kawai: The Jets of SS 433: Second Order Effects. Astronomy and Astrophysics **363**, 640-646 (2000).

Brinkmann, W., M Gliozzi, C.M. Urry, L. Maraschi and R. Sambruna: The Soft X-Ray Variability of PKS 2155-304. Astronomy and Astrophysics **362**, 105-112 (2000).

Brinkmann, W., M. Gliozzi, H. Negoro, I.E. Papadakis, E. Detsis and I. Papamastorakis: Optical and X-ray monitoring of the NLS1 Galaxy Ark 561. In: New Century of Astronomy. (Eds.) H. Inoue, H. Kunieda. ASP Conference Series Vol. 251, Astronomical Society of the Pacific, San Francisco, USA, 340-341 (2001).

Brinkmann, W., M. Gliozzi, H. Scheingraber et al.: Optical and X-ray Monitoring of the NLS1 Galaxy Ark 561, in: New Century of Astronomy, (Eds.) H. Inoue, H. Kunieda, ASP Conf. Series, Vol. **251**, 340-341 (2001).

Brinkmann, W., S. Sembay, R.G. Griffiths et al.: XMM-Newton Observations of Markarian 421. Astronomy and Astrophysics **365**, L162-L167 (2001).

Brinkmann, W., E. Ferrero and M. Gliozzi: XMM-Newton observations of the BAL quasar PHL 5200: The big surprise. Astron. Astrophys. **385**, L31-L35 (2002).

Brinkmann, W., M. Gliozzi, H. Scheingraber, H. Negoro, I.E. Papadakis, E. Detsis and I. Papamastorakis: Optical and X-ray monitoring of the NLS1 Galaxy Ark 564. In: MAXI Workshop on AGN Variability. (Eds.) N. Kawai, H. Negoro, A. Yoshida, T. Mihara. Vol., Seiyo Press, Saitama, Japan, 131-136 (2002).

Brinkmann, W., D. Grupe, G. Branduardi-Raymont and E. Ferrero: XMM-Newton observation of PG 0844-309. Astron. Astrophys. **398**, 81-87 (2003).

Brinkmann, W., I.E. Papadakis, J.W.A den Herder and F. Haberl: Temporal Variability of Mrk 421 from XMM-Newton Observations. Astron. Astrophys. **402**, 929-947 (2003).

Brinkmann, W., V. Burwitz, I.E. Papadakis and J.W.A. den Herder: Recent X-ray observations of BL Lac objects, in: High Energy Blazar Astronomy, (Eds.) L.O. Takalo, E. Valtaoja, APS Conference Series Vol. **299**, Ann Arbor, Michigan, p. 53-62 (2003).

Brinkmann, W., I.E. Papadakis and E. Ferrero: XMM-Newton observations of the two X-ray weak quasars PG 1411+442 and Mrk 304. Astron. Astrophys. **414**, 107-116 (2004).

Brinkmann, W., P. Arevalo, M. Gliozzi and E. Ferrero: X-ray variability of the Narrow Line Seyfert 1 Galaxy PKS 0558-504. Astron. Astrophys. **415**, 959-969 (2004).

Bryant, P: Floating potential of spherical probes and dust grains in collisional plasmas. J. Phys. (D) **36**, 2859-2868 (2003).

Bullen, A.J., K.E. O'Hara, D.G. Cahill, O. Monteiro and A. von Keudell: Thermal Conductivity of Amorphous Carbon Thin Films. Journal of Applied Physics **88**, 6317-6320 (2000).

Bunk, W., F. Jamitzky, R. Pompl, C. Räth and G. Morfill: Local Scaling Properties for Diagnostic Purposes. In: Proc. The Science of Disasters. (Eds.) A. Bunde, J. Kropp, H.J. Schellnhuber., Springer Berlin 2002, 283-313.

Carrington, M.E., T. Fugleberg, D. Pickering, and M.H. Thoma: Dielectric Functions and Dispersion Relations of Ultra-Relativistic Plasmas with Collisions, Can. J. Phys. **82**, 671 (2004).

Caticha, A. and R. Preuss: Maximum Entropy and Bayesian Data Analysis: Entropic Prior Distributions. Physical Review E **70**, 046127-1-046127-12 (2004).

Chakraborty, P., M. G. Mustafa, and M.H. Thoma: Quark Number Susceptibility in Hard Thermal Loop Approximation, Eur. Phys. J. C **23**, 591 (2002).

Chakraborty, P., M. G. Mustafa, and M.H. Thoma: Chiral Susceptibility in Hard Thermal

Loop Approximation, Phys. Rev. D **67**, 114004 (2003).

Chakraborty, P., M.G. Mustafa, and M.H. Thoma: Quark Number Susceptibility, Thermodynamic Sum Rule, and Hard Thermal Loop Appproximation, Phys. Rev. D **68**, 085012 (2003).

Collins, C.A., L. Guzzo, H. Böhringer et al.: The ROSAT-ESO Flux-Limited (REFLEX) Galaxy Cluster Survey II: The Spatial Correlation Function. Mon. Not. R. Astron. Soc. **319**, 939-948 (2000).

Constantinescu, O.D., K.-H. Glassmeier, R. Treumann and K.-H. Fornacon: Magnetic Mirror Structures Oberserved by Cluster in the Magnetosheath. Geophysical Research Letters **30**, 4-1 – 4-4 (2003).

Cremer, M. and M. Scholer: On a Nonlinear State of the Electromagnetic Ion/Ion Cyclotron Instability. Nonlinear Processes in Geophysics **7**, 173-177 (2000).

Cremer, M. and M. Scholer: Structure of the Reconnection Layer and the Associated Slow Shocks: Two-dimensional Simulations of a Riemann Problem. Journal of Geophysical Research **105**, A12, 27,621-27,632 (2000).

Cruddace, R.G., W. Voges, H. Böhringer et al.: A Catalog of Clusters of Galaxies in a Region of 1 Ster Around the South Galactic Pole, Derived From a Systematic Search of the ROSAT All-Sky Survey. Astrophys. J. Supp. **140**, 239-264 (2002).

Czaykowska, A., T.M. Bauer, R.A. Treumann and W. Baumjohann: Magnetic Field Fluctuations across the Earth's Bow Shock. Annales Geophysicae **19**, 1-13 (2001).

Dose, V., P. Pecher and R. Preuss: Formulas for Cross Sections and Rate Coefficients for Partial Electron Impact Ionization of CH_4 and H_2. Journal of Physical and Chemical Reference Data **29**, 1157-1164 (2000).

Dose, V., J. Neuhauser, B. Kurzan et al.: Tokamak Edge Profile Analysis Employing Bayesian Statistics. Nuclear Fusion **41**, 1671-1685 (2001).

Dose, V., R. Preuss and J. Roth: Evaluation of Chemical Erosion Data for Carbon Materials at High Ion Fluxes using Bayesian Probability Theory. Journal of Nuclear Materials **288**, 153-162 (2001).

Dose, V.: Bayes in Five Days. Lecture Notes from a Ten Hour Tutorial on Bayesian Analysis Given at the International Max-Planck- Research School on Bounded Plasmas, Greifswald. CIPS Report No. 83 (2001).

Dose, V.: Bayesian Inference in Physics: Case Studies. Reports on Progress in Physics **66**, 1421-1461 (2003).

Dose; V.: Hyperplane Priors. In: Bayesian Inference and Maximum Entropy Methods in Science and Engineering, C.J. Williams (Ed.). American Institute of Physics 2003, 350-357.

Dose, V. and A. Menzel: Bayesian Analysis of Climate Change Impacts in Phenology. Global Change Biology **10**, 259-272 (2004).

Eckstein, W. and R. Preuss: New Fit Formulae for the Sputttering Yield. Journal of Nuclear Materials **320**, 209-213 (2003).

Erkaev, N.V., V.S. Semenov and F. Jamitzky: Rec-onnection Rate for the Inhomogeneous Resistivity Model. Physical Review Letters **84**, 1455-1458 (2000).

Ferrero, E. and W. Brinkmann: XMM-Newton observations of four high-z quasars, Astron. Astrophys. **402**, 465-476 (2003).

Fischer, R., K.M. Hanson, V. Dose and W. von der Linden: Background Estimation in Experimental Spectra. Physical Review E **61**, 1152-1160 (2000).

Fischer, R.: Depth Profiles and Resolution Limits in Accelerator-based Solid State Analysis. Analytical Bioanalytical Chemistry **374**, 619-625 (2002).

Fischer, R., C. Wendland, A. Dinklage, S. Gori, V. Dose and the W7-AS team: Thomson Scattering Analysis with the Bayesian Probability Theory. Plasma Physics and Controlled Fusion **44**, 1501-1519 (2002).

Fischer, R. and V. Dose: Physical Mixture Modeling with Unknown Number of Components. CP617, Bayesian Inference and Maximum Entropy Methods in Science and Engineering: 21 Intern. Workshop, (Ed.) R.L. Fry, 143-154 (2002).

Fischer, R., A. Dinklage and E. Pasch: Bayesian Modelling of Fusion Diagnostics. Plasma Physics and Controlled Fusion **45**, 1095-1111 (2003).

Fischer, R.: Bayesian Group Analysis of Plasma-enhanced Chemical Vapour Deposition

Data. New Journal of Physics **6**, 25.1-25.19 (2004).

Fischer, R.: Bayesian Experimental Design – Studies for Fusion Diagnostics. In: Bayesian Inference and Maximum Entropy Methods in Science and Engineering, R. Fischer, R. Preuss, U. von Toussaint (eds.), American Institute of Physics 2004, 76-83.

Fleishman, G. and K. Arzner: Saturation of Electron Cyclotron Maser by Lower-hybrid Waves. Astron. Astrophys. **358**, 776-788 (2000).

Fortov, V.E,. O.S. Vaulina, O.F. Petrov, V. I. Molotkov, A.V. Chernyshev, A.M. Lipaev, G. Morfill, H. Thomas, H. Rothermel, S.A. Khrapak, Yu.P. Semenov, A.I. Ivanov, S. K. Krikalev and Yu.P. Gidzenko. Dynamics of macroparticles in a dusty plasma under microgravity conditions. JETP **96**, 704 (2003).

Fortov, V.E., O.S. Vaulina, O.F. Petrov, V.I. Molotkov, A.M. Lipaev, V.M. Torchinsky, H.M. Thomas, G.E. Morfill, S.A. Khrapak, Y.P. Semenov, A.I. Ivanov, S.K. Krikalev, A.Y. Kalery, S.V. Zaletin and Y.P. Gidzenko: Transport of microparticles in weakly ionised gas-discharge plasmas under microgravity conditions. Phys. Rev. Lett. **90**, 245005-1-245005-4 (2003).

Fortov, V.E., O.S. Vaulina, O.F. Petrov, V.I. Molotkov, A.M. Lipaev, A.V. Chernyshev, A.V. Gavrikov, I.A. Shakhova, H. Thomas, G.E. Morfill, S.A. Khrapak, Y.P. Semenov, A.I. Ivanov, S.K. Krikalev, A.Y. Kalery, S.V. Zaletin and Y.P. Gigzenko: Dusty plasma in gas-discharges under ground-based and micrograviton conditions. In: 30th EPS Conference on Controlled Fusion and Plasma Physics, St. Petersburg 2003, ECA Vol. 27A, 0-1.1B (1-4) (2003).

Fortov, V.E,. A. G. Khrapak, S.A. Khrapak, V. I. Molotkov and O. F. Petrov. Dusty Plasmas. Phys. Uspekhi **47** (5) 447 (2004). .

Fortov, V.E., O.S. Vaulina, O.F. Petrov, V. I. Molotkov, A.M. Lipaev, G. Morfill, H. Thomas, S. Khrapak, Yu.P. Semenov and A.I. Ivanov. Dynamics and structural properties of dusty plasma liquid in microgravity: experiments onboard the International Space Station. Plasma Phys. Control. Fusion (in press, 2004).

Gaidashev, D.G. and S.K. Zhdanov: On the transverse instability of the two-dimensional Benjamin-Ono solitons. Phys. Fluids. **16**, 1915-1921 (2004).

Gioia, I.M., J.P. Henry, C.R. Mullis et al.: Cluster Evolution in the ROSAT North Ecliptic Pole Survey. Astrophys. J. Lett. **553**, L105-L108 (2001).

Gliozzi, M., Th. Boller, W. Brinkmann and W.N. Brandt: ROSAT HRI Monitoring of X-ray Variability in the NLS1 Galaxy PKS 0558-504. Astronomy and Astrophysics **356**, L17-L20 (2000).

Gliozzi, M., W. Brinkmann, P.T. O'Brien et al.: XMM-Newton Monitoring of X-ray Mariability in the Quasar PKS 0558-504. Astronomy and Astrophysics **365**, L128-L133 (2001).

Gliozzi, M., W. Brinkmann, S.A. Laurent-Muehleisen, E.C. Moran and J. Whalen: BeppoSax Observations of the Narrow-Line Seyfert 1 Galaxy RX J1702.5+3247. Astron. Astrophys. **377**, 44-51 (2001).

Golan, A. and V. Dose: A Generalized Information Theoretical Approach to Tomographic Reconstruction. Journal of Physics A: Mathematical and General **34**, 1271–1283 (2001).

Gliozzi, M., W. Brinkmann and C. Räth: Nonlinear analysis of AGN light curves. In: Lighthouses of the universe: the most luminous celestial objects and their use for cosmology-Proceedings of the MPE/ESO workshop, 289-291(2002).

Gliozzi, M., W. Brinkmann, C. Räth, I.E. Papadakis, H. Negoro and H. Scheingraber: On the Nature of X-ray Variability in Ark 564. Astron. Astrophys. **391**, 875-886 (2002).

Golan, A. and V. Dose: Tomographic Reconstruction from Noisy Data. CP617, Bayesian Inference and Maximum Entropy Methods in Science and Engineering: 21 Intern. Workshop, (Ed.) R.L. Fry, 248-258 (2002).

Gozadinos, G., A.V. Ivlev and J.P. Boeuf: A fluid model for colloidal plasmas under microgravity conditions. New Journal of Physics **5**, 32.1-32.9 (2003).

Gridneva, E.A., V.A. Kurnaev, N.N. Trifonov and S.K. Zhdanov: Molecular Effect in the Formation of the Energy Spectrum upon the Transmission of Low-Energy Hydrogen Ions through Ultrathin Carbon Foils. JETP Letters **77**, L12-L14 (2003).

Griessl, S. J. H., M. Lackinger, F. Jamitzky, T. Markert, M. Hietschold and W.M. Heckl: Room Temperature STM Manipulation of Single C60 Molecules at the Liquid Solid Interface - Playing

Nano-Soccer, J. Phys. Chem. B. **108**(31), 11556-11560 (2004).

Griessl, S. J. H., M. Lackinger, F. Jamitzky, T. Markert, M. Hietschold, W.M. Heckl: Single molecular rotation in an organic template structure. Langmuir **20**(21), 9403-9407 (2004).

Guglielmetti, F., R. Fischer and V. Dose: Mixture Modeling for Background and Sources in "Bayesian Inference and Maximum Entropy Methods in Science and Engineering", Editors: R. Fischer and R. Preuss and U. von Toussaint, AIP CP **735,** 111 (2004).

Guglielmetti, F., R. Fischer, V. Dose, W. Voges and G. Boese: Source Detection and Background Estimation with Bayesian Inference in "The Integral Universe", Editors: V. Schoenfelder, G. Lichti and C. Winkler", ESA SP **552**, 847 (2004)

Guglielmetti, F., R. Fischer, V. Dose, W. Voges and G. Boese: Source Detection with Bayesian Inference on ROSAT All-Sky Survey Data Sample, in Astronomical Society of the Pacific Conference Series, 253 (2004)

Hallatschek, K. and D. Biskamp: Transport Control by Coherent Zonal Flows in the Core/Edge Transitional Regime. Phys. Rev. Lett. **86**, 1223-1226 (2001).

Hallatschek, K. and P.H. Diamond: Modulational instability of drift waves. New Journal of Physics **5**, 29.1-9 (2003).

Hallatschek, K.: Thermodynamic potential in local turbulence simulations. Phys. Rev. Lett. **93**, 125001-1 - 4 (2004).

Hallatschek, K.: Turbulent saturation of tokamak core zonal flows. Phys. Rev. Lett. **93**, 65001-1-4 (2004).

Hallatschek, K.: Thermodynamic Potential in Local Turbulence Simulations. Physical Review Letters **93**, 125001-1-125001-4 (2004).

Hartquist, T.W., O. Havnes, G.E. Morfill: The effects of charged dust on Saturn's rings, Astronomy & Geophysics **44**, 26-30 (2003).

Hashimoto, Y., X. Barcons, H. Böhringer et al.: Abundance Constraint and Direct Redshift Measurement of Diffuse X-ray Emission from Distant Clusters of Galaxies. Astron. Astrophys. **417**, 819-825 (2004).

Havnes, O., T.W. Hartquist, A. Brattli, G.M.W. Kroesen and G. Morfill: Dynamic Mach cone as a diagnostic method in reactive dusty plasma experiments. Phys. Rev (E) **65**, 045403, 1-4 (2002).

Helmberger, H., N. Sorger, C. Raeth, G.E. Morfill et al.: Volumetry from spiral CT data sets for response evaluation during neoadjuvant chemotherapy of gastric cancer, Radiology **217**, 532 (2000).

Hopf, C., T. Schwarz-Selinger, W. Jacob and A. von Keudell: Surface Loss Probabilities of Hydrocarbon Radicals on Amorphous Hydrogenated Carbon Film Surfaces. Journal of Applied Physics **87**, 2719-2725 (2000).

Hopf, C., A. von Keudell and W. Jacob: Chemical Sputtering of Hydrocarbon Films by Low-Energy A+ Ion and H Atom Impact. Letter. Nuclear Fusion **42**, 27-30 (2002).

Hopf, C., A. von Keudell and W. Jacob: Chemical Sputtering of Hydrocarbon Films. Journal of Applied Physics, **94**, 2373-2380(2003).

Hopf, C., A. von Keudell and W. Jacob: Direct Verification of the Ion-Neutral Synergism During Hydrocarbon Film Growth.Journal of Applied Physics. **93**, 3352-3358 (2003).

Hopf, C., A. von Keudell and W. Jacob: The Influence of Hydrogen Ion Bombardment on Plasma-Assisted Hydrocarbon Film Growth. Diamond and Related Materials **12**, 85-89 (2003).

Itoh, K., K. Hallatschek, S. Toda, H. Sanuki and S. Itoh: Coherent structure of zonal flow and nonlinear saturation. Journal of the Physical Society of Japan **73**, (2004).

Itoh, K., K. Hallatschek, S. Toda, S.-I. Itoh, P.H. Diamond, M. Yagi, H. Sanuki: Collisional effect on coherent structures of zonal flows and turbulent transport. Plasma Physics and Controlled Fusion **46**, A335-A340 (2004).

Ivlev, A.V., R. Sütterlin, V. Steinberg, M. Zuzic and G. Morfill: Nonlinear Vertical Oscillations of a Particle in a Sheath of a rf Discharge. Phys. Rev. Lett. **85**, 4060-4063 (2000).

Ivlev, A.V., U. Konopka and G. Morfill: Influence of Charge Variation on Particle Oscillations in the Plasma Sheath. Physical Review E **62**, 2739-2744 (2000).

Ivlev, A.V. and G. Morfill: Anisotropic Dust Lattice Modes. Physical Review E **63**, 016409-1-016409-3 (2000).

Ivlev, A.V. and G. Morfill: Acoustic Modes in a Collisional Dusty Plasma: Effect of the charge variation. Physics of Plasmas **7**, 1094-1102 (2000).

Ivlev, A.V. and G. Morfill: Dust Acoustic Solitons with Variable Particle Charge: Role of the Ion Distribution. Physical Review E **63**, 026412-1–026412-5 (2000).

Ivlev, A.V., G.E. Morfill. and U. Konopka: Coagulation of Charged Microparticles in Neutral Gas and Charge-Induced Gel Transitions. Phys. Rev. Lett., **89**, 195502-1-195502-4 (2002).

Ivlev, A.V., A.G. Khrapak, S.A. Khrapak, B.M. Annaratone, G. Morfill and K. Yoshino: Rodlike particles in gas discharge plasmas: Theoretical model. Phys. Rev. (E) **68**, 026403-1-026403-10 (2003).

Ivlev, A.V., M. Kretschmer, M. Zuzic, G. Morfill, H. Rothermel, H. Thomas, V.E. Fortov, V.I. Molotkov, A.P. Nefedov, A.M. Lipaev, O.F. Petrov, Y.M. Baturin, A.I. Ivanov and J. Goree: Decharging of complex plasmas: First kinetic observations. Phys. Rev. Lett. **90**, 5, 055003 (2003).

Ivlev, A.V., S.K. Zhdanov and G.E. Morfill: Coupled dust-lattice solitons in monolayer plasma crystals. Phys. Rev. (E) **68**, 066402-1-066402-4 (2003).

Ivlev, A.V., U. Konopka, G.E. Morfill and G. Joyce: Melting of monolayer plasma crystals. Phys. Rev. (E) **68**, 026405-1-026405-4 (2003).

Ivlev, A.V., S.A. Khrapak, S.K. Zhdanov, G. Joyce and G.E. Morfill: Force on a charged test particle in a collisional flowing plasma. Phys. Rev. (E). **92**, 205007-1-205007-4 (2004).

Ivlev, A.V., S.K. Zhdanov, B.A. Klumov, V.N. Tsytovich, U. de Angelis and G.E. Morfill: Kinetics of ensembles with variable charges. Phys. Rev. (E). (in press, 2004)

Ivlev, A.V., S.K. Zhdanov, S.A. Khrapak and G.E. Morfill: Kinetic approach for the ion drag force in a collisional plasma. Phys. Rev. (E). (in press, 2004).

Ivlev, A.V., S.A. Khrapak, S.K. Zhdanov and G.E. Morfill: Ion drag force in dusty plasmas. Plasma Phys. Control. Fusion. (in press, 2004).

Iyudin, A.F., H. Böhringer, V. Dogiel and G. Morfill: Gamma-Ray Line Emission from Galaxy Clusters. Astron. Astrophys. **413**, 817-825 (2004).

Jacob, W., C. Hopf, A. von Keudell and T. Schwarz-Selinger: Surface Loss Probabilities of Hydrocarbon Radicals on Amorphous Hydrogenated Carbon Film Surfaces: Consequences for the Formation of Re-deposited Layers in Fusion Experiments. In: Hydrogen Recycling at Plasma Facing Materials, Chung-Hsiung Wu (Ed.), Kluwer Academic Publishers, Dordrecht, The Netherlands, 331-337, 2000.

Jacob, W., A von Keudell and T. Schwarz-Selinger: Infrared Analysis of Thin Films: Amorphous, Hydrogenated Carbon on Silicon. Brazilian Journal of Physics **30**, 508-516 (2000).

Jacob, W., A. von Keudell and T. Schwarz-Selinger: ERRATUM: Infrared Analysis of Thin Films: Amorphous, Hydrogenated Carbon on Silicon. Brazilian Journal of Physics **31**, 109 (2001).

Jacob, W., C. Hopf, A. von Keudell, M. Meier and T. Schwarz-Selinger: Particle-beam Experiment to Study Heterogeneous Surface Reactions Relevant to Plasma-assisted Thin Film Growth and Etching. Review of Scientific Instruments **74**, 5123-5136 (2003).

Jacobs, G ., Yaroshenko,V., and F. Verheest: Low-frequency electrostatic waves in self-gravitating dusty plasmas with dust-ion collisions, Phys. Rev. E, **66**, 026407 (2002).

Jamitzky, F., R.W. Stark, W. Bunk, S. Thalhammer, C. Räth, T. Aschenbrenner, G.E. Morfill and W.M. Heckl: Scaling -index method as an image processing tool in scanning-probe Microscopy. Ultramicroscopy **86**, 241-246 (2001).

Jamitzky, F., M. Stark, W. Bunk, W. M. Heckl and R. W. Stark: Nonlinear dynamics of a microcantilever in close proximity to a surface. Proc. 2004 4th IEEE Conf. Nanotechnology (17.-19. Aug), Munich, Germany (ISBN 0-7803-8537-03).

Jaroschek C. H., H. Lesch and R. A. Treumann, Relativistic fast reconnection as the possible energy source for high variability and flat spectra in extragalactic radio sources, Astrophys. J. Lett. **605**, L9-L12 (2004).

Jaroschek, C.H., R.A. Treumann, H. Lesch and M. Scholer: Fast Reconnection in Relativistic Pair Plasmas: Analysis of Particle Acceleration in Self-consistent Full Particle Simulations. Physics of Plasmas **11**, 1151-1163 (2004).

Jaroschek, C. H., H. Lesch and R. A. Treumann: Self-consistent diffusive lifetimes of Weibel magnetic fields in gamma ray bursts. Astrophys. J. **616**, 1065-1071 (2004).

Jaroschek, C. H., H. Lesch, and R. A. Treumann: Ultra-relativistic plasma shell collisions in g-ray burst sources: Dimensional effects on the final steady-state magnetic field. Astrophys. J., **618**, 822-831 (2005).

Kaastra, J.S., T. Tamura, J. Peterson et al.: Spatially resolved X-ray spectroscopy of cooling clusters of galaxies. Astron. Astrophys. **413**, 415-439 (2004).

Kang, H. D. and V. Dose: Radical Detection in a Methane Plasma. Journal Vacuum Science and Technology A **21**, 1978-1980 (2003).

Kempe, A., F. Jamitzky, W: Altermann, B. Baisch, T. Markert and W.M. Heckl: Discrimination of Aqueous and Aeolian Paleoenvironments by Atomic Force Microscopy-A Database for the Characterization of Martian sediments. Astrobiology **4** (1), 51-64 (2004).

Keudell, A. von, T. Schwarz-Selinger, M. Meier and W. Jacob: Direct Identification of the Synergism between Methyl Radicals and Atomic Hydrogen during Growth of Amorphous Hydrogenated Carbon Films. Applied Physics Letters **76**, 676-678 (2000).

Keudell, A. von, T. Schwarz-Selinger, M. Meier and W. Jacob: Erratum: Direct Identification of the Synergism between Methyl Radicals and Atomic Hydrogen during Growth of Amorphous Hydrogenated Carbon Films. Applied Physics Letters **77**, 459 (2000).

Keudell, A. von: Surface Processes during Thin Film Growth. Plasma Sources Science and Technology **9**, 455-467 (2000).

Keudell, A. von, T. Schwarz-Selinger and W. Jacob: Simultaneous Interaction of Methyl Radicals and Atomic Hydrogen with Amorphous Hydrogenated Carbon Films. Journal of Applied Physics **89**, 2979-2986 (2001).

Keudell, A. von, M. Meier and T. Schwarz-Selinger: Simultaneous Interaction of Methyl Radicals and Atomic Hydrogen with Amorphous Hydrogenated Carbon Films, as Investigated with Optical In Situ Diagnostics. Applied Physics A **72**, 551-556 (2001).

Keudell, A. von, T. Schwarz-Selinger, W. Jacob and A. Stevens: Surface Reactions of Hydrocarbon Radicals: Suppression of the Re-deposition in Fusion Experiments via a Divertor Liner. Journal of Nuclear Materials **290-293**, 231-237 (2001).

Keudell, A. von and J.R. Abelson: Advantages of the "Optical Cavity Substrate" for Real Time Infrared Spectroscopy of Plasma-surface Interactions. Journal of Applied Physics **91**, 4840-4845 (2002).

Keudell, A. von: Formation of Polymer-like Hydrocarbon Films from Radical Beams of Methyl and Atomic Hydrogen. Thin Solid Films **402**, 1-37 (2002).

Khodataev, Y.K., R. Bingham, V.P. Tarakanov, G.E. Morfill, et al.: The free boundary dust-plasma crystal, Physica Scripta **T89**, 95-100 (2001).

Khodataev, Y.K., G.E. Morfill, V.N. Tsytovich: Role of neutral-particle bombardment in dust-dust interactions in plasmas, Journal Of Plasma Physics **65**, 257-272 (2001).

Khrapak, S.A. and G.E. Morfill: Waves in Two Component Electron-dust Plasma. Physics of Plasmas **8**, 2629-2634 (2001).

Khrapak, S.A., A.V. Ivlev and G. Morfill: Interaction Potential of Microparticles in a Plasma: Role of Collisions with Plasma Particles. Physical Review E **64**, 046403-1-046403-7 (2001).

Khrapak, S.A. and G.E. Morfill: Dust Diffusion across a Magnetic Field due to Random Charge Fluctuations. Physics of Plasmas **9**, 619-623 (2002).

Khrapak, S.A., A.V. Ivlev, G.E. Morfill and H.M. Thomas: Ion Drag Force in Complex Plasmas. Physical Review E **66**, 046414-1-046414-4 (2002).

Khrapak, S.A., A.V. Ivlev, G.E. Morfill and H.M. Thomas: Ion drag in complex plasmas. Dusty Plasmas in the New Millenium: Third International Conference on the Physics of Dusty Plasma, AIP Conference Proceedings **649**, (Eds.) R. Bharuthram, M.A. Hellberg, P.K. Shukla et al., American Institute of Physics, Melville NY 2002, 341-344 (2002).

Khrapak, S.A. and V.V. Yaroshenko: Low-frequency Waves in Collisional Complex Plasmas with an Ion Drift. Physics of Plasmas **10**, 4616-4621 (2003).

Khrapak, S.A., D. Samsonov, G. Morfill, H. Thomas, V. Yaroshenko, H. Rothermel, T. Hagl, V. Fortov, A. Nefedov, V. Molotkov, O. Petrov, A. Lipaev, A. Ivanov and Y. Baturin:

Compressional waves in complex (dusty) plasmas under microgravity conditions. Phys. Plasmas **10**, 1, L1-L4 (2003).

Khrapak, S.A., A.V. Ivlev, G.E. Morfill and S.K. Zhdanov: Scattering in the Attractive Yukawa Potential in the Limit of Strong Interaction. Phys. Rev. Lett. **90**, 225002-1-225002-4 (2003).

Khrapak, S.A., A.V. Ivlev, G.E. Morfill, H.M. Thomas, S.K. Zhdanov, U. Konopka, M.H. Thoma and R.A. Quinn: Comment on "Measurement of the ion drag force on falling dust particles and its relation to the void formation on complex (dusty) plasmas" Physics of plasmas **10**, 1278, 4579-4581 (2003).

Khrapak, S.A., A.V. Ivlev, S. K. Zhdanov and G.E. Morfill. Hybrid approach to the ion drag force. (Phys. Plasmas accepted, 2004).

Khrapak, S.A. and G.E. Morfill: Dusty Plasmas in a Constant Electric Field: Role of the Electron Drag Force. Physical Review E **69**, 066411-1-066411-5 (2004).

Khrapak, S.A., A.V. Ivlev, G.E. Morfill, S.K. Zhdanov and H.M. Tomas: Scattering in the attractive Yukawa potential: application to the ion-drag force in complex plasmas. IEEE Trans. On Plasma Sci. **32**, 555-560 (2004).

Khrapak, S.A., A.V. Ivlev and G.E. Morfill. Momentum transfer in complex plasmas. Phys. Rev. E **70**, 056405 (2004).

Kikuchi, K., C. Itho, A. Kushino et al.: Detection of an X-Ray Hot Region in the Virgo Cluster of Galaxies. Astrophys. J. Lett. **531**, 95-98 (2000).

Kis, A., M. Scholer, B. Klecker, E. Möbius, E. A. Lucek, H. Reme,J. M. Bosqued, L. M. Kistler and H. Kucharek: Multi-spacecraft observations of diffuse ions upstream of Earth's bow shock. Geophys. Res. Lett. **31**, L20801, doi:10.1029/2004GL020759 (2004).

Klindworth, M., A. Melzer, A. Piel, U. Konopka and G.E. Morfill: Langmuir probe measurements in a complex plasma under microgravity conditions. In: Dusty Plasmas in the New Millennium:Third Intern. Conf. Durban 2002, R. Bharuthram et al. (Eds.) AIP Conf. Proc. 649, 345-348 (2002).

Klumov, B.A., A.V. Ivlev and G. Morfill: Complex Plasma Experiments: the Role of Negative Ions. Dusty Plasmas in the New Millenium: Third International Conference on the Physics of Dusty Plasma, AIP Conference Proceedings **649**, (Eds.) R. Bharuthram, M.A. Hellberg, P.K. Shukla et al., American Institute of Physics, Melville NY 2002, 349-352.

Klumov, B.A., A.V. Ivlev and G. Morfill: The role of negative ions in experiments with complex plasma. JETP Letters **78**, 300-304 (2003).

Komossa, S., D. Breitschwerdt, H. Böhringer and M. Janek: X-ray Emission Mechanisms of LINERs. In: Proc. Astrophysical Dynamics. (Eds.) D. Berry, D. Breitschwerdt, A. daCosta and J. Dyson. Astrophys. Space Sci. **272**, 295-298 (2000).

Kompaneetz, R., V. Tsytovich, G. Morfill: Weak dust ion-acoustic and dust-acoustic solitons with absorption of ions, ionization, and ion drag, IEEE Transactions On Plasma Science **32**, 561-568 (2004).

Konopka, U., D. Samsonov, A.V. Ivlev et al.: Rigid and Differential Plasma Crystal Rotation induced by Magnetic Field. Physical Review E **61**, 1890-1898 (2000).

Konopka, U., G. Morfill and L. Ratke: Measurement of the Interaction Potential of Microspheres in the Sheath of a rf Dischage. Phys. Rev. Lett. **84**, 891-894 (2000).

Konz, C., H. Lesch, G.T. Birk and H. Wiechen: The Critical Velocity Effect as a Cause for the Hα Emission from the Magellanic Stream. The Astrophys. J. **548**, 249-252 (2001).

Kretschmer,M. S.A.Khrapak, S.K. Zhdanov, H.M. Thomas, G.E. Morfill, V.E. Fortov, A.M. Lipaev, V.I. Molotkov, A.I.Ivanov: "Trampoline effect" and the force field inside the void in complex plasmas, Submitted to Phys. Rev. E (2004).

Kruger, H., E. Grun, A. Graps, G.E. Morfill, et al.: One year of Galileo dust data from the Jovian system: 1996, Planetary And Space Science **49**, 1285-1301 (2001).

Kruger, H., E. Grun, M. Landgraf, G.E. Morfill, et al.: Four years of Ulysses dust data: 1996-1999, Planetary And Space Science **49**, 1303-1324 (2001).

Kucharek, H., M. Scholer and A.P. Matthews: Three-dimensional Simulation of the Electromagnetic Ion/Ion Beam Instability: Cross Field Diffusion. Nonlinear Processes in Geophysics **7**, 167-172 (2000).

Kucharek, H., E. Möbius, M. Scholer et al.: On the origin of field-aligned beams at the quasi-perpendicular bow shock: multi-spacecraft observations. Annales Geophysicae **22**, 2301 - 2308 (2004).

LaBelle, J. and R. A. Treumann, Auroral radio emissions, 1. Hisses, roars and bursts, Space Sci. Rev. **101**, 295-440 (2002).

LaBelle, J., R.A. Treumann, P.H. Yoon and M. Karlicky: A Model of Zebra Emission in Solar Type IV Radio Bursts. The Astrophys. J. **593**, 1195-1207 (2003).

Lackinger, M., S. Griessl, T. Markert, F. Jamitzky and W.M. Heckl: Self-assembly of benzene-dicarboxylic acid isomers at the liquid solid interface - steric aspects of hydrogen-bonding. J. Phys. Chem. B. **108**(36), 13652-13655 (2004).

Langer, U., E. Taglauer, R. Fischer and W7 AS Team: Investigation of the Hydrogen Fluxes in the Plasma Edge of W7-AS during H-mode Discharges. Journal of Nuclear Materials **290-293**, 658-662 (2001).

Lee, B. C., S. S. Allam, D.L. Tucker et al.: A Catalog of Compact Groups of Galaxies in the SDSS Commissioning Data. Astron. J. **127**, 1811-1859 (2004).

Lembege, B., J. Giacalone, M. Scholer et al.: Selected problems in collisionless-shock physics. Space Science Reviews **110**, 161 - 226 (2004).

Livina, V.N., Y. Ashkenazy, P. Braun, R. Monetti, S. Havlin, and A. Bunde: Non-linear Volatility of River Flux Fluctuations. Phys. Rev. E **67**, 042101 (2003).

Loredo, T.: Bayesian Inference in Astronomy & Astrophysics. A Short Course. Lecture Notes from a Short Course on Bayesian Inference in Astronomy & Astrophysics (Five Lectures), Garching. CIPS Report No. 93 (2002).

Iyudin, A.F., H. Bohringer, V. Dogiel, G.E. Morfill et al.: Gamma-ray line emission from galaxy clusters, Astronomy & Astrophysics **413**, 817-825 (2004).

Mamun, A.A., P.K. Shukla and G.E. Morfill: New Resonance and Cut-off for Low-frequency Electromagnetic Waves in Dusty Magnetoplasmas. Physics of Plasmas **11**, 2307-2310 (2004).

Mamun, A.A., P.K. Shukla, G.E. Morfill: Theory of Mach cones in magnetized dusty plasmas with strongly correlated charged dust grains, Physical Review Letters **92**, 095005 (2004).

Maruyama, K., W. Jacob and J. Roth: Formation of Hard Amorphous Hydrogenated Carbon Films with Low Hydrogen Concentration and their Erosion in Air. Japanese Journal of Applied Physics **40**, 788-793 (2001).

Matsukiyo, S. and M. Scholer: Modified Two-stream Instability in the Foot of High Mach Number Quasi-perpendicular Shocks. Journal of Geophysical Research **108**, A12, SMP 19-1-19-6 (2003).

Matsukiyo, S., R.A. Treumann and M. Scholer: Coherent Waveforms in the Auroral upward Current Region. Journal of Geophysical Research **109**, A06212-1-A06212-5 (2004).

McKee, G.R., R.J. Fonck, M. Jakubowski et al.: Experimental characterization of coherent, radially-sheared zonal flows in the DIII-D tokamak. Physics of Plasmas **10**, 1712 - 1719 (2003).

McKee, G.R., R.J. Fonck, M. Jakubowski et al.: Observation and characterization of radially-sheared zonal flows in DIII-D. Plasma Physics and Controlled Fusion **45**, A477 - A482 (2003).

Meier, M. and A. von Keudell: Hydrogen Elimination as a Key Step for the Formation of Polymerlike Hydrocarbon Films. Journal of Applied Physics **90**, 3585-3594 (2001).

Meier, M. and A. von Keudell: Temperature Dependence of the Sticking Coefficient of Methyl Radicals at Hydrocarbon Film Surfaces. Journal of Chemical Physics **116**, 5125-5136 (2002).

Meier, M., R. Preuss and V. Dose: Interaction of CH3 and H with Amorphous Hydrocarbon Surfaces: Estimation of Reaction Cross Sections using Bayesian Probability Theory. New Journal of Physics **5**, 133.1-133.24 (2003).

Melandso, F., A . Bjerkmo, G. Morfill, H. Thomas and M. Zuzic: Detection of Stochastic Waves in Plasma Monolayer Crystals from Video Images. Phys. Plasmas **7**, 4368-4378 (2000).

Melzer, A., S. Nunomura, D. Samsonov, Z.W. Ma and J. Goree: Laser-excited Mach cones in a dusty plasma crystal, Phys. Rev. E 62 (3), 4162-4176 (2000).

Melzer, A., S. Nunomura, D. Samsonov, Z.W. Ma and J. Goree: Laser-excited Mach cones in plasma crystals. Mater. Sci. Forum 382, 41-46 (2000).

Memola, E., C. Fendt and W. Brinkmann: Theoretical X-ray spectra of relativistic MHD jets, Astron. Astrophys. **385**, 1089-1094 (2002).

Merz, B.P. and R.A. Treumann: Relaxation Oscillation Phenomena in Cyrogenic Si Diodes. Applied Physics Letters **78**, 1876-1878 (2001).

Metz S., H. Daldrup-Link, T. Richter, C. Räth, M. Settles and M. Piert: Detection and quantification of early necrosis in breast cancers by MR imaging: Value of the necrosis specific contrast agent Gadophrin. Radiol. **225** (Suppl. S), 112 (2002).

Metz S., H. Daldrup-Link, T. Richter, C. Räth, W. Ebert, M. Settles, E. Rummeny, T. Link and M. Piert: Detection and quantification of breast tumor necrosis with MR imaging: Value of the necrosis-avid contrast agent Gadophrin-3. Acad. Radiol. **10**, 484-490 (2003).

Mikikian, M, L. Boufendi, A. Bouchoule, G.E. Morfill, H.M. Thomas, H. Rothermel, T. Hagl, A.P. Nefedov, V.E. Fortov, V.I. Molotkov, O. Petrov. A. Lipaev, Y.P. Semenov, A.I. Ivanov, V. Afanasev et al.: Dust Particles Growth and Behavior under Mivrogravity Condition. Dusty Plasmas in the New Millenium: Third International Conference on the Physics of Dusty Plasma, AIP Conference Proceedings **649**, (Eds.) R. Bharuthram, M.A. Hellberg, P.K. Shukla et al., American Institute of Physics, Melville NY 2002, 135-138.

Mikikian, M., L. Boufendi, A. Bouchoule, H.M. Thomas, G.E. Morfill, A.P. Nefedov, V.E. Fortov and the PKE-Nefedov team: Formation and behaviour of dust particle clouds in a radio-frequency discharge: results in the laboratory and under microgravity conditions. New Journal of Physics **5**, 3, 19.1-19.12, (2003).

Mimica, P., M.A. Aloy, E. Müller and W. Brinkmann: Synthetic light curves of BL Lacs from relativistic hydrodynamic simulations, Astron. Astrophys. **418**, 947-958 (2004).

Mimica, P., M.A. Aloy, E. Müller, and W. Brinkmann: Computation of X-Ray Blazar Light Curves using RHD simulations, Astrophys. Sp. Sci. **293**, 165-172 (2004).

Mokler, F. and B. Stelzer: X-ray emission near the substellar limit: The sigma Orionis and Taurus star forming regions. Astron. Astrophys. **391**, 1025-1032 (2002).

Monetti, R., H. Böhm, D. Müller, D. Newitt, S. Majumdar, E. Rummeny, T.M. Link and C. Räth: Scaling index method: a novel nonlinear technique for the analysis of high resolution MRI of human bones, Proc. of the SPIE: Medical Imaging: Image Processing, **5032**, 1777-1786 (2003).

Monetti, R., H. Böhm, D. Müller, E. Rummeny, G. Morfill, S. Majumdar, D. Newitt, T. Link and C. Räth: Structure Analysis of High Resolution MRI of the Proximal Femur Using a 3D Anisotropic Method for the Prediction of Mechanical Strength In Vitro, J. Bone Min. Res. **19**, S235 (2004).

Monetti, R., H. Böhm, D. Müller, E. Rummeny, T. Link and C. Räth: Assessing the biomechanical strength of trabecular bone in vitro using 3D anisotropic non-linear texture measures: the scaling vector method, Proc. of the SPIE: Medical Imaging: Image Processing, **5370**, 215-224 (2004).

Morfill, G. and V.N Tsytovich: Ionization Instability and Dusty Plasma Structurization. Plasma Physics Reports **26**, 682-690 (2000).

Morfill, G. and W. Bunk: New Designs on Complex Patterns. Physics World, April, 41-45 (2000).

Morfill, G. and V.N. Tsytovich: Modelling of Complex Plasmas under Micro-gravity Conditions. Physics of Plasmas **9**, 4-16 (2002).

Morfill, G.E., V.N. Tsytovich and H. Thomas: Complex Plasmas: II. Elementary Processes in Complex Plasmas. Plasma Phys. Rep. **29**, 1-30 (2002).

Morfill, G.E., B.M. Annaratone, P. Bryant, A.V. Ivlev, H.M. Thomas, M. Zuzic and V.E. Fortov: A Review of Liquid and Crystalline Plasmas – New Physical States of Matter? Plasma Physics and Controlled Fusion **44**, B263-B277 (2002).

Morfill, G.E.: A Synopsis of Recent Experimental Developments in Complex (Dusty) Plasma Physics. Dusty Plasmas in the New Millenium: Third International Conference on the Physics of Dusty Plasma, AIP Conference Proceedings **649**, (Eds.) R. Bharuthram, M.A. Hellberg, P.K. Shukla et al., American Institute of Physics, Melville NY 2002, 507-511.

Morfill, G.E., H.M. Thomas, B.M. Annaratone, A.V. Ivlev, R.A. Quinn, A.P. Nefedov and V.E.. Fortov PKE-Nefedov Team: Complex Plasmas under Microgravity Conditions: First Results from PKE-Nefedov. Dusty Plasmas in the New Millenium: Third International Conference on the Physics of Dusty Plasma, AIP Conference Proceedings **649**, (Eds.) R. Bharuthram, M.A.

Hellberg, P.K. Shukla et al., American Institute of Physics, Melville NY 2002, 91-109.

Morfill, G.E., M. Rubin-Zuzic, H. Rothermel, A.V. Ivlev, B. A. Klumov, H.M. Thomas and U. Konopka: Highly Resolved Fluid Flows - "Liquid Plasmas" at the Kinetic Level, Phys. Rev. Lett., **92** (2003).

Morfill, G.E., V.N. Tsytovich, H. Thomas: Complex plasmas: II. Elementary processes in complex plasmas
Plasma Physics Reports **29**, 1-30 (2003).

Morfill, G.E,. A.V. Ivlev, S.A. Khrapak, B. A. Klumov, M. Rubin-Zuzic, U. Konopka and Thomas. H. M,. Ten years of plasma crystals – from ICPIG (Bochum) to ICPIG (Greifswald). Contrib. Plasma Phys. **44**, 450 (2004).

Morfill, G.E,. S.A. Khrapak, A.V. Ivlev, B. A. Klumov, M. Rubin-Zuzic and H.M. Thomas. From fluid flows to crystallization: New results from complex plasmas. Physica Scripta T107, **59** (2004).

Müller, D., T. M. Link, J. Bauer, G. Morfill, E. Rummeny and C. Räth: A newly developed 3D-based scaling index algorithm to optimize struture analysis of trabecular bone in patientes with and without osteoporotic spine fractures, Radiol., **225** (Suppl. S), 603-604 (2002).

Müller, D., T.M. Link, J. Bauer, G.E. Morfill, E.J. Rummeny, C. Räth and T.M. Link: A Newly Developed 3D-based Scaling Index Algorithm to Optimize Structure Analysis of Trabecular Bone in Patients with and without Osteoporotic Spine Fractures. In: Proceedings of the 88th Annual Meeting of the RSNA, Chicago, IL (USA), 2002. (Ed.). Supplement to Radiology Vol. **225**, Radiological Society of North America, 581 (2002).

Müller, D., T.M. Link, R.A. Monetti, G.E. Morfill, E.J. Rummeny and C. Räth: 3D structure analysis of high-resolution magnetic resonance imaging of the proximal femur in relationship with biomechanical bone strength in vitro. In: The 89th annual meeting of the RSNA. Supplement to Radiology 229, Radiological Society of North America, Chicago, 518 (2003).

Müller, D., T. Link, R. Monetti, G. Morfill, E. Rummeny and C. Räth: 3D structure analysis of high-resolution magnetic resonance imaging of the proximal femur in relationship with biomechanical strength in vitro, Radiol., **229** (Suppl. S), 518 (2003).

Müller, D., T. Link, R. Monetti, j. Bauer, E. Rummeny and C. Räth: Age-related changes of 3D trabecular structure parameters in comparison with bone mineral density, Radiol., **229** (Suppl. S), 572 (2003).

Müller, D., T. Link, R. Monetti, J. Bauer, E. Rummeny and C. Räth: Structure analysis of the distal radius using the scaling index algorithm in the prediction of osteoporotic spine fractures, J. Bone Min. Res., **18**, S254 (2003).

Müller, D., R. Monetti, S. Majumdar, D. C. Newitt, H. Böhm, C. Räth, E. J. Rummeny and T. M. Link: Relationship Between Structure Analysis Based on the 3D Scaling Index Method and DXA in Postmenopausal Women with Osteoporotic Spine Fractures, J. Bone Min. Res., **19**, S113 (2004).

Müller, D., R. Monetti, S. Majumdar, H. Böhm, C. Räth, E. J. Rummeny and T. M. Link: Structure Analysis of High Resolution Magnetic Resonance Images of the Calcaneus using the Anisotropic 3D Scaling Vector Method, J. Bone Min.. Res., **19**, S127 (2004).

Müller, D., R. Monetti, H. Böhm, J. Bauer, E. Rummeny, T. Link and C. Räth: Three-dimensional-based scaling index algorithm to optimize structure analysis of trabecular bone in postmenopausal women with and without osteoporotic spine fractures, Proc. of the SPIE: Medical Imaging: Image Processing, **5370**, 225-232 (2004).

Müller, T.G.: Thermophysical Analysis of Infrared Observations of Asteroids. In: Proceedings of The Physical Properties of Potential Earth Impactors: Know Your Enemy, Erice, Italy, 2001. (Ed.). Meteoritics and Planetary Science Vol. **37**, Meteoritical Society, Fayetteville, AR, 1700-1710 (2002).

Müller, W.-Ch., A. Zeiler and G.E. Morfill: Direct Numerical Simulation of Yukawa Systems by Particle-in-cell Methods. Dusty Plasmas in the New Millenium: Third International Conference on the Physics of Dusty Plasma, AIP Conference Proceedings **649**, (Eds.) R. Bharuthram, M.A. Hellberg, P.K. Shukla et al., American Institute of Physics, Melville NY 2002, 365-368.

Müller, W.-Ch. and D. Carati: Dynamic Gradient-diffusion Subgrid Models for Incompressible Magnetohydrodynamik Turbulence. Physics of Plasmas **9**, 824-834 (2002).

Müller, W.-Ch. and R. Grappin: The residual energy in freely decaying magnetohydrodynamic turbulence. Pasma Physics and Controlled Fusion **46** (2004).

Müller, W.-Ch., D. Biskamp and R. Grappin: Statistical Anisotropy of Magnetohydrodynamic Turbulence. Physical Review E **67**, 066302-1-066302-4 (2003).

Mullis, C.R., J.P. Henry, I.M. Gioia et al.: The North Ecliptic Pole Supercluster. Astrophys. J. Lett. **553**, L115-L118 (2001).

Mustafa, M.G., and M.H. Thoma: Quenching of Hadron Spectra due to the Collisional Energy Loss of Partons in the Quark-Gluon Plasma, Acta Phys. Hung. A (in press).

Mustafa, M.G., M.H. Thoma, and P. Chakraborty: Screening of a Moving Parton in the Quark-Gluon Plasma, Phys. Rev. C **71**, 017901 (2005).

Nakamura, M. and M. Scholer: Structure of the Magnetopause Reconnection Layer and of Flux Transfer Events: Ion Kinetic Effects. J. Geophys. Res. **105**, 23179-23191 (2000).

Nakamura, R., W. Baumjohann,T. Nagai, M. Fujimoto, T. Mukai, B. Klecker, R. Treumann, A. Balogh, H. Reme, J. A. Sauvaud, L. Kistler, C. Mouikis, C. J. Owen, A. N. Fazakerley, J. P. Dewhurst, and Y. Bogdanova: Flow shear near the boundary of the plasma sheet observed by Cluster and Geotail, J. Geophys. Res. **109**, A05204 (2004).

Namiki, M., N. Kawai, T. Kotani and W. Brinkmann: The X-ray Lobes of the W50/SS433 System. Adv. Space Res. **25**, 709-712 (2000).

Neagu, E., S.P. Gary, J.E. Borovsky, W. Baumjohann and R.A. Treumann: Constraints on Magnetic Fluctuation Energies in the Plasma Sheet. Geophys. Res. Lett. **28**, L919-L922 (2001).

Neagu E., J. E. Borovsky, M. F. Thomsen, S. P. Gary, W. Baumjohann and R. A. Treumann: Statistical survey of magnetic field and ion velocity fluctuations in the near-Earth plasma sheet: Active Magnetospheric Particle Trace Explorers Ion Release Module (AMPTE IRM) measurements, J. Geophys. Res. **107**, doi:10.1029/2001JA000318 (2002).

Nefedov, A.P., G.E. Morfill, V.E. Fortov, H.M. Thomas, H. Rothermel, T. Hagl, A.V. Ivlev, M. Zuzic, B.A. Klumov, A.M. Lipaev, V.I. Molotkov, O.F. Petrov, Y.P. Gidzenko, S.K. Krikalev, W. Shepherd, A.I. Ivanov, M. Roth, H. Binnenbruck, J.A. Goree and Y.P. Semenov: PKE-Nefedov: plasma crystal experiments on the International Space Station. New Journal of Physics **5**, 3, 33.1-33.10 (2003).

Nilsson, K., T. Pursimo, J. Heidt, L.O. Takalo, A. Sillanpää and W. Brinkmann: R-band imaging of the host galaxies of RGB BL Lacertae objects, Astron. Astrophys. **400**, 95-118 (2003).

Nunomura, S., D. Samsonov and J. Goree : Transverse Waves in a Two-Dimensional Screened-Coulomb Crystal (Dusty Plasma). Physics Review Letters **84**, 5141-5144 (2000).

Nunomura, S., J. Goree, S. Hu, X. Wang and A. Bhattacharjee: Dispersion relations of longitudinal and transverse waves in two-dimensional screened Coulomb crystals. Phys. Rev (E) **65**, 066402, 1-11 (2002).

Nunomura, S., J. Goree, S. Hu, X. Wang, A. Bhattacharjee and K. Avinash: Phonon spectrum in a plasma crystal. Phys. Rev. Lett. **89**, 035001, 1-4 (2002).

Nunomura, S., J. Goree, S. Hu, X. Wang, B.M. Annaratone and J.E. Allen: A Radiofrequency sustained double layer in a plasma reactor. J. Appl. Phys. **91**, 6321-6324 (2002).

Nunomura, S., S. Zhdanov, G.E. Morfill and J. Goree: Nonlinear longitudinal waves in a two-dimensional screened Coulomb crystal. Phys. Rev. (E) **68**, 026407-1-026407-7 (2003).

Nunomura, S., S. Zhdanov, D. Samsonov and G. Morfill: Wave spectra in solid and liquid complex (dusty) plasmas, Submitted to Phys. Rev. Lett. (2004).

Nunomura, S., D. Samsonov, S. Zhdanov, G. Morfill, Heat transfer in a two-dimensional crystalline complex (dusty) plasma, Submitted to Phys. Rev. Lett. (2004).

O'Brien, P.T., J.N. Reeves, M.J.L. Turner et al.: XMM-Newton Detection of a Comptonized Accretion Disk in the Quasar PKS 0558-504. Astron. Astrophys. Lett. **365**, L122-L127 (2001).

Onishchenko O. G., O. A. Pokhotelov, R. Z. Sagdeev, L. Stenflo, R. A. Treumann and M. A. Balikhin: Generation of convective cells by kinetic Alfvin waves in the upper ionosphere, J. Geophys. Res. **109**, A03306, doi:10.1029/2003JA010248 (2004).

Ortiz-Gil, A., L. Guzzo, P. Schuecker, H. Böhringer and C.A. Collins: The X-ray Luminosity - Velocity Dispersion Relation in the REFLEX Cluster Survey. Mon. Not. R. Astr. Soc., **348**, 325-332 (2004).

Ostrikov, K.N., S.V. Vladimirov, M.Y. Yu and G.E. Morfill: Dust-acoustic Wave Instabilities in

Colloidal Plasmas. Physical Review, **61**, 4 (2000).

Ostrikov, K.N., S.V. Vladimirov, M.Y. Yu and G.E. Morfill: Low-frequency Dispersion Properties of Plasmas with Variable-charge Impurities. Physics of Plasmas **7**, 461-465 (2000).

Papadakis, I.E., W. Brinkmann, H. Negoro and M. Gliozzi: Detection of a high frequency break in the X-ray power spectrum of Ark 564, Astron. Astrophys. **382**, L1- 4 (2002).

Peitzmann, T. and M.H. Thoma: Direct Photons from Relativistic Heavy-Ion Collisions, Phys. Rep. **364**, 175 (2002).

Pokhotelov, O.A., O.G. Onishchenko, M.A. Balikhin, R.A. Treumann and V.P. Pavlenko: Drift Mirror Instability in Space Plasmas, 2, Nonzero Electron Temperature Effects. Journal of Geophysical Research **106**, 13,237-13,246 (2001).

Pokhotelov, O.A., M.A. Balikhin, R.A. Treumann and V.P. Pavlenko: Drift Mirror Instability Revisited, 1, Cold Electron Temperature Limit. Journal of Geophysical Research **106**, 8455-8463 (2001).

Pokhotelov, O.A., R. A. Treumann, R. Z. Sagdeev et al.: Linear theory of the mirror instability in non-Maxwellian space plasmas, J. Geophys. Res. **107**, 1312, 10.1029/2001JA009125 (2002).

Pokhotelov, O.A., O. G. Onishchenko, R. Z. Sagdeev and R. A. Treumann, Nonlinear dynamics of inertial Alfvin waves in the upper ionosphere: Parametric generation of electrostatic convective cells. J. Geophys. Res. **108**, 1291, doi:10.1029/2003JA009888 (2003).

Pokhotelov, O.A., I. Sandberg, R.Z. Sagdeev, R.A.Treumann, O.G Onishchenko., M.A Bakikhin and V.P.Pavlenko: Slow Drift Mirror Modes in Finite Electron-Temperature Plasma: Hydrodynamic and Kinetic Drift Mirror Instabilities. Journal of Geophysical Research **108**, 1-1-1-12 (2003).

Pokhotelov, O.A., O.G. Onishchenko, R.Z. Sagdeev and R.A. Treumann: Nonlinear Dynamics on Inertial Alfvén Waves in the Upper Ionosphere: Parametric Generation of Electrostatic Convective Cells. Journal of Geophysical Research **108**, A7, SMP 15-1–15-8 (2003).

Pokhotelov, O.A., R. Z. Sagdeev, M. A. Balikhin and R. A. Treumann: The mirror instability at finite ion-Larmor radius wavelengths, J. Geophys. Res. **109**, A09213,doi:10.1029/2004JA010568 (2004).

Pompl, R., W. Bunk, A. Horsch et al.: MELDOQ: Ein System zur Unterstützung der Früherkennung des maglignen Melanoms durch digitale Bildverarbeitung. Informatik aktuell (Bildverarbeitung für die Medizin 2000), Springer Verlag, pp 234-238.

Popel, S.I., A.P. Golub', T. V. Losseva, A.V. Ivlev and G.E. Morfill: Dust ion-acoustic solitons: Role of trapped electrons. Dusty Plasmas in the New Millenium: Third International Conference on the Physics of Dusty Plasma, AIP Conference Proceedings **649**, (Eds.) R. Bharuthram, M.A. Hellberg, P.K. Shukla et al., American Institute of Physics, Melville NY 2002, 386-389.

Popel, S.I,. A.P. Golub', T. V. Losseva, A.V. Ivlev, S.A. Khrapak and G. Morfill. Weakly dissipative dust-ion-acoustic solitons. Phys. Rev. E **67**, 056402 (2003).

Popesso, P. H. Böhringer, J. Brinkmann, W. Voges and D.G. York: ROSAT-SDSS Galaxy Clusters Survey. I. The Catalog and the correlation of X-ray and optical properties. Astron. Astrophys. **423**, 449-467 (2004).

Porquet, D., J.N. Reeves, P.O. Brien and W. Brinkmann: XMM-Newton EPIC observations of 21 low-redshift PG quasars. Astron. Astrophys. **422**, 85-95 (2004).

Pottelette, R., R.A. Treumann and M. Berthomier: Auroral Plasma Turbulence and the Cause of Auroral Kilometric Radiation Fine Structure. J. Geophysical Research **106**, No. A5, 8465-8476 (2001).

Pottelette, R., R.A. Treumann, M. Berthomier and J. Jasperse: Electrostatic Shock Properties Inferred from AKR Fine Structure. Nonlinear Processes in Geophysics **10**, 87-92 (2003).

Pottelette, R., R. A. Treumann and E. Georgescu: Crossing a narrow-in-altitude turbulent auroral acceleration region, Nonlin. Proc. Geophys. **11**, 197-204, SRef-ID: 1607-7946/npg/2004-11-197 (2004).

Preuss, R., H. Kang, T. Schwarz-Selinger and V. Dose: Quantitative Analysis of Multicomponent Mass Spectra. CP617, Bayesian Inference and Maximum Entropy Methods in Science and Engineering: 21 Intern. Workshop, (Ed.) R.L. Fry 155-162 (2002).

Preuss, R., M. Maraschek, H. Zohm and V. Dose: Bayesian Analysis of Magnetic Island Dynamics of Tearing Modes in Asdex Upgrade. In: Proceedings 29th EPS Conference on Plasma Physics and Controlled Fusion, Montreux, 2002. ECA 26B. Europ. Phys. Soc., P-1.042.

Preuss, R., M. Daghofer, and V. Dose: Modeling Energy Confinement in Plasma Devices by Neural Networks. In: Bayesian Inference and Maximum Entropy Methods in Science and Engineering, R. Fischer, R. Preuss, U. von Toussaint (eds.), American Institute of Physics 2004, 363-370.

Quinn, R.A. and J. Goree: Particle interaction measurements in a Coulomb crystal using caged particle motion. Phys. Rev. Lett. **88**, 195001, 1-4 (2002).

Räth, C., W. Bunk, B. Schulte et al.: Segmentierung und Volumetrie von Tumorentitäten mit CT-Datensätzen, Bildverarbeitung für die Medizin 2000. (Eds.) A. Horsch and T. Lehmann., Springer Verlag, Berlin, 449-453 (2000).

Räth, C., W. Bunk, M.B. Huber, G.E. Morfill, J. Retzlaff and P. Schuecker: Analysing large-scale structure- I. Weighted scaling indices and constrained randomization. Mon. Not. R. Astron. Soc. **337**, 413-421 (2002).

Räth, C. and P. Schuecker: Analysing large scale structure: II. Testing for primordial non-Gaussianities in CMB maps using surrogates, Month. Not. Roy. Astr. Soc., **344**, 115-128 (2003).

Räth, C., R. Monetti, D. Müller, H. Böhm, E. Rummeny and T.M. Link: Analysing and selecting measures for quantifying trabecular bone structures using surrogates, Proc. of the SPIE: Medical Imaging: Image Processing, **5032**, 1748-1756 (2003).

Räth, C., W. Bunk, P. Schuecker, J. Retzlaff, M. Huber and G. Morfill: Analysing cosmic large scale structure using surrogate data. In: Statistical challenges in astronomy. (Eds.) E.D. Feigelson, G.J. Babu., Springer, New York, 481-482 (2003).

Räth, C., R. Monetti, D. Müller, H. Böhm, E. Rummeny and T. Link: Comparing nonlinear texture measures for quantifying trabecular bone structures using surrogates, Proc. of the SPIE: Medical Imaging: Image Processing, **5370**, 207-214 (2004).

Räth, C., R. Monetti, D. Müller, T. Link and H. Böhm: Modelling Trabecular Changes using Cellular Automata, J. Bone Min. Res., **19**, S371 (2004).

Ratynskaia, S., S. Khrapak, A. Zobnin, M. H. Thoma, M. Kretschmer, A. Usachev, V. Yaroshenko, R. A. Quinn, G.E. Morfill, O. Petrov and V. Fortov. Experimental determination of dust particle charge in a discharge plasma at elevated pressures. Phys. Rev. Lett. **93**, 085001 (2004).

Ratynskaia, S., M. Kretschmer, S. Khrapak, R. A. Quinn, M. H. Thoma, G.E. Morfill, A. Zobnin, A. Usachev, O. Petrov and V. Fortov. Dust mode in collisionally dominated complex plasmas with particle drift. IEEE Trans. on Plasma Sci. **32**, 613 (2004).

Ratynskaia, S., C. Knapek, K. Rypdal, S. Khrapak and G. E.Morfill: Statistics of particle transport in a 2D dusty plasma cluster, Phys. Plasmas, **12,** 022302 (2005).

Reich, W., E. Fürst, P. Reich et al.: Radio-loud Active Galaxies in the Northern ROSAT All-Sky Survey: IV. Properties of Sources Stronger than 100 mJy at 5 GHz. Astron. Astrophys. **363**, 141-156 (2000).

Reiter, M., F. Jamitzky, F. Trixler and W.M. Heckl: STM Structure Determination of Adenine Bilayers by Moire Interpretation. Phys. Stat. Sol. (a) **187**(1), 171-176 (2001).

Resendes, D. P., P. K. Shukla and G.E. Morfill: Electrostatic Interaction in a Colloidal Plasma and Ordered Structures. Physica Scripta. 62, 491-498 (2000).

Ricci, P., G. Lapenta, U. de Angelis and V.N. Tsytovich: Plasma Kinetics in Dusty Plasmas. Phys. Plasmas **8**, 769-776 (2000).

Rothermel, H., T. Hagl, G.E. Morfill, M.H. Thoma and H.M. Thomas: Gravity Compensation in Complex Plasmas by Application of a Temperature Gradient. Phys. Rev. Lett. **89**, 175001, 1-4 (2002).

Rüll T., R. Brosow, C. Räth, M. Brügel, W. Weber and T.M. Link: Response evaluation of neoadjuvant therapy in esophageal squamous cell cancer: Comparison of CT-volumetry and FDG-PET, Radiol., **225** (Suppl. S), 581 (2002).

Rüll, T., R. Brosow, C. Räth, M. Brügel, W. Weber and T.M. Link: Response Evaluation of Neoadjuvant Therapy in Esophageal Squamous Cell Cancer: Comparison of CT-Volumetry and FDG-PET. In: Proceedings of the 88th Annual

Meeting of the RSNA, Chicago, IL (USA), 2002. (Ed.). Supplement to Radiology Vol. 225, Radiological Society of North America, **581** (2002).

Runov, A., R. Nakamura, W. Baumjohann, R.A. Treumann, T.L. Zhang, M. Volwerk, Z. Vörös, A. Balogh, K.-H. Glaßmeier, B. Klecker, R. Rème and. L. Kistler: Current Sheet Structure Near Magnetic X-line Observed by Cluster. Geophysical Research Letters **30**, 33-1 –33-4 (2003).

Rypdal, K. and S. Ratynskaia: Statistics of low-frequency plasma fluctuations in a simple magnetized torus. Phys. Plasmas **10**, 7, 2686-2695 (2003).

Salimullah, M., P. K. Shukla, I. Sandberg and G.E. Morfill: Excitation of dipole oscillons in a dusty plasma containing elongated dust rods. New Journal of Physics **5**, 3, 40.1-40.7 (2003).

Salimullah, M., P.K. Shukla and G.E. Morfill: Wake potentials in plasmas containing elongated dust rods. Journal of Plasma Physics **69**, 4, 363-369 (2003).

Samsonov, D., J. Goree, H.M. Thomas and G.E. Morfill: Mach Cone Shocks in a Two-dimensional Yukawa Solid Using a Complex Plasma. Physical Review E **61**, 5557-5572 (2000).

Samsonov, D., A.V. Ivlev, G.E. Morfill and J. Goree: Long-range Attractive and Repulsive Forces in a Two-dimensional Complex (Dusty) Plasma. Phys. Rev. (E) **63**, 025401(R)-025405(R) (2001).

Samsonov, D., A.V. Ivlev, R.A. Quinn, G. Morfill and S. Zhdanov: Dissipative longitudinal solitons in a two-dimensional strongly coupled complex (dusty) plasma. Phys. Rev. Lett. **88** (9), 095004 (2002).

Samsonov, D., G. Morfill, H. Thomas, T. Hagl, H. Rothermel, V. Fortov, A. Lipaev, V. Molotkov, A. Nefedov, O. Petrov, A. Ivanov and S. Krikalev: Kinetic measurements of shock wave propagation in a three-dimensional complex (dusty) plasma. Phys. Rev. (E) **67**, 036404 (2003).

Samsonov, D., S. Zhdanov, G. Morfill and V. Steinberg: Levitation and agglomeration of magnetic grains in a complex (dusty) plasma with magnetic field, New J. Phys. **5**, 24 (2003).

Samsonov, D.¸ S. K. Zhdanov, R. A. Quinn, S. I. Popel and G.E. Morfill: Shock Melting of a Two-Dimensional Complex (Dusty) Plasma, Phys. Rev. Lett. **92**, 255004 (2004).

Samsonov, D., S. Zhdanov and G. Morfill: Shock waves and solitons in complex (dusty) plasmas, AIP Conf. Proc. **706**, 111 (2004).

Samsonov, D., S. Zhdanov and G. Morfill: Vertical wave packets in a two-dimensional strongly coupled complex (dusty) plasma. Phys. Rev.(E). (in press, 2004).

Sanservino M. A, A. Lopez, E. V. Albano and R. A. Monetti: Study of a monomer-monomer reaction system with short-range repulsive interactions. Eur. Phys. J. B **40**, 305-312 (2004).

Scholer, M., H. Kucharek and J. Giacalone: Cross-field Diffusion of Charged Particles and the Problem of Ion Injection and Acceleration at Quasi-perpendicular Shocks. Journal of Geophysical Research **105**, 18,285-18,293 (2000).

Scholer, M.: Ion Dynamics during Magnetotail Reconnection. Adv. Space Res. **26**, 405-414 (2000).

Scholer, M. and R.A. Treumann: Particle Acceleration in Magnetic Fields. In: Encyclopedia of Astron. Astrophys. Vol. **3**, (Ed.) P. Murdin. Insitute of Physics, Bristol and Philadelphia, 1974-1978 (2001).

Scholer, M.: (Chapter 14) Global Magnetospheric Modelling. I.A. Daglis (Ed.), Space Storms and Space Weather Hazards, 363-388 (2001).

Scholer, M., H. Kucharek and C. Kato: On Ion Injection at Quasiparallel Shocks. Physics of Plasmas **9**, 4293-4300 (2002).

Scholer, M., H. Kucharek and I. Shinohara: Short-large amplitude magnetic structures and whistler wave precursors in full-particle quasi-parallel shock simulations. J. Geophys. Research **108**, doi:10.1029/2002JA009820 (2003).

Scholer, M., I. Shinohara and S. Matsukiyo: Quasi-perpendicular shocks: Length scale of the cross-shock potential, shock reformation and implication for shock surfing. J. Geophys. Res. **108**, 1014 (2003).

Scholer, M., I. Sidorenko, C. H. Jaroschek, R. A. Treumann and A. Zeiler: Onset of collisionless magnetic reconnection in thin current sheets: Three-dimensional particle simulations. Phys. Plasmas **10**, 3521-3527 (2003).

Scholer, M.: Magnetic reconnection on the Sun and in the Earth's Magnetosphere. In Energy Conversion and Particle Acceleration in the Solar Corona, Lecture Notes in Physics, (Ed.) K.-L. Klein, Springer, 9 - 27 (2003).

Scholer, M.: Magnetic reconnection on the sun and in the earth's magnetosphere. In: Energy Conversion and Particle Acceleration in the Solar Corona. (Ed.) K.-L. Klein. Lecture Notes in Physics **612**, Springer Berlin, 9-27 (2003).

Scholer, M. and S. Matsukiyo: Nonstationarity of Quasi-perpendicular Shocks: A Comparison of Full Particle Simulations with Different Ion to Electron Mass Ratio. Annales Geophysicae **22**, 2345-2353 (2004).

Scholer, M.: Kinetic structure of the reconnection layer. In Physics of Reconnection in High-Temperature Plasmas. Research Signpost, (Ed.) M. Ugai, 267 - 289 (2004).

Scholer, M., H. Kucharek, V.V. Krasnosselskikh and K.-H. Trattner: Injection and Acceleration of Ions at Collisionless Shocks: Kinetic Simulations. ACE 2000 Symposium, Acceleration and Transport of Energetic Particles Observed in the Heliosphere, CP 528.

Schuecker, P., H. Böhringer and W. Voges: Detection of X-ray Clusters of Galaxies by Matching RASS Photons and SDSS Galaxies within GAVO. Astron. Astrophys. **420**, 61-74 (2004).

Schuecker, P., H. Böhringer, K. Arzner and T.H. Reiprich: Cosmic Mass Functions from Gaussian Stochastic Diffusion Processes. Astron. Astrophys. **370**, 715-728 (2001).

Schuecker, P., H. Böhringer, L. Guzzo et al.: The ROSAT-ESO Flux-Limited X-Ray (REFLEX) Galaxy Cluster Survey III: The Power Spectrum. Astron. Astrophys. **368**, 086-106 (2001).

Schuecker, P., H. Böhringer, T.H Reiprich and L. Feretti: A Systematic Study of X-ray Substructure of Galaxy Clusters Detected in the ROSAT All-Sky Survey. Astron. Astrophys. **378**, 408-427 (2001).

Schuecker, P., H. Böhringer, C.A. Collins and L. Guzzo: The REFLEX Galaxy Cluster Survey VII: Ω_m and σ_8 from cluster abundance and large-scale structure clustering. Astron. Astrophys. **398**, 867-877 (2002).

Schuecker, P., L. Guzzo, C.A. Collins and H. Böhringer: The ROSAT-ESO Flux-Limited X-ray (REFLEX) Galaxy Cluster Survey VI: Constraints on the cosmic matter density from the KL power spectrum. Mon. Not. R. Astr. Soc., **335**, 807-816 (2002).

Schuecker, P., R.R. Caldwell, H. Böhringer et al.: Observational Constraints on General Relativistic Energy Conditions, Cosmic Matter Density and Dark Energy from X-Ray Clusters of Galaxies and Type-Ia Supernovae. Astron. Astrophys. **402**, 53-63 (2003).

Schwarz-Selinger, T., A. von Keudell and W. Jacob: Novel Method for Absolute Quantification of the Flux and Angular Distribution of a Radical Source for Atomic Hydrogen. Journal of Vacuum Science and Technology A **18**, 995-1001 (2000).

Schwarz-Selinger, T., R. Preuss, V. Dose and W. von der Linden: Analysis of Multicomponent Mass Spectra Applying Bayesian Probability Theory. Journal of Mass Spectrometry **36**, 866-874 (2001).

Schwarz-Selinger, T., V. Dose, W. Jacob and A. von Keudell: Quantification of a Radical Beam Source for Methyl Radicals. Journal of Vacuum Science and Technology A **19**, 101-107 (2001).

Shemmer, O., P. Romano, R. Bertram et al.: Multiwavelength Monitoring of the Narrow-Line Seyfert 1 Galaxy Arakelian 564. III. Optical Observations and the Optical-UV-X-Ray Connection. Astrophys. J. **561**, 162-170 (2001).

Shinohara, I., H. Suzuki, M. Fujimoto and M. Hoshino: Rapid Large-scale Magnetic-field Dissipation in a Collisionless Current Sheet via Coupling between Kelvin-Helmholtz and Lower-Hybrid-Drift Instabilities. Physical Review Letters **87**, L950011-L950014 (2001).

Shukla, P. K., L. Stenflo and G.M. Morfill: Nonlinear Instabilities in a Dusty Plasma Sheath. IEEE Transactions on Plasma Science, **29**, No.2, 198-201 (2001).

Shukla, P.K., L. Stenflo, G.E. Morfill: Nonlinear instability of dust ion-acoustic waves in a plasma with strongly correlated dust grains IEEE Transactions On Plasma Science **31**, 119-122 (2003).

Shukla, P.K., M. Salimullah, G.E. Morfill: Instability of dust acoustic waves in an accelerating dusty plasma, Physica Scripta **67**, 354-356 (2003).

Shukla, P.K., M. Torney, R. Bingham, G.E. Morfill et al.: Streaming instabilities in plasmas with strongly coupled dust grains, Physica Scripta **67**, 350-353 (2003).

Shukla, P.K., A.A. Mamun, B. Eliasson, and G.E. Morfill: Oscillonic Mach cones in a dusty magnetoplasma, Physics Of Plasmas **11**, 4142-4145 (2004).

Shukla, P.K., R. Bharuthram, A.A. Mamun, G.E. Morfill et a: Response to "Comment on 'Instability of the Shukla mode in a dusty plasma containing equilibrium density and magnetic field inhomogeneities' and 'New resonance and cutoff for low-frequency electromagnetic waves in dusty magnetoplasmas' " [Phys. Plasmas 11, 4154 (2004)], Physics Of Plasmas **11**, 4156-4158 (2004).

Siebert, J., W. Brinkmann, S. Laurent-Muehleisen and M. Matsuoka: The Broad Band X-ray Spectra of Intermediate BL Lacs. Adv. Space Res. **25**, 729-732 (2000).

Sorger N., H. Helmberger, C. Räth: C. Ganter, U. Fink and G.E. Morfill: Volumetry using scaling indices: A clinically useful technique for response evluation during neoadjuvant therapeutical concepts. Radiol. **221** (Suppl. S), 369-370 (2001).

Steinberg, V., R. Sütterlin, A.V. Ivlev and G. Morfill: Vertical Pairing of Identical Particles Suspended in the Plasma Sheath. Phys. Rev. Lett. **86**, 4540-4543 (2001).

Sugiyama, T., M. Fujimoto and M. Scholer: Injection of He^{2+} Ions at a Parallel Shock. Adv.Space Res. **27**, 637-642 (2001).

Terasawa, T., K. Shibata and M. Scholer: Comparative Study of Flares and Substorms. Adv. Space Res. **26**, 573-576 (2000).

Terry, J.L., S.J. Zweben, K. Hallatschek et al.: Observations of the turbulence in the scrape-off-layer of Alcator C-Mod and comparisons with simulation. Physics of Plasmas **10**, 1739-1747 (2003).

Thoma, M.H.: Absence of Thermophoretic Flow in Relativistic Heavy-Ion Collisions as an Indicator for the Absence of a Mixed Phase, Phys. Rev. Lett. **88**, 202303 (2002).

Thoma, M.H., M. Kretschmer, H. Rothermel, H.M. Thomas, and G.E. Morfill: The Plasma Crystal, Am. J. Phys. (in press).

Thoma, M.H.: The Quark-Gluon-Plasma Liquid, J. Phys. G **31**, L7 (2005).

Thoma, M.H., J. Trümper, and V. Burwitz: Strange Quark Matter in Neutron Stars? -- New Results from Chandra and XMM, Proc. 7th Int. Conf. ``Strangeness in Quark Matter'' (Atlantic Beach, USA, 2003), J. Phys. G **30**, S471 (2004).

Thoma, M.H.: Strongly Coupled Plasmas in High-Energy Physics, Proc. "10th Workshop on the Physics of Dusty Plasmas" (St. Thomas, US Virgin Islands, 2003), IEEE Trans. Plasma Sci. **32**, 738 (2004).

Thoma, M.H., H. Höfner, S.A. Khrapak, M. Kretschmer, R.A. Quinn, S. Ratynskaia, G.E. Morfill, A. Usachev, A. Zobnin, O. Petrov, and V. Fortov, Measurement of the ion drag force in a complex dc plasma using the PK-4 experiment, Proc. Int. Conf. "Dusty Plamas in Applications", (Odessa, Ukraine, 2004), Ukrainian J. Phys (in press).

Thomas, E. Jr., W. Amatucci and G.E. Morfill: Boundary Phenomena in RF and DC Glow Discharge Dusty Plasmas. In: Dusty Plasmas in the New Millenium: Third International Conference on the Physics of Dusty Plasma, AIP Conference Proceedings **649**, (Eds.) R. Bharuthram, M.A. Hellberg, P.K. Shukla et al., American Institute of Physics, Melville NY 2002, 243-246.

Thomas, E., Jr., B.M. Annaratone, G.E. Morfill and H. Rothermel: Measurements of forces acting on suspended microparticles in the void region of a complex plasma. Phys. Rev. (E) **66**, 016405 -016411 (2002).

Thomas, H.M., D. D. Goldbeck, T. Hagl et al.: Complex Plasmas under microgravity conditions: Parabolic flights. Physica Scr. **T89**, 16-19 (2001).

Thomas, H.M., G.E. Morfill, Complex Plasmas – An introduction to a new field of research, Contrib. Plasma Phys. 41, 255-258, (2001).

Thomas, H. M, G.E. Morfill and V.N. Tsytovich: Complex plasmas: III. Experiment on Strong Coupling and Long Range Interactions. Plasma Phys. Rep. **29**, 895-954 (2003).

Thomas, H.M., G.E.Morfill, A.P. Nefedov, V.E. Fortov, H. Rothermel, A.V. Ivlev, M. Zuzic, A.M. Lipaev, V.I. Molotkov, O.F. Petrov: The Physics of Complex Plasmas and the Microgravity Programme on Plasma Crystal (PK) Research, Proceedings of the 55th International Astronautical Congress 2004 - Vancouver, Canada, IAC-04-T.4.03 and IAC-04-J.3.02 (2004).

Toussaint, U. von, S. Gori and V. Dose: Bayesian Neural-networks-based Evaluation of Binary Speckle Data. Applied Optics **43**, 5356-5363 (2004).

Toussaint, U. von, V. Dose and A. Golan: Maximum Entropy Decomposition of Quadrupole Mass Spectra. Journal of Vacuum Science and Technology A **22**(2), 401-406 (2004).

Toussaint, U. von, S. Gori, and V. Dose: A Prior for Neural Networks Utilizing Enclosing Spheres for Normalization. In: Bayesian Inference and Maximum Entropy Methods in Science and Engineering, R. Fischer, R. Preuss, U. von Toussaint (eds.), American Institute of Physics 2004, 328-335.

Treumann, R. A., M. Berthomier and R. Pottelette: Theory of Alfvénic Solitons and the Nonlinear State of the Auroral Magnetosphere. OFFPRINT – Verlag der Österreichischen Akademie der Wissenschaften (2000).

Treumann, R. A. and W. Baumjohann: Collisionless Mirror Mode Trapping. Nonlinear Processes in Geophysics **7**, 179-184 (2000).

Treumann, R. A., A. Kull and H. Böhringer: Neutrino Dark Matter in Clusters of Galaxies. New Journal of Physics **2**, 11.1-11.13 (2000).

Treumann, R. A., E. Georgescu and W. Baumjohann: Lion Roar Trapping in Mirror Modes. Geophysical Research Letters **27**, 1843-1846 (2000).

Treumann, R.A. and A. Kull: Kullback's Contrast and Lorentzian Entropy. Physica Scr. **61**, 403-405 (2000).

Treumann, R. A. and M. Scholer: Collisionless Plasmas in Astrophysics. Encyclopedia of Astronomy and Astrophysics. (Ed.) P. Murdin. Institute of Physics Publishing, Bristol and Nature Publishing, London, UK **1**, 398-408 (2000).

Treumann, R. A. and M. Scholer: The Magnetosphere as a Plasma Laboratory. The Century of Space Science, Kluwer Academic Publishers, 1495-1528 (2001).

Treumann, R. A. and T. Terasawa: Electron acceleration in the heliosphere. Space Sci. Rev. **99**, 135-150 (2001).

Treumann, R. A.: Origin of Resistivity in Reconnection. Earth Planet Space **53**, 453-462 (2001).

Treumann, R. A.: Statistical Mechanics of Stable States far from Equilibrium: Thermodynamics of Turbulent Plasmas. Astrophysics and Space Science **277**, 81-95 (2001).

Treumann, R. A. and M. Scholer: Collisionless Processes in Astrophysical Plasmas, In: Encyclopedia of Astron. Astrophys. Vol. **1**, (Ed.) P. Murdin. Institute of Physics, Bristol and Philadelphia, 398-408 (2001).

Treumann, R. A. and M. Scholer: The magnetosphere as a plasma laboratory, The Century of Space Science. (Eds.) J. Bleeker, J. Geiss, M.C.E. Huber. Kluwer Acad. Publ., Dordrecht, Holland, 1495-1528 (2002).

Treumann, R. A.: An attempt of formulating the principles of a generalized-Lorentzian quantum mechanics. Phys. Scripta **66**, 417-424 (2002).

Treumann, R. and J. Labelle: Auroral Radio Emissions, 1. Hisses, Roars. and Bursts. Space Science Reviews **101**, 295-440 (2002).

Treumann, R. A. and R. Pottelette: Particle acceleration in the magnetosphere and its immediate environment. Adv. Space Res. **30** (7), 1623-1628 (2003).

Treumann R. A., C. H. Jaroschek and M. Scholer, Stationary plasma states far from thermal equilibrium. Phys. Plasmas **11**, 1317-1325 (2004).

Treumann, R. A., C. H. Jaroschek, O. D. Constantinescu, R. Nakamura, O. A. Pokhotelov, and E. Georgescu: The strange physics of low-frequency mirror mode turbulence in high temperature plasma, Proc. Geophys. **11**, 647-657 (2004).

Tsytovich, V.N. and U. de Angelis: Kinetic Theory of Dusty Plasmas. III.- Dust-dust Collision Integrals. Phys. Plasmas **8**, 1141-1153 (2001).

Tsytovich, V.N., U. de Angelis and R. Bingham: Low-frequency Responses and Wave Dispersion in Dusty Plasmas. Phys. Rev. Lett. **87**, 185003/1-4 (2001).

Tsytovich, V.N., S.V. Vladimirov, G.E. Morfill and J. Goree: Theory of Collision-dominated Durst Voids in Plasmas. Phys. Rev. E **63**, 056609/1-11 (2001).

Tsytovich, V.N.: Evolution of Voids in Dusty Plasmas. Phys. Scr. **T89**, 89-94 (2001).

Tsytovich, V.N. and G.E. Morfill: Collective attraction of equal-sign charged grains in plasmas. Plasma Phys. Rep. **28**, 171-176 (2002).

Tsytovich, V.N. and G.E. Morfill: Physics of collective dust-dust attraction and dust structure formation. Dusty Plasmas in the New Millenium: Third International Conference on the Physics of Dusty Plasma, AIP Conference Proceedings **649**, (Eds.) R. Bharuthram, M.A. Hellberg, P.K. Shukla et al., American Institute of Physics, Melville NY 2002, 110-118 (2002).

Tsytovich, V.N. and U. de Angelis: Kinetic theory of dusty plasmas. IV. Distribution and fluctuations of dust charges. Phys. Plasmas **9**, 2497-2506 (2002).

Tsytovich, V.N., G.E. Morfill and H. Thomas: Complex plasmas: I. Complex plasmas as unusual state of matter. Plasma Phys. Rep. **28**, 623-651 (2002).

Tsytovich, V.N.: Collective plasma corrections to thermonuclear reaction rates in dense plasmas. JETP 94 (5), 927-942 (2002).

Tsytovich, V.N., A.P. Nefedov, V.E. Fortov, O.F. Petrov and G.E. Morfill: Effects of Ultraviolet Radiation on Dusty Plasma Structures at Microgravity. Physics of Plasmas **10**, Articles, 2633-2642 (2003).

Tsytovich, V.N., G. Morfill, U. Konopka and H. Thomas: Collision Dominated Dust Sheaths and Voids-observations in Micro-gravity Experiments and Numerical Investigation of the Force Balance Relations. New Journal of Physics **5**, 1.1-1.27 (2003).

Tsytovich, V.N., G.E. Morfill and A.V. Ivlev: Van der Waal's approach in the theory of phase transitions in complex plasmas. Contrib. Plasma Phys. **43**, 439-446 (2003).

Tsytovich, V.N., N. Gusein-Zade and G. Morfill: Helical Dust Structures in Laboratories and Space. In: 30th European Physical Society Conference on Plasma Physics and Controlled Fusion. Published electronically: http://eps2003.ioffe.ru/public/pdfs/O-35B-pre.pdf., (2003).

Tsytovich, V.N., N. Sato and G.E. Morfill: Note on the charging and spinning of dust particles in complex plasmas in a strong magnetic field. New. J. Phys. **5**, 43.1-43.9 (2003).

Tsytovich, V., N. Gusein-Zade, G. Morfill: Dust-dust interactions and formation of helical dust structures, IEEE Transactions On Plasma Science 32, 637-652 (2004).

Uchida, G., U. Konopka, G. Morfill: Wave dispersion relation of two-dimensional plasma crystals in a magnetic field, Physical Review Letters **93**, 155002 (2004).

Usachev, A., A. Zobnin, O. Petrov, V. Fortov, M.H. Thoma, M. Kretschmer, S. Ratynskaia, R.A. Quinn, H. Höfner, and G.E. Morfill: The Project “Plasmakristall - 4" (PK-4) - a Dusty Plasma Experiment in a Combined DC/RF(i) Discharge Plasma under Microgravity Conditions, Proc. ``21st Symposium on Plasma Physics and Technology" (Praha, Czechia, 2004), Czech. J. Phys. (in press)

Vasquez-Borucki, S., W. Jacob and C. A. Achete: Amorphous Hydrogenated Carbon Films as Barrier for Gas Permeation through Polymer Films. Diamond and Related Materials **9**, 1971-1978 (2000).

Vasquez-Borucki, S., C.A. Achete and W. Jacob: Hydrogen Plasma Treatment of Poly(ethylene terephtalate) Surfaces. Surface and Coating Technology **138**, 256-263 (2001).

Vaulina, O., S. Khrapak and G. Morfill: Universal Scaling in Complex (Dusty) Plasmas. Physical Review E **66**, 016404-1-016404-5 (2002).

Verheest, F., V.V. Yaroshenko and M. Hellberg: Dust distribution in self-gravitating dusty plasmas. Phys. Plasmas **9**, 2479-2485 (2002).

Verheest, F, Yaroshenko,V.: Oblique Electrostatic Modes in Self-Gravitating Plasmas, Phys. Rev. E, **65**, 036415 (2002).

Verheest, F., M. Hellberg and V.V. Yaroshenko: Electrostatic modes in dusty plasma with continuous size distributions. Phys. Rev. (E) **67**, 1, 016406-1-016406-4 (2003).

Verheest, F., P.K. Shukla, G. Jacobs and V.V. Yaroshenko: Jeans instability in partially ionized self-gravitating dusty plasmas. Phys. Rev. (E) **68**, 027402 (2003).

Vladimirov, S.V., G.E. Morfill, V.V. Yaroshenko and N.F. Cramer: Oscillatory modes of magnetized grains in a plasma. Phys. Plasmas **10**, 7, 2659-2662 (2003).

Vladimirov, S.V., K. Ostrikov, M.Y. Yu and G.E. Morfill: Ion-acoustic waves in a complex plasma with negative ions. Physical review E **67**, 036406-036406 (2003).

Vörös Z., W. Baumjohann, R. Nakamura, M. Volwerk, A. Runov, T.L. Zhang, H. U. Eichelberger, R. A. Treumann, E. Georgescu, A. Balogh, B. Klecker, and H. Rème: Magnetic turbulence in the plasma sheet, J. Geophys. Res., **109**, A11215, doi:10.1029/2004JA010404, (2004).

Voitsenya, V. S., A.F. Bardamid, V.N. Bondarenko et al.: Some Problems Arising due to Plasma-Surface-Interaction for Operation of the In-vessel Mirrors in a Fusion Reactor. Journal of Nuclear Materials **290-293**, 336-340 (2001).

Volwerk M., R. Nakamura, W. Baumjohann et al.: Statistical study of compressional waves in the tail current sheet. J. Geophys. Res. **108**, 1429, doi:10.1029/2003JA010155 (2003).

Volwerk M., W. Baumjohann, K.-H. Glaßmeier et al: Compressional waves in the Earth's neutral sheet. Ann. Geophys. **22**, 303-315 (2004).

Wang, T., W. Brinkmann, M. Matsuoka, J.X. Wang and W. Yuan: X-ray and UV Spectral Properties of the X-ray Transient Quasar PG 0844+349. Astrophys. J. **533**, 113-119 (2000).

Wang, T.G., W. Brinkmann, W. Yuan, J. X. Wang and Y.Y. Zhou: The X-ray Absorber in Broad Absorption Line Quasars. Astrophys. J. **545**, 77-85 (2000).

Wiechen, H. and G.T. Birk: Kelvin-Helmholtz Instabilities in Dusty Plasma-neutral Gas Systems. Proceedings of ISSS-6, 184-187 (2001).

Wu, C.H., C. Alessandrini, J.P. Bonal et al.: Progress of the European R&D on Plasma-Wall Interactions, Neutron Effects and Tritium Removal in ITER Plasma Facing Materials. Fusion Engineering and Design **56-57**, 179-187 (2001).

Yaroshenko, V. and G.E. Morfill: Parametric Excitation of Low Frequency Waves in Complex (Dusty) Plasmas. Physics of Plasmas **9**, 4495-4499 (2002).

Yaroshenko,V., Voitenko Y. and M.Goossens: Linear coupling of electromagnetic and Jeans modes in self-gravitating plasma streams, Phys. Plasmas, **9**, No 5, 1520-1525 (2002).

Yaroshenko, V.V. and G.E. Morfill: Instability of dust lattice waves due to periodically varying charges of dust particles. Dusty Plasmas in the New Millenium: Third International Conference on the Physics of Dusty Plasma, AIP Conference Proceedings **649**, (Eds.) R. Bharuthram, M.A. Hellberg, P.K. Shukla et al., American Institute of Physics, Melville NY 2002, 487-490.

Yaroshenko, V., A. Debousscher, M.Goossens, and G.E. Morfill: On Possible stationary equilibrium of dusty self-gravitating space plasmas, Problems of Atomic Science and Technology (Voprocy Atomnoy Nauki i Tekhniki), Series: Plasma Physics, **4(7)**, 115-118 (2002).

Yaroshenko, V.V. and G.E. Morfill: Vibrational Modes in Plasma Crystals Due to Nonlinear Temperature Distribution in Gas Discharge Plasmas. Physical Review **66**, 065401-1-065401-3 (2002).

Yaroshenko,V. and G. Morfill: Instability of dust lattice waves due to periodically varying charges of dust particles, In: "Dusty Plasmas in the New Millennium", (edited by R. Bharuthram, M.A. Hellberg, P.K. Shukla, and F. Verheest) AIP press, p.487490 (2002).

Yaroshenko, V.V., G.E. Morfill and S.V. Vladimirov: Vibrational modes in the plasma crystal due to nonlinear temperature distribution in gas discharge plasmas. Phys. Rev. (E) **66**, 065401, 1-3 (2002).

Yaroshenko, V.V., F. Verheest and M. Hellberg: Dust-acoustic instability in inhomogeneous complex plasmas. Phys. Plasmas **10**, 3834-3840 (2003).

Yaroshenko, V.V., G.E. Morfill, D. Samsonov and S.V. Vladimirov: Mutual interactions of magnetized particles in complex plasmas. New Journal of Physics **5**, 18.1-18.8 (2003).

Yaroshenko, V.V., B.M. Annaratone, S.A. Khrapak, H.M. Thomas, G.E. Morfill, V.E. Fortov, A.M. Lipaev, V.I. Molotkov, O.F. Petrov, A.I. Ivanov and M.V. Turin: Electrostatic Modes in Collisional Complex Plasmas under Microgravity Conditions. Physical Review E **69**, 066401-1-066401-7 (2004).

Yaroshenko, V.V., G.E. Morfill and D. Samsonov: Vertical Oscillations of Paramagnetic Particles in Complex Plasmas. Physical Review E **69**, 016410-1-016410-5 (2004).

Yaroshenko, V., G.E. Morfill, D. Samsonov and S.V. Vladimirov: Agglomeration of Magnetized Dust Particles in Complex Plasmas, IEEE Transactions on Plasma Science, vol. 32, No 2, p.675-679 (2004)

Yaroshenko, V.V., A. V. Ivlev, G.E. Morfill: Charge-gradient instability of dust lattice waves, Phys. Plasmas, Accepted for publication

Yaroshenko, V.V., A. V. Ivlev, G. E. Morfill: Coupled dust lattice modes in complex plasmas, Phys. Rev. E. submitted, October, 2004

Yuan, W., W. Brinkmann, M. Gliozzi, Y. Zhao and M. Matsuoka: X-ray Observation of the Super-luminal Quasar 4C+73.18 (1928+738) by ASCA. Astronomy and Astrophysics **362**, 19-26 (2000).

Zarka, Ph., R.A. Treumann, B.P. Ryabov and V.B. Ryabov: Magnetically-driven Planetary Radio Emissions and Application to Extrasolar Planets. Astrophysics and Space Science **277**, 293-300 (2001).

Zeiler, A., D. Biskamp, J. F. Drake, B. N. Rogers, M. A. Shay and M. Scholer: Three-dimensional particle simulations of collisionless magnetic reconnection. J. Geophys. Research, doi:10.1029/2001JA000287 (2002).

Zhang, Y.-Y., A. Finoguenov, H. Böhringer, Y. Ikebe, K. Matsushita and P. Schuecker: Temperature gradients in XMM-Newton observed REFLEX-DXL galaxy clusters at z≈0.3. Astron. Astrophys. **413**, 49-63 (2004).

Zhdanov, S. K., D. Samsonov and G.E. Morfill: Anisotropic plasma crystal solitons. Phys. Rev. (E) **66**, 026411, 1-11 (2002).

Zhdanov, S., R.A. Quinn, D. Samsonov and G.E. Morfill: Large-scale steady-state structure of a 2D plasma crystal. New Journal of Physics **5**, 74.1-74.11 (2003).

Zhdanov, S., S. Nunomura, D. Samsonov and G. Morfill: Polarization of wave modes in a two-dimensional hexagonal lattice using a complex (dusty) plasma. Phys. Rev. E 68 (3), 035401 (2003).

Zhdanov, S.K., G.E. Morfill, D. Samsonov, M. Zuzic and O. Havnes: Origin of the Curved Nature of Mach Cone Wings in Complex Plasmas. Physical Review E **69**, 026407-1-026407-8 (2004).

Zhdanov,S.K. A.V. Ivlev, ,G.E. Morfill: Non-Hamiltonian dynamics of grains with spatially varying charges, submitted to Phys. Rev. E (2004).

Zuzic, M., A.V. Ivlev, J. Goree, G.E. Morfill, H.M. Thomas, H. Rothermel, U. Konopka, R. Sütterlin and D.D. Goldbeck: Three-Dimensional Strongly Coupled Plasma Crystal under Gravity Conditions. Phys. Rev. Lett. **85**, No. 19, 4064-4067 (2000).

www.cips.mpg.de